STYLOLITIZATION MECHANISMS, PERMEABILITY BARRIERS AND PRESSURE SOLUTION GENERATED-CEMENTS

STYLOLITIZATION MECHANISMS, PERMEABILITY BARRIERS AND PRESSURE SOLUTION GENERATED CEMENTS: EXAMPLES FROM THE LOCKPORT FORMATION (MIDDLE SILURIAN) OF DUNDAS, ONTARIO AND NISKU FORMATION (UPPER DEVONIAN) OF CENTRAL ALBERTA

By

M. CRAIG RICE B.Sc.

A Thesis

Submitted to the Faculty of Science

in Partial Fulfillment of the Requirements

for the Degree

Master of Science

McMaster University

September, 1986

MASTER OF SCIENCE (1986)
(Geology)

McMASTER UNIVERSITY
Hamilton, Ontario

TITLE:	Stylolitization Mechanisms. Permeability Barriers And Pressure Solution Generated-Cements
AUTHOR:	M. Craig Rice B. Sc.
SUPERVISOR:	Dr. P.M. Clifford
NUMBER OF PAGES:	xx, 316

To My Wife, Ann

ABSTRACT

The study of stylolites found in the Lockport (Middle Silurian) dolostones and Nisku Formation (Upper Devonian) limestones has led to the development of two stylolitization mechanisms. The amalgamation mechanism (Lockport Formation) forms a stylolite by the amalgamation of microstylolites through pressure solution of intervening dolomite. Microstylolites originated as primary "organic" layers. Dolomitization-stylolitization (Nisku Formation) forms a stylolite by pressure-dissolution of matrix calcite against concentrations of dolomite. Dolomite acts as a stress perturbation that ultimately leads to pressure solution and stylolitization.

Statistical analysis of Nisku Formation core data suggests that there is a reversal in the trend of vertical permeability reduction once a stylolite grows to centimetre-scale. The most effect permeability barriers are millimetre- and millimetre to centimetre-scale stylolites.

Cathodoluminescent observations suggest that stylolites generate carbonate cements. The mode of transport of dissolved material away from the stylolite is by ionic transfer in porosity and diffusion through intracrystalline/matrix micrite mediums. Stylolitization is responsible for recrystallization and dedolomitization textures seen in the vicinity of stylolites. The isotopic composition of main mineral phases in the Nisku Formation supports these interpretations.

ACKNOWLEDGEMENTS

Many people have contributed to the production of this thesis from its inception to its completion. First, I would like to thank Dr. Paul Clifford whose efforts made my graduate work possible. Texaco Canada Resources Ltd., notably Murray Coppold, were generous enough to give me a research grant and provide their services to help minimize my expenses. Nigel Watts, at Texaco, suggested some of the ideas in this thesis. Thank you Nigel for all your help and patience.

Dr. Roger Walker deserves much recognition. Without his help I never would have been able to go to Calgary to collect the bulk of the samples used in this research. Dr. Gerry Middleton was of great assistance in helping me learn and understand the statistical analysis used in this thesis. He was also always available to let me bounce my ideas off him to test their soundness.

Len Zwicker not only made excellent thin sections, his lab door was always open (except fridays) to me. Many entertaining and hilarious times have been spent in his company that will remain unforgetable. Bill Buhay was one of the best office-mates that any one could ask for. In

many of our more leisurely moments we have invented new indoor office sports and pulled more practical jokes than we would care to admit (if only the faculty knew what went on..)

Many other persons have been of great assistance over these years who deserve more recognition than I can give them in these pages. Thank you to Dr. Henry Schwarcz, John Cekr, Jack Whorwood, David Collins, Fereydoun Ghazban, and the secretaries. Steve Zymela is responsible for the production of this text. His knowledge of computers virtually made it possible for me to meet my deadline. Steve, how do I get the computer to do....?

Yet, though all these people helped in one way or another, the person most deserving of recognition is my wife, Ann. She supported me when I decided to do graduate work, and put up with me when came I home in one of my crazy moods. This thesis is as much hers as it is mine.

TABLE OF CONTENTS

LIST OF FIGURES

LIST OF TABLES

CHAPTER 1

INTRODUCTION

1.1 INTRODUCTION

Stylolitization is a phenomenon that is often recognized, but poorly understood by many carbonate geologists. In recent years, with the advent of burial diagenetic studies, our understanding of pressure solution phenomena has improved but is still in its developing stages. This research is an attempt at contributing to that understanding.

Pressure solution, and ultimately stylolitization, plays an important role in the post-depositional alteration of carbonate sediments. Stylolitization of a carbonate rock unit proceeds through the dissolution of material induced by overburden pressures. The dissolved material may be removed from the "system" and reprecipitated elsewhere, or it may be reprecipitated locally. In the subsurface environment, pressure solution is believed to be the source for volumes of cement otherwise unaccounted for.

An artifact of stylolitization is the accumulation of insoluble materials (clays, organics) at the stylolite surface. These act as barriers to fluid-flow that reduce the vertical permeability of the rock. For a reservoir geologist, stylolites may prove to be the cause of many problems not found in non-stylolitic rocks, such that the geologist might wish he had never seen them. To circumvent these problems a better understanding of the process of stylolitization is required.

1.2 NATURE OF THE PROBLEM

The purpose of this research is three-fold. First, stylolites are the result of pressure-dissolution of the rock. How do they develop? Why do they form where they do? How do they grow vertically and laterally? Do stylolites in different types of carbonate form and grow in the same way? This research will look at stylolites that occur within beds in order to answer these questions.

Secondly, bedding-parallel stylolites are commonly thought to behave as permeability barriers to vertical flow. Using core data for one set of samples of this study, an attempt will be made to look a permeability reduction relative to stylolite occurrence.

Thirdly, pressure solution dissolves carbonate material at stylolite surfaces and/or grain contacts. Is there any evidence that indicates if this material was reprecipitated locally, and if so, are there direct links between the reprecipitated material and stylolites?

This research will look at two different sample suites and attempt to answer these questions in an effort to better understand the pressure solution phenomenon.

1.3 PREVIOUS WORK

1.3.1 PRESSURE SOLUTION

When first recognized over a century ago, stylolites were so named because they resembled the trace of a "stylus". They were believed by these early investigators to be fossiliferous, some sort of organism that was preserved in the rock.

In the first half of this century, it was Stockdale (1922, 1926, 1943) who proposed the idea of stylolites developing as the result of a pressure-dissolution process, the SOLUTION-PRESSURE theory. Shaub (1939, 1949) proposed an alternative explanation by modelling stylolite formation via the CONTRACTION-PRESSURE theory. This requires deposition of a mud with a clay layer on top of it that will act as an impermeable barrier to escaping water. A subsequent mud layer is deposited on top of the clay layer, and then the sediments are subaerially exposed. Contractions resulting from the drying-out of this last mud unit would result in localized reduced pressure zones and the underlying wet mud and clay layers would be injected upwards into these zones. This would form a "stylolite" as the lower layers interpenetrate the dried and cracked upper layer.

Prokopovich (1952) suggested that stylolites develop due to lime mud dissolution at the sediment-water interface, the SUBAQUEOUS-SOLUTION theory. The result would be an etched and pitted surface with insoluble materials left as a "veneer" over the irregular surface. Renewed deposition would trap the layer of insoluble material, thus forming a stylolite.

A return to the general theory of Stockdale was proposed by Dunnington (1954) who dismissed the contraction-pressure theory as being the result of poor investigation on the part of Shaub. Additionally, the subaqueous-solution theory of Prokopovich was dismissed because its analogies were strained and it did not offer satisfactory explanations of normal stylolitic features found in sediments other than lime muds.

Dunnington (1954) generally accepted the theory of Stockdale, that pressure solution of hardened rock is the reason for stylolites, but suggested that pressure solution features begin as microscopic serrations that in turn amalgamate to features of macroscopic size. In this sense, he may have been ahead of his time.

More recently, the focus of pressure solution studies has been on the degree of consolidation of the rock at the onset of pressure solution. Park and Schot (1968) suggest that stylolites are of pre-complete cementation origin. Similarly, Bathurst (1971) believes that stylolites begin in limestones which are only lightly cemented and that the process releases $CaCo_3$ to drive cementation to completion. Once cementation is complete the process may come to an end due to transport problems away from the site of dissolution.

Purser (1978) has noticed a progressive increase in the degree of compaction of burrows and in the abundance of stylolites below hardgrounds. This led him to the conclusion that stylolitization occurred in sediments that lacked early near-surface cementation and were presumably buried in a "friable" state.

The experimental compaction experiments of Shinn and Robbin (1983) produced "stylolite-like" organic layers and pressure-dissolution penetration of particles by quartz grains. These authors envisage pressure solution as a continuation of mechanical compaction in unlithified lime muds.

Wanless (1979) proposed a classification of pressure solution features that relates the responsiveness of a limestone to stress, to the type of pressure-solution texture observed. The style of pressure solution feature that develops is dependent upon the degree of resistance to stress inherent in the rock. For example, sutured solution seams form at the contact between two resistant "units". Non-sutured solution seams form at the contact between a resistant and a responsive "unit". Non-seam solution develops within responsive units. This last style of pressure solution does not result in stylolitic features but distorts primary sedimentological textures.

Most recently Schofield (1984) proposed that dolomitization, neomorphism and pressure solution are genetically related. Dolomitization of a marine sediment will induce neomorphism of micritic sediments and particles under burial conditions. With increased burial, the rock responds by passing out of the neomorphism field into that of pressure solution; the result is seen as non-seam solution analagous to that of Wanless (1979). He also suggested that stylolites may propagate laterally by non-seam solution of dolomitic limestone but offered no mechanism for propagation.

1.3.2 PERMEABILITY BARRIERS

Stylolites have long been recognized to impede the flow of fluids and hydrocarbons across their surfaces (Dunnington 1967, Bathurst 1971). However, no one has attempted to quantify permeability reduction by stylolites in the literature.

1.3.3 PRESSURE SOLUTION DERIVED CEMENTS

Numerous workers have noted close spatial relationships between stylolite occurrence and low porosity (Dunnington 1967, Purser 1978, Nelson 1981). The best documented example is that of Wong and Oldershaw (1981), for a Devonian reef in Alberta. These authors were able to establish the relative timing of stylolite growth and cementation.

To link pressure solution directly to burial cements requires a "certain leap of faith" as Scholle and Halley (1983) so aptly phrase it. To be able to do so requires direct links but often only spatial and temporal relationships can be found. Oldershaw and Scoffin (1967) propose that much of the calcite spar in the Halkin and Wenlock Limestones is of pressure solution origin. However, this is inferred. They do not directly relate the two processes by citing evidence of calcite filled veinlets propagating away from stylolites. Purser (1978) believes that pressure solution generated a locally reprecipitated calcite spar, a belief based upon temporal relationships and isotopic evidence. However, nowhere has there been published an account of direct evidence linking stylolites to pore--occluding cement.

Wanless (1979) believes that pressure solution may be an agent by which dolomitization takes place. Dissolved carbonate from along a stylolite surface may enter into magnesium-enriched pore waters and be reprecipitated locally as dolomite of a distinctive character (size, zonation, luminescence) different from dolomite elsewhere in the rock. The author suggests that this may be a mechanism that can account for stratiform dolomite observed in ancient carbonates.

1.4 LOCATION

The two sets of sample suites for this research come from two different localities. The Lockport Formation (Middle Silurian) samples were collected from a quarry approximately 5 kilometres north of the town of Dundas, Ontario on Highway 5. It is owned by Steetley Industries Ltd. from whom permission must be obtained before entering.

The Nisku Formation (Upper Devonian) samples are from the borehole Texaco Bigoray 6-12-52-9W5, located in west-central Alberta. The cored interval penetrates a pinnacle reef that rests on a carbonate platform approximately 2400 metres below the surface.

CHAPTER 2

STYLOLITIZATION MECHANISMS I

2.1 GENERAL OBSERVATIONS-LOCKPORT FORMATION

The samples used for this study are from the Eramosa Member of the Lockport Formation (Middle Silurian). These are sediments of a subtidal-intertidal environment which have experienced penecontemporaneous dolomitization and a later, more complete, dolomitization in a phreatic zone of mixing (Shukla and Friedman 1983). Dolomitization has completely obliterated all details of any precursor carbonate phase.

Stylolites abound in these samples and display many different styles and relationships. They are all essentially bedding parallel. Nowhere is there evidence to suggest that stylolitization was succeeded by dolomitization. All stylolites are post-dolomite, hence stylolitization occurred in a relatively homogeneous, monominerallic medium.

Thick, undulose accumulations of black insoluble material are found at what appear to be bedding planes. Previous workers have called these "carbonaceous partings", but Simpson (1985) refers to features similar to these as pseudo-bedding. Contacts such as these resemble, though may not be, bedding surfaces. In the Lockport Formation, it is believed that these are stylolites that have either enhanced a bedding surface or resemble one.

The lateral extent of any one stylolite is believed to reflect the degree of development, such that long stylolites are more mature than short stylolites. One can find those that are laterally extensive, metres long, or ones that are only a few centimetres long. In any one "bed" an extremely long seam may have as its nearest neighbour a seam that is equally as long, or very short, or any combination thereof. As a result stylolite density and frequency is variable. Stylolite occurrence resembles a number of very long seams with shorter ones nestled between them.

A number of morphologic styles and relationships of stylolites were found. To generalize, well-developed stylolites are metres long and may be sutured or undulose. Commonly, they are branched, bifurcating into smaller stylolites along their length. On the other hand, short stylolites are mostly finely sutured and are most always associated with other seams and swarms of microstylolites. It is common to find short stylolites, centimetres long that fan-outward into "horsetail-like" projections at their lateral tips.

To examine stylolite development and ultimately model a stylolitization mechanism, only those features within "beds" were studied. The variability of stylolites in these units is believed to represent various stages of development "frozen" in the rock. The following sections emphasize those processes occurring only within "beds".

2.2 SOLUTION SEAM MORPHOLOGY

Six morphological types of stylolites and related features were recognized within "bedding" layers. These are:

i) Microswarms - looks like regions of minute, wispy stylolites (Figure 1). These may or may not occur associated with stylolites. The thickness of a microswarm is variable, ranging from less than 1 centimetre to several centimetres. The lateral extent of a microswarm gradually decreases until it is no longer recognizable.

ii) Regular sutured - resembles a near-rectiplanar stylolitic solution seam, the amplitude of which rarely exceeds 2 millimetres (Figure 2a).

iii) Irregular sutured - resembles a sutured waveform superimposed upon an irregular waveform of varying wavelength and amplitude (Figure 2b). The amplitude of the sutured seam rarely exceeds 2 millimetres.

Figure 1 Close-up photograph of a microstylolite swarm (microswarm) as seen in thin section. This microswarm occurs in the absence of a stylolite. Note the diffuse boundaries of the swarm and the dense concentration of microstylolites within it. Scale bar = 1 cm.

12

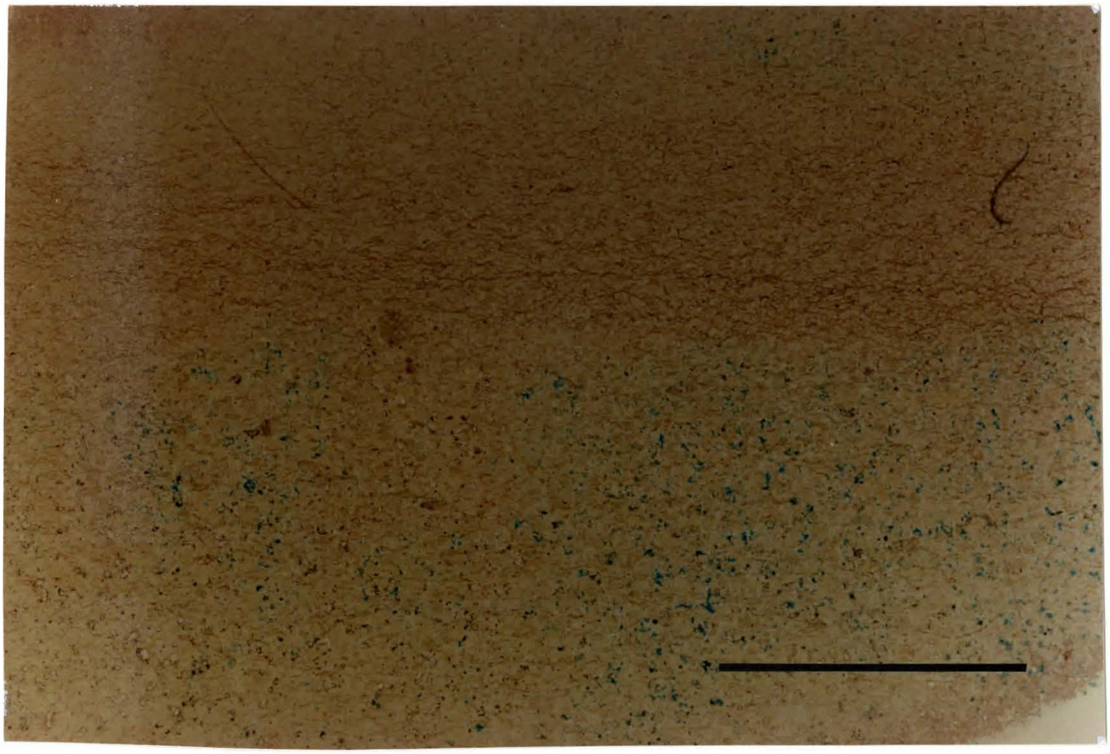

Figure 2 Close-up photographs of stylolite morphologies as seen in thin section. 2a) Regular sutured morphology. The stylolite resembles a near-rectiplanar digitate surface. 2b) Irregular sutured morphology. The stylolite resembles an irregular digitate waveform. Scale bar = 1 cm.

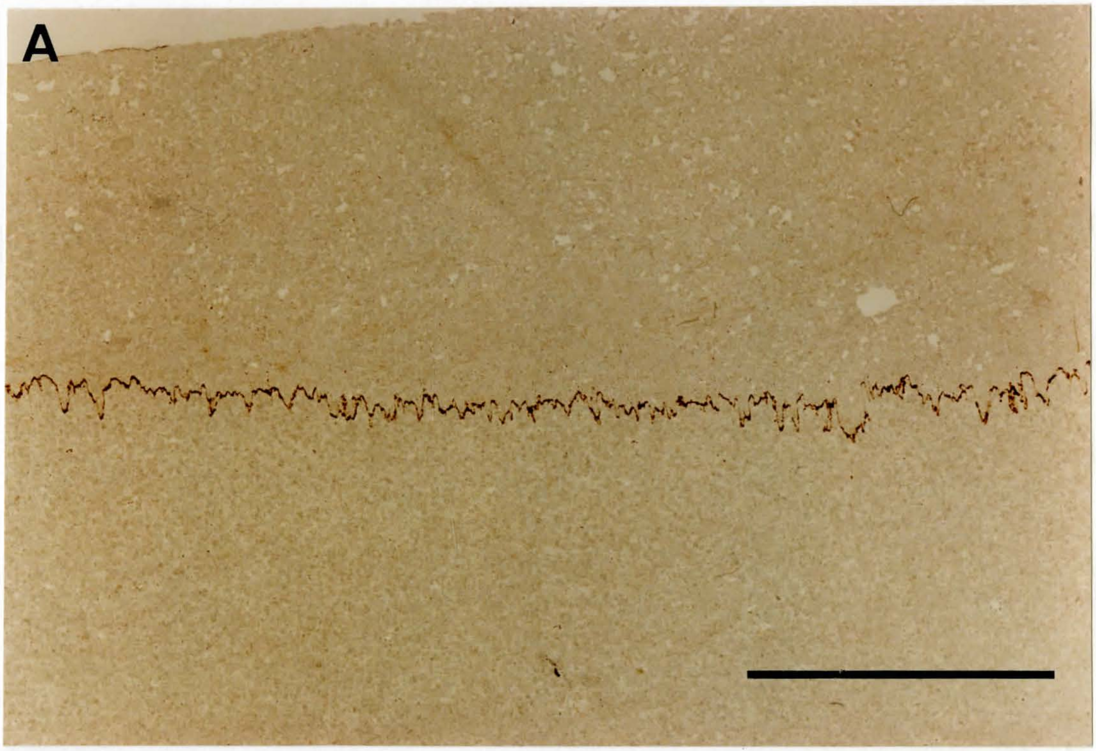
A

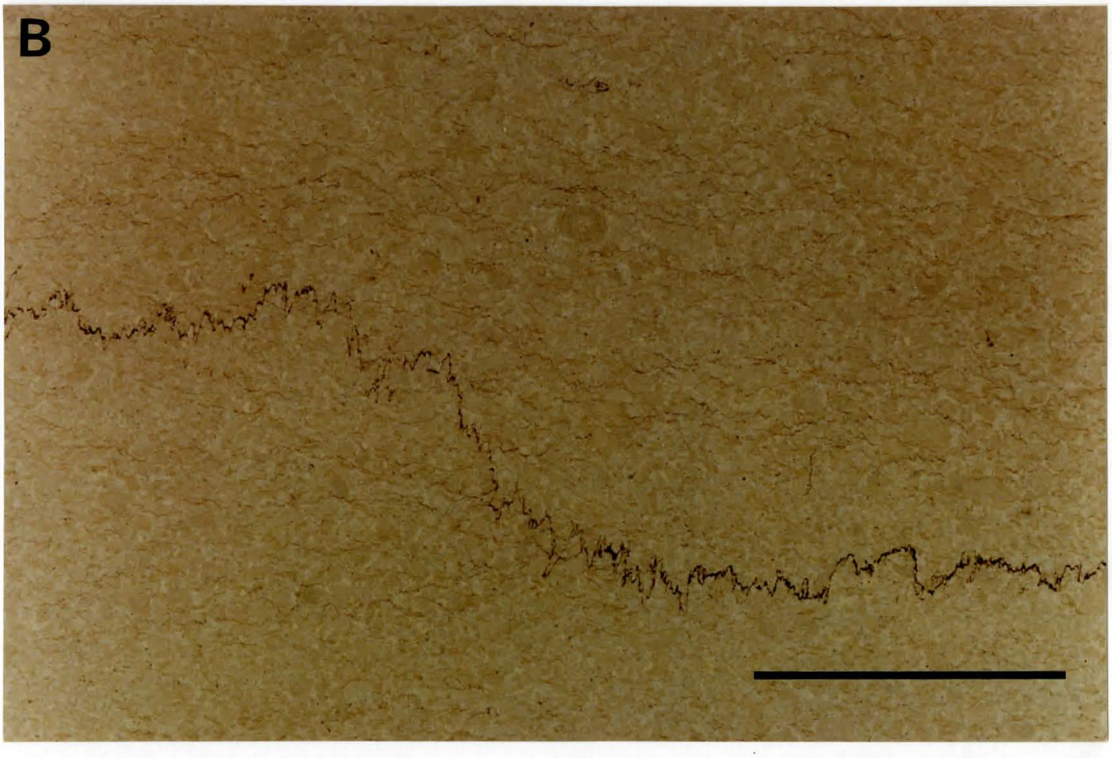
B

iv) <u>Amalgamated seams</u> - usually are regular or irregular sutured seams that resemble an anastamosing network of seams (Figure 3). The amplitude of the sutured seam is usually less than 1 millimetre. The zone in which these seams occur is variable, though usually less than 1 centimetre thick.

v) <u>Undulatory non-sutured</u> - a low frequency, gentle, undulatory accumulation (<2 millimetres thick) of black insoluble material of very low amplitude (Figure 4). Amplitude rarely exceeds 1 centimetre.

vi) <u>Bifurcating lateral tips</u> - resembles a wispy horsetail at the terminus of a solution seam (Figure 5). These have been recognized by Mossop (1972).

Of these morphological types, some are frequently found in association with one another. The following combinations have been observed:

a) Bifurcating lateral tips, as an inherent part of sutured stylolites.

b) Microswarms found in a form resembling an anastamosing microstylolite network, usually with a sutured stylolite.

Figure 3 Close-up photograph of amalgamated stylolite morphology as seen in thin section. Visible are stylolites that have merged together to form one seam which represents the net thickness of all seams. Scale bar = 1 cm.

15

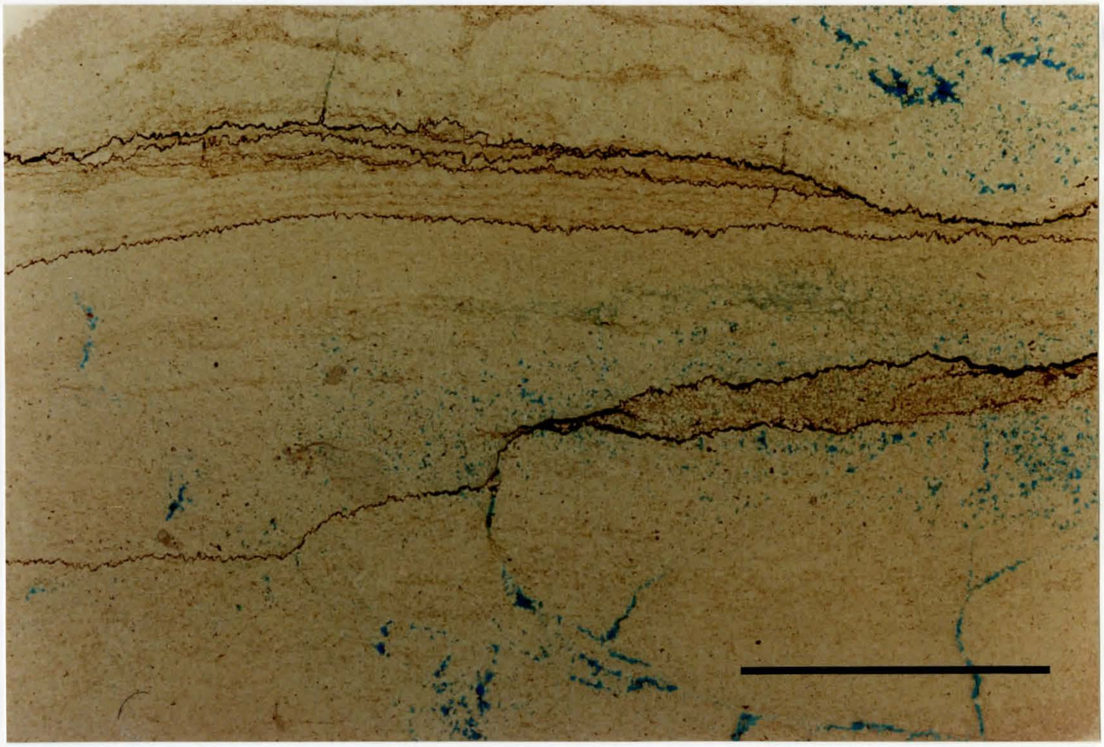

Figure 4 Close-up photograph of undulatory non-sutured stylolite morphology as seen in thin section. The undulatory seam is extremely thick relative to other sutured seams seen elsewhere in the photograph. The undulatory nature is not well shown due to the low frequency and amplitude of the overall waveform. Scale bar = 1 cm.

16

Figure 5 Close-up photograph of stylolite terminations as seen in thin section. Both sutured stylolites shown in the photograph bifurcate at their tips into what resemble wispy horsetails made up of microstylolites. These, in turn, gradually fade away into the host dolomite. Scale bar = 1 cm.

17

c) Sutured stylolites seem as branches of other sutured seams, undulatory non-sutured seams, or sections of seams.

2.3 MICROMORPHOLOGY

Pressure solution features were found in all thin sections studied, even those without stylolites. Over seventy thin sections have been looked at; 60% of these are from 4 metres of discontinuous section, the remaining 40% come from assorted samples that were chosen for selected features. The observations made and the data collected are presented here in order from crystal scale through to stylolite scale. Data are summarized and presented in Tables 1 and 2.

2.3.1 CRYSTAL CONTACTS

Crystal-to-crystal contacts are of an irregular sutured form (Figure 6). Interpenetration depths of adjacent dolomite crystals vary, ranging from less than 5 microns up to 60 microns. Even within one contact the degree of suturing (interpenetration) may be variable. Extremely low interpenetration depths may not always be the result of solution, but may be a primary artifact of crystal growth (xenotopic texture).

TABLE 1: GEOMETRIC PARAMETERS OF CRYSTAL CONTACTS AND STYLOLITES - LOCKPORT FORMATION

(all measurements in microns)

		Grain Contacts		Microstylolites						Stylolites				Seam Thickness			
	Degree of	Interpenetration Depth		Wavelength		Amplitude		Length		Wavelength		Amplitude		Microstylolites		Stylolites	
Sample	Pressure Solution	Max	Min	Max	Min	Max	Min	Max	Min	Max	Min	Max	Min	Max	Min	Max	Min
1.2	sutured seam and 2 microswarms	20	5	80	10	30	3	5000	200	220	60	140	20	5	2	15	5
1.3	not visible	60	5	40	--	20	--	450	---	---	---	---	--	3	1	--	--
1.4	incipient seam	10	3	40	10	25	4	3500	250	60	20	30	8	5	2	8	2
1.5	sutured seam	20	5	60	15	25	3	1300	200	300	100	125	20	5	1	60	10
	incipient seam									50	60	100	20			25	5
1.6	incipient seam	20	5	80	20	25	5	2500	200	80	40	40	10	5	2	25	7
1.7a	incipient seam and microswarm	15	5	80	15	20	3	2500	150	200	40	60	20	5	2	20	5
1.7b	propagating tip	20	5	60	30	20	5	1500	260	475	100	200	40	5	2	25	5.
1.7c	sutured stylolite with microswarm	40	5	100	15	30	5	1500	100	600	140	300	40	15	3	30	10
1.8	not visible	10	3	50	--	15	--	12000	---	---	---	---	--	--	--	--	--
1.9	sutured stylolite with microswarm and indiv. swarm	15	2	100	30	40	10	2500	80	350	50	200	20	6	1	30	2
2.1	anastomosed	15	3	--	--	--	--	----	---	450	150	250	20	--	--	40	5
2.2	poorly defined microstylolites	20	3	60	--	16	--	4500	120	---	---	---	--	5	1	--	--
2.3	sutured seams with microstylolites	20	5	60	30	20	10	7500	100	140	30	60	10	10	2	20	4

TABLE 1: GEOMETRIC PARAMETERS OF CRYSTAL CONTACTS AND STYLOLITES - LOCKPORT FORMATION (cont'd)

(all measurements in microns)

		Grain Contacts		Microstylolites						Stylolites				Seam Thickness			
	Degree of	Interpenetration Depth		Wavelength		Amplitude		Length		Wavelength		Amplitude		Microstylolites		Stylolites	
Sample	Pressure Solution	Max	Min	Max	Min	Max	Min	Max	Min	Max	Min	Max	Min	Max	Min	Max	Min
2.4	anastomosed seams	20	3	50	30	20	10	3000	200	550	60	200	30	8	3	100	10
2.5a	microswarm	10	3	160	20	40	5	4500	160	---	---	---	--	5	2	--	--
2.5b	poorly defined microswarm	40	3	100	35	40	8	3000	200	---	---	---	--	10	3	--	--
2.6	anastomosed sutured with microswarm	40	5	80	15	30	4	2250	200	350	80	200	30	8	1	70	10
2.7	sutured seam with microswarm and indiv. swarm	20	5	65	20	15	5	3500	125	360	100	120	30	10	2	60	10
2.9	sutured stylolite with microstylolites	20	4	80	15	30	5	3000	220	400	70	150	20	15	3	70	15
2.10	not visible	30	3	35	50	15	10	1000	150	---	---	---	--	4	1	--	--
2.11	not visible	30	2	100	30	40	8	1500	160	---	---	---	--	5	1	--	--
2.12	microswarm	20	5	140	25	40	10	5000	200	---	---	---	--	8	2	--	--
2.13	undulatory non-sutured and sutured stylolite	25	4	120	30	40	5	2250	260	550	8	120	0	6	2	100	40

-- not measurable

TABLE 2: GEOMETRIC PARAMETERS RELATIVE TO STYLOLITE GROWTH STAGES–LOCKPORT FORMATION

Sample	Degree of Pressure Solution	Classification	Maximum Wavelength	Maximum Amplitude	Seam Thickness	
					Max	Min
1.4	Incipient	Early Adol.	60 micron	30 micron	8 micron	2 micron
1.6	Incipient	" "	80 "	40 "	25 "	7 "
1.7a	Incipient	" "	200 "	60 "	20 "	5 "
1.5	Incipient	" "	250 "	100 "	25 "	5 "
2.3	Sutured with microswarm	Adolescent	140 "	60 "	20 "	4 "
2.7	Sutured with microswarm	" "	360 "	160 "	60 "	10 "
2.9	Sutured with microswarm	" "	400 "	150 "	70 "	15 "
1.7c	Well sutured with microswarm	Late Adol.	600 "	300 "	30 "	10 "
1.2	Sutured	Adult	220 "	140 "	15 "	5 "
2.6	Anastomosed Sutured	" "	350 "	200 "	70 "	10 "
2.1	Anastomosed Sutured	" "	450 "	250 "	40 "	5 "
2.4	Anastomosed Sutured	" "	550 "	200 "	100 "	10 "
2.13	Undulatory Non-sutured	" "	550 "	120 "	100 "	40 "
1.9	Lateral tip	Propagating	350 "	200 "	30 "	2 "
1.7b	Lateral tip	" "	475 "	200 "	25 "	5 "

Figure 6 Photomicrograph of an interstylolitic region showing penetrative contacts of dolomite crystals. Contacts show very little insoluble material between crystals. Polarized light. Magnification 158x. Scale bar = 50 microns.

21

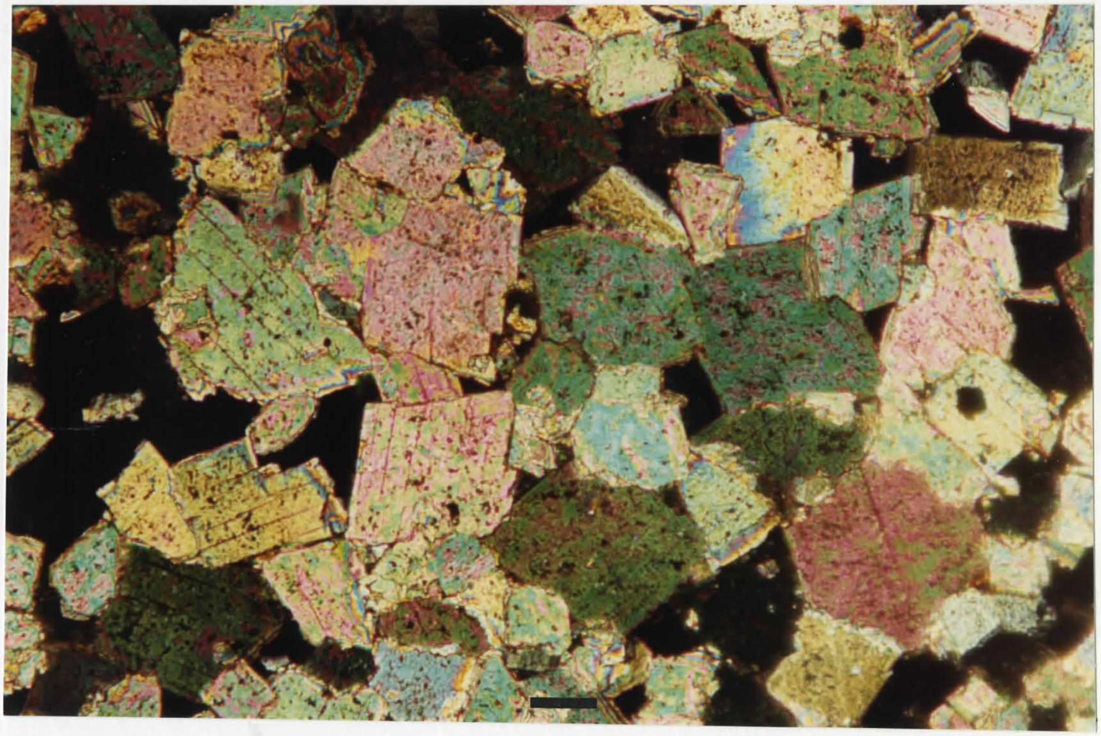

Even in thin sections that show no visible pressure solution features, crystal contacts are penetrative. The distribution of these contacts is patchy, but extends throughout the thin section. These two observations suggest that pressure solution was pervasive throughout the rock body.

Penetrative crystal contacts occur normal to or at angles to bedding, and not all contacts are penetrative. Some are essentially straight. Recognizing that penetrative contacts are patchily distributed, yet pervasive throughout all samples, and that straight and non-penetrative contacts do occur, it is suggested that penetrative contacts are the result of differential solubility at a crystal scale, and that straight contacts are the result of equal solubilities at the same scale.

There appears to be no discernible increase in the interpenetration depth as one proceeds from background to solution seam in any one thin section.

2.3.2 MICROSTYLOLITES

The microstylolites observed in thin section are predominantly irregularly sutured, though some may be undulatory or well-sutured. Microstylolites are found in several modes of occurrence. These are:

a) <u>Individual microstylolites</u> - those not associated with any other pressure solution feature besides interpenetrative crystal contacts (Figure 7).

b) <u>Microswarms</u> - those that occur as multiple individual seams or as an anastomosing network. The boundaries of a microswarm may be sharp or diffuse (Figure 8a).

c) <u>Microswarms associated with solution seams</u> - microstylolites that wholly or partially envelop a stylolite, and those that occur at the bifurcating lateral tip of a solution seam (Figure 5,8b).

d) <u>Straggler microstylolites</u> - those that occur associated with a stylolite, yet their numbers are so few that to call them a microswarm is misleading (Figure 9).

Lengths of microstylolites are variable, ranging from 100 to 7500 microns. The average length is approximately 3000 microns. Longer microstylolites commonly occur in samples that contain stylolites.

The amplitude and wave length of microstylolites is also variable, ranging from less than 5 to 40 microns amplitude, and 10 to 160 microns wavelength. Unlike the length, higher values of amplitude and wavelength most

Figure 7 Photomicrograph of an individual microstylolite that occurs in the presence of penetrative crystal contacts. Other microstylolites and stylolites are absent in the immediate vicinity. Plane polarized light. Magnification 40x. Scale bar = 200 microns.

24

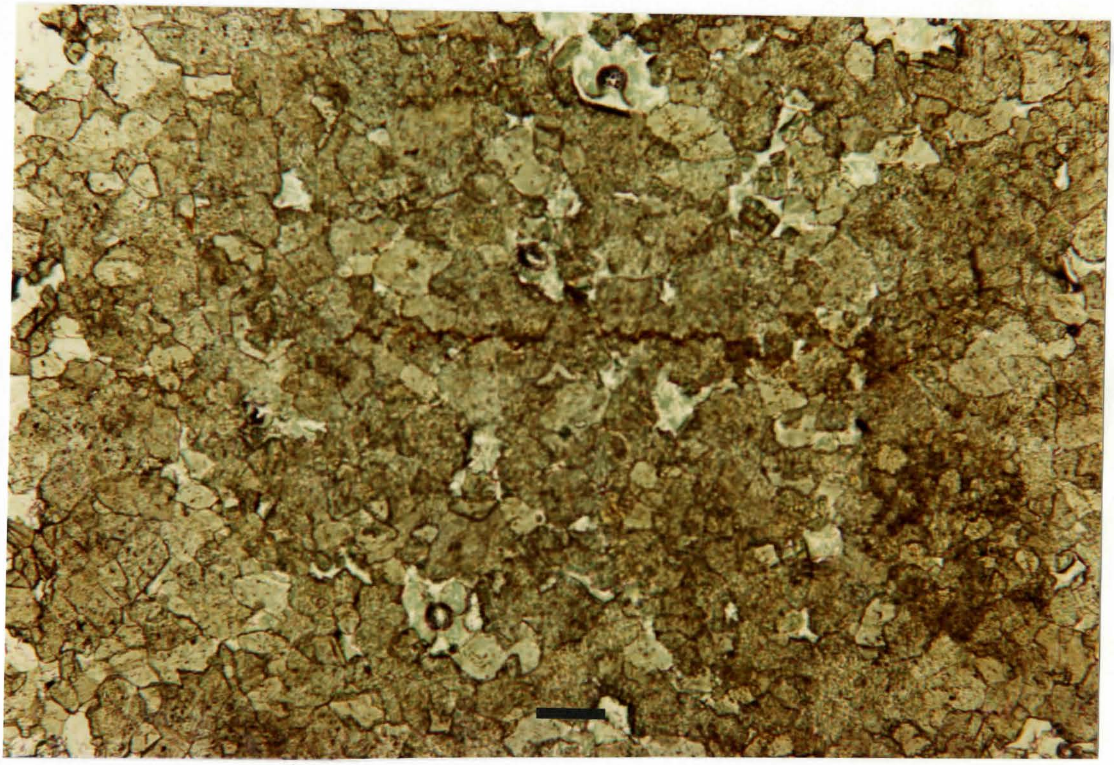

Figure 8 Photomicrographs of microstylolite occurrences. 8a) Microstylolites as seen in a microswarm that display singular and anastomosed network characteristics. 8b) Microstylolites as seen in a microswarm associated with a stylolite. The stylolite is enveloped by the microstylolites. Plane polarized light. Magnification 40x. Scale bar = 200 microns.

25

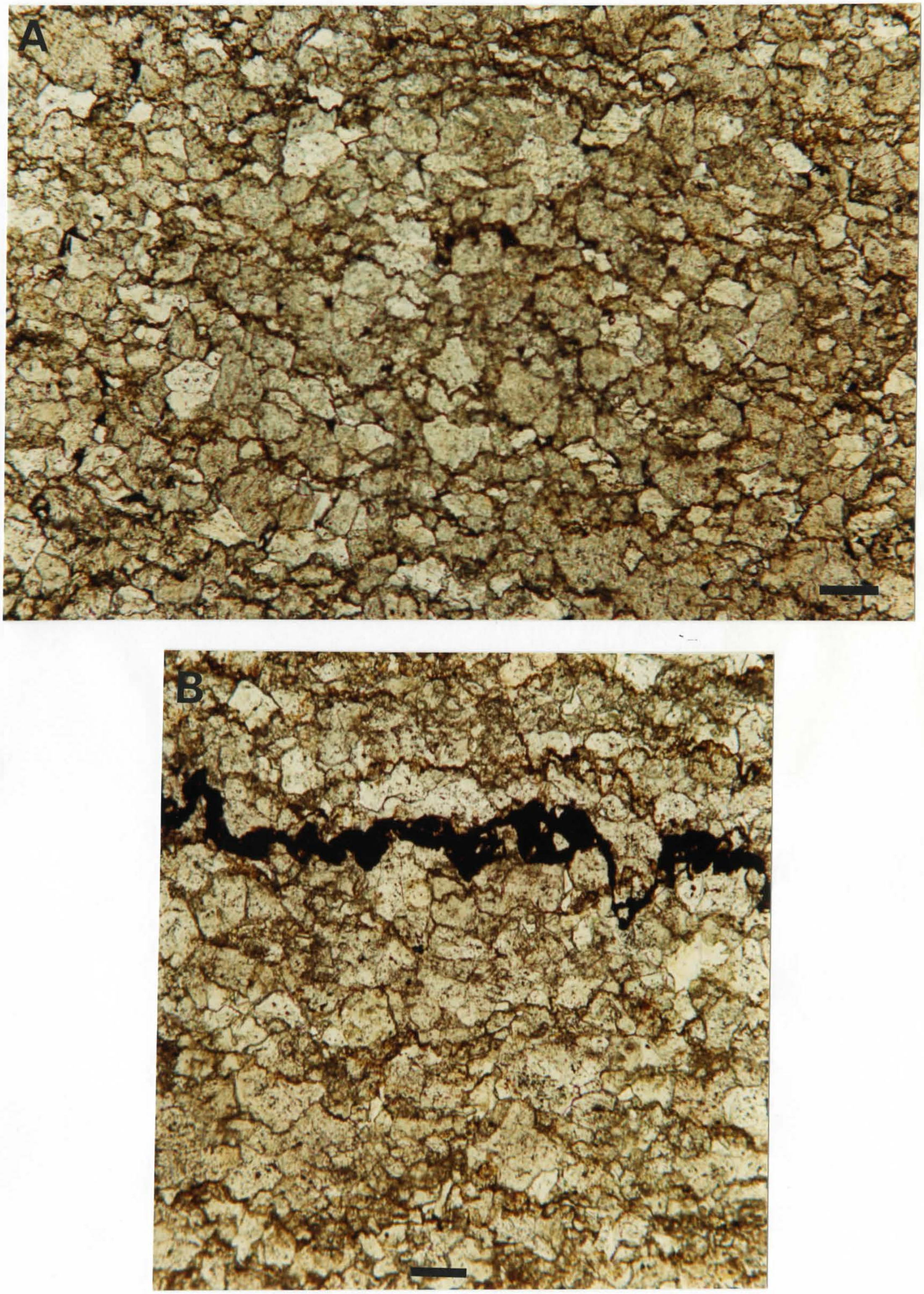

Figure 9 Photomicrograph of a straggler microstylolite found adjacent to a stylolite. Stylolite suture can be seen in top right corner of photo. Plane polarized light. Magnification 40x. Scale bar = 200 microns.

26

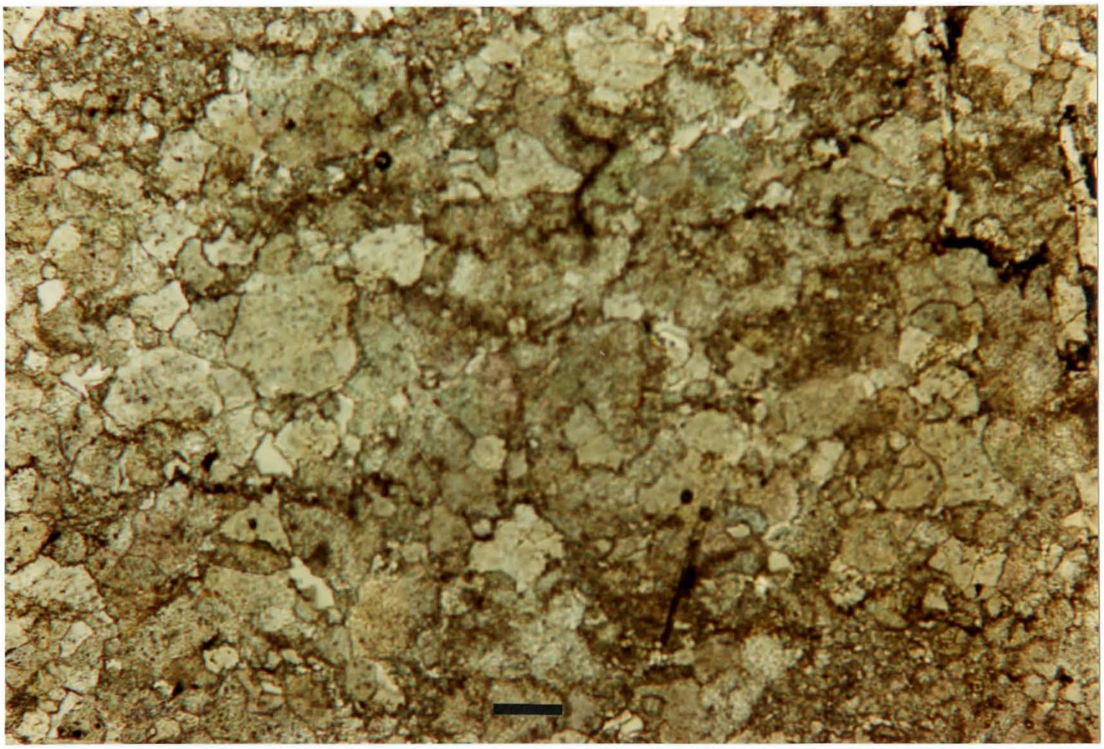

frequently occur in samples that contain microswarms, but are devoid of stylolites. Microstylolite thickness is commonly from 1 to 5 microns, up to 15 microns. These geometric parameters may be variable within and between individual seams.

2.3.3 STYLOLITES

As noted earlier, stylolites occur in five morphological styles and combinations thereof. In thin section, morphological traits are not as critical as the character of the seams themselves.

Stylolite character is variable, ranging from those that are incipient, those that are associated with microswarms, to those without microswarms. The sutured habit of stylolites is variable. Commonly they display simple to peaked and/or columnar suturing, though they may sometimes be undulatory. These are analagous to the sutured-seam and non-sutured seam classification of Wanless (1979).

Incipient stylolites (Figure 10) are not laterally extensive; usually they are only a couple of centimetres long. Frequently these seams are found in the midst of a microswarm or where a microswarm is lacking there are always microstylolites associated with the incipient seam. Incipient stylolites display an anastomosing character of the seam itself, and/or associated microstylolites. This

Figure 10 Photomicrograph of an incipient stylolite that occurs in a microswarm. Microstylolites and the stylolite display an anastomosing character. Plane polarized light. Magnification 16x. Scale bar = 2 mm.

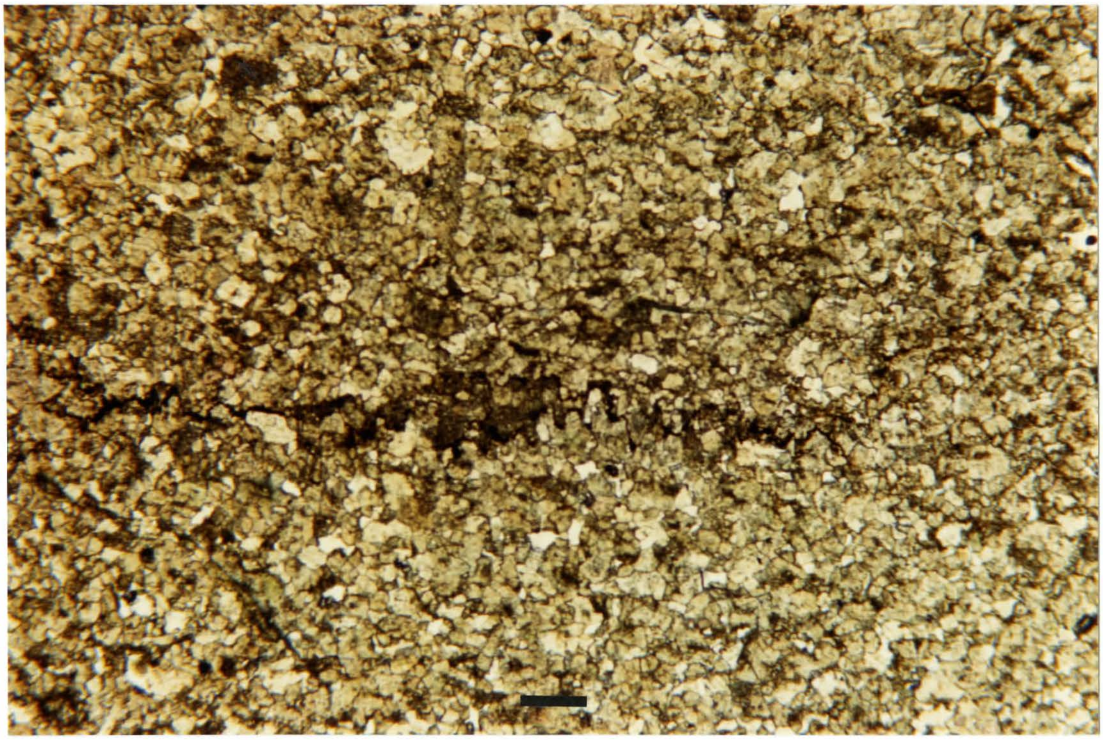

suggests amalgamation of microstylolites and/or stylolites (if there are multiple seams) through pressure-dissolution of interstitial dolomite.

Geometrically, incipient seams have amplitudes ranging from 30 to 100 microns, and wavelengths of 60 to 250 microns. Seam thickness is also variable, maximum values approach 25 microns, minimum values range from 2 to 7 microns. As with microstylolites, these geometric parameters are variable within and between individual seams.

Stylolites that are found associated with microswarms are always within the swarm (Figure 11). These stylolites appear to truncate microstylolites at the tips and along the limbs of sutures. This relationship is interpreted as the incorporation of microstylolites into the stylolite itself by dissolution of intervening carbonate. The microstylolites within the swarm may or may not display an anastamosing character. It is suggested here that the process of microstylolite incorporation is amalgamation through pressure-dissolution.

Stylolites with microswarms have amplitudes ranging from 60 to 150 microns. Wavelength values are variable from 140 to 400 microns. Maximum seam thickness ranges from 20 to 70 microns, minimum values are from 4 to 15 microns. Once again all these values are variable within and between individual seams.

Figure 11 Photomicrograph of a stylolite in a microswarm. The sutures of the stylolite truncate microstylolites at their tips and along their limbs suggestive of microstylolite incorporation through pressure-dissolution of intervening dolomite. Plane polarized light. Magnification 40x. Scale bar = 200 microns.

30

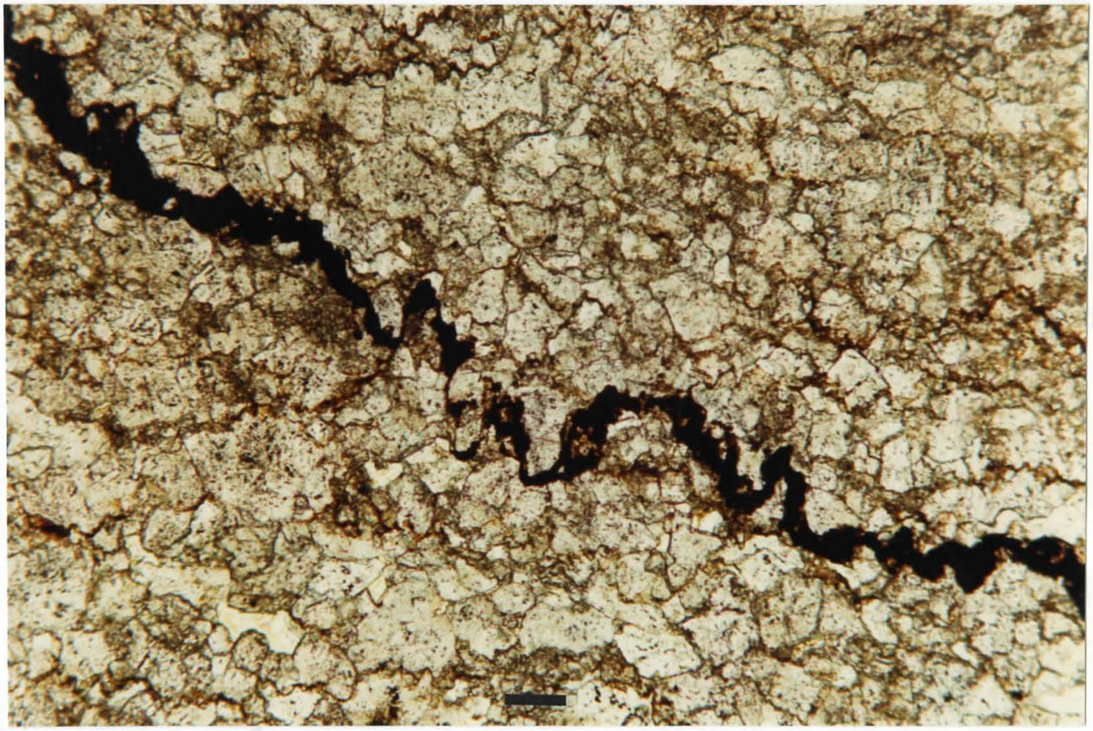

Stylolites that occur in the absence of associated microswarms may or may not have microstylolites nearby (Figure 12a,12b). If microstylolites do occur, they are the straggler variety. As above, these seams appear to be truncating microstylolites at their tips and along the limbs of the sutures by amalgamation.

Stylolites of this type of are also observed to merge with other seams that are proximal to them especially if the seams are irregular in their form (Figure 13). This habit of seam incorporation is recognized as amalgamation at the solution seam, not microstylolite scale.

The amplitude of these seams ranges from 120 to 250 microns. Wavelength values are from 220 to 550 microns. Maximum values of seam thickness vary from 15 to 100 microns, minimum values are from 5 to 40 microns. As before, these geometric parameters vary within and between individual seams.

2.3.4 STYLOLITE TERMINATIONS

Stylolites terminate by bifurcating outwards into a microswarm or several smaller solution seams (Figure 14). Both the microswarms and smaller solution seams converge upon the terminus of the seam itself. In the best of examples the convergence of microstylolites is symmetrical

Figure 12 Photomicrographs of stylolites that occur in the absence of microswarms. 12a) Sutured stylolite with some straggler microstylolites in the immediate vicinity. 12b) Sutured stylolite with no microstylolites in the immediate vicinity. Plane polarized light. Magnification 16x. Scale bar = 2 mm.

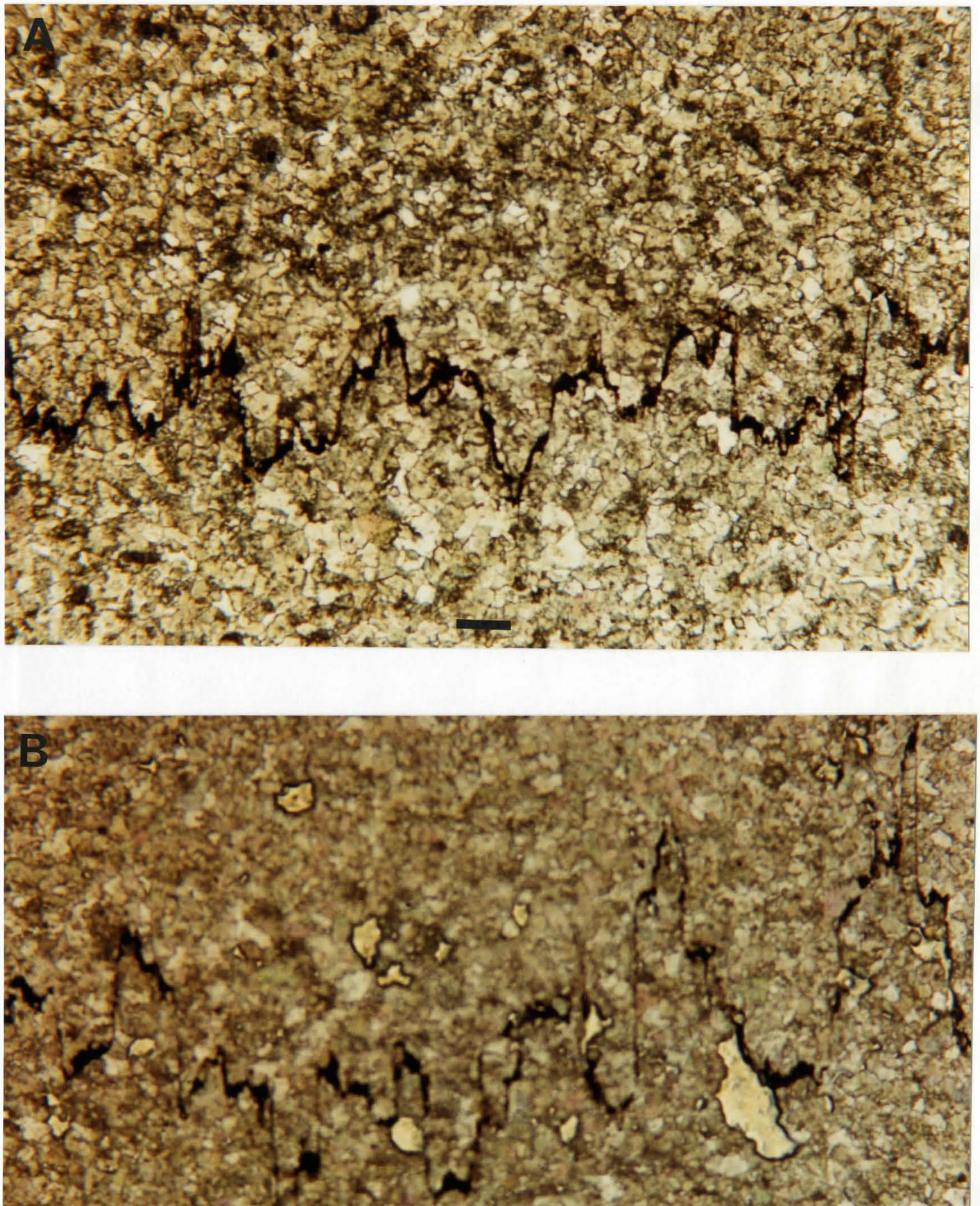
A
B

Figure 13 Photomicrograph of stylolites that have merged together along a portion of their length. The thickness of the merged section of the seam is the net thickness of all seams that have merged together. Plane polarized light. Magnification 16x. Scale bar = 2 mm.

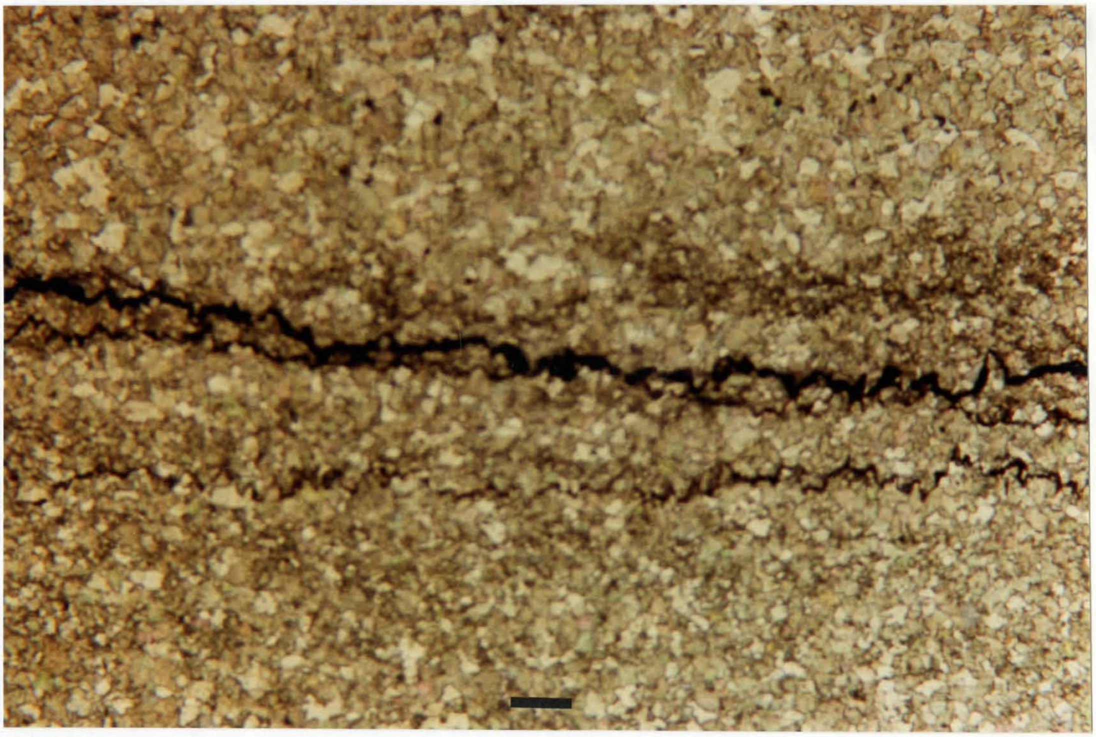

Figure 14 Close-up photograph of the lateral termination of a stylolite. The sutured seam bifurcates outward into a wispy horsetail-like array made up of smaller stylolites and microstylolites in a swarm. Scale bar = 1 cm.

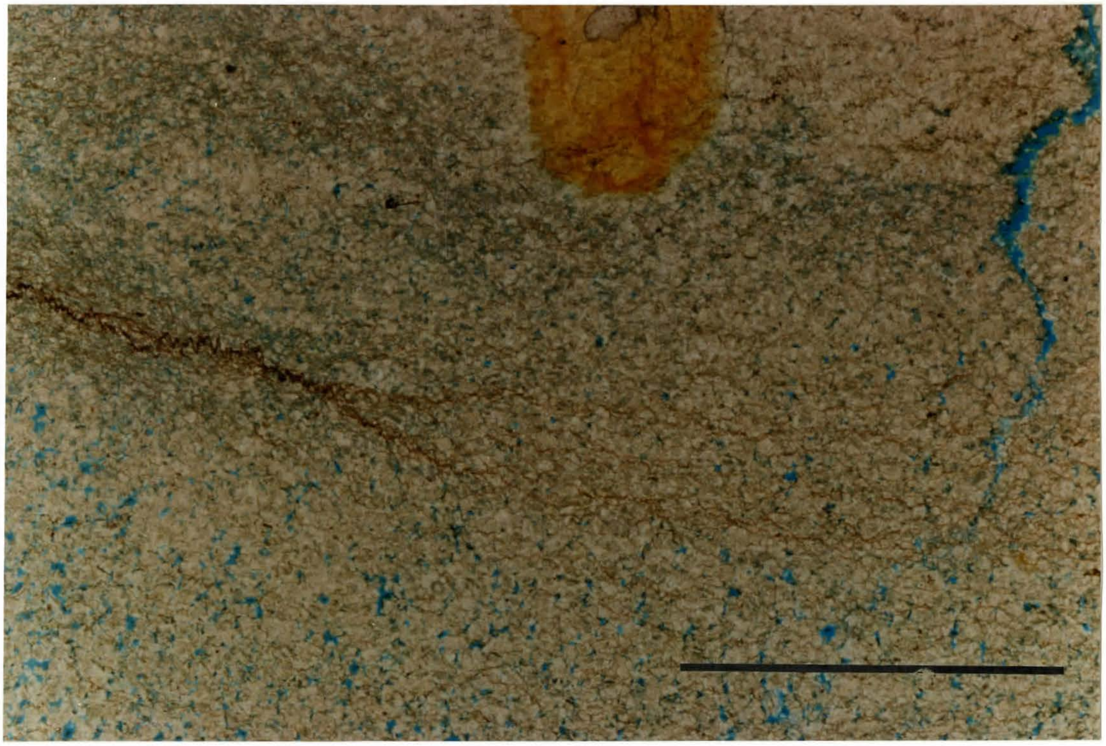

about the stylolite. Symmetry is lost in some of the poorer examples of seam terminations. For example, where abundant microstylolites are absent the seams still bifurcate into geometrically smaller seams that eventually die out laterally.

The terminations of incipient stylolites also bifurcate, though this may not be as easily recognized as it is in the more mature seams. Usually, it is seen as a stop to the anastomosing fabric of the incipient seam. It is suggested here that bifurcated stylolite terminations are actually the propagating lateral tip of the stylolite.

2.4 CRYSTAL SIZE ASSOCIATIONS

There is a relationship between microstylolite, stylolite occurrence and crystal size of the dolomite. To further examine this relationship the most obvious place to look is in a sample showing a not yet fully developed stylolite.

Such a sample was slabbed three times. Slab one contained an amalgamating seam in a microswarm, several centimetres long, and bifurcating at both ends. In slab two the microswarm dominated over the solution seam, and in slab three the microswarm was hardly visible, the stylolite gone. Six thin sections were made from each slab, all similarly oriented in same positions as their counterparts in the other slabs. The thin sections were examined for solution seam and/or microstylolite relationships to crystal size in the background and visible pressure solution zones.

Of the 18 thin sections studied the average composition was 85% coarse dolomite (50-300 microns) and 15% dolomicrite (<20 microns) for the background zone, (Table 3). Interpenetrative crystal contacts were found between coarse dolomite crystals and also at dolomicrite-coarse dolomite contacts. Microstylolite were most often found at dolomicrite-coarse dolomite contacts. The abundance of microstylolites in this background zone is commonly less than 5 in a field of view of 4.5 millimetres. Wherever insolubles were present between crystal contacts microstylolites were present.

In the pressure solution zone the average composition was 55% coarse dolomite and 45% dolomicrite (Table 3). Where the stylolite is best developed the average composition is reversed, being 55% dolomicrite and 45% coarse dolomite. Microstylolites are very abundant in this zone, approximately 40 in a field of view of 4.5 millimetres. Based upon these observations alone it seems reasonable to suggest that microstylolites develop in greater numbers were smaller crystal sizes dominate. Furthermore, stylolites develop in these zones through the amalgamation of abundant microstylolites.

TABLE 3: CRYSTAL SIZE PERCENTAGES-LOCKPORT FORMATION

	Background Zone		Pressure Solution Zone	
Sample	% cd	% dm	% cd	% dm
S1a	80	20	40	60
S1b	85	15	50	50
S1c	85	15	40	60
S1d	90	10	40	60
S1e	85	15	50	50
S1f	90	10	80	20
S2a	80	20	75	25
S2b	90	10	50	50
S2c	90	10	50	50
S2d	85	15	40	60
S2e	90	10	40	60
S2f	85	15	50	50
S3a	80	20	-	-
S3a	85	15	-	-
S3c	85	15	-	-
S3d	80	20	70	30
S3e	90	10	75	25
S3f	80	20	-	-

cd = coarse dolomite 50 - 300 microns

dm = dolomicrite <20 microns

\- = not visible

To further study this relationship 23 other thin sections were examined. In the majority of these the background crystal size is 50-300 microns, the remainder being 50-250 or 50-350 microns (Table 4). Twenty of these twenty-three thin sections contain microstylolites. Of these, seven have 20% or more dolomicrite associated with the microstylolites. Three of these seven also have a coarse dolomite component of less than 150 microns. Eight other thin sections show that the crystal size associated with the microstylolites is predominantly less than 150 microns. Several are even less than 50 microns. The remaining five thin sections show no noticeable difference between the background crystal size and that associated with microstylolites, or they have a minor component of dolomicrite.

Crystal sizes associated with stylolites show much the same trends as those associated with microstylolites. Fourteen of the twenty-three thin sections contain stylolites. Of these, ten have smaller crystal sizes associated with the stylolite than in the background (<150 microns). In five samples the crystal sizes are similar to those for microstylolites. The other five have coarser crystal sizes than those associated with microstylolites. In some there were no microstylolites to use for comparison. The remain-

TABLE 4; CRYSTAL SIZE DISTRIBUTIONS - LOCKPORT FORMATION

Sample	Degree of Pressure Solution	Background Crystal Size	Crystal Size Associated With Microstylolites	Crystal Size Associated With Stylolites
1.2	sutured seam and 2 swarms	50-250 micron	50-250 micron	50-250 micron
1.3	not visible	50-250 "	50-250 "	———
1.4	incipient seam	50-250 "	50-250 "	50-250 "
1.5	sutured seam incipient seam	50-250 "	50-250 " 20% dolomicrite	50-250 " minor dolomicrite
1.6	incipient seam	50-250 "	<150 micron	0 micron50-250 "
1.7a	incipient seam and microswarm	50-300 "	30-150 "	30-150 "
1.7b	propagating tip	50-350 "	<50 micron	<50 micron
1.7c	sutured stylolite with microswarm	50-300 "	<50 "	<100 "
1.8	not visible	50-300 "	<100 "	———
1.9	sutured seam with microswarm and individ. swarm	50-250 "	<150 " 40% dolomicrite	<150 " minor dolomicrite
2.1	anastomosed	50-300 "	———	<150 least developed <250 best developed
2.2	poorly defined microstylolites	50-300 "	<150 " 20% dolomicrite	———
2.3	sutured stylolites with microstylolites	50-300 "	<50 "	50-300 "
2.4	anastomosed stylolites	50-250 "	———	<150 "
2.5a	microswarm	50-300 "	60% dolomicrite 40% 50-250 micron	———

TABLE 4; CRYSTAL SIZE DISTRIBUTIONS - LOCKPORT FORMATION

(cont'd)

Sample	Degree of Pressure Solution	Background Crystal Size	Crystal Size Associated With Microstylolites	Crystal Size Associated With Stylolites
2.5b	poorly defined microswarm	50-300 "	<150 "	———
2.6	anastomosed sutured with microswarm	50-300 "	<150 " 25% dolomicrite	<150 " minor dolomicrite
2.7	sutured stylolite with microswarm and indiv. swarm	50-300 "	<150 "	<150 "
2.9	sutured stylolite with microstylolites	50-300 "	<150 "	<150 "
2.10	not visible	50-300 "	minor dolomicrite	———
2.11	not visible	50-300 "	30% dolomicrite 50-300 "	———
2.12	microswarm	50-300 "	<150 " 20% dolomicrite	———
2.13	undulatory non-sutured and sutured stylolite	50-300 "	———	50-300 "

ing four thin sections show no apparent difference between background and pressure solution zone crystal sizes.

From these results and those from the slabbed sections, two generalizations can be made about the occurrence of microstylolites and stylolites relative to crystal size variations.

First, a predominance of smaller crystal sizes are associated with the occurrence of microstylolites. However, microstylolites do occur where there are no detectable changes in crystal sizes relative to the background. It may be that these seams are the result of factors other than crystal size control (e.g intercrystalline clays/organics, point contacts of adjacent crystals, solubility differences, fabric anisotropy).

Second, smaller crystal sizes are also associated with the occurrence of stylolites, though the crystals may be somewhat larger than those associated with microstylolites. However, some seams do occur where there is no detectable change in crystal size. This may be an artifact of other less obvious factors, or it may just be that the smaller sizes have been reduced in numbers as a result of amalgamation processes.

The key point is that microstylolites and stylolites generally do occur where crystal sizes are smaller than those in the background.

2.5 STYLOLITE DEVELOPMENT:THE AMALGAMATION MECHANISM

Interpretation of the morphological styles and observations made in thin section has lead to the development of a "model" for stylolite formation.

Two simple assumptions have been made based upon the various observations. These are:

a) that the thickness of the seam (microstylolite or stylolite) is an indicator of its maturity.

b) that increasing amplitude is associated with increasing development of stylolites i.e. the more mature the seam is, the greater the amplitude becomes, all other things being equal.

Based upon the observations of where a stylolite occurs, it appears that the seam itself need not originate at a natural lithological parting. The focus of this study is on those that develop within a "bed". The development of a solution seam is an evolutionary process. It can be subdivided into three stages. Stage one corresponds to the birth of microstylolites. Stage two is the amalgamation of these "neonatal" microstylolites resulting in "adolescent" stylolites. The last stage is the maturing of "adolescent" seams into full-fledged "adult" seams.

The numerical data cited in this section may be found in Table 1 and 2.

2.5.1 INITIAL RESPONSE TO PRESSURE SOLUTION

Several factors govern the initiation of pressure solution in rock body. These are:

a) reaching the critical magnitude of directed stress created by overburden or tectonism.

b) the correct nature of the pore fluid (water, gas, oil).

c) adequate porosity and permeability so that the pore fluid may invade the rock body.

Once these factors are met, the initial response of the rock body is seen as pervasive pressure solution. The result of pervasive pressure solution is dissolution at crystal contacts throughout the rock body. As observed in all thin sections, crystal contacts may be sutured or non-sutured. The patchy yet pervasive distribution of these suggests that not all crystals respond to pressure solution, but that the majority do.

At the onset of pressure solution, crystal-crystal penetration and the amount of material removed was minimal. With time, penetration and material removal increases, and continues increasing until pressure solution ceases. In thin section the maximum crystal-crystal penetration depth measured was 60 microns. This is significant considering that the maximum crystal size approaches 350 microns in some samples. Penetration to this depth suggests a maximum 16% of material was lost due to pervasive pressure solution.

To further substantiate the suggestion that pressure solution is pervasive at this level is the observation that there is no discernible increase in suturing of crystals as one approaches a stylolite. In other words, pervasive pressure solution was going on before, as well as during the formation of stylolites and did not increase near stylolite zones. The seams just overprint the pervasive solution signature.

2.5.2 MICROSTYLOLITE DEVELOPMENT-NEONATAL STAGE

The mechanism by which microstylolites are "born" is essentially a very simple one. Once pressure solution is operative in the rock, the initial result is pressure-solved crystal contacts. With time and continued dissolution the contacts are enlarged. Microstylolite development is seen as the extension of pressure-solved contacts beyond crystal pairs due to the enlargement of the contact area (Figure 15). From the crystal size/microstylolite relationships, microstylolites are more abundant in the finer dolomite where the smaller crystal size easily permits lateral propagation of a continuous contact. Extension may also be brought about by the vertical alignment of two or more

Figure 15 Schematic diagrams of microstylolite formation. 15a) Simplest case microstylolite formation. Initiation of pressure solution results in material being lost at crystal contacts. Continued pressure solution results in extension of contacts beyond crystal pairs to form a continuous pressure-solved surface. 15b) Analogous to above, but with the addition of an "organic"layer between crystal contacts. Initiation and continuation of pressure solution results in the formation of a microstylolite about the organic layer. 15c) Analagous to above two scenarios. Microstylolite formation in a dolostone. Organic layer and smaller crystal sizes are favoured sites for microstylolite formation.

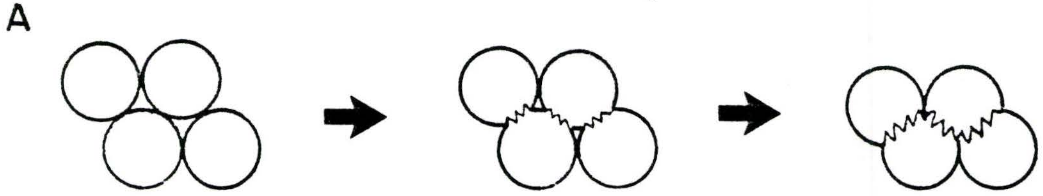
A

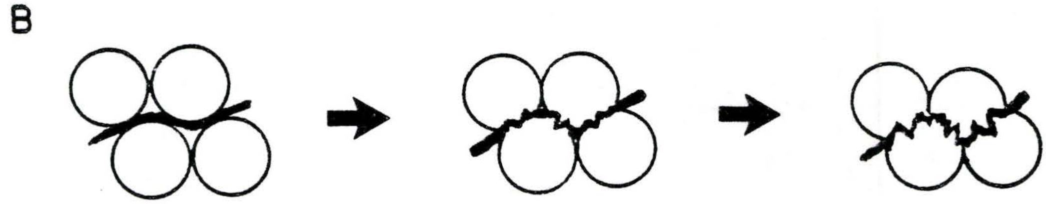
B

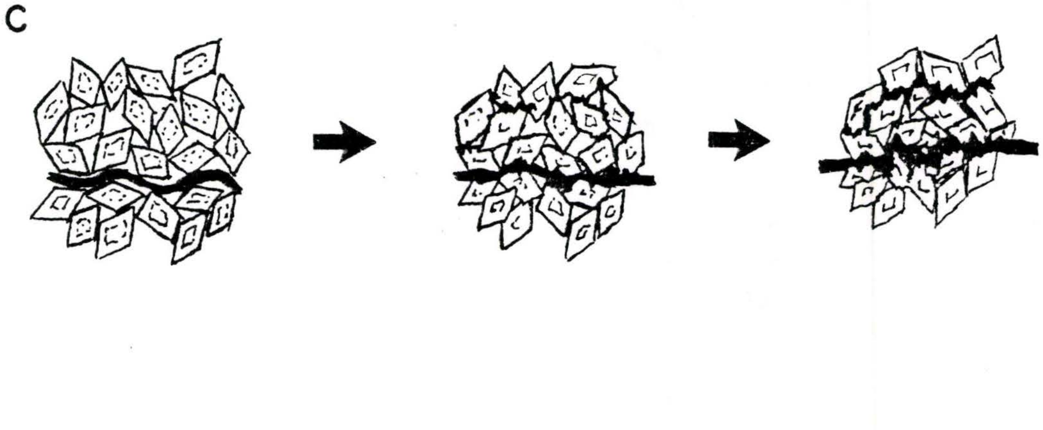
C

crystal contacts. Through continued solution the vertical separation of such contacts may be decreased.

Insoluble material (clay/organics) occurrence is a major factor that determines where and how many microstylolites occur. The reasoning for this is based upon petrological and experimental evidence. Microstylolites are believed to develop by the extension of contacts beyond crystal pairs suggesting that the insoluble material is in part a net accumulation of material released by pressure solution between crystal contacts. But, crystal contacts seen have very little accumulated material between them; not enough to account for 1 to 15 microns thickness of accumulated insolubles in microstylolites, except through large volumes of material lost. This suggests that the majority of insoluble material accumulated in microstylolites is originally of a primary sedimentary origin.

In the compaction experiments of Shinn et al. (1977) and Shinn and Robbin (1983) features were produced that resemble microstylolites and incipient stylolites found throughout the geologic record, and also in these samples. These are wavy organic "stylolite-like" layers made up of squashed blades and roots of seagrass and other plant materials indigenous to marine mud sediments.

Similar to Pratt (1982) and Shinn and Robbin (1983) it is believed that these organic stringers initiate pressure solution with increasing depth of burial and result ultimately in accumulation of clays and other insolubles contained in the rock. Pressure-dissolution, once initiated, would occur along these organic layers and at grain-to-grain contacts.

An implication of these experiments is that early cementation (marine, vadose, or phreatic) would prohibit the formation of these stringers, and hence no pressure solution. These stylolite-like layers are the result of soft-sediment compaction and would not form if the sediment was cemented earlier, at a shallower depth.

Thus, the mechanism of microstylolite development is the extension of pressure solution contacts beyond crystal pairs but where they occur is mainly a factor of the occurrence of primary organic material in the original sediment. Very little insoluble material between crystal contacts suggests that either large volumes of material have to be dissolved to account for the accumulated thicknesses of insolubles in microstylolites, or that microstylolite occurrence is determined by organic stringers of mechanical compaction origin. The latter is favored for two reasons. First, there is no evidence of large amounts of volume loss associated with microstylolites. Second, primary concentrations of organic materials would easily explain the existence of microswarms.

To summarize, smaller crystal sizes easily permit the extension of pressure solution contacts beyond crystal pairs and primary organic material concentrations are the main determinant as to where the majority of microstylolites occur by this mechanism.

2.5.3 AMALGAMATION-ADOLESCENT STAGE

Stylolites form by the amalgamation of microstylolites (in a swarm) through the dissolution of interstitial dolomite. Removal of dolomite by pressure solution along numerous microstylolite surfaces allows for the formation of a larger surface of dissolution, the stylolite. This period of growth marks a major accumulation of insoluble materials. Eventually, with continued pressure solution, all the microstylolites in a swarm will amalgamate to form a stylolite, such that the insoluble material of the stylolite is the net of all the microstylolites that amalgamated (Figure 16).

Incipient stylolites mark the formation of a stylolite early in its amalgamation history. They are found in microswarms and can be seen to truncate microstylolites along their length or show an anastomosed texture with microstylolites. These textures represent the amalgamation mechanism "frozen" into the rock and not two episodes of stylolitization as suggested by Mossop (1972). Had pressure

Figure 16 Schematic diagram of stylolite formation by microstylolite amalgamation through pressure-dissolution of intervening dolomite. Stage I: microstylolites in a swarm. Stage II: pressure-dissolution of intervening dolomite results in anastomosed network of microstylolites. Stage III: continued removal of dolomite results in microstylolites amalgamating to form an incipient stylolite (early adolescent stage). Stage IV: continued amalgamation results in a further developed stylolite in a microswarm (middle adolescent stage) with microstylolites truncated at sutures and along limbs. Stage V: amalgamation process is near complete, the microswarm is nearly gone due to incorporation of microstylolites into growing stylolite. Microstylolites are seen truncated as before. Stylolite thickness represents accumulation of all microstylolites amalgamated (late adolescent stage).

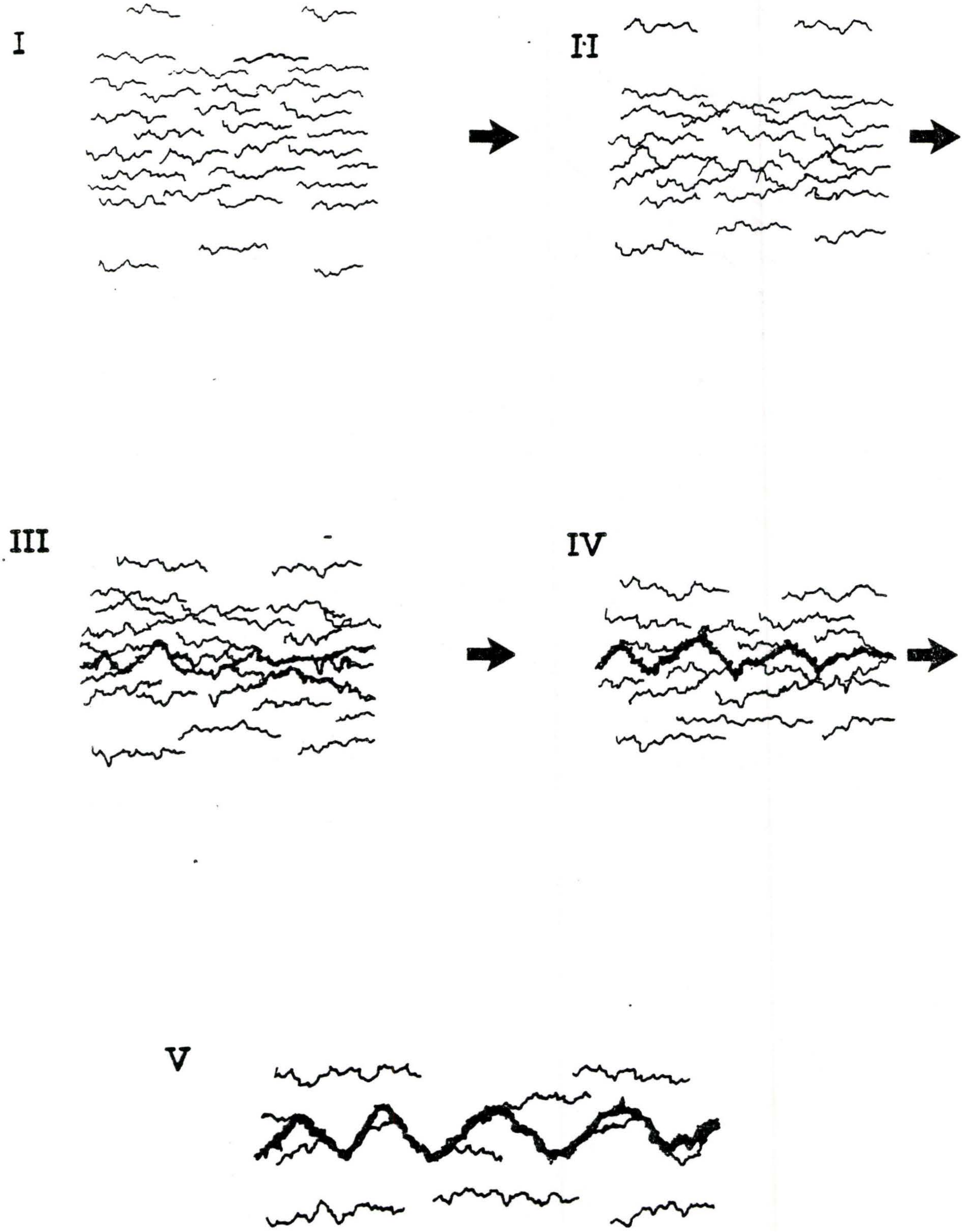
I
I·I
III
IV
V

solution continued for a longer period of time, these truncated and anastomosed microstylolites would have been incorporated into the stylolite.

Stylolites that occur in microswarms represent a stage of formation later in the amalgamation history, beyond the incipient stage. These stylolites are further developed because more microstylolites have amalgamated to form them. They display similar amalgamation textures as incipient stylolites do and only differ in size. Their maximum wavelengths, amplitudes and thicknesses (wavelength=140 to 400 microns, amplitude=60 to 150 microns, thickness=20 to 70 microns) are greater than those for incipient stylolites (wavelength=60 to 250 microns, amplitude=30 to 100 microns, thickness=8 to 25 microns). These, in turn, are larger than microstylolites (wavelength=40 to 160 microns, amplitude=15 to 40 microns, thickness=1 to 15 microns). These progressively greater thickness are in agreement with the concept of evolutionary growth through amalgamation of microstylolites. The larger wavelengths and amplitudes need further explanation.

Amalgamation is analagous to the superposition of waveforms principle. A combination of constructive and destructive interference of two or more waveforms (microstylolites) results in a geometrically larger or smaller waveform. The geometry of the resultant waveform is a function of the phase relationship (in-phase or out-of-phase) of the amalgamating waveforms. See Figures 17 and 18.

The measurements cited for stylolites suggest that amalgamation of microstylolites was more constructive than destructive interference. Stylolites that are further developed than others are also larger in their geometry and thickness. Thus amalgamation microstylolites results in progressively larger and thicker stylolites with continued growth.

This stage of stylolite growth has been termed "adolescent" because these stylolites are experiencing a major period of growth that will end when the microswarm no longer exists. At this point, amalgamation basically ends, and stylolites grow in a different fashion.

2.5.4 STYLOLITE GROWTH-ADULT STAGE

An adolescent stylolite grows by the amalgamation of microstylolites in a swarm, through pressure solution of interstitial carbonate. This growth period results in a major accumulation of insoluble material. Conversely, the growth of the adult solution seam involves only a minor accumulation of insoluble seam material due to growth in a different fashion.

Figure 17 Superposition of waveforms principle. 17a) Represents perfect constructive interference. Superpositioning (addition) of two waveforms that are in-phase with one another results in a waveform of twice the amplitude and thickness. 17b) Represents perfect destructive interference. Superpositioning (addition) of two waveforms that are out of phase relative to one another results in cancellation, a waveform with no amplitude, but twice the thickness.

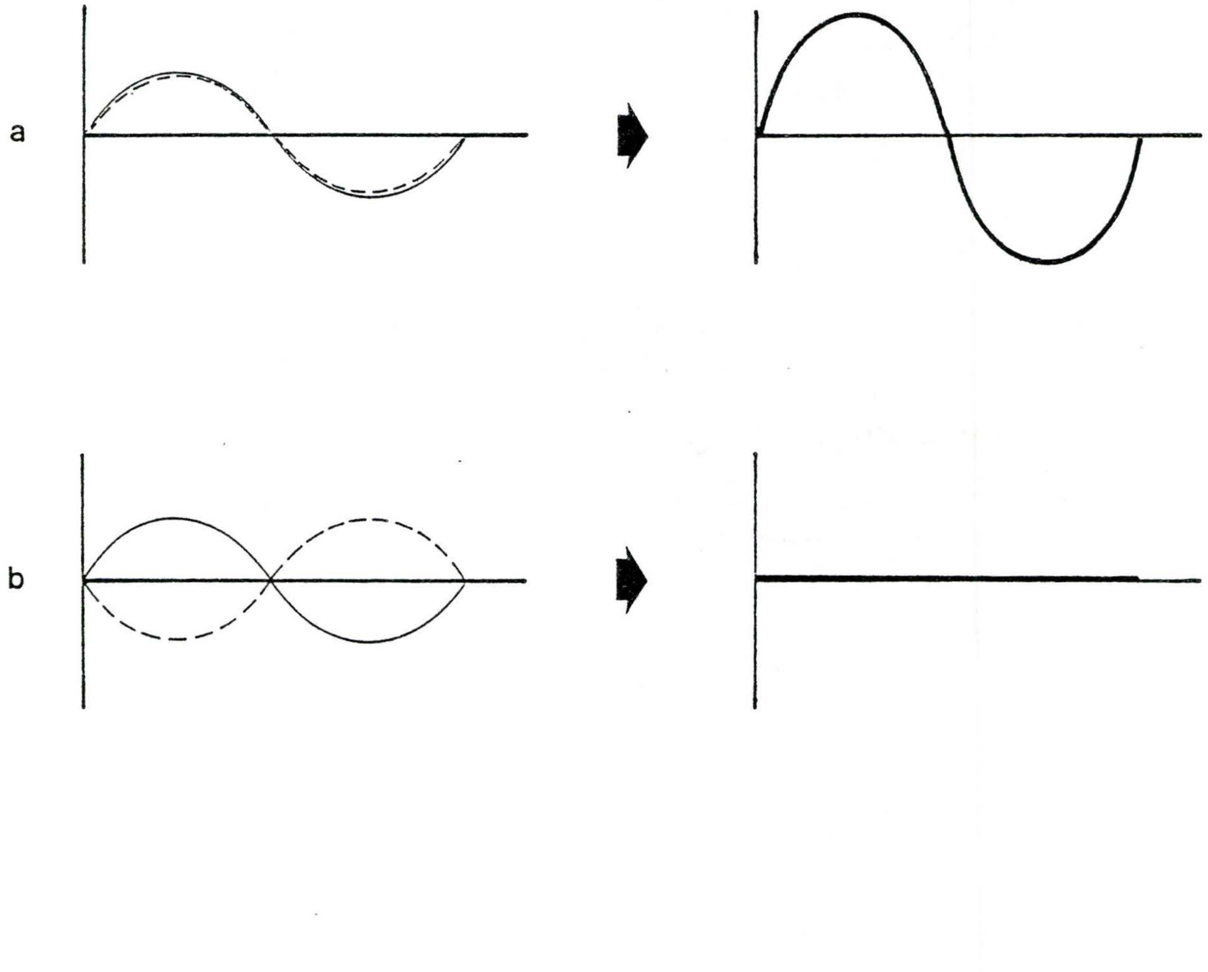
a
b

Figure 18 Schematic representation of microstylolite amalgamation via the superposition of waveforms principle. Two microstylolites merge together such that they become superimposed on top of one another (A). Through constructive and destructive interference they form a resultant seam that is thicker and of differing geometry (B). In turn, this seam merges with another, forming the one in (C) which is thicker and different again. Amalgamation of another microstylolite results in the stylolite in D. Through constructive and destructive interference, the resultant seam "grows", ever changing through these stages.

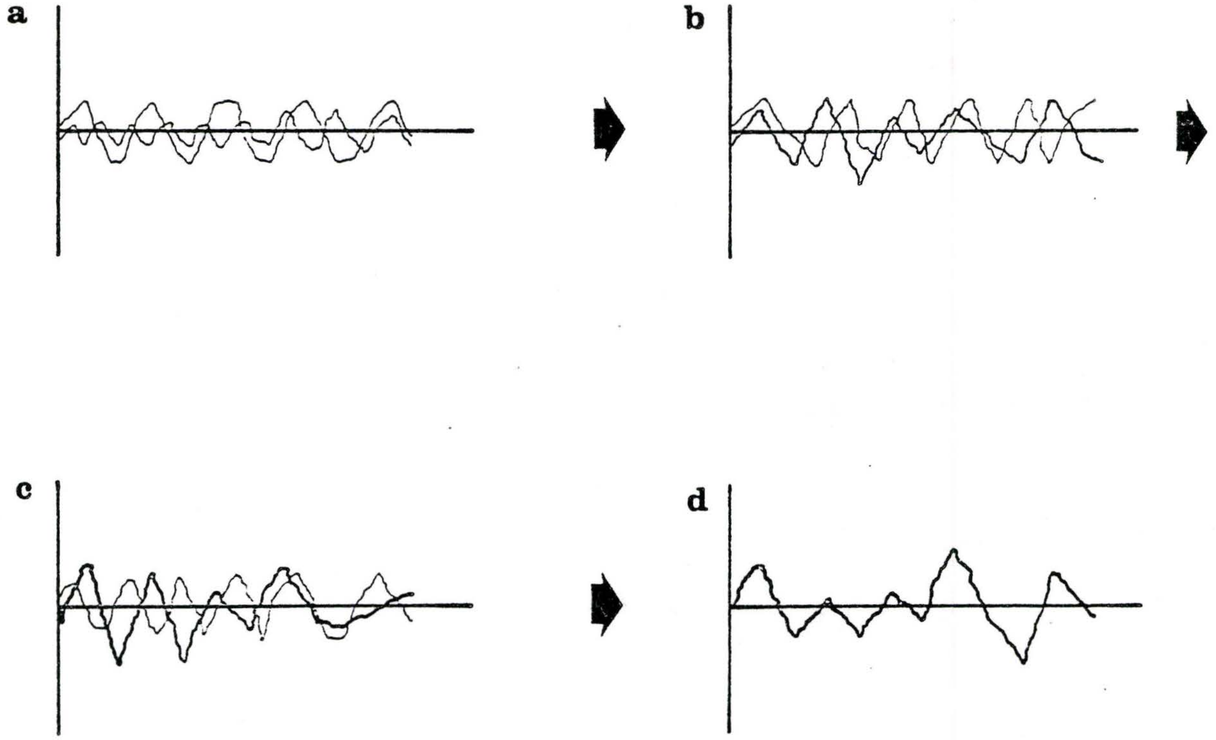
a
b
c
d

2.5.4.1 Growth in the Direction of Shortening

Adult stylolites are those that occur without an associated microswarm. The maximum wavelengths and amplitudes are greater than those for adolescent stylolites (wavelength=220 to 550 microns, amplitude=140 250 microns) and maximum seam thickness ranges from 15 to 100 microns. This considerable overlap with thickness values of adolescent stylolites is in agreement with the suggestion that minor accumulation of insoluble seam material occurs in this stage of growth.

Observation suggests that growth proceeds by dissolution of the sockets, at near equal rates, on both sides of the stylolite surface, not by the amalgamation of microstylolites. The increase in stylolite wavelength and amplitude and the absence of cumulative growth (amalgamation) on both sides of the seam confirms this.

For growth to proceed in the fashion observed there must be a solubility difference between the socket and the tip of a suture column. The socket must be more soluble than the tip. The difference may be inherent in the anisotropic dolomite crystals.

It is believed that differing stress solubilities are the result of a variation in stress of a body acted upon by a point load. In this case the sutured column acts as the point load, and the socket is the stressed body. The point vertical stress (in the socket) is maximum when the point load (the column tip) is at an angle of zero degrees relative to the maximum stress (Figure 19).

Crystals in the sockets are in a stressed state due to point loading by the column tips. According to Rieke's Principle mineral crystals that are under stress have higher solubilities i.e. they dissolve in preference to unstressed crystals of the same mineral. Hence, the sockets on both sides of a solution surface will dissolve at equivalent rates, assuming that the applied stress is constant.

The result of dissolution of the sockets about the seam can be seen in thin section. The geometry of the adolescent seam tends to a higher degree of suturing, becoming sharp-peaked to sub-rectangular in the adult seam. Striations are evident, due to deep interpenetration (vertical shearing of contacts) of the columns, in this mode of stylolite growth.

Insoluble material is drawn out along the limbs, and caps the tip of the column (Figure 20). This is characteristic of advanced stylolite growth. Since the major source of insoluble material, the microswarm, is gone, the growing stylolite attenuates what material it already has along the limbs of a suture. The production of striations is associated with this thinning phenomenon.

Figure 19 Diagramatic representation of the stress distribution in a body acted upon by a point load (P). The stress in the body is greatest when the point load is at zero degrees relative to the applied stress.

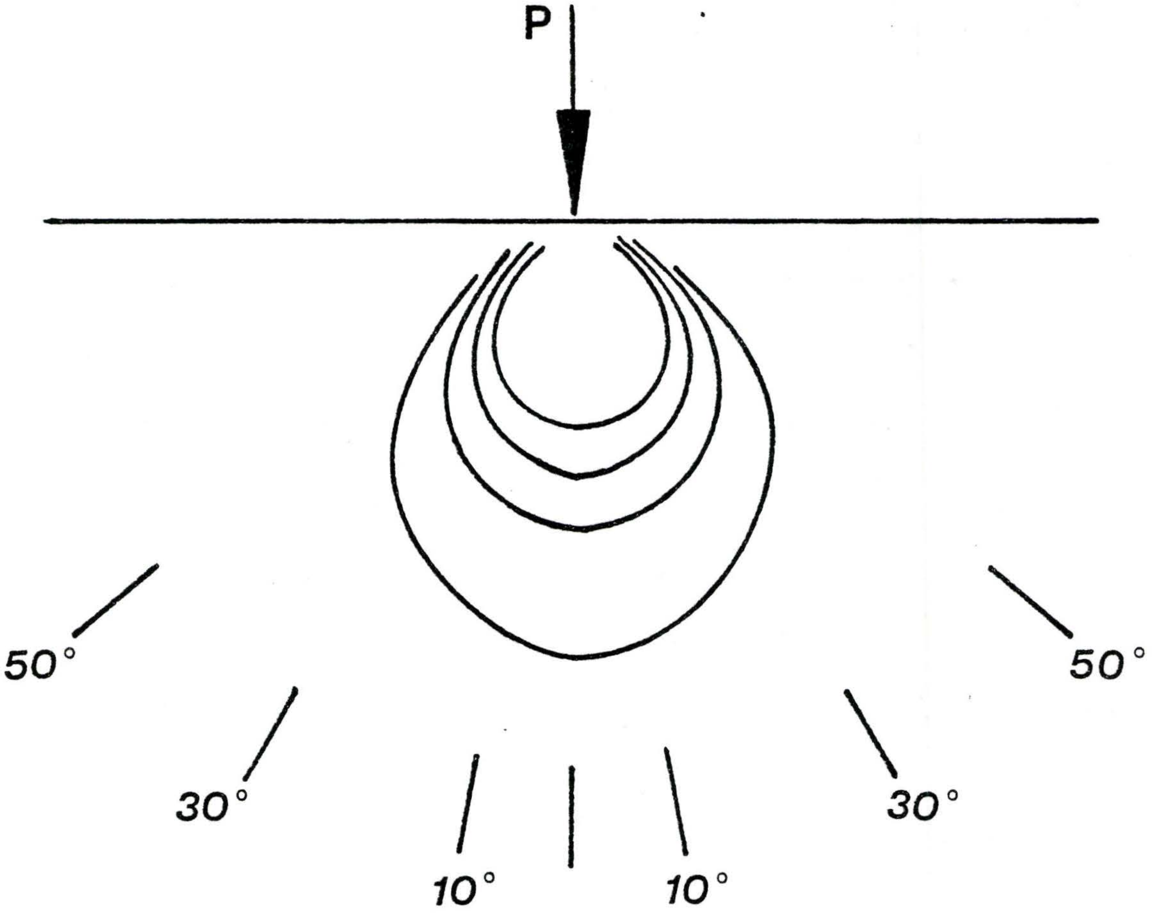
P
50°
50°
30°
30°
10°
10°

Figure 20 Schematic representation of adult stage stylolite growth. Stage I: a late adolescent/young adult stylolite grows by dissolution of the sockets due to point load stresses induced by the suture columns. Stage II: through pressure-dissolution of the sockets the sutures penetrate deeper (dashed line represents their former position, arrows indicate deeper penetration). Seam material becomes thinned along socket walls due to the shearing action. Straggler microstylolites become incorporated into the growing stylolite. Stage III: continued growth in this fashion results in the production of striations and extreme thinning of the seam material. Where the shearing action is not active, the seam material is thickest capping the suture.

I

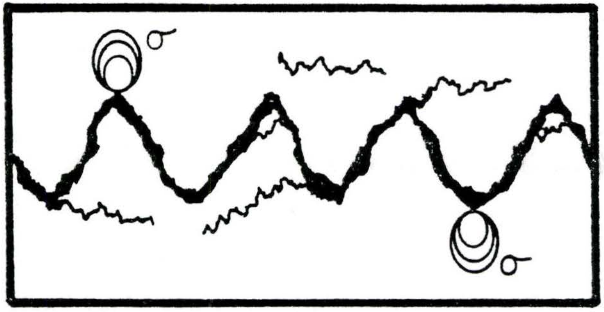

II

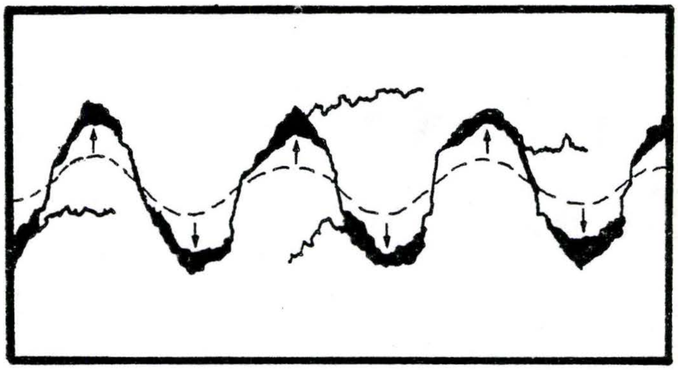

III

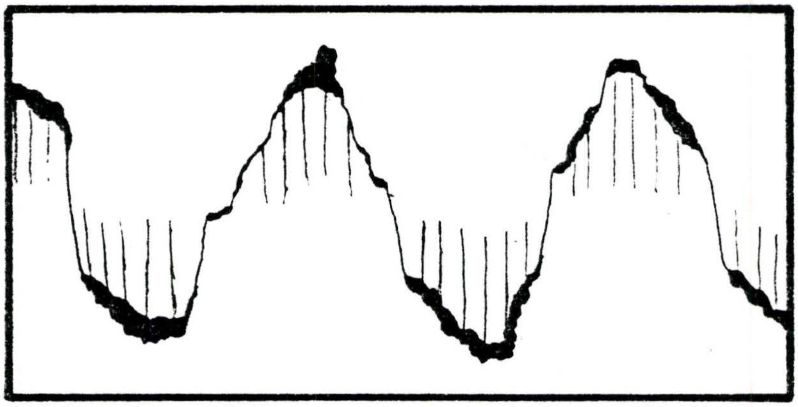

2.5.4.2 Propagation of Stylolites

Both adolescent and adult stylolites bifurcate into microstylolite swarms resembling "horsetails" at their terminations. Observation suggests that the seam propagates by incorporation of the bifurcating microstylolites through dissolution of carbonate between them. From a view of material lost, compaction is much greater in the central portion of the stylolite than at its termination, where the stylolite is in early stages of development. This differential compaction sets up a stress concentration symmetrical about the stylolite surface and centered at the terminations (Figure 21).

The stress concentration set up by differential compaction provides a means for enhancing pressure solution at this site. The result is seen as microswarms resembling "horsetails". Via the amalgamation mechanism, these microstylolites converge at the terminus of the solution seam, extending it laterally in an effort to relieve built-up stresses. This action resembles that of "pinching" a fan-like array of microstylolites along the stylolite surface, extending it outwards (Figure 22). The newly formed extension then goes through growth stages similar to that of an adolescent and adult stylolite.

Figure 21 Diagramatic representation of the compressive stresses acting upon a solution surface (2a), in the plane XY. Uniform remote compressive stresses σ_{yy}^{∞} and σ_{xx}^{∞} act normal and parallel to the surface. Compressive stresses σ_{yy} act upon the solution. σ_{yy} corresponds to the thickness of rock dissolved away along the surface. In this case the compressive stresses exceed the remote stresses and displacement occurs in the Y direction. V^{c} represents this normal displacement and one half of the material removed. In the region of the surface tip there is a strong stress concentration, symmetrical about the solution plane. This results in propagation in the X direction and relaxes the compressive stress acting upon the surface (after Fletcher and Pollard, 1981).

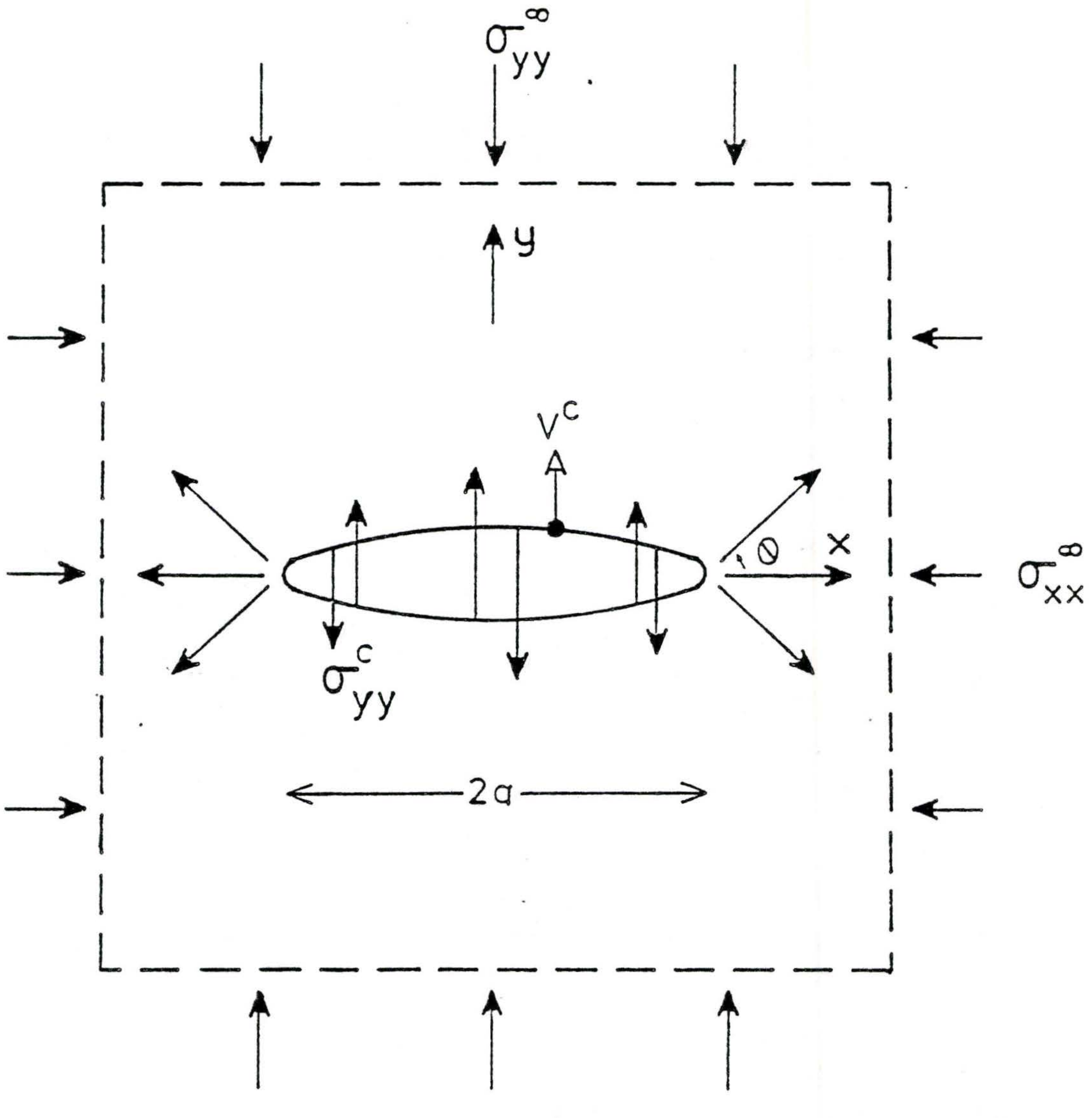
σ_{yy}^{∞}
y
V^c
θ
x
σ_{xx}^{∞}
σ_{yy}^{c}
2a

Figure 22 Schematic representation of stylolite propagation. Stage I: no pressure solution. Black line represents a marker horizon depicting a relative degree of compaction. Stage II: early adolescent stage. The marker horizon is depressed. The volume lost at the stylolite surface (represented by the ellipse) results in a symmetrical distribution of stresses centered at the lateral tips. This results in the "horsetail" of microstylolites. Stage III: amalgamation of microstylolites along the seam and at its tips (represented by arrows) results in lateral propagation and vertical growth. More volume lost means greater stresses at the tips and a larger "horsetail". Stage IV: continued propagation and vertical growth results in a larger seam, more volume lost and greater compaction. This results in a greater stresses which in turn, form a larger "horsetail". Through these steps it can be seen how stylolite growth is self-perpetuating.

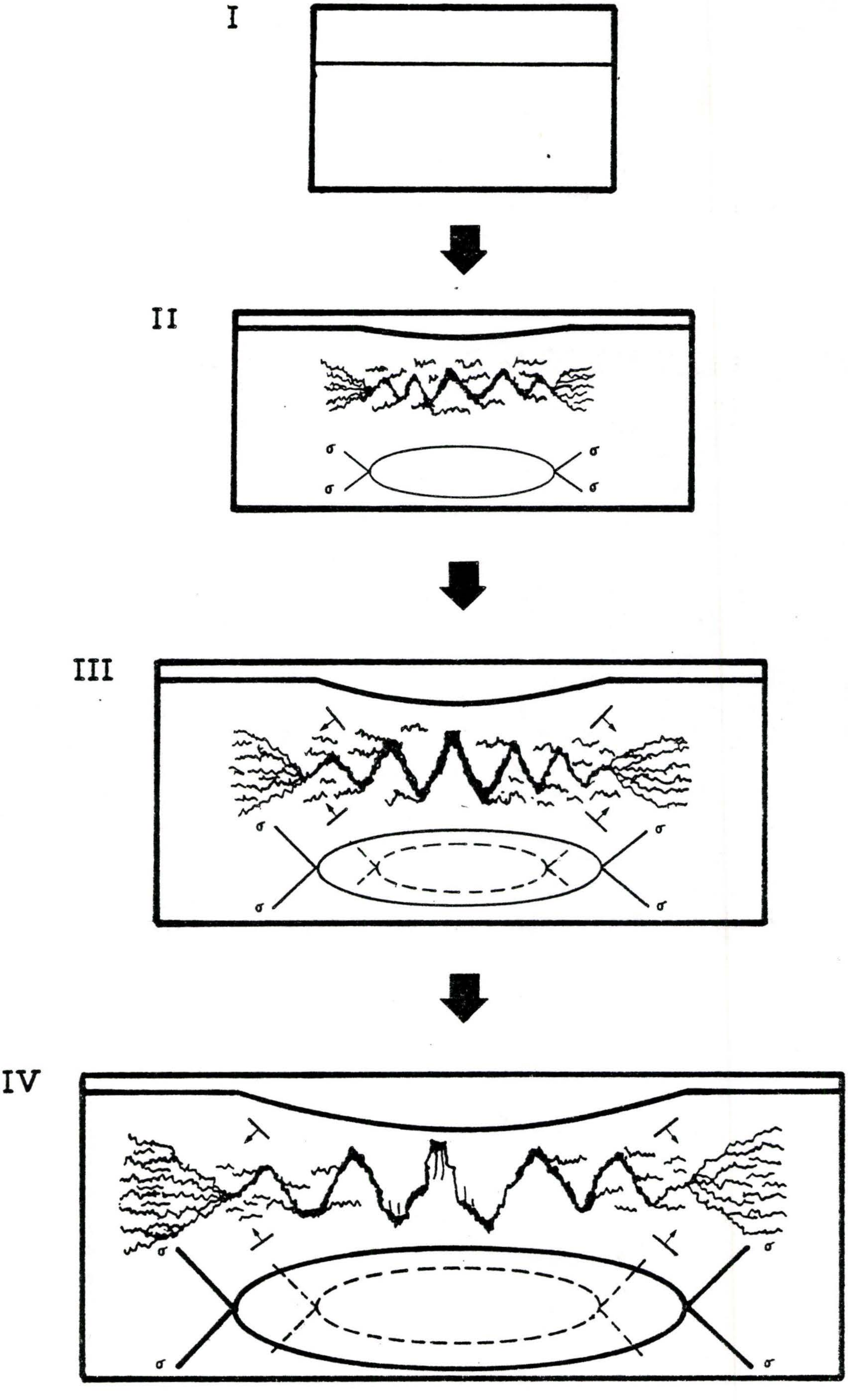
I
II
σ
σ
σ
σ
III
σ
σ
σ
σ
IV
σ
σ
σ
σ

2.6 SUMMARY

Amalgamation is proposed as the mechanism of stylolite development that was active in the Lockport Formation dolomites. This response of the dolomite to pressure solution is dependent upon primary features (possibly organic) that were formed as a result of mechanical compaction. Had these "stylolite-like" layers not been formed, it is doubtful that stylolites of the type described would have formed.

The complete mechanism of stylolite formation is shown in Figure 23. The initial response to pressure solution is seen as pervasive pressure solution throughout the entire rock body. This mode is operative during the time of stylolitization, not only at the beginning. Concommittant with or after, the onset of pervasive pressure solution, microstylolites form at sites favored by "organic" layers and smaller crystal sizes. These mark the neo-natal stage of stylolite development. Pressure solution is enhanced along microstylolites. With continued pressure solution, microstylolites in a swarm amalgamate, through the dissolution of dolomite between them, and form stylolites. Incipient stylolites are an early adolescent stage of development. Stylolites in microswarms are later in the adolescent stage. This stage of growth records a major accumulation of insoluble material. When the microswarm no

Figure 23 Schematic diagram of stylolite formation and development. Stage I: no pressure solution. Stage II: initial response is crystal contact dissolution. Stage III: continued pressure solution results in formation of a microswarm where organic layers are densely concentrated. Stage IV: amalgamation of microstylolites forms an incipient stylolite. The volume lost allows for propagation. Stage V: continued amalgamation and greater volume loss results in a larger seam and greater stresses at the tips. Stage VI: continued growth, the central portion of the seam is maturing while the tips propagate. Stage VII: continued growth, the central body is an adult, while the extremities are still maturing.

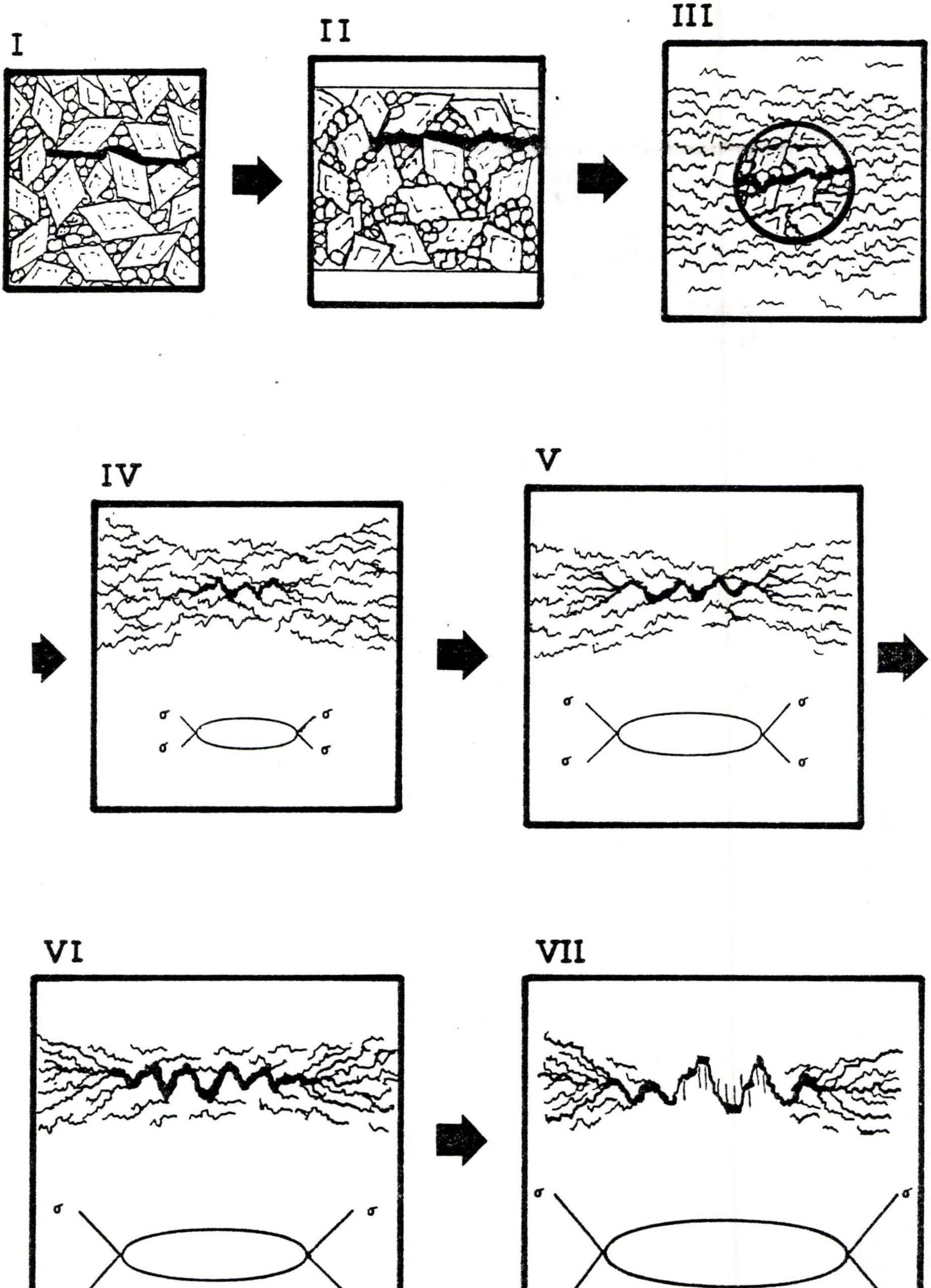
I
II
III
IV
σ
σ
σ
σ
V
σ
σ
σ
σ
VI
σ
σ
σ
σ
VII
σ
σ
σ
σ

longer exists, the source of much of this material, the adolescent stage comes to an end. Adult stage stylolites grow by dissolution at the sockets and accumulate lesser amounts of insoluble material. Striations are produced which draw insoluble materials out along the limbs of sutures.

The volume of material that is lost along a stylolite surface is responsible for setting-up a concentration of stresses at the lateral tips of stylolites. To relieve these built-up stresses, stylolites bifurcate at their tips into microstylolites which subsequently amalgamate to form an extension of the stylolite surface. Because of the dependence of microstylolite occurrence on mechanically produced "organic" layering, the lateral extent of a stylolite may be limited by primary accumulations of this material in the sediment.

Within any one stylolite that is well-developed, one should be able to recognize all the stages of growth described here. The propagating lateral tips should show features characteristic of neonatal and adolescent stage growth. Progressing towards the center of a stylolite, adolescent features will give way to adult stage growth features, such that striations and thinned insoluble accumulations should be found.

Amalgamation is not only associated with microstylolites. Two or more stylolites can amalgamate together to form a thicker stylolite by the mechanism described in the adolescent stage. Whether the wavelength and amplitude becomes larger is dependent upon the phase relationships of the individual stylolites. The examples described and shown in Figure 3 and 13 can be attributed to this mechanism.

CHAPTER 3

STYLOLITIZATION MECHANISMS II

3.1 GENERAL OBSERVATIONS-NISKU FORMATION

The samples for this study of stylolitization mechanisms are from the Nisku Formation, Zeta Lake Member (Upper Devonian). They were obtained from the borehole Texaco Bigoray 6-12-52-9W5.

Evidence of pressure solution is abundant throughout the cored interval. It is seen as stylolites of variable sizes, up to six centimetres in amplitude. Fitted-fabric textures typical of grainstones and packestones are not seen in any core samples, suggesting that the bulk of the rock was well-cemented before significant burial. Fossils are well-preserved in these samples. There is no sign of pressure solution distortion of the original shapes, except where fossils were dissolved along stylolite surfaces.

The stylolites found in Zeta Lake Member are of the sutured variety, commonly regular or irregular sutured and simple to very complex. They can be found at bedding planes and within beds. Spacing of individual stylolites shows no regularity and appears random. This suggests no facies control over stylolite occurrence.

Stylolites are common to the micritic or dolomitized matrix of this rock. They show no affinity for any specific mineral phase and appear to cross-cut all phases, except for anhydrite, which is the last mineralization episode (Watts 1984). Where the matrix is dolomitized the dolomite appears to have accumulated at the stylolite surface. This relationship is important to the mechanism of stylolitization.

3.2 DIAGENETIC HISTORY

Unlike the Lockport Formation, these samples are extremely heterogeneous. The Zeta Lake Member of the Nisku Formation is a carbonate of pinnacle reef origin. It is made up of marine sediments and a variety of marine organisms (dendroid and fasiculate rugose corals, tabulate corals, stromatoporoids, and calcareous algae) that have been preserved as wackestones, packestones, rudstones, framestones, and boundstones.

The diagenesis of the Zeta Lake Member is extremely complex. Two diagenetic histories have been proposed for these rocks (Machel 1984, Watts 1984), and of these, the diagenesis of Watts (1984) is favoured.

In brief, Nisku reefs were subjected to fairly extensive marine cementation resulting in an ubiquitous fibrous calcite cement, syntaxial rim cements, and micritization of the sediment. Following this, meteoric cementation was short-lived, as evidenced by rare occurrences of thin dogtooth spar and cross-cutting spar. Subsequently, karstification and leaching were not extensive in these reefs (Watts 1984).

Calcite spar began to precipitate at shallow burial and through continued burial. Watts (1984) does not recognize different episodes of calcite spar cementation, but it is suggested in subsequent chapters that the last phase of calcite spar precipitation is post-compactional and of pressure solution origin.

After initial calcite spar cementation but before the last episode of spar precipitation, dolomitization of the micritic matrix occurred. It began as a shallow matrix dolomite of hypersaline reflux origin and continued through the recrystallization of this dolomite and continued growth (pervasive dolomite) at intermediate to deep burial. Pervasive dolomite is not fabric selective and obliterates original components (Watts 1984). In this well, pervasive dolomite is rare (fossils are not dolomitized) but the matrix dolomite does show evidence of recrystallization.

Following dolomitization, and as this study indicates, precipitation of a late calcite spar, porosity was further occluded by Fe-dolomite and then anhydrite. These were the last mineral phases to precipitate before hydrocarbon migration (Watts 1984).

Stylolitization, as proposed by Watts (1984), took place after matrix dolomitization and then again after pervasive dolomitization. The latter was the main event. Because of the paucity of pervasive dolomite, two events are not easily recognized.

By the time of stylolitization, Nisku reefs were well-cemented by marine and early burial precipitates, and had been matrix dolomitized. This, as will be seen, is critical to the mechanism that results in stylolitization of the rock.

3.3 STYLOLITE MORPHOLOGY

Stylolites of the Zeta Lake Member occur in all sizes. They vary from micron-scale stylolites that are just visible , to centimetre-scale stylolites that reach up to six centimetres in amplitude. Microstylolites are not recognized in hand sample. This variety of sizes enabled the classification of stylolites by scale for permeability studies (Chapter 4).

Of the different sizes, micron- and micron to millimetre scale stylolites are the most abundant, centimetre-scale ones least. The smaller sizes mainly occur individually but are also found in swarms of up to ten or more (Figure 24a,24b). Within these swarms micron-scale seams are seen to branch away from other seams. As stylolites become larger it is uncommon to observe them occurring as a swarm. Larger stylolites typically occur individually or with very few seams in the immediate vicinity.

Other than in swarms, branched textures are not common with small-scale stylolites. They are more often found with larger stylolites. The seams that branch-off the main "trunk" seam are smaller than the main stylolite itself (Figure 25a). Mossop (1972) interpreted this texture as indicative of two stylolitization events. Besides branching, smaller stylolites show an anastomosed texture along the main stylolite (Figure 25b). Analogues of these two textures, branched and anastomosed, were seen at a much smaller scale in the Lockport Formation. Similarly, it is believed that an amalgamation mechanism can explain these textures.

As stylolites get larger their suturing becomes more variable. Micron-scale stylolites show simple-peaked to peaked suturing along their length (Figure 26). Millimetre-scale stylolites can be peaked or peaked and undulatory within the width of the core (Figure 27a,27b). Centimetre-scale stylolites display columnar, peaked, and undulatory styles of suturing (Figure 28a,28b). Larger stylolites are sometimes seen to have smaller stylolites within the interior of a suture resembling bridges joining the suture walls (Figure 29). It is believed that the variation in suturing can be explained by constructive and destructive interference of an amalgamation mechanism during growth. Bridging stylolites cannot all be explained by anamalgamation mechanism, but require a consideration of secondary stylolitization.

An unfortunate artifact of a core study is that stylolites cannot be traced-out along their lateral extent. Only micron-scale stylolites can be seen to terminate, and these terminate abruptly (Figure 30). There is no evidence of any "horsetails" (as found in the Lockport Formation) associated with micron-scale seams. It is possible that the branched texture seen with larger stylolites are the equivalent of "horsetails" and that only a section of it is seen in core, but this can not be confirmed.

3.4 STYLOLITE-DOLOMITE ASSOCIATIONS

Dolomite concentrations are easy to recognize in these core samples. Because the core had been slabbed and etched, dolomite could be distinguished based on its color (grey, brown, pale green) and greater relief relative to calcite. For these reasons the following observations were made.

An estimated 70% of stylolites have recognizable accumulations of dolomite along their length. This is most common with micron-scale stylolites that occur at the edges of dolomite concentrations or within dolomitic regions of the matrix (Figure 31a,31b). For stylolites that are larger this association becomes less obvious. For example, millimetre-scale stylolites show dolomite concentrations in their sutures, making up the bulk of a suture. To a lesser degree dolomite is concentrated along the length of these stylolites (Figure 32a). Centimetre-scale stylolites show dolomite mainly in the sutures, as the main mineral phase of the suture, or capping the top of it (Figure 32b).

For large seams, stylolite-dolomite associations become less common, such that larger stylolites show no relationship to any specific mineral phase (Figure 33). This is believed to be a function of originally low dolomite occurrence prior to stylolitization at these sites and not due to the removal of dolomite through pressure solution.

3.5 MICROSCOPIC PRESSURE SOLUTION TEXTURES AND RELATED FEATURES

Evidence of pervasive pressure solution is lacking in all thin sections studied. Microfossils and macrofossils within the matrix are well-preserved and show no signs of volume loss about their boundaries (Figure 34). This suggests that pressure solutions was active only at discrete horizons in these carbonates.

3.5.1 NEOMORPHIC AND RECRYSTALLIZED TEXTURES

Micrite and the microfossils that make-up the matrix do show evidence of neomorphism, resulting in micrite transformation to microspar and partial obliteration of structural textures (Figure 35a,35b). It is difficult to characterize these neomorphic textures as related to any particular mode of occurrence. Neomorphism appears patchy yet evenly distributed in some thin sections and is difficult to recognize in others. It may be greatest nearest stylolites and dolomite concentrations or show no spatial correlation at all.

In cathodoluminescence the matrix shows a patchy, variably intense luminescence. It is dominantly dull but with patches of non-luminescent and bright cements throughout it. Microfossil morphologies do not show well under luminescence suggesting that the chemistry of the micrite has been "rearranged" (Schofield 1984).

Dolomite shows neomorphic textures that can be spatially related to stylolites. The best examples are those that show increasing recrystallization towards stylolites. In cathodoluminescence, individual crystals lose their faint zonation and their luminescence becomes more uniform towards a stylolite. This texture is shown in Chapter 6, Figure 85. Also, mosaics of coarse dolomite crystals are found adjacent to stylolites. The mosaics show a coalesced texture and have an undulatory extinction (Figure 36) suggesting plastic deformation of the crystal structures. Mosaics similar to these have not been recognized in the absence of stylolites.

3.5.2 DEDOLOMITE TEXTURES

As well as recrystallization textures, dolomite crystals are found showing dedolomite textures adjacent to stylolites. Dedolomitization is the replacement of dolomite by calcite. It is seen in these samples as the replacement of the dolomite core and partial corrosion of the crystal boundaries (Figure 37). Crystals susceptible to calcitization are both matrix-replacement and cement crystals in the immediate vicinity of stylolites, or those millimetres away. There is a general pattern of intense dedolomitization nearest a stylolite but it is not uniform and does not decrease uniformly away from the seam. Dedolomite textures have not been recognized in the absence of stylolites.

3.5.3 NON-STYLOLITIC PRESSURE SOLUTION TEXTURE

It was said at the beginning of this section pervasive pressure solution is not recognized in these rocks. Other pressure solution features are recognized that are non-stylolitic nor do they resemble a pervasive mode. These features are isolated examples of non-stylolitic solution associated with individual or clusters of dolomite rhombs. For example, dolomite rhombs are seen penetrating original bioclastic particles in a distinctive pressure-dissolution fashion (Figure 38a). Along laminar concentrations of dolomite, a number of boundary dolomite rhombs are seen penetrating micritic matrix material (Figure 38b). The porosity created by a penetrating dolomite crystal suggests that the dolomite crystals involved were part of a rigid framework of crystals that responded to compactive pressures by dissolving the adjacent calcite. Similar non-stylolitic textures were not recognized associated with any calcite component.

3.5.4 STYLOLITE-DOLOMITE TEXTURAL RELATIONSHIPS

Microstylolites are not recognized in hand sample but can be found in thin section. They are not abundant as in the Lockport Formation examples, nor do they resemble them. These microstylolites are found associated with dolomite crystals. Usually a linear arrangement of dolomite defines the microstylolite. The smallest of these seams has only a few dolomite crystals along it and as they get bigger, more dolomite crystals are found (Figure 39a,39b). They can occur individually as in Figure 39 or in an anastomosed network associated with a stylolite (Figure

40). Microstylolites without dolomite along their length are not seen.

Micron-scale stylolites show similar dolomite relationships. These stylolites commonly occur at the edges of dolomite concentrations, suggesting a causative association, or they occur in dominantly dolomitic matrix (Figure 41a,41b). The dolomite along their length may make up all or part of the sutures or just cap them. In the most ideal examples, dolomite concentration decreases away from the stylolite and calcitic matrix material increases in abundance.

Similar relationships were observed with larger scale seams. The pattern of dolomite concentration is not as clear for these larger stylolites due to the complexity of the suturing, but dolomite is found capping and making-up integral parts of the sutures (Figure 42a,42b).

3.5.5 SUTURE MORPHOLOGIES

As recognized in hand sample, the larger a stylolite is, the more variable the suturing is. At micron-scale, stylolites may have a relatively simple peaked or very complex suturing (Figure 43a,43b). Along larger stylolites, the suturing may show signs of amalgamated stylolites incorporated into the main stylolite. The result is that the suturing may be even more complex or more simple (Figure

44a,44b). The resultant morphology of the stylolite appears to be dependent upon the phase relationships of an amalgamation mechanism.

Complex suturing of stylolites seems to have concentrations of insoluble material capping the individual sutures and thinned-to-minimal concentrations of insolubles along the limbs (Figure 45). This thinning is not characteristic of any particular scale of stylolite. It is found in micron- through centimetre-scale seams, but is more common in centimetre-scale seams that display complex-columnar suturing.

Dolomite appears to have contributed to the development of sutures. Dolomite crystals can be found at the edges of sutures in positions that suggest that through pressure solution, they have sheared the socket walls of the suture. Along the limbs, the result is seen as planar socket walls, thinned insoluble material accumulations, and created porosity (Figure 46a). Where they occur at the tip of a suture they may create an even more complex suture (Figure 46b). These features are more typical of larger stylolites, with deep penetrating sutures.

The bridged structure described in the preceding section can similarly be attributed to dolomite concentrations. These bridging stylolites commonly occur at the edge of laminar dolomite concentrations in suture interiors

(Figure 47a). They cannot be correlated between sutures and are difficult to explain by an amalgamation mechanism.

Occasionally, where dolomite concentrations are low, very irregular pressure solution textures are found within large sutures (Figure 47b). These features are not stylolites but pressure-dissolved particles and cements. The cause of this dissolution can be related to dolomite crystals and detrital grains that penetrate the particle. Both this texture and the bridged structure are seen as a secondary response to pressure solution as the result of built-up stresses localized about the main stylolite.

3.5.6 STYLOLITE TERMINATIONS

Only the terminations of microstylolites and micron-scale stylolites could be observed. Where seen, the associated stylolite always had dolomite along its length. These stylolites terminate in two ways. Where dolomite abundances are low, the stylolite terminated abruptly into the matrix. It did not fan outwards into a "horsetail" feature similar to those seen in the Lockport Formation (Figure 48a). Where dolomite abundances were higher, the stylolite terminated outwards into a dolomite concentration, sometimes abruptly or sometimes resembling a fan-like array of dolomite crystals (Figure 48b). Microstylolites were not observed propagating from these features.

Stylolitization, as proposed by Watts (1984), took place after matrix dolomitization and then again after pervasive dolomitization. The latter was the main event. Because of the paucity of pervasive dolomite, two events are not easily recognized.

By the time of stylolitization, Nisku reefs were well-cemented by marine and early burial precipitates, and had been matrix dolomitized. This, as will be seen, is critical to the mechanism that results in stylolitization of the rock.

3.3 STYLOLITE MORPHOLOGY

Stylolites of the Zeta Lake Member occur in all sizes. They vary from micron-scale stylolites that are just visible , to centimetre-scale stylolites that reach up to six centimetres in amplitude. Microstylolites are not recognized in hand sample. This variety of sizes enabled the classification of stylolites by scale for permeability studies (Chapter 4).

Of the different sizes, micron- and micron to millimetre scale stylolites are the most abundant, centimetre-scale ones least. The smaller sizes mainly occur individually but are also found in swarms of up to ten or more (Figure 24a,24b). Within these swarms micron-scale seams are seen to branch away from other seams. As stylolites

Figure 24 Core photographs of micron-scale stylolite occurrence. 24a) An individual micron-scale stylolite with no others in the immediate vicinity. 24b) Micron-scale stylolites that are so numerous they constitute a swarm. Note how some stylolites branch away from others.

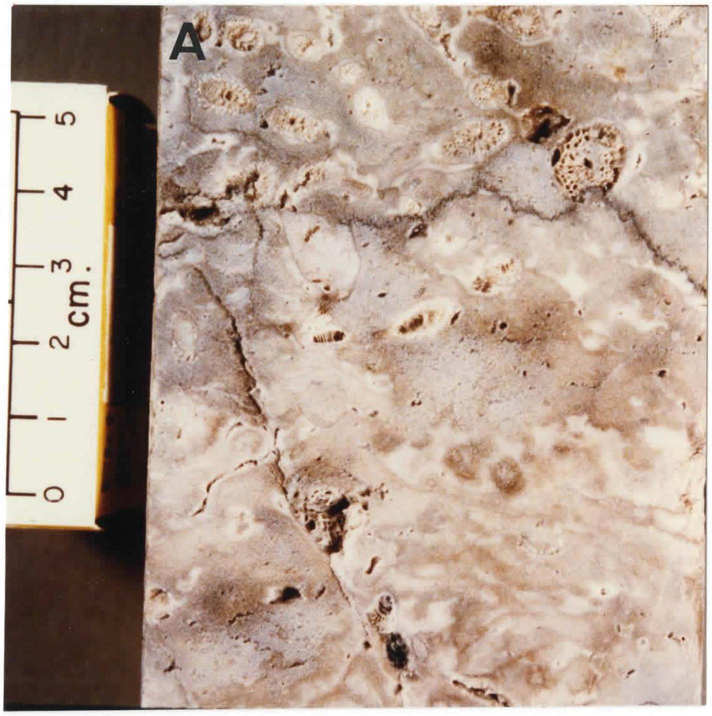
A
0
1
2
3
4
5
cm.

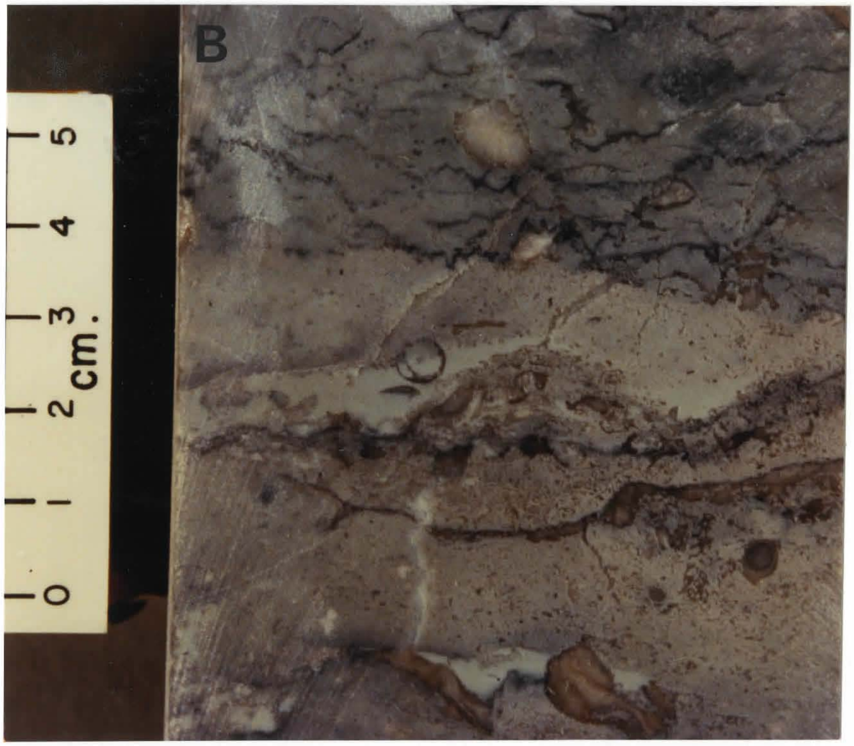
B
0
1
2
3
4
5
cm.

become larger it is uncommon to observe them occurring as a swarm. Larger stylolites typically occur individually or with very few seams in the immediate vicinity.

Other than in swarms, branched textures are not common with small-scale stylolites. They are more often found with larger stylolites. The seams that branch-off the main "trunk" seam are smaller than the main stylolite itself (Figure 25a). Mossop (1972) interpreted this texture as indicative of two stylolitization events. Besides branching, smaller stylolites show an anastomosed texture along the main stylolite (Figure 25b). Analogues of these two textures, branched and anastomosed, were seen at a much smaller scale in the Lockport Formation. Similarly, it is believed that an amalgamation mechanism can explain these textures.

As stylolites get larger their suturing becomes more variable. Micron-scale stylolites show simple-peaked to peaked suturing along their length (Figure 26). Millimetre-scale stylolites can be peaked or peaked and undulatory within the width of the core (Figure 27a,27b). Centimetre-scale stylolites display columnar, peaked, and undulatory styles of suturing (Figure 28a,28b). Larger stylolites are sometimes seen to have smaller stylolites within the interior of a suture resembling bridges joining the suture walls (Figure 29). It is believed that the variation in

Figure 25 Core photographs of branched and anastomosed large scale stylolites. 25a) The stylolite branching off the "trunk" stylolite is smaller. 25b) A smaller stylolite that departs then rejoins the "trunk" stylolite in an anastomosed manner.

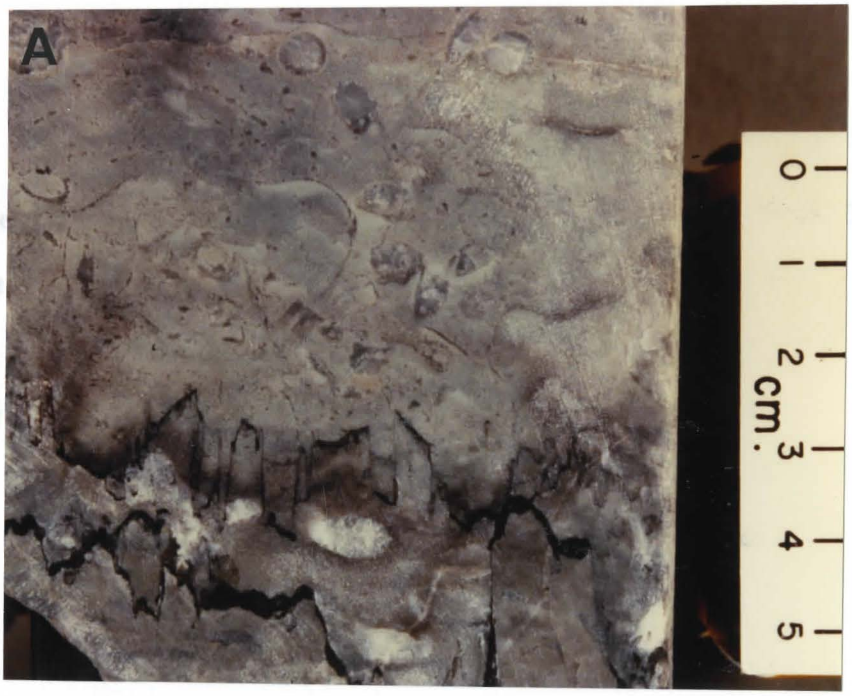
A
0
1
2
cm.
3
4
5

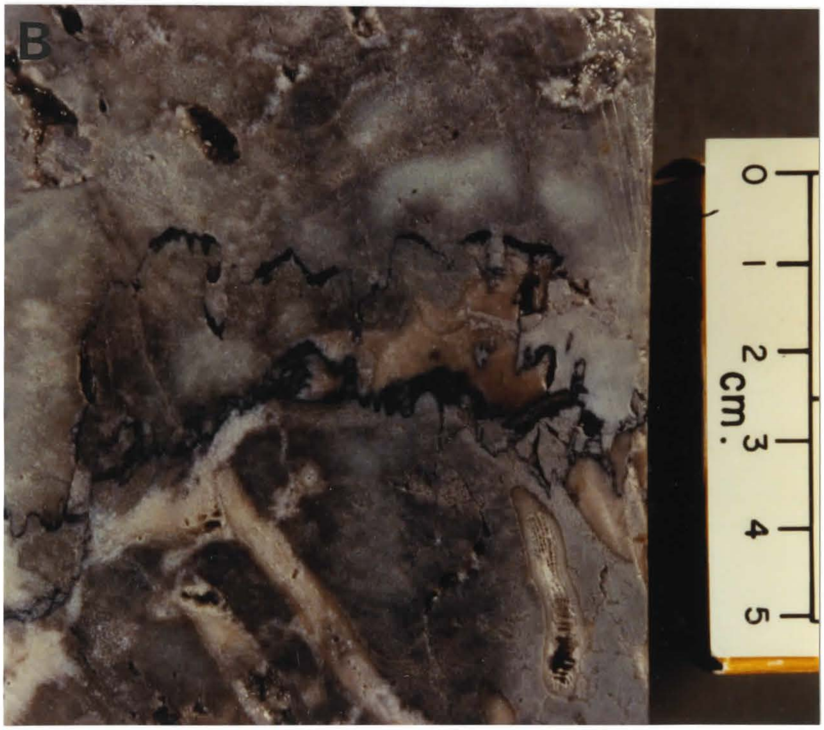
B
0
1
2
cm.
3
4
5

Figure 26 Core photograph of a micron-scale stylolite showing its peaked suturing. This is an exceptional case where a micron-scale seam has two centimetre-scale sutures. This is suggestive of exceptional volume loss.

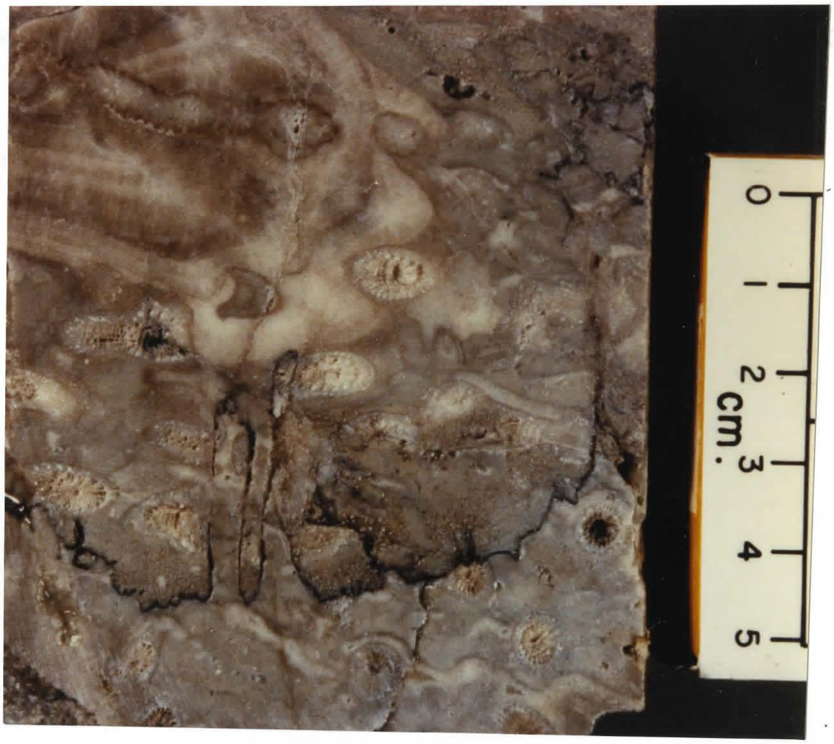
0
1
2
3
4
5
cm.

Figure 27 Core photographs of millimetre-scale stylolites and their suture morphologies. 27a) Peaked suturing. 27b) Peaked and undulatory suturing.

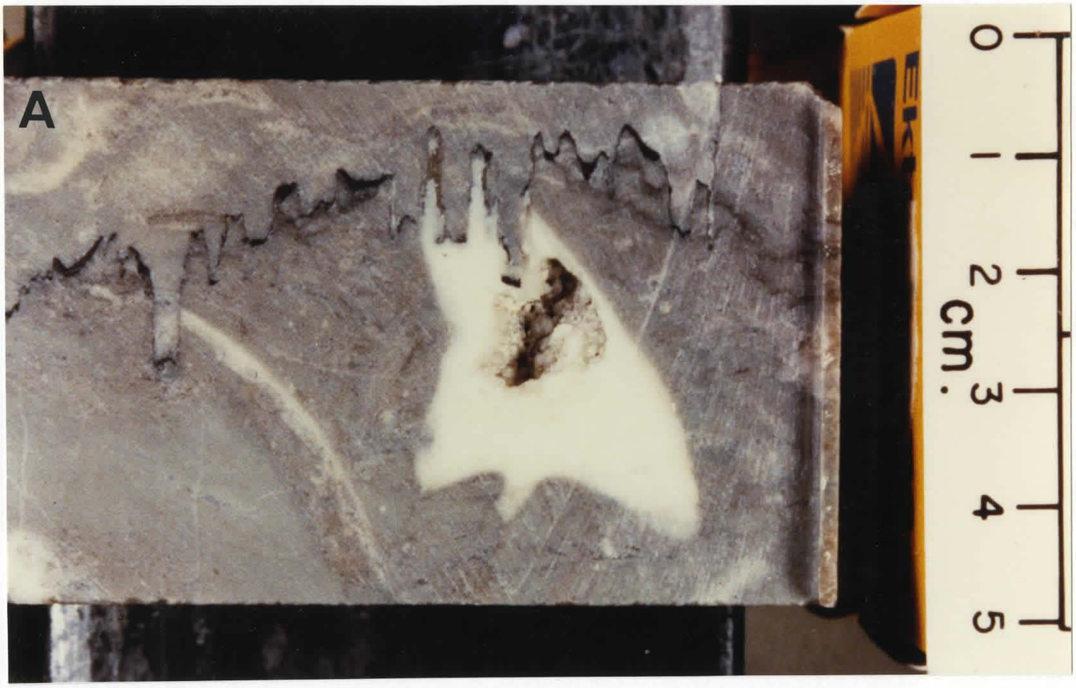
A
0
1
2
cm.
3
4
5

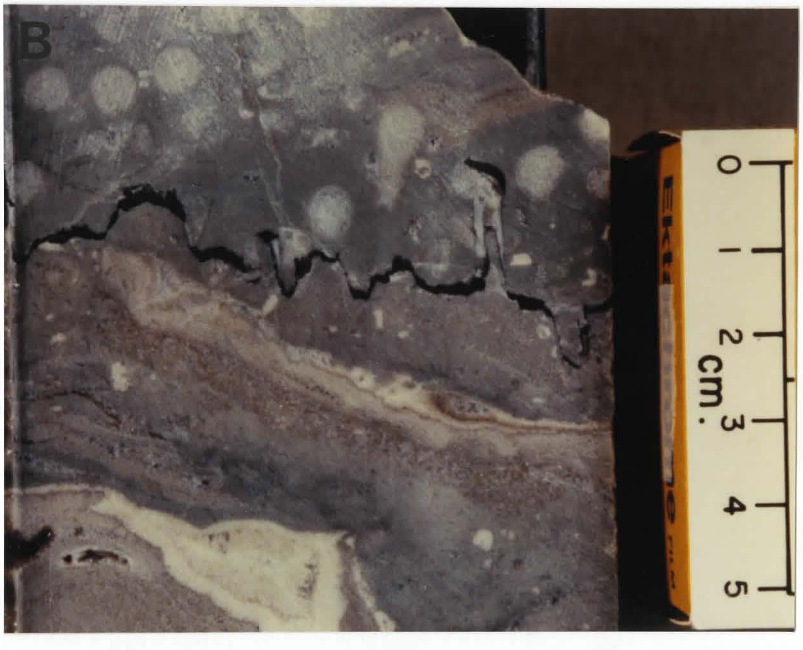
B
0
1
2
cm.
3
4
5

Figure 28 Core photographs of centimetre-scale stylolites and their suture morphologies. 28a) Peaked and columnar suturing. 28b) Columnar and undulatory suturing. Note the branching micron-scale seam in the center of the photo.

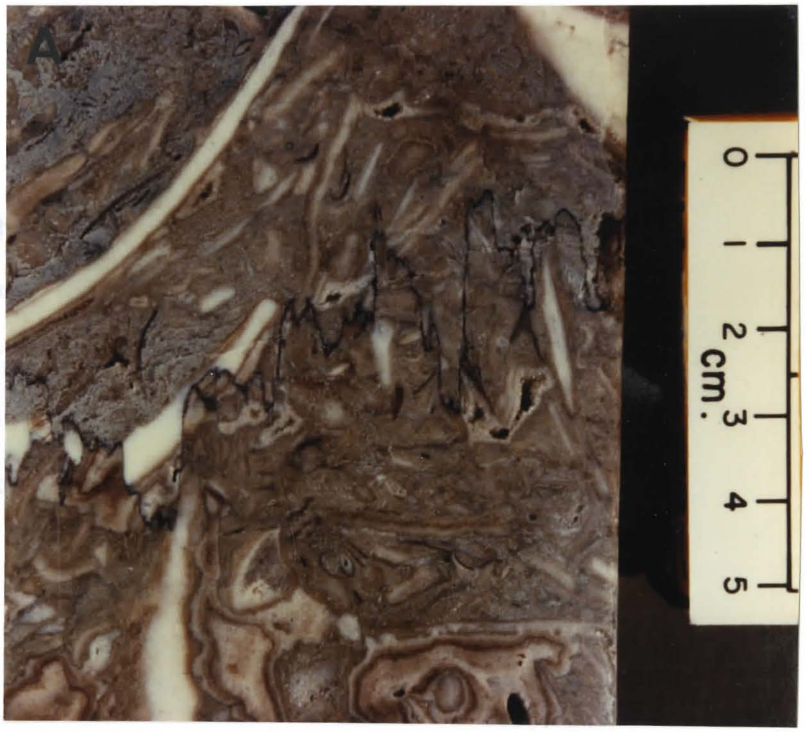
A
0
1
2
3
4
5
cm.

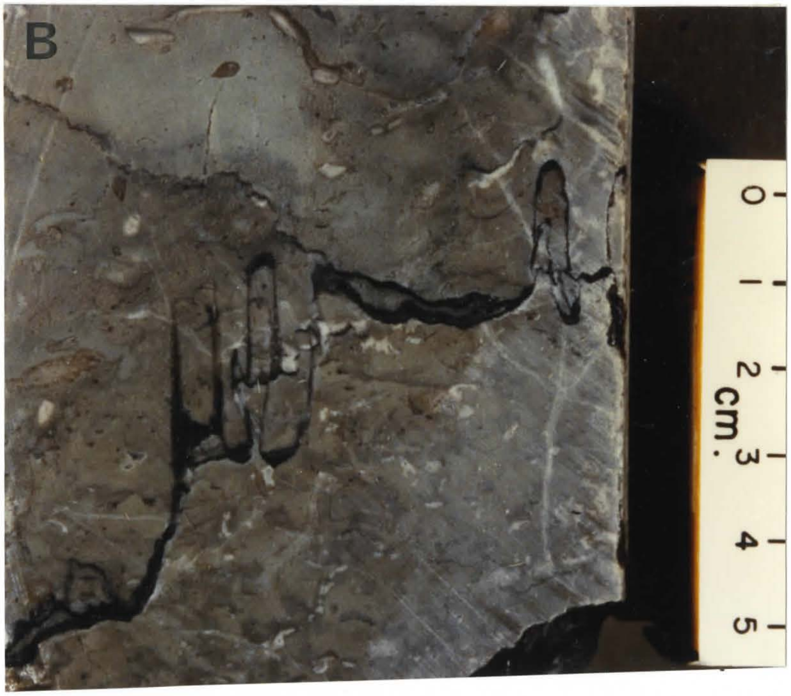
B
0
1
2
3
4
5
cm.

Figure 29 Core photograph of a centimetre-scale stylolite that displays smaller stylolites within the suture interiors that form bridges between the socket walls. These bridging stylolites cannot be correlated across sutures.

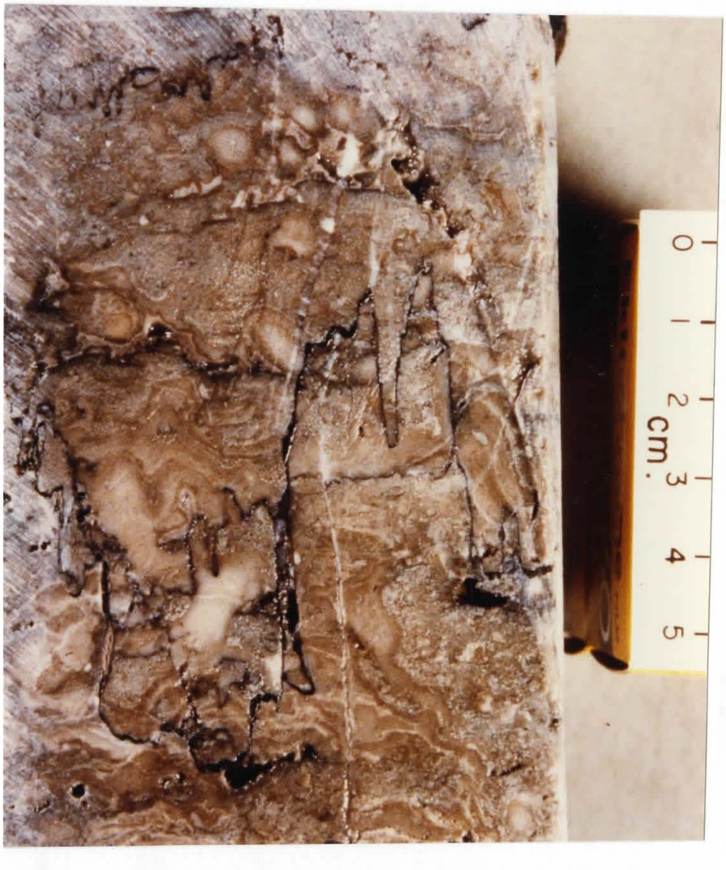
0
1
2
cm.
3
4
5

suturing can be explained by constructive and destructive interference of an amalgamation mechanism during growth. Bridging stylolites cannot all be explained by anamalgamation mechanism, but require a consideration of secondary stylolitization.

An unfortunate artifact of a core study is that stylolites cannot be traced-out along their lateral extent. Only micron-scale stylolites can be seen to terminate, and these terminate abruptly (Figure 30). There is no evidence of any "horsetails" (as found in the Lockport Formation) associated with micron-scale seams. It is possible that the branched texture seen with larger stylolites are the equivalent of "horsetails" and that only a section of it is seen in core, but this can not be confirmed.

3.4 STYLOLITE-DOLOMITE ASSOCIATIONS

Dolomite concentrations are easy to recognize in these core samples. Because the core had been slabbed and etched, dolomite could be distinguished based on its color (grey, brown, pale green) and greater relief relative to calcite. For these reasons the following observations were made.

An estimated 70% of stylolites have recognizable accumulations of dolomite along their length. This is most common with micron-scale stylolites that occur at the edges

Figure 30 Core photograph of the terminations at both ends of a micron-scale stylolite. Note how the stylolite terminates abruptly in the upper half of the photo.

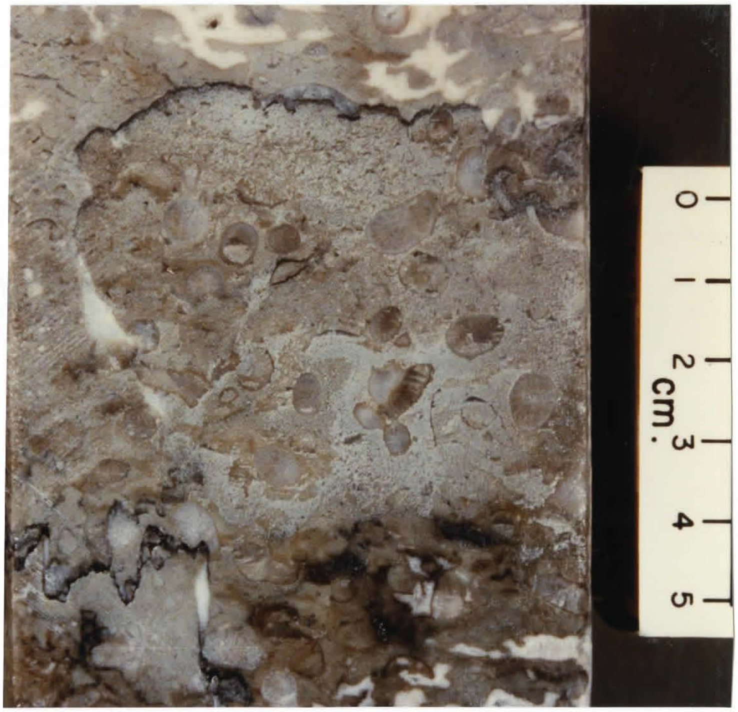
0
1
2
cm.
3
4
5

of dolomite concentrations or within dolomitic regions of the matrix (Figure 31a,31b). For stylolites that are larger this association becomes less obvious. For example, millimetre-scale stylolites show dolomite concentrations in their sutures, making up the bulk of a suture. To a lesser degree dolomite is concentrated along the length of these stylolites (Figure 32a). Centimetre-scale stylolites show dolomite mainly in the sutures, as the main mineral phase of the suture, or capping the top of it (Figure 32b).

For large seams, stylolite-dolomite associations become less common, such that larger stylolites show no relationship to any specific mineral phase (Figure 33). This is believed to be a function of originally low dolomite occurrence prior to stylolitization at these sites and not due to the removal of dolomite through pressure solution.

3.5 MICROSCOPIC PRESSURE SOLUTION TEXTURES AND RELATED FEATURES

Evidence of pervasive pressure solution is lacking in all thin sections studied. Microfossils and macrofossils within the matrix are well-preserved and show no signs of volume loss about their boundaries (Figure 34). This suggests that pressure solutions was active only at discrete horizons in these carbonates.

Figure 31 Core photographs of stylolite-dolomite associations. 31a) A micron-scale stylolite that occurs at an abrupt boundary between matrix dolomite (grey) and fossiliferous limestone. 31b) A micron-scale seam that occurs in dolomitic matrix on both sides.

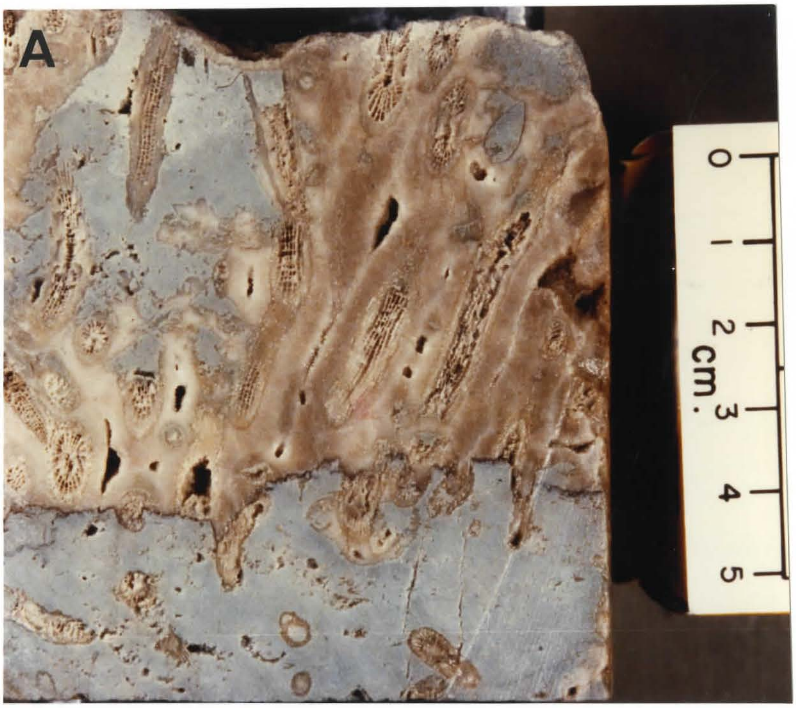
A
0
1
2
3
4
5
cm.


B
0
1
2
3
4
5
cm.

Figure 32 Core photographs of stylolite-dolomite associations. 32a) A millimetre-scale stylolite with abundant dolomite in its sutures and partially along its length. 32b) A centimetre-scale stylolite with dolomite capping and making up the bulk of some sutures.

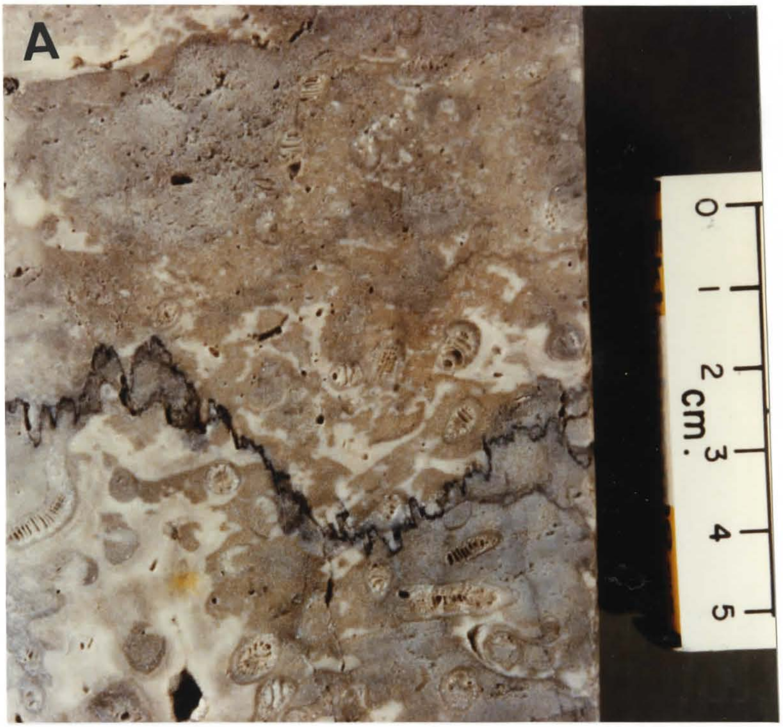
A
0
1
2
3
4
5
cm.

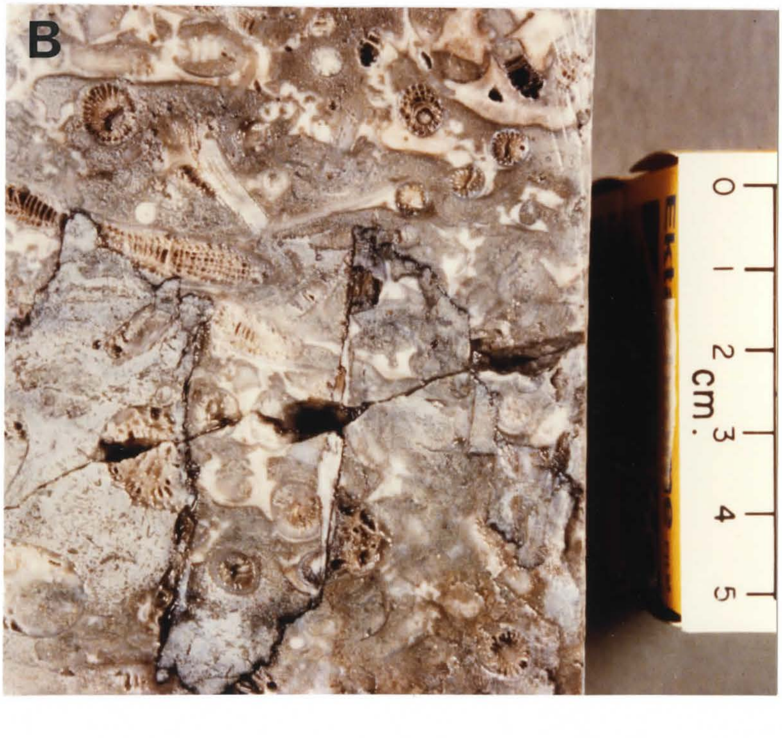
B
0
1
2
3
4
5
cm.

Figure 33 Core photograph of a large stylolite that shows no specific relationship to any specific mineral phase.

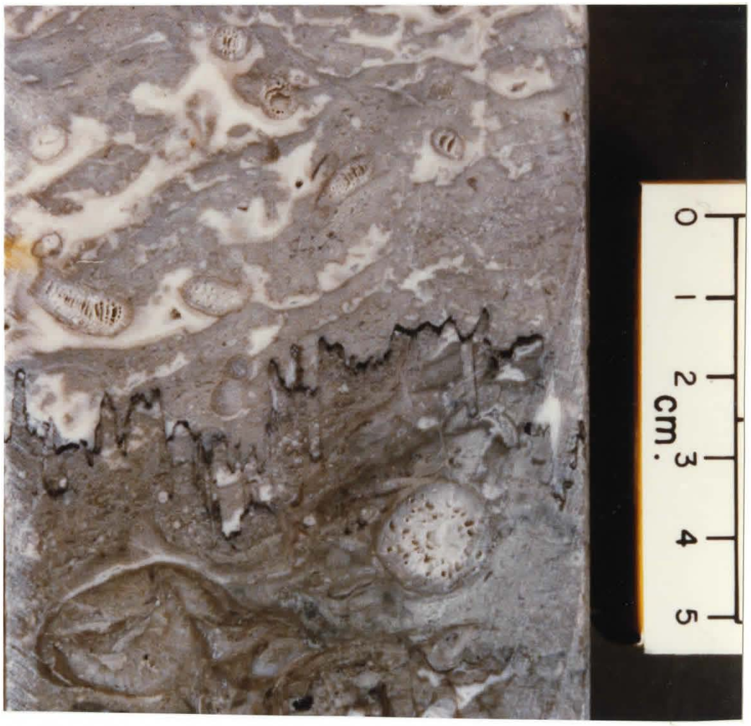
0
1
2
cm.
3
4
5

Figure 34 Photomicrograph of bioclastic particles within the matrix showing no signs of pressure solution. Particle boundaries are well-defined. Plane-polarized light. Magnification 16x. Scale bar = 2 mm.

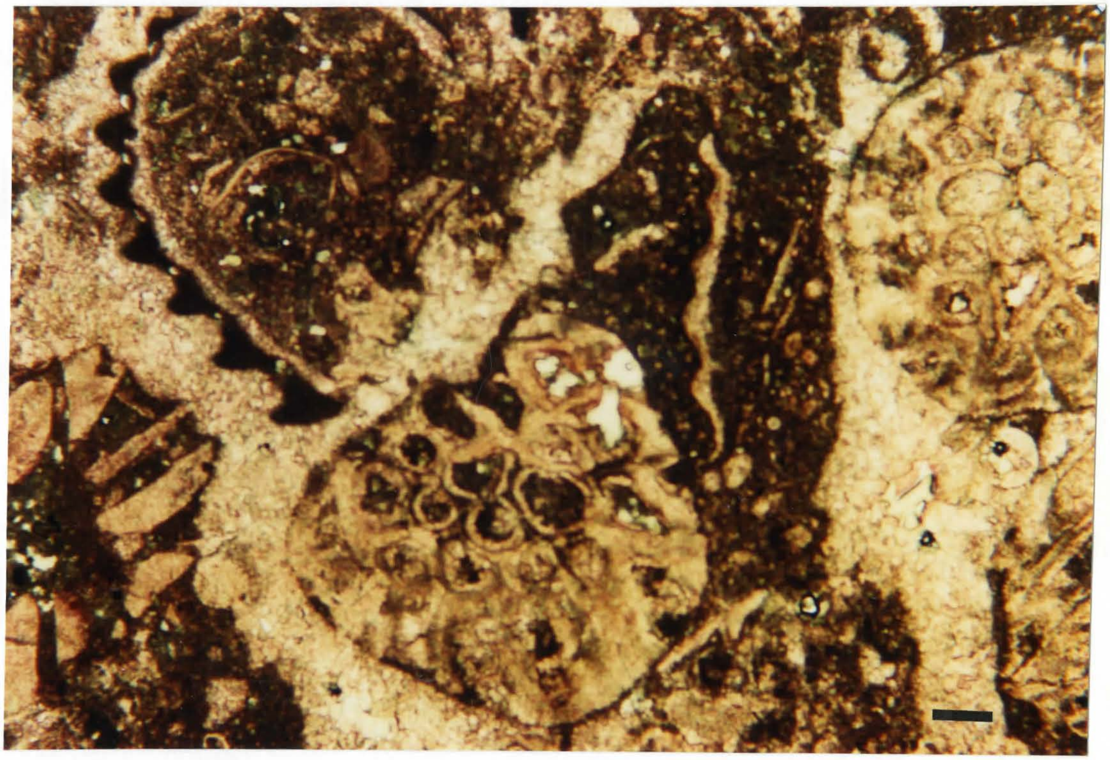

3.5.1 NEOMORPHIC AND RECRYSTALLIZED TEXTURES

Micrite and the microfossils that make-up the matrix do show evidence of neomorphism, resulting in micrite transformation to microspar and partial obliteration of structural textures (Figure 35a,35b). It is difficult to characterize these neomorphic textures as related to any particular mode of occurrence. Neomorphism appears patchy yet evenly distributed in some thin sections and is difficult to recognize in others. It may be greatest nearest stylolites and dolomite concentrations or show no spatial correlation at all.

In cathodoluminescence the matrix shows a patchy, variably intense luminescence. It is dominantly dull but with patches of non-luminescent and bright cements throughout it. Microfossil morphologies do not show well under luminescence suggesting that the chemistry of the micrite has been "rearranged" (Schofield 1984).

Dolomite shows neomorphic textures that can be spatially related to stylolites. The best examples are those that show increasing recrystallization towards stylolites. In cathodoluminescence, individual crystals lose their faint zonation and their luminescence becomes more uniform towards a stylolite. This texture is shown in Chapter 6, Figure 85. Also, mosaics of coarse dolomite crystals are found adjacent to stylolites. The mosaics show

Figure 35 Photomicrographs of neomorphic matrix materials. 35a) Micrite that has been transformed to microspar. 35b) Partial obliteration of a microfossil that occurs in a matrix of microspar. Vertical structure in center of photo is believed to be former microfossil. Plane polarized light. Magnification 100x. Scale bar = 100 microns.

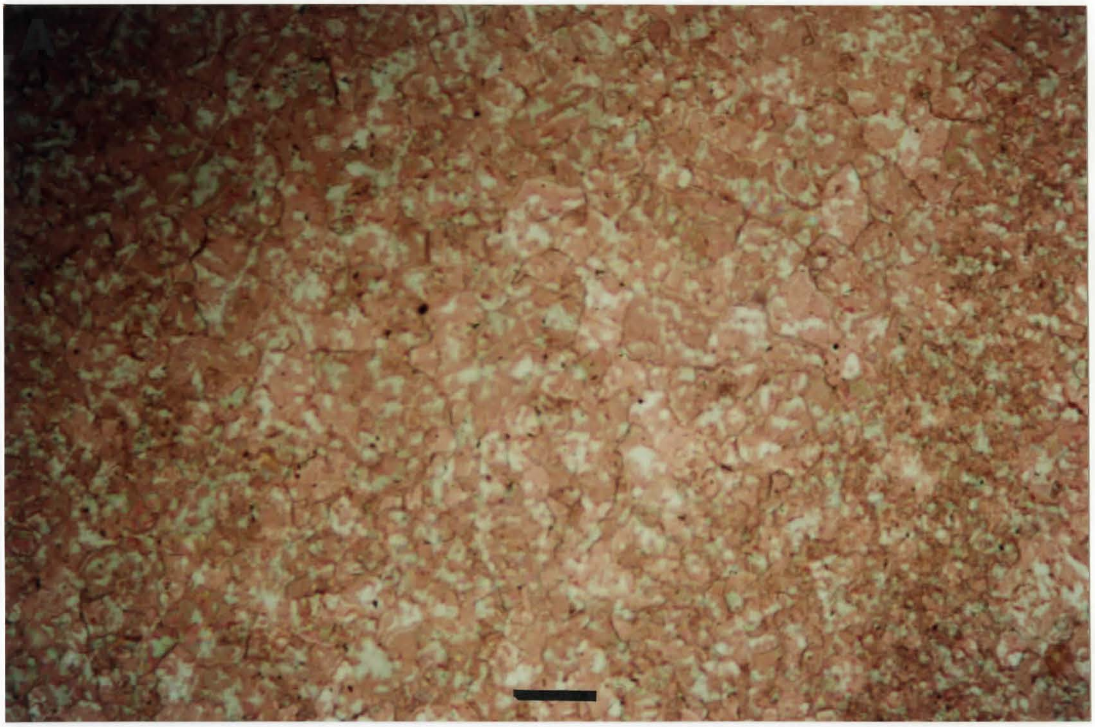
A

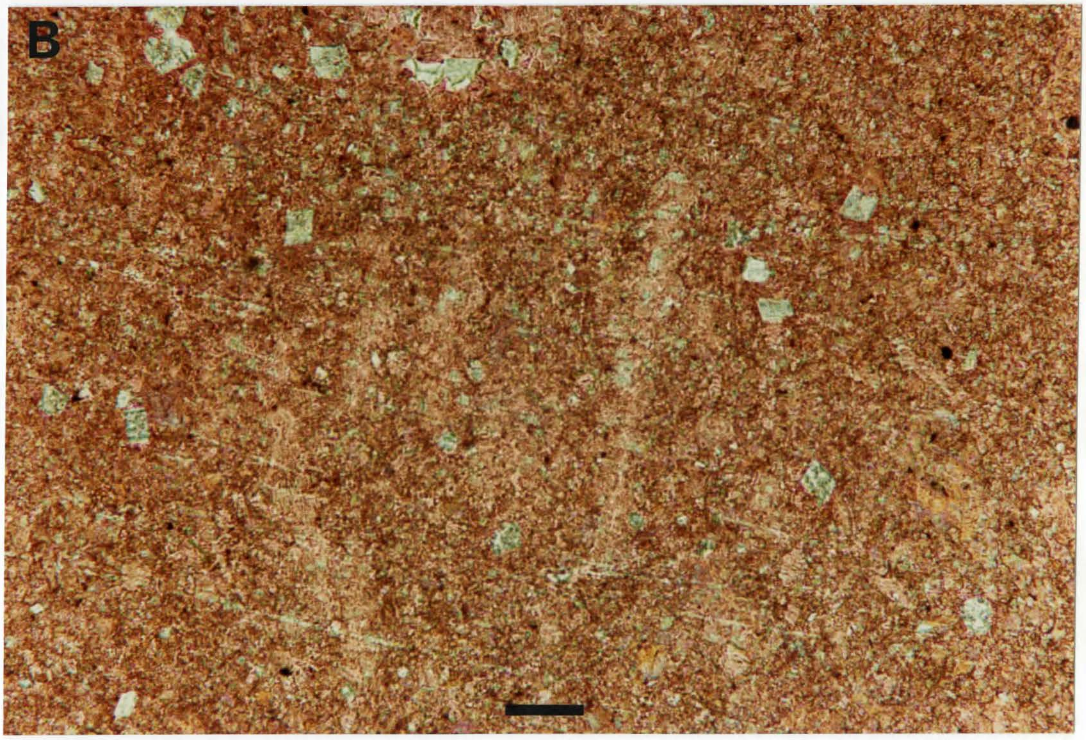
B

a coalesced texture and have an undulatory extinction (Figure 36) suggesting plastic deformation of the crystal structures. Mosaics similar to these have not been recognized in the absence of stylolites.

3.5.2 DEDOLOMITE TEXTURES

As well as recrystallization textures, dolomite crystals are found showing dedolomite textures adjacent to stylolites. Dedolomitization is the replacement of dolomite by calcite. It is seen in these samples as the replacement of the dolomite core and partial corrosion of the crystal boundaries (Figure 37). Crystals susceptible to calcitization are both matrix-replacement and cement crystals in the immediate vicinity of stylolites, or those millimetres away. There is a general pattern of intense dedolomitization nearest a stylolite but it is not uniform and does not decrease uniformly away from the seam. Dedolomite textures have not been recognized in the absence of stylolites.

3.5.3 NON-STYLOLITIC PRESSURE SOLUTION TEXTURE

It was said at the beginning of this section pervasive pressure solution is not recognized in these rocks. Other pressure solution features are recognized that are non-stylolitic nor do they resemble a pervasive mode. These features are isolated examples of non-stylolitic

Figure 36 Photomicrograph of an undulatory mosaic of coarse dolomite crystals that occurs adjacent to a stylolite at top of photo. Cross polarized light. Magnification 40x. Scale bar = 200 microns.

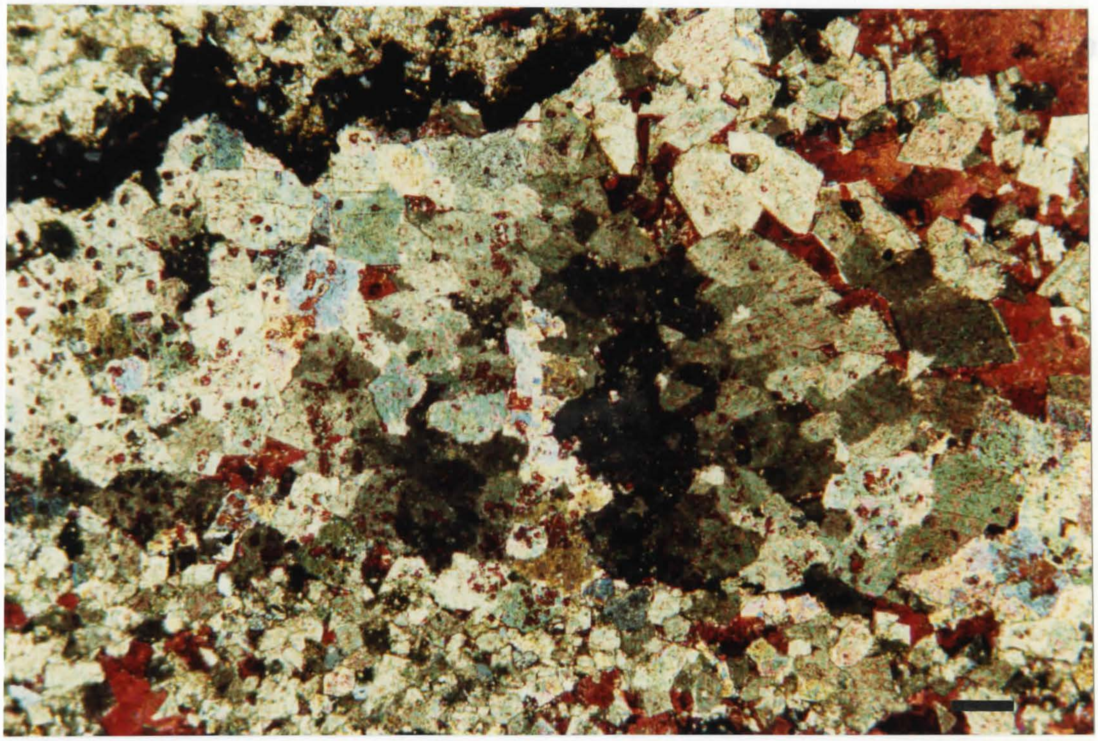

Figure 37 Photomicrograph of dedolomitization textures as seen in both cement and matrix dolomite crystals. Non-ferroan calcite replaces the cores of crystals. The outer boundary of dolomite crystals appear corroded as well. Plane polarized light. Magnification 100x. Scale bar = 100 microns.

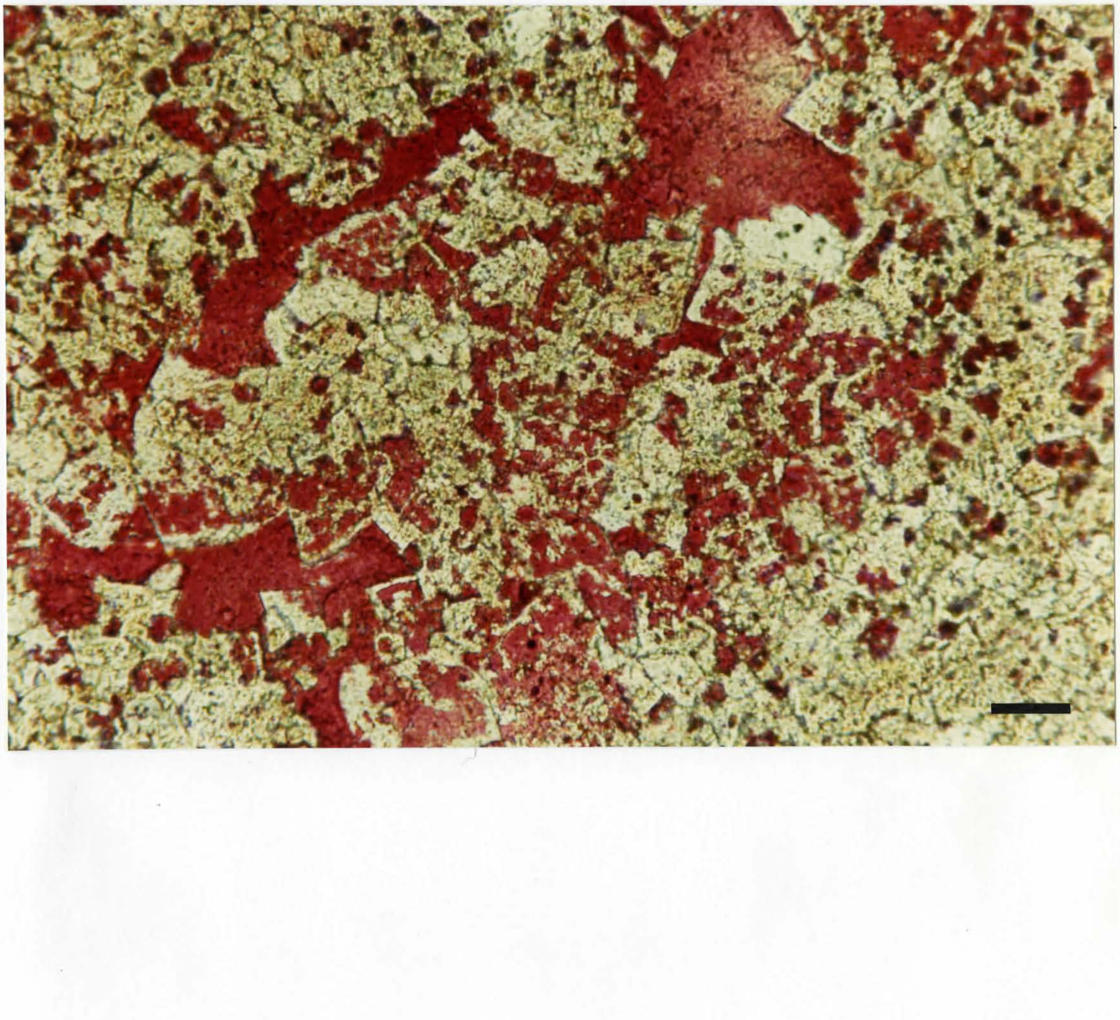

solution associated with individual or clusters of dolomite rhombs. For example, dolomite rhombs are seen penetrating original bioclastic particles in a distinctive pressure-dissolution fashion (Figure 38a). Along laminar concentrations of dolomite, a number of boundary dolomite rhombs are seen penetrating micritic matrix material (Figure 38b). The porosity created by a penetrating dolomite crystal suggests that the dolomite crystals involved were part of a rigid framework of crystals that responded to compactive pressures by dissolving the adjacent calcite. Similar non-stylolitic textures were not recognized associated with any calcite component.

3.5.4 STYLOLITE-DOLOMITE TEXTURAL RELATIONSHIPS

Microstylolites are not recognized in hand sample but can be found in thin section. They are not abundant as in the Lockport Formation examples, nor do they resemble them. These microstylolites are found associated with dolomite crystals. Usually a linear arrangement of dolomite defines the microstylolite. The smallest of these seams has only a few dolomite crystals along it and as they get bigger, more dolomite crystals are found (Figure 39a,39b). They can occur individually as in Figure 39 or in an anastomosed network associated with a stylolite (Figure

Figure 38 Photomicrographs of non-stylolitic pressure solution textures. 38a) Dolomite crystals that penetrate a skeletal particle. Plane polarized light. 38b) Dolomite crystals that have penetrated micritic matrix material. The penetrating action has created porosity behind the advancing crystals. Cross polarized light. Magnification 40x. Scale bar = 200 microns.

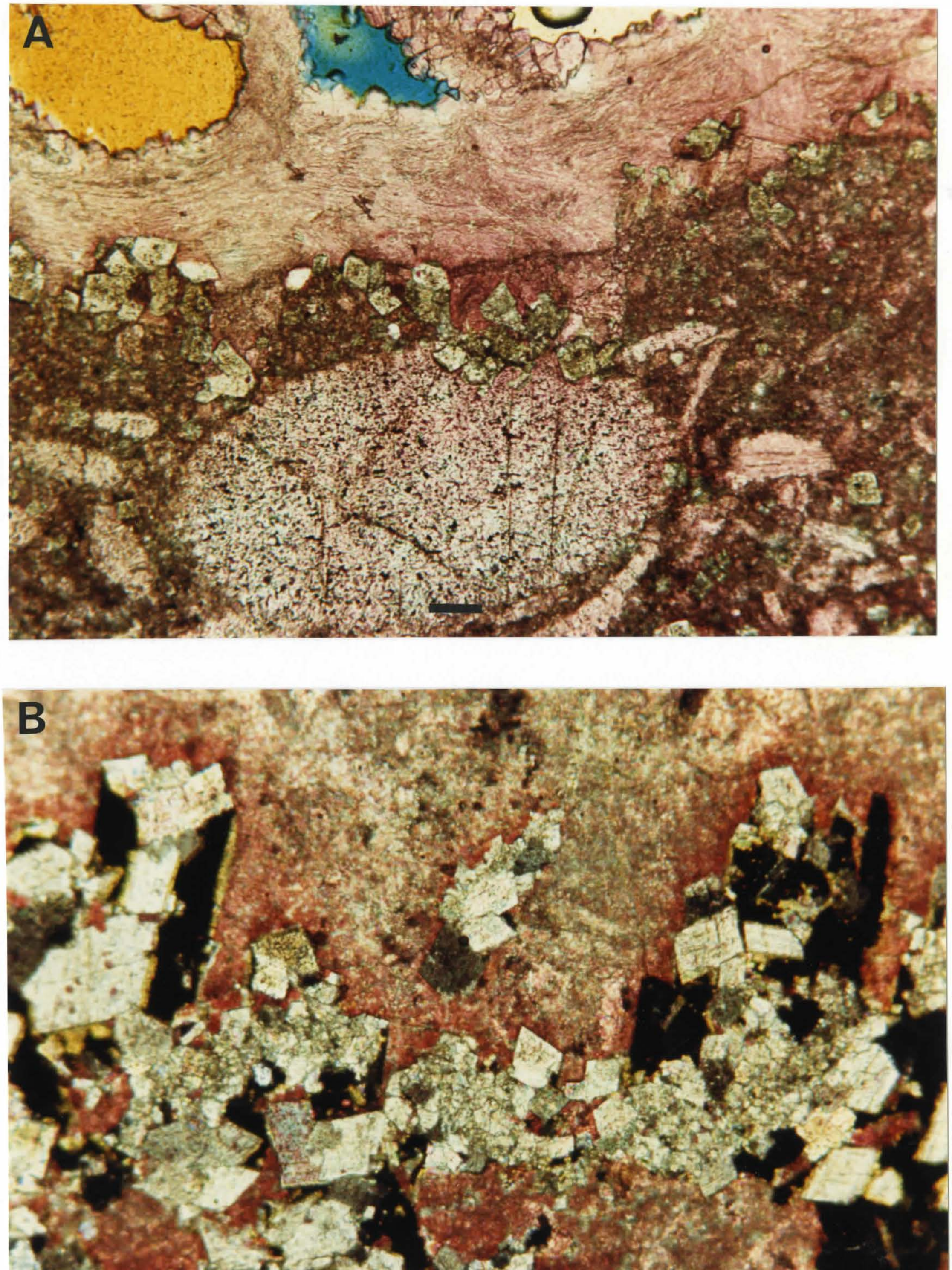
A
B

Figure 39 Photomicrographs of stylolite-dolomite relationships. 39a) A very small microstylolite that has very few dolomite crystals along its length. 39b) A larger microstylolite that has a greater number of dolomite crystals along its length. Plane polarized light. Magnification 40x. Scale bar = 200 microns.

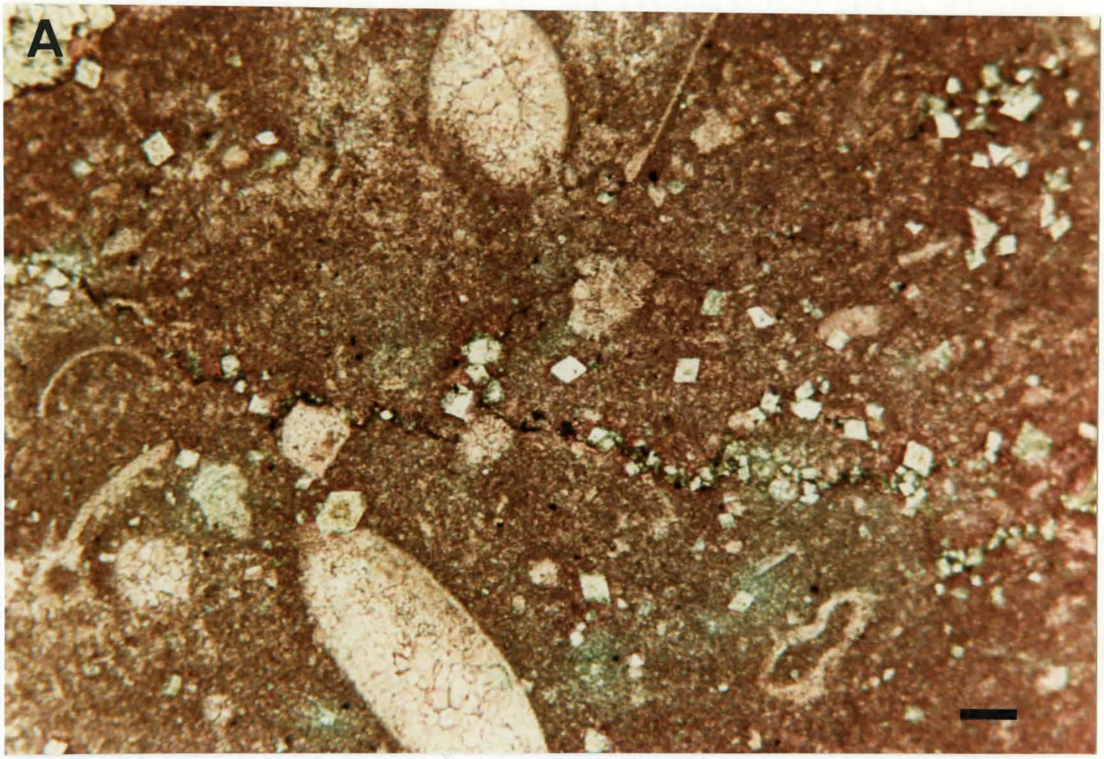
A

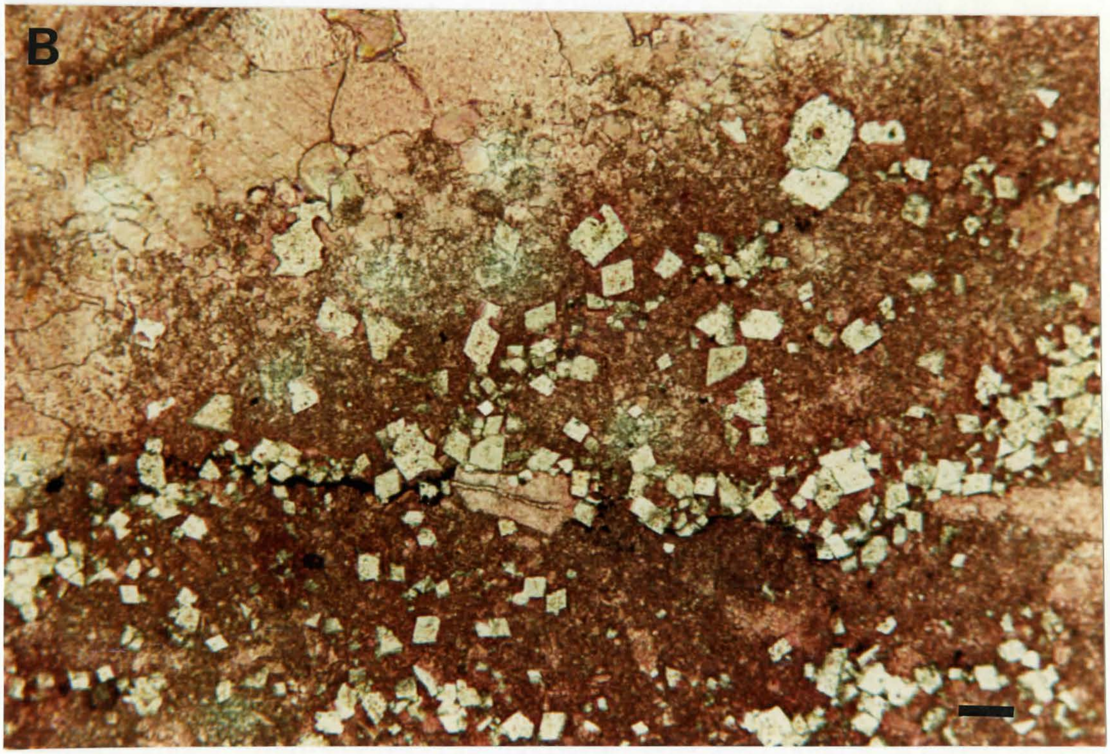
B

Figure 40 Photomicrograph of an anastomosed network of microstylolites associated with a micron-scale seam at top of photo. Microstylolites are defined by dolomite crystals along their length. Plane polarized light. Magnification 40x. Scale bar = 200 microns.

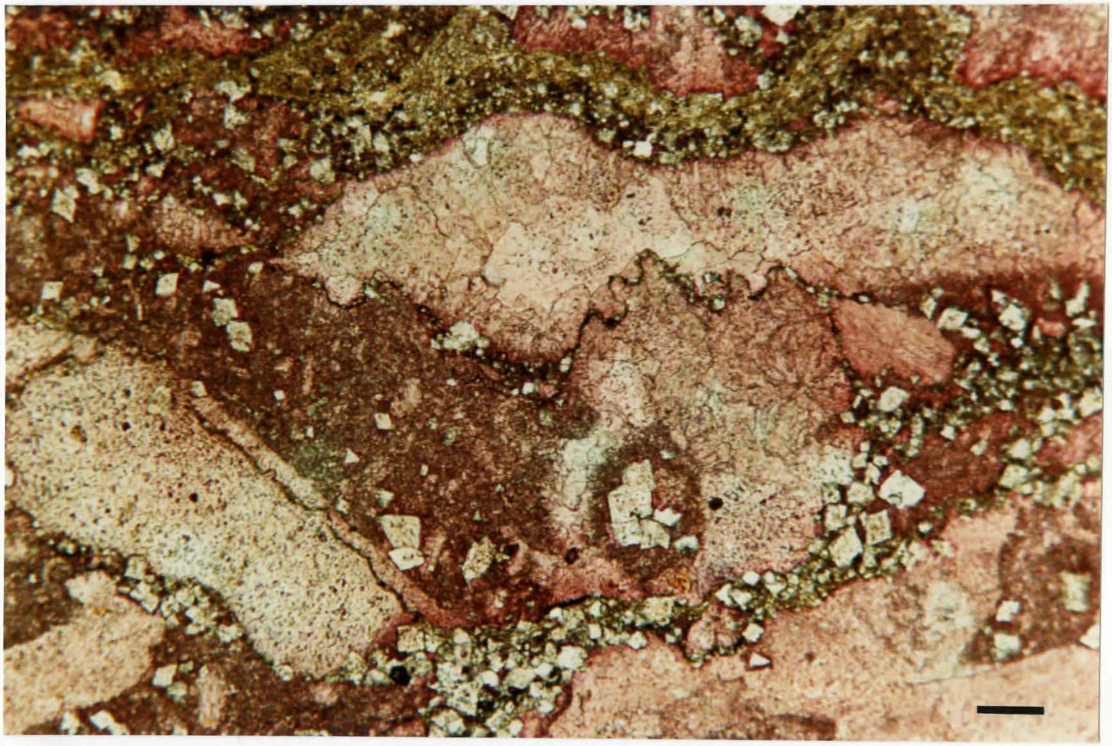

40). Microstylolites without dolomite along their length are not seen.

Micron-scale stylolites show similar dolomite relationships. These stylolites commonly occur at the edges of dolomite concentrations, suggesting a causative association, or they occur in dominantly dolomitic matrix (Figure 41a,41b). The dolomite along their length may make up all or part of the sutures or just cap them. In the most ideal examples, dolomite concentration decreases away from the stylolite and calcitic matrix material increases in abundance.

Similar relationships were observed with larger scale seams. The pattern of dolomite concentration is not as clear for these larger stylolites due to the complexity of the suturing, but dolomite is found capping and making-up integral parts of the sutures (Figure 42a,42b).

3.5.5 SUTURE MORPHOLOGIES

As recognized in hand sample, the larger a stylolite is, the more variable the suturing is. At micron-scale, stylolites may have a relatively simple peaked or very complex suturing (Figure 43a,43b). Along larger stylolites, the suturing may show signs of amalgamated stylolites incorporated into the main stylolite. The result is that the suturing may be even more complex or more simple (Figure

Figure 41 Photomicrographs of stylolite-dolomite relationships. 41a) Micron-scale seam that occurs at the edge of a concentration of dolomite crystals. 41b) Micron-scale seam that occurs in a dolomitic matrix with dolomite crystals on both sides of the seam. Plane polarized light. Magnification 16x. Scale bar = 2 mm.


A

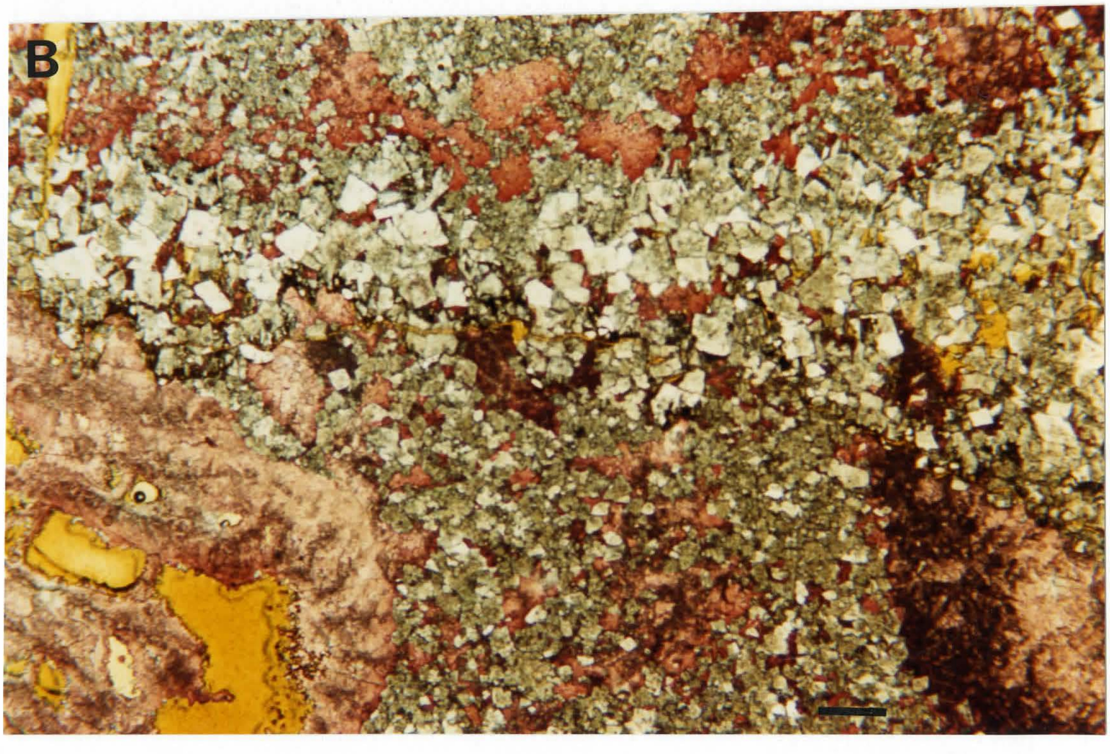
B

Figure 42 Close-up photographs of stylolite-dolomite relationships. 42a) Large scale stylolite that has dolomite crystals capping the top of its sutures. 42b) Large scale stylolite that has dolomite crystals in the bulk of the suture interiors. Scale bar = 1 cm.

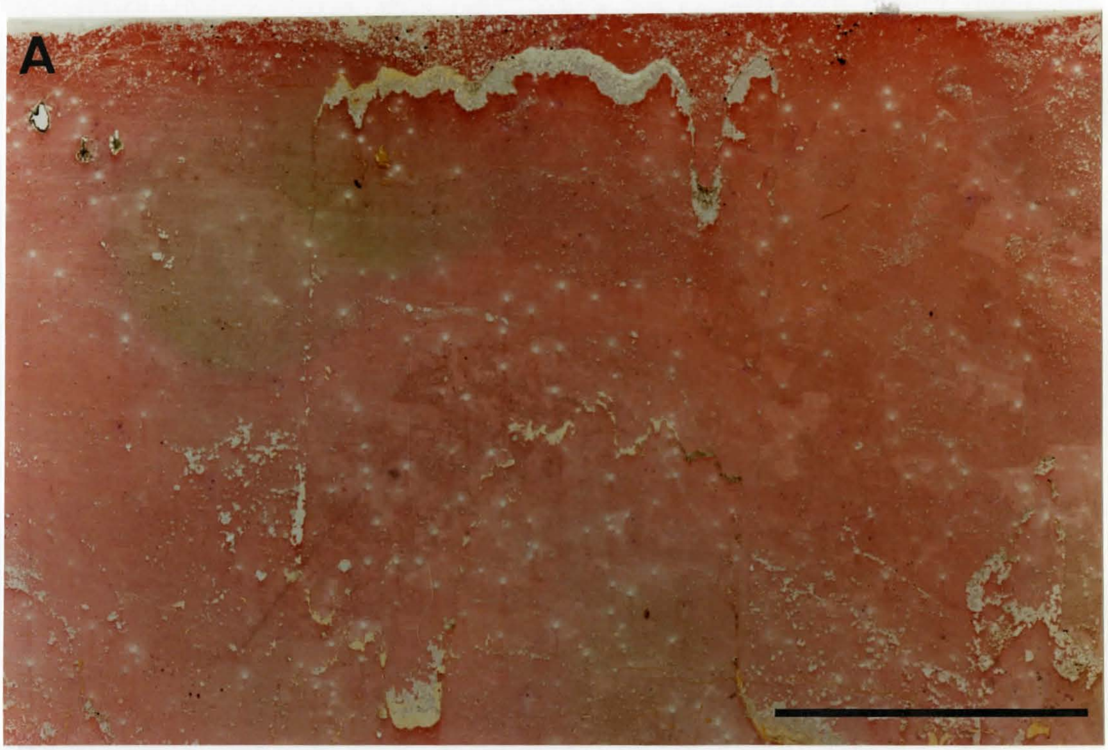
A

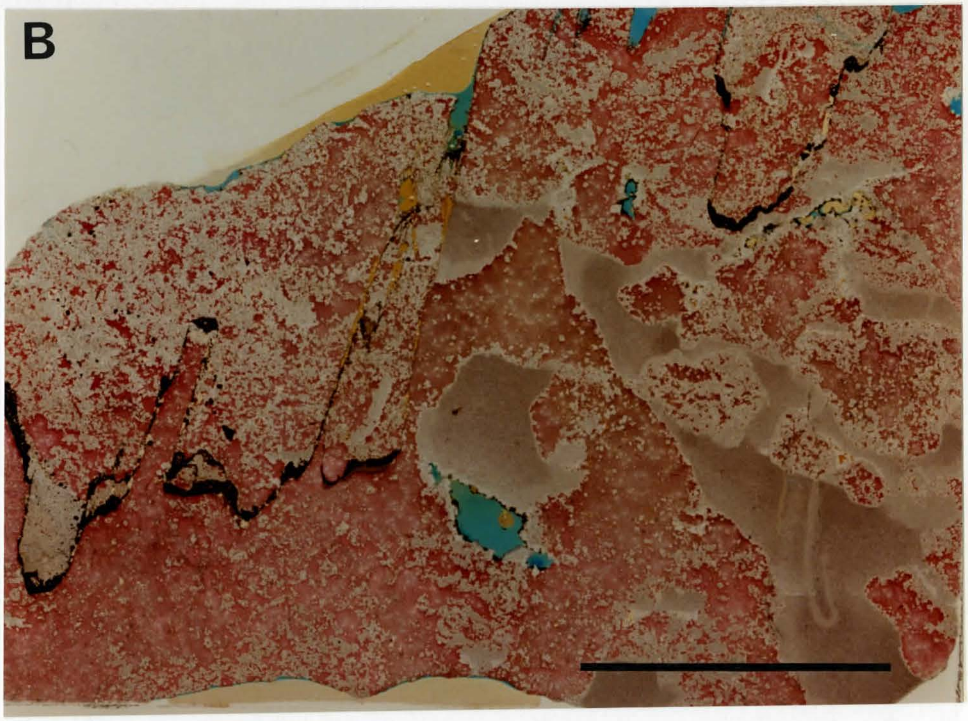
B

Figure 43 Photomicrographs of stylolite suture morphologies. 43a) Micron-scale stylolite that shows a simple peaked suture morphology. 43b) Micron-scale stylolite that shows a complex peaked suture morphology. Plane polarized light. Magnification 40x. Scale bar = 200 microns.

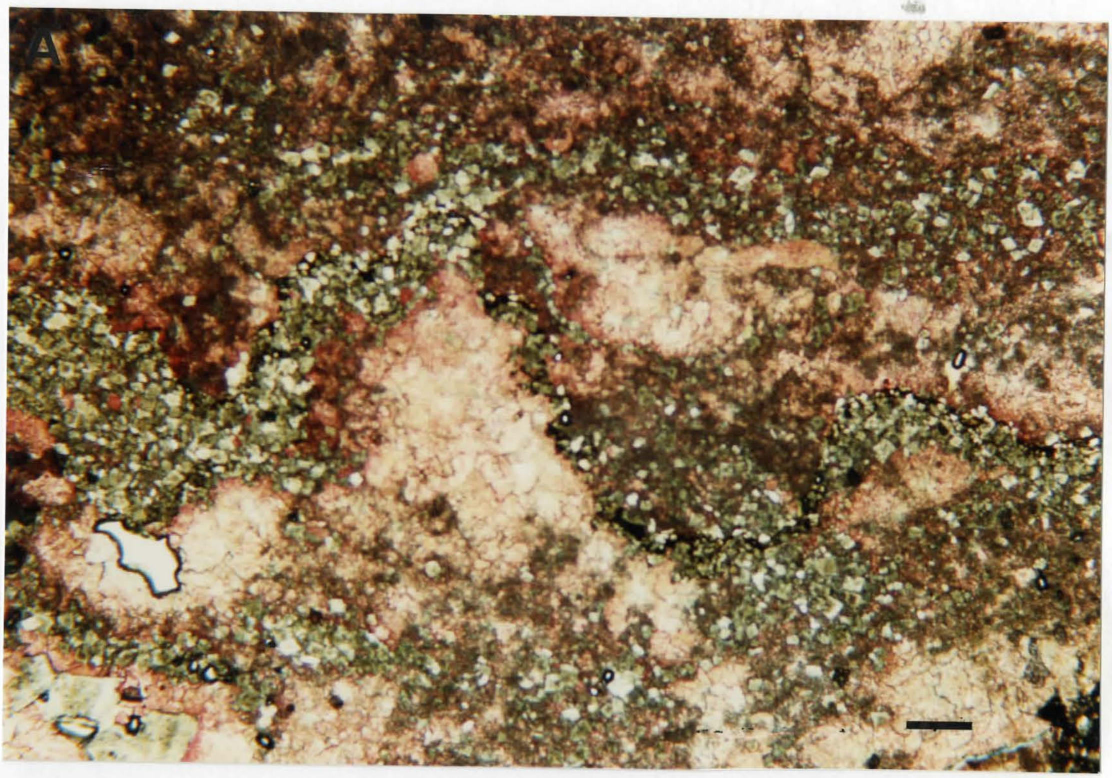
A

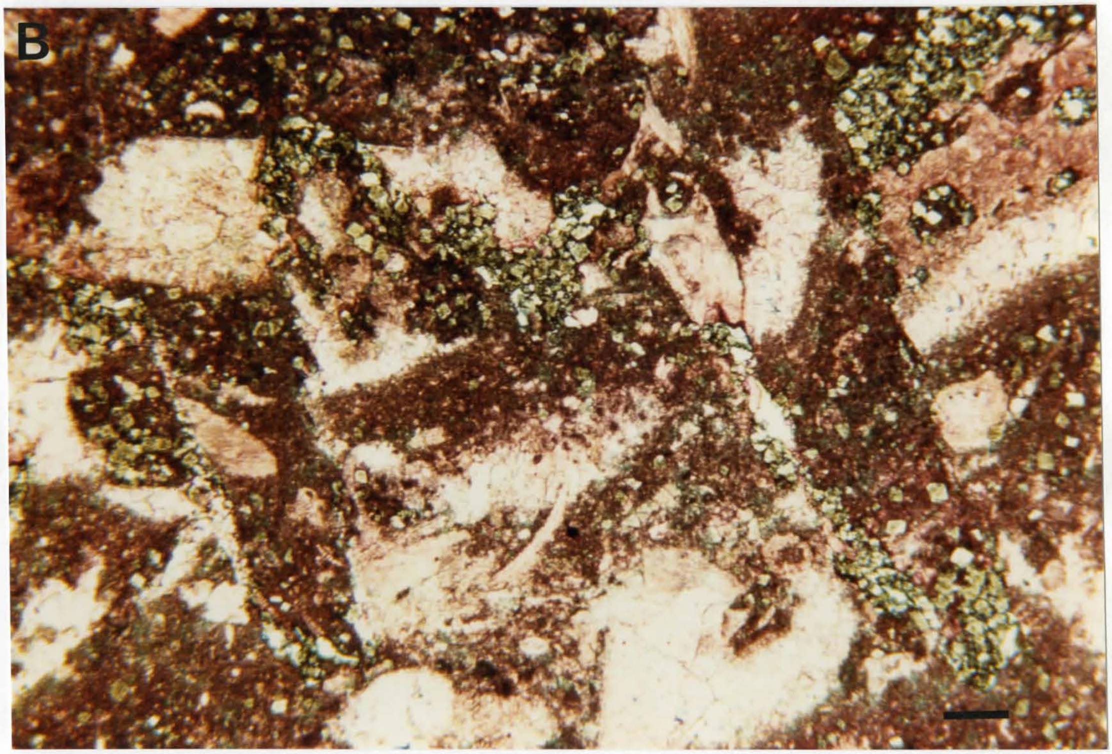
B

Figure 44 Close-up photographs of stylolite suture morphologies. 44a) Large scale stylolite that shows a complex suture morphology suggestive of amalgamation. 44b) Large scale stylolite that shows a simple suture morphology suggestive of amalgamation. Note the "islands" of dolomite included in the seam material. Scale bar = 1 cm.

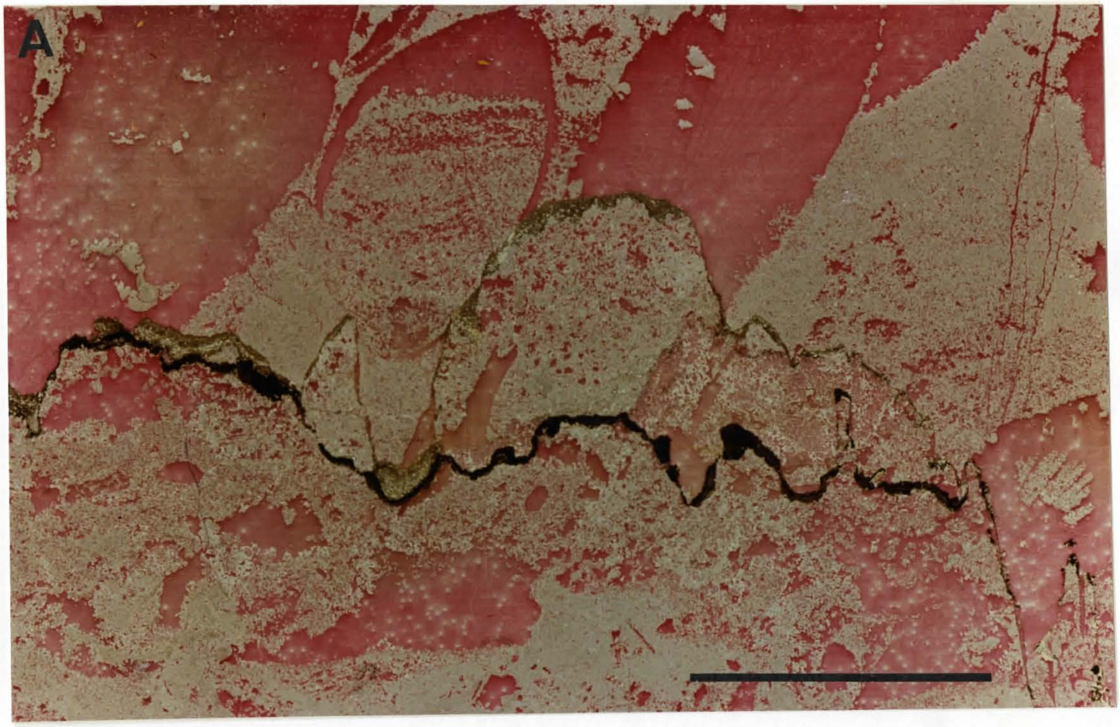
A

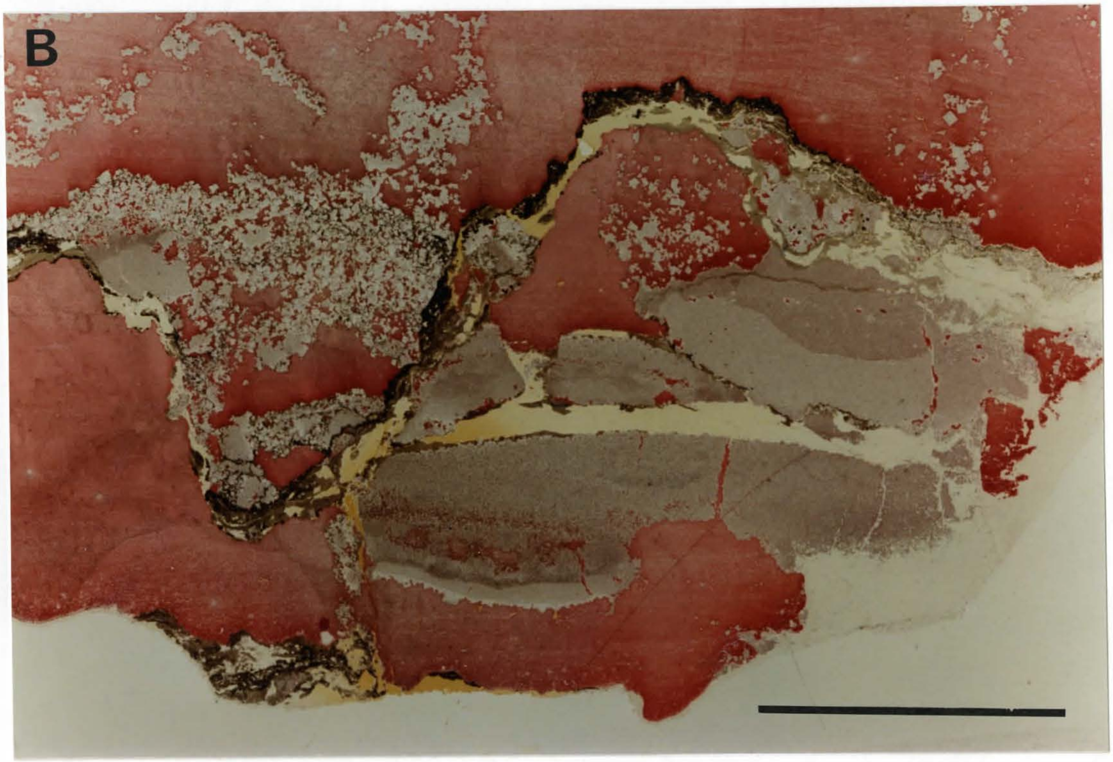
B

44a,44b). The resultant morphology of the stylolite appears to be dependent upon the phase relationships of an amalgamation mechanism.

Complex suturing of stylolites seems to have concentrations of insoluble material capping the individual sutures and thinned-to-minimal concentrations of insolubles along the limbs (Figure 45). This thinning is not characteristic of any particular scale of stylolite. It is found in micron- through centimetre-scale seams, but is more common in centimetre-scale seams that display complex-columnar suturing.

Dolomite appears to have contributed to the development of sutures. Dolomite crystals can be found at the edges of sutures in positions that suggest that through pressure solution, they have sheared the socket walls of the suture. Along the limbs, the result is seen as planar socket walls, thinned insoluble material accumulations, and created porosity (Figure 46a). Where they occur at the tip of a suture they may create an even more complex suture (Figure 46b). These features are more typical of larger stylolites, with deep penetrating sutures.

The bridged structure described in the preceding section can similarly be attributed to dolomite concentrations. These bridging stylolites commonly occur at the edge of laminar dolomite concentrations in suture interiors

Figure 45 Close-up photograph of a sutured stylolite that displays thinned insoluble material along suture limbs and thick accumulations capping the sutures. Note the porosity where the socket has separated from the suture, and calcite has begun to infill. Scale bar = 1 cm.

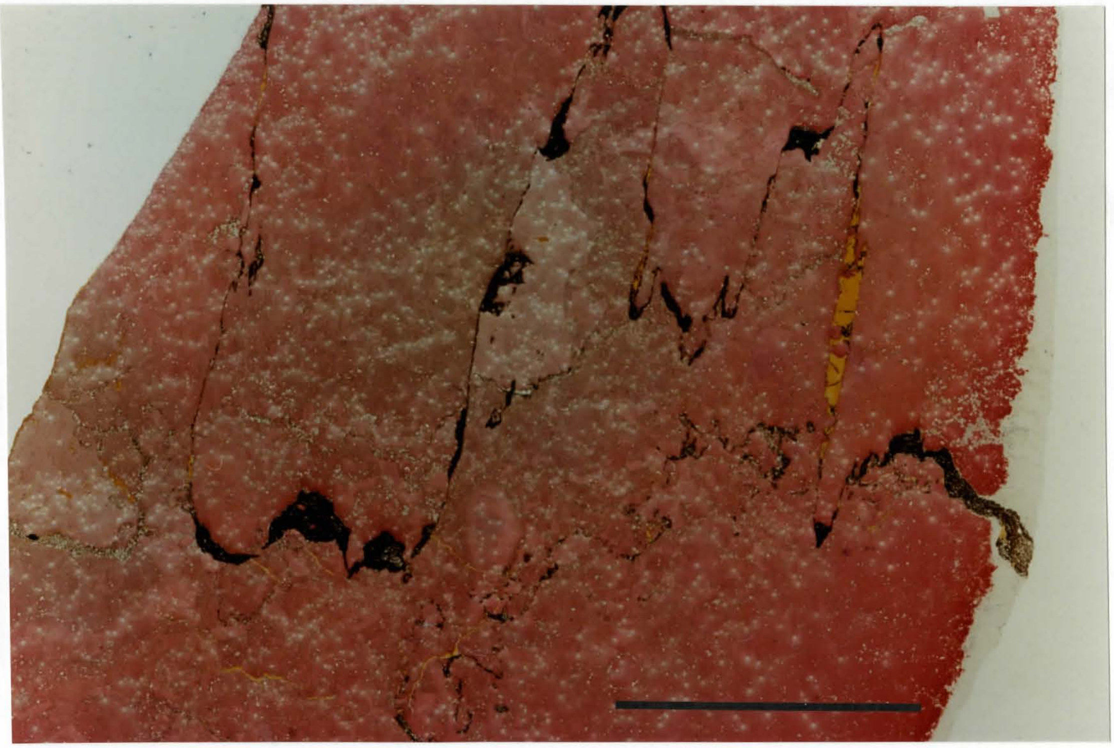

Figure 46 Photomicrographs of suture morphologies that have been altered by dolomite crystals. 46a) Dolomite crystals that have sheared the socket walls and created porosity. Plane polarized light. Magnification 40x. Scale bar = 200 microns. 46b) Dolomite crystals at the top of a suture that penetrate deeply, resulting in a more complex suture. Plane polarized light. Magnification 16x. Scale bar = 2 mm.

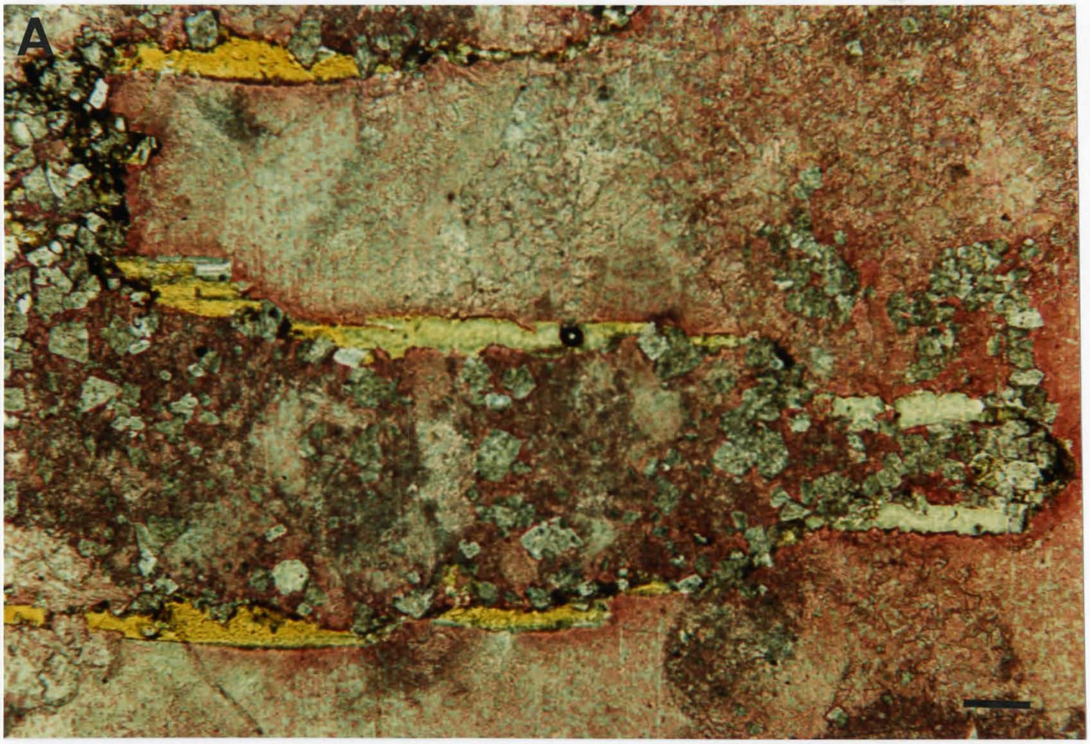
A


B

(Figure 47a). They cannot be correlated between sutures and are difficult to explain by an amalgamation mechanism.

Occasionally, where dolomite concentrations are low, very irregular pressure solution textures are found within large sutures (Figure 47b). These features are not stylolites but pressure-dissolved particles and cements. The cause of this dissolution can be related to dolomite crystals and detrital grains that penetrate the particle. Both this texture and the bridged structure are seen as a secondary response to pressure solution as the result of built-up stresses localized about the main stylolite.

3.5.6 STYLOLITE TERMINATIONS

Only the terminations of microstylolites and micron-scale stylolites could be observed. Where seen, the associated stylolite always had dolomite along its length. These stylolites terminate in two ways. Where dolomite abundances are low, the stylolite terminated abruptly into the matrix. It did not fan outwards into a "horsetail" feature similar to those seen in the Lockport Formation (Figure 48a). Where dolomite abundances were higher, the stylolite terminated outwards into a dolomite concentration, sometimes abruptly or sometimes resembling a fan-like array of dolomite crystals (Figure 48b). Microstylolites were not observed propagating from these features.

Figure 47 Close-up photographs of stylolite-related pressure solution features. 47a) Bridging micron-scale stylolite that occurs at the edge of a laminar dolomite concentration (arrows). 47b) Non-stylolitic irregular pressure solution features in which dolomite crystals penetrate matrix cements. A bridging stylolite is seen proximal to these features. Scale bar = 1 cm.

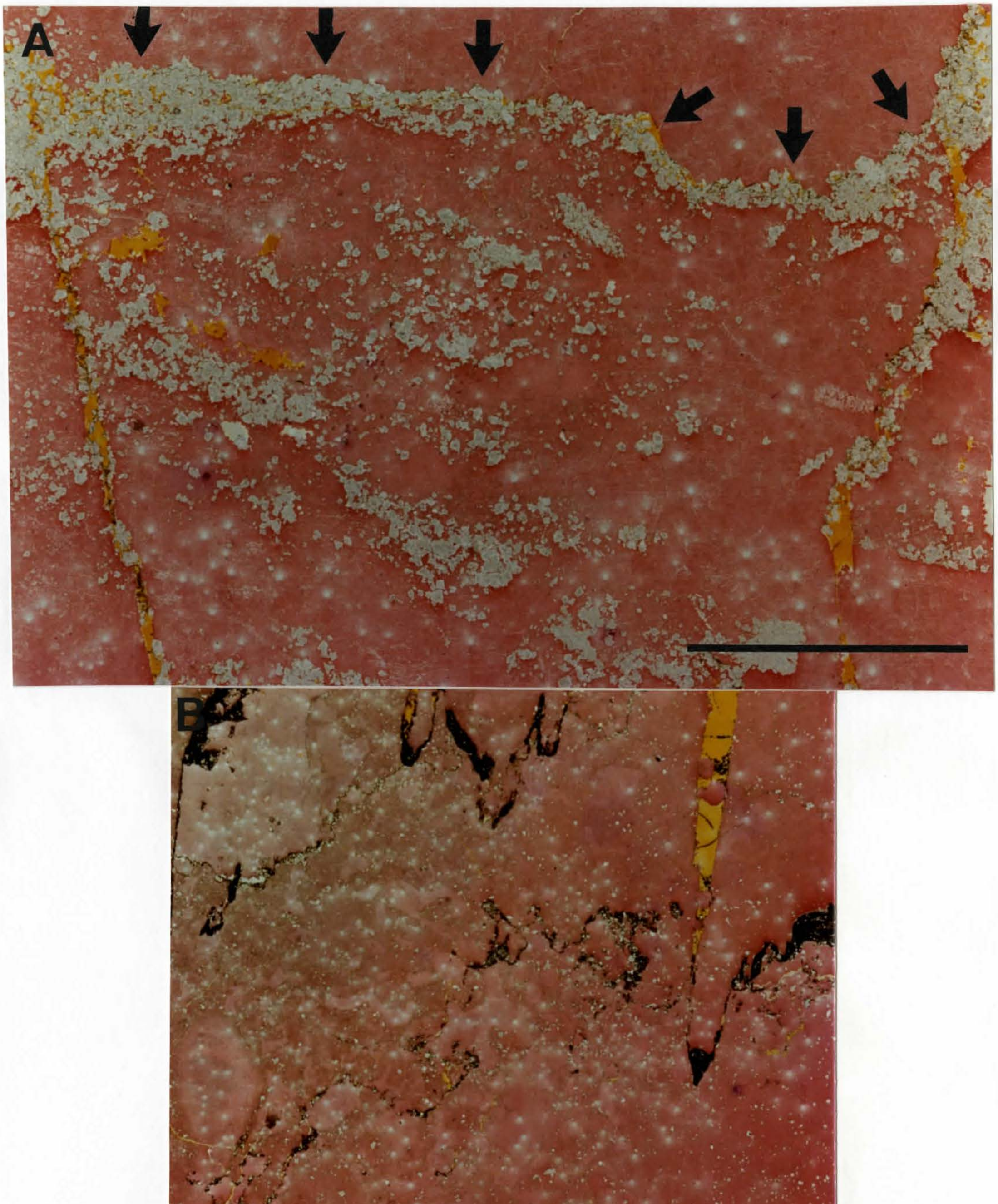
A
B

Figure 48 48a) Photomicrograph of a micron-scale stylolite (marked by arrows) that terminates abruptly into dolomitic matrix. Plane polarized light. Magnification 16x. Scale bar = 2 mm. 48b) Close-up photograph of a large micron-scale stylolite that terminates at a fan-like array of dolomite crystals. Scale bar = 1 cm.

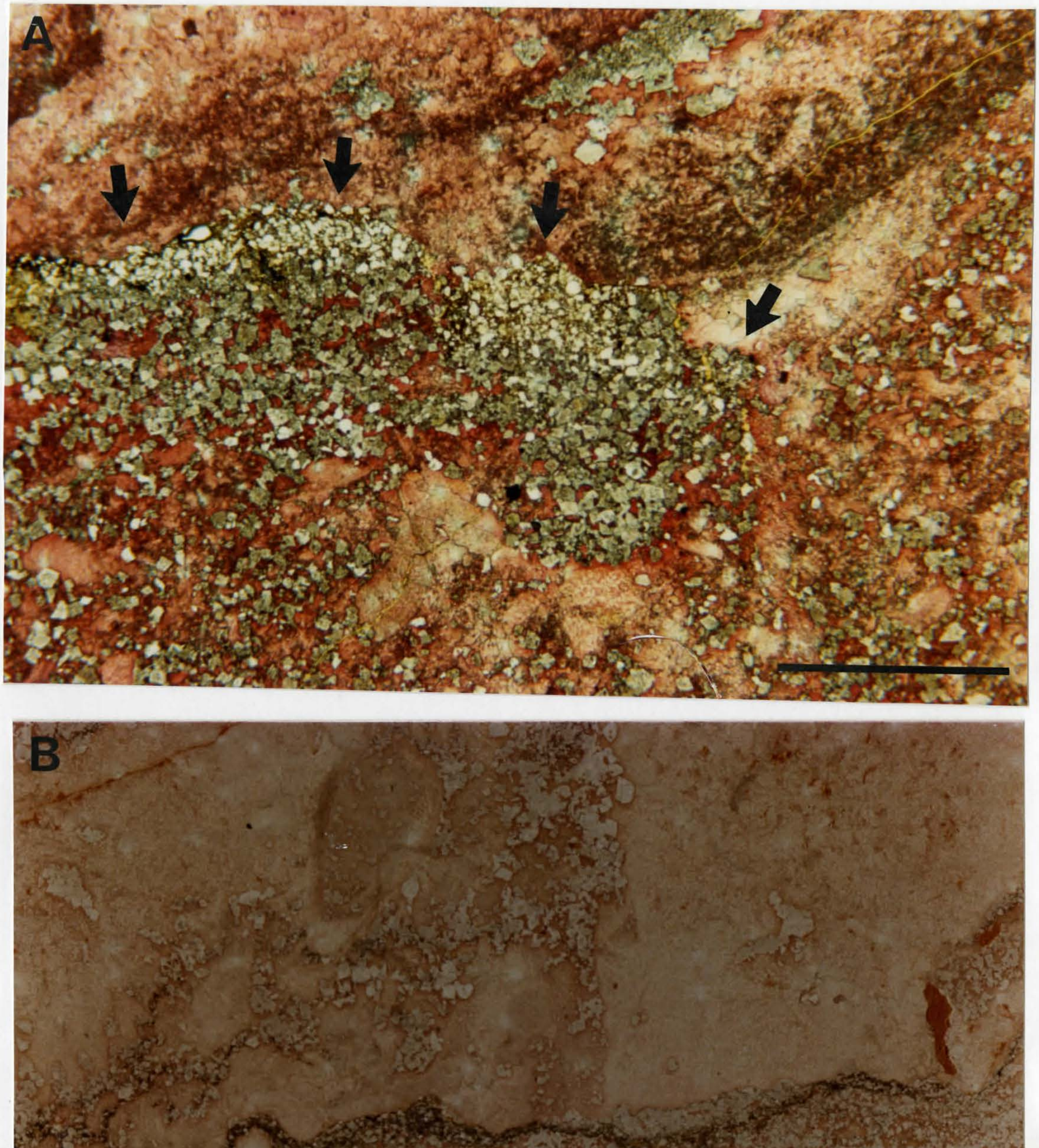
A
B

3.6 STYLOLITE DEVELOPMENT:DOLOMITIZATION-STYLOLITIZATION

Interpretation of stylolite morphology, neomorphic textures, and dolomite associations has lead to the development of a "model" for stylolite formation that is genetically related to dolomite occurrence. This "model" is an extension of work already done by Schofield (1984) who proposed that neomorphism is a response to greater differential stresses, brought about by dolomitization, that may ultimately result in non-seam pressure solution.

In this case, stylolitization is seen as the response to stress perturbations caused by clusters and concentrations of dolomite crystals. Once initiated, growth proceeds by dissolution at the sockets on both sides of the stylolite. There is no adolescent stage analogy in this model. Amalgamation does occur, but this is amalgamation of "adult" stylolites, not amalgamation to form the stylolite. For these reasons, dolomitization-stylolitization should not be thought of a occurring stages. It would be better to think of this mechanism as developing continuously.

As in the preceding chapter, it is assumed that greater thicknesses and larger amplitudes are indicative of the degree of stylolite development.

3.6.1 DOLOMITE AS A STRESS PERTURBATION

The lack of pressure solution textures in the inter-stylolitic domain of the rock suggests that pressure solution was activated along discrete planes. Bathurst (1980) states that activation of the process is dependent upon "inhomogeneities in the distribution of stresses in the solid phase". Commonly, investigators into the pressure solution phenomenon relate stress inhomogeneities to bedding contacts, early diagenetic nodules, burrow, or large allochem fragments. When features such as these are lacking, causes such as grain contacts, clay occurrences, and organic layers are invoked.

None of these features other than bedding contacts were observed showing causative association with stylolites. This suggests that some other factor influenced the distribution of stress in the beds of these rocks. As in Schofield (1984), it is proposed that dolomite will provide the necessary anomaly to stylolitize the interior of beds.

Schofields' (1984) reasoning for this proposal is based upon theoretical analyses of stress and strain patterns developed around inhomogeneities in a previously homogeneous medium. The work of Shimamoto (1975) and Selkman (1983) show that stress and strain "shadows" are developed around crystalline inhomogeneities within the surrounding less resistant media. These "shadows" are limited to one to three particle diameters of the anisotropy. In theory, this demonstrates that a crystalline inhomogeneity introduced into a previously homogeneous medium could lead to increased stresses "conducive to the initiation of pressure solution" (Schofield 1984). This conclusion, though, is based upon materials of highly contrasting physical properties that produce large, easily measured effects.

More applicable, in terms of material contrasts and the absence of directed stresses, is the study of porphyroblast growth in regionally and thermally metamorphosed rocks (Ferguson et al. 1972). These authors state that conditions suitable for the initiation of pressure solution may be found in the compressibility differences between a porphyroblast and its surrounding matrix. At metamorphic conditions, those mechanical differences will be dissipated through permanent creep deformation. Similarly, these increased stresses diminish within two particle-diameters of the porphyroblast. This work, and that of Shimamoto (1975) and Selkman (1983) are for metamorphic conditions. Hence, these results are not directly analagous to those for burial diagenetic conditions.

Schofield (1984) believes that the mechanical contrast between dolomite and calcite can be as great as that between a porphyroblast and its matrix. Citing the lists of Wuerker (1962) for the mechanical properties of dolostones and limestones, Schofield (1984) states that "there is indeed a fairly considerable contrast between dolomite and limestone". Assuming that the mechanical properties of the rock are equivalent to those of the minerals, dolomite would create the necessary stress inhomogeneity to promote pressure solution in a limestone.

In support of this is the experimental work of Rutter (1976), who shows that the most likely mode of deformation for crystals 100 microns in diameter, bathed in a fluid phase, is pressure solution. At lower diagenetic temperatures, creep deformation is only viable at large grain-sizes.

Thus, dolomitization of a limestone should cause local perturbations in the stress field. Individual dolomite crystals and small clusters of crystals would not result in significant perturbations. As dolomite abundances increase, the inhomogeneity will become more significant such that Schofield (1984) envisages three stages of deformation as the degree of dolomitization increases and the anisotropy developed becomes greater.

Increasing stress around growing dolomite crystal-clusters enhances the probability that calcite will pass into solution along a migrating dissolution front, but will retain its chemical composition despite repeated solution and reprecipitation. With continued dolomitization, the anisotropy increases and the calcite will lose its chemical identity due to increased neomorphism and the migration of ions passed into solution along the dissolution front being precipitated elsewhere. Before the amalgamation of dolomite crystals to form a "framework", the increased differential stresses about dolomite concentrations will result in movement out of the neomorphism field, into that of pressure solution. This requires the movement of dissolved material out of the immediate vicinity of be precipitated elsewhere.

3.6.2 INITIAL RESPONSE TO PRESSURE SOLUTION

To understand how a partially-dolomitized limestone responds to pressure solution it seems logical to look at the smallest pressure solution features. It is assumed that because these features are the smallest and contain the least accumulated insoluble materials, they represent the beginning stages of pressure solution. For these reasons, the initial response to pressure solution is seen as dissolution at abrupt boundaries (Figure 38a) between dolomite concentrations and matrix micrite and allochems. It can also be seen as penetration of allochems by individual or small clusters of dolomite crystals (Figure 38b) and the formation of microstylolites along microscopic linear/planar arrangements of dolomite crystals (Figure 39a). For each case, calcite is preferentially dissolved (due to its greater solubility) and dolomite remains as an "insoluble residue".

The mechanism by which these features form is simple pressure-dissolution about a stress inhomogeneity, with dolomite acting as the anomaly (Figure 49). The presence of microspar as well as random luminescent patterns of the matrix micrite and microfossils suggests that this style of pressure solution proceeds by a mechanism similar to that of neomorphism, but enhanced by dolomite and more extreme. Due to anisotropies caused by dolomite concentrations, the limestone responds to stress by dissolution at these sites. The solute is then transported by thin fluid films away from the site of dissolution and precipitated elsewhere.

Maintenance of this transport system over a wide area may be difficult, as diffusion is extremely slow and saturation is quickly achieved. In the absence of an open pore system, transport by diffusion is viable only over small distances. Even with the enhanced efficiency of diffusion at depths it poses a major problem (Pingitore 1982) which may explain why some pressure solution features are extremely small and never well-developed.

Figure 49 Schematic representation of the initial response to pressure solution. Stage I: before the onset of pressure solution, burial conditions promote the development of stress shadows about clusters of dolomite crystals. Stage II: due to the stresses induced by dolomite crystals, the matrix responds by non-seam solution. Porosity may be created by the advance of a framework supported crystal (shown as black zones behind the advancing crystal). Though the microfossil is now closer to the dolomite cluster, non-seam solution can not be detected in the absence of created porosity. Stage III: continued non-seam solution is recognizable by created porosity and penetration of microfossil by dolomite rhomb.

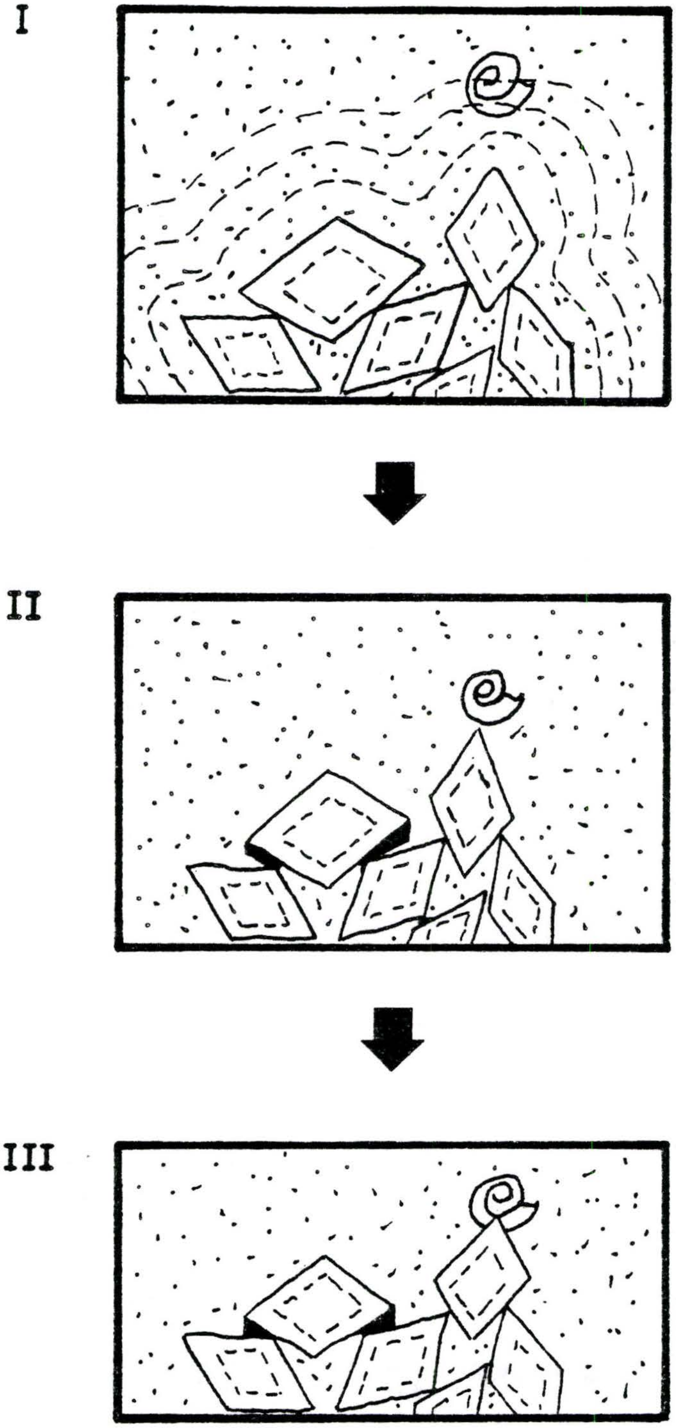
I
II
III

These problems may be overcome by the emergence of the thin fluid film into an open pore system where ionic transfer by fluid flow could efficiently dispose of the solute elsewhere (Schofield 1984, Pingitore 1982). A transport mechanism such as this is necessary to the development of stylolites.

3.6.3 STYLOLITE EVOLUTION-GROWTH IN THE DIRECTION OF SHORTENING

The transition from the initial response to stylolite formation follows naturally with continued pressure solution about stress perturbations. Along abrupt boundaries between dolomite concentrations and matrix carbonate, continued pressure solution will result in a dissolution surface with accumulated insoluble residues that mimic the topography of the dolomite "front" (Figure 50). This would now be a micron-scale stylolite similar to that shown in Figure 41a.

Where dolomite does not form an abrupt boundary with the matrix a stylolite must form by propagation of the dissolution surface(s) along a widespread inhomogeneity in the rock. For example; this may be a concentration of macro-fossils, early diagenetic nodules, of a bedding surface. Or, it may be in zones which lack extensive early cementation, where stress inhomogeneities may arise adjacent

Figure 50 Schematic representation the formation of a stylolite at an abrupt dolomite boundary. Stage I: no pressure solution. Stage II: non-seam pressure solution response results in accumulation of insoluble materials at the dolomite "front" through pressure-dissolution of matrix calcite. The microfossil is closer to the dolomite concentration. Stage III: continued pressure solution accumulates sufficient insoluble materials that form the stylolite. The stylolite formed mimics the topography of the dolomite "front". Through pressure-dissolution at this site the microfossil is even closer to the stylolite now formed.

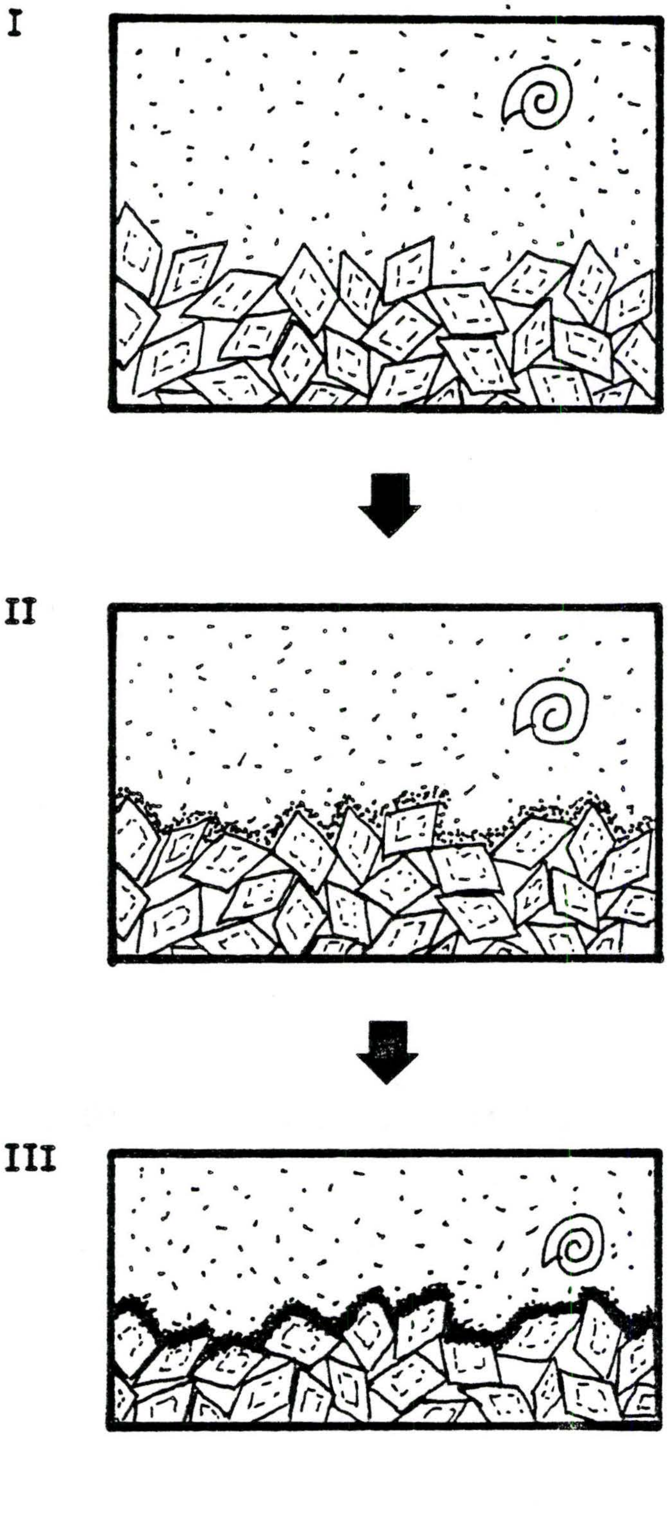
I
II
III

to grain contacts of poorly-cemented particles. Not to be ruled out as possible inhomogeneities are lesser abundances of dolomite that do not form abrupt boundaries but are still abundant enough to pose as a stress perturbation. Stylolites may also form by the amalgamation of microstylolites that occur in an anastomosed network through the same mechanism as in the Lockport Formation (Figure 51a,51b).

Once formed, a stylolites' topography is determined (as it grows) by minor local variations in the degree of cementation of the sediment, minor solubility differences between allochems and matrix, and the nature and amount of residue (Schofield 1984). In these samples, dolomite constitutes an insoluble residue such that calcite is being preferentially dissolved and dolomite accumulates at the stylolite surface. When the stylolites are small their suturing closely follows the pattern of dolomite occurrence (Figure 41). As stylolites get larger, dolomite crystals are found showing evidence of having sheared the socket walls and penetrated deeper into the socket than the suture itself (Figure 46).

The only possible explanation for the presence of these crystals is that they were included in the seam material as an insoluble residue. The sheared and penetration textures are evidence that they formed as a result of active pressure solution and that they have made significant

Figure 51 Schematic representations of stylolite formation by alternative dolomitic associations. 51a) Stage I: dolomite clusters in micritic matrix. No pressure solution. Stage II: non-seam solution induced by the clusters begins to accumulate insoluble materials at the sites of material removal. Stage III: continued pressure-dissolution at the clusters results in extension of the solution surface to form a continuous surface, the stylolite. Through this process the initial topography of the stylolite is determined. 51b) Stage I: low abundances of dolomite crystals in micritic matrix. No pressure solution. Stage II: non-seam solution response about individual crystals results in microstylolite formation by extension of the solution surface beyond individual crystals to form continuous surfaces represented by insoluble material accumulation. Stage III: continued pressure-dissolution at the microstylolite surfaces results in the amalgamation of two seams by removal of intervening matrix material.

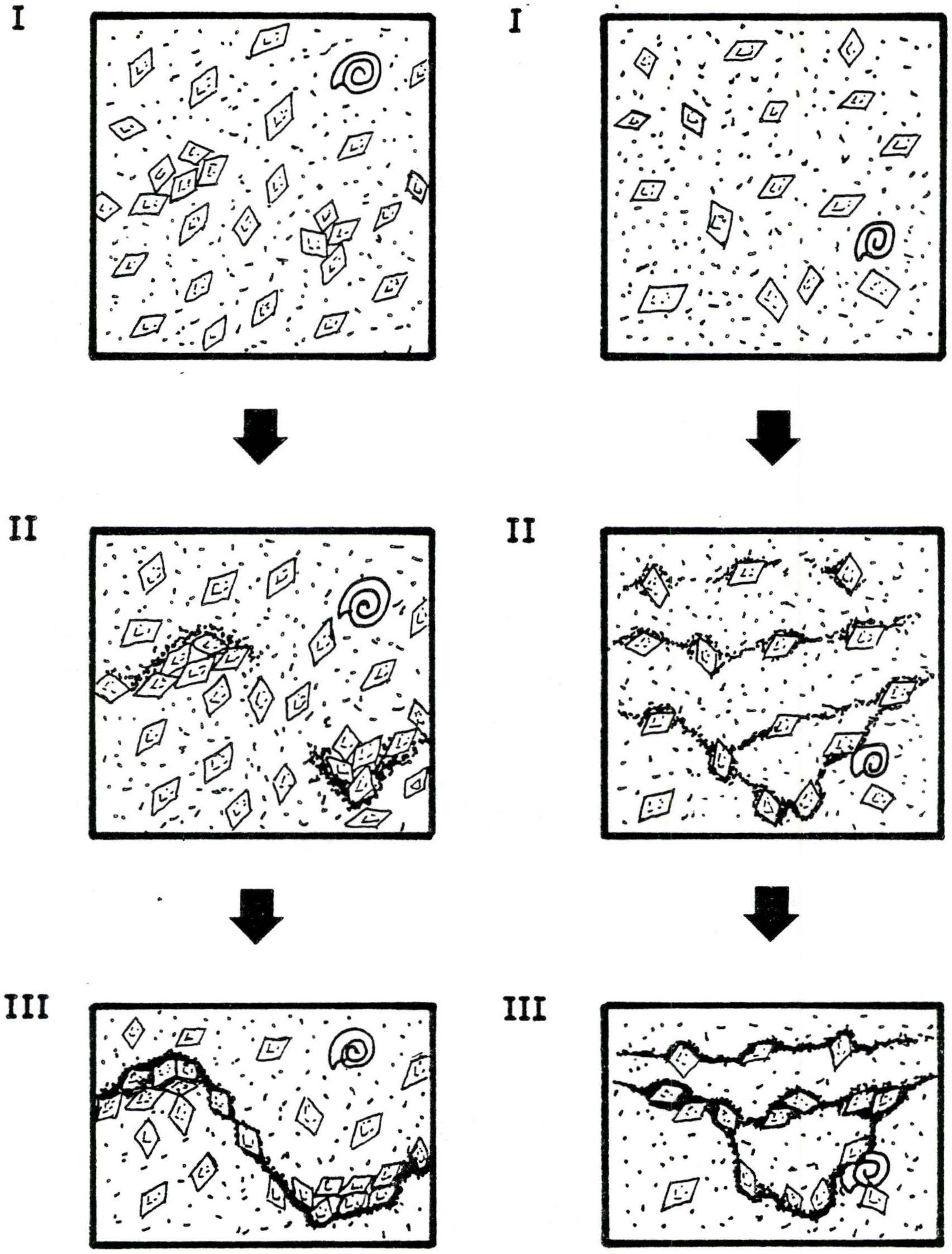
I
I
II
II
III
III

contributions to the morphology of the stylolites (Figure 52).

As stylolites become larger, rather than being accumulated along the length of seams, dolomite is sometimes found capping or in the interior of a suture (Figure 42). Generally, it is observed that these sutures penetrated deeper relative to others in the immediate vicinity that lack abundant dolomite. This suggests that because of the presence of dolomite these sutures were able to penetrate deeper than the others.

Following suggestions made by Schofield (1984), it is believed the presence of dolomite along a stylolite may provide and/or help maintain the anisotropy necessary for the growth of a stylolite. This is not to say that dolomite is the main contributor to the morphology of a stylolite. It is believed in the early stages of stylolitization, because dolomite is the "trigger", the morphology of the "young" stylolite is strongly influenced by dolomite concentrations. As stylolites get larger, a departure from this pattern is seen such that dolomite associations are more difficult to recognize. This suggests that other factors are influencing the stylolites' growth. For example, there may be a change in the degree of cementation or differential solubility of the material being dissolved

Figure 52 Schematic representation of dolomite crystals altering the morphology of a suture through inclusion in the seam material. Stage I: simple sutured stylolite with dolomite crystals in the sutures in a dolomitic matrix. Stage II: continued growth by pressure-dissolution of the sockets results in larger sutures and inclusion of dolomite crystals at tops and along limbs of sutures. Stage III: continued growth results in shearing of socket wall by dolomite crystals, creating porosity, and a change from peaked to columnar suture morphology.

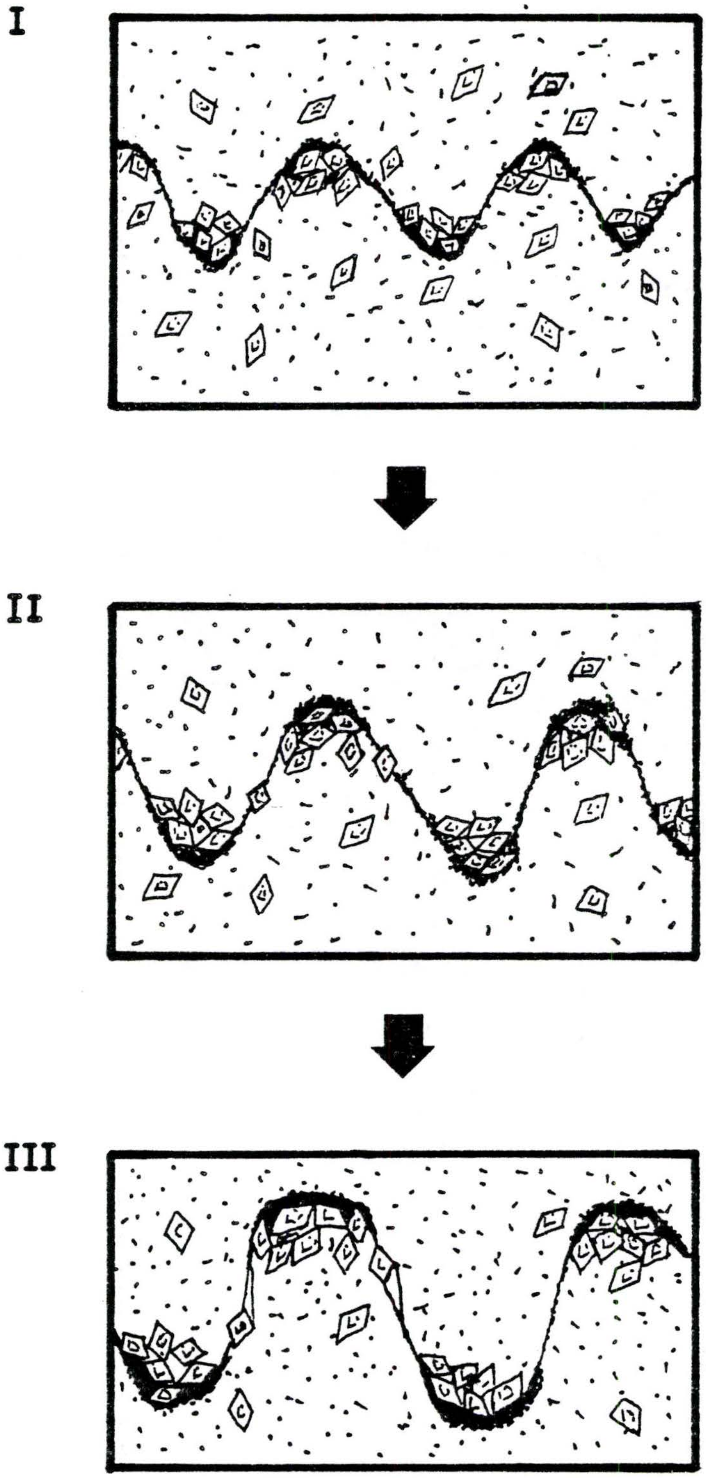
I
II
III

that enhances or inhibits pressure solution, the result being a change in growth.

For dolomitization-stylolitization, the growth of a stylolite is envisaged to be as follows: incipient stylolites form along matrix/allochem contacts with some type of dolomite concentration (clusters, laminae, etc..). Early in the development of the stylolite, its morphology is strongly influenced by the dolomite. For example, a stylolite formed at a laminar dolomite and micrite contact would essentially be straight. Those found in lower abundances of dolomite of variable concentrations would be expected to be highly irregular.

As the stylolite grows, it accumulates more dolomite, its amplitude gets greater, the frequency of sutures becomes less, and new material is available to be dissolved at the stylolite surface. Accummulation of more dolomite is beneficial to the stylolite as it results in larger stress perturbations localized at the stylolite surface and may shear the socket walls. This promotes more dissolution and greater amplitudes of sutures. As new material is encountered by the growing stylolites, it may respond differently to pressure solution, which may ultimately result in the enhancement or inhibition of the process. For these reasons, fewer dolomite associations are seen in larger rather than smaller scale stylolites.

3.6.4 STYLOLITE EVOLUTION-LATERAL PROPAGATION

The only stylolite terminations observed were those of micron-scale seams. Terminations of larger stylolites were not recognized in the core samples. As a result, the mechanism by which a stylolite propagates can only be discussed tentatively based upon the few examples that were seen.

Two styles of stylolite terminations are seen; both are associated with dolomite. Commonly, micron-scale stylolites terminate abruptly into the matrix (Figure 48a). There are no signs of a bifurcating lateral tip or a swarm of microstylolites. The stylolite just dissipates into a dolomitic matrix. Differences in the abundance of dolomite along the stylolite and at the tip are hard to detect. On the other hand, a fan-like array of dolomite crystals was observed at the termination of one stylolite (Figure 48b). It is this example that suggests that the mechanism of lateral propagation is similar to that for the Lockport Formation.

Greater volume loss in the more central regions of a stylolite surface results in differential stresses being built-up symmetrically about the lateral tip. In an effort to relieve these stresses the rock responds by pressure solution, thus forming an extension of the stylolite surface. It responds by pressure-dissolution about dolomite crystals or clusters of crystals and is analagous to the type of pressure solution response described by Schofield (1984). The mechanism is one of thin fluid-film migration away from the anomaly at the tip and precipitation elsewhere. The development of the anisotropy is inherent in stylolite growth such that growth in the direction of shortening cannot proceed without growth by lateral propagation. Figure 53 is a schematic of how lateral propagation is envisioned to occur.

3.6.5 SECONDARY RESPONSE TO PRESSURE SOLUTION

Bridged, and irregular pressure solution fabrics seen within some suture interiors are believed to be a secondary response to pressure-dissolution at the stylolite surface. These features do not correlate across sutures and cannot be explained by an amalgamation mechanism. Instead, their association with dolomite (Figure 47) and larger stylolites suggests that they formed in response to greater stresses associated with well-developed stylolites.

In response to increased stresses due to deep penetration or inhibition of a large stylolite suture, it is envisioned that a secondary stress is "felt" within the suture interior. In essence, a smaller inhomogeneity is locally produced by a suture experiencing increased stresses. In order to accommodate them, the presence of

Figure 53 Schematic representation of lateral propagation of a stylolite. Stage I: volume lost at the stylolite surface (represented by ellipse) results in built-up stresses centered symmetrically at the tips of the seam. These stresses promote non-seam solution at the tips (stippled area) extending the seam laterally. Stage II: continued growth of the above seam results in larger volume lost due to pressure solution. As a result, stresses built-up at the tips are greater and the region of non-seam solution response is greater. Stage III: continued growth of the above seam results in greater volume loss and built-up stresses promoting propagation by non-seam solution in the stippled area.

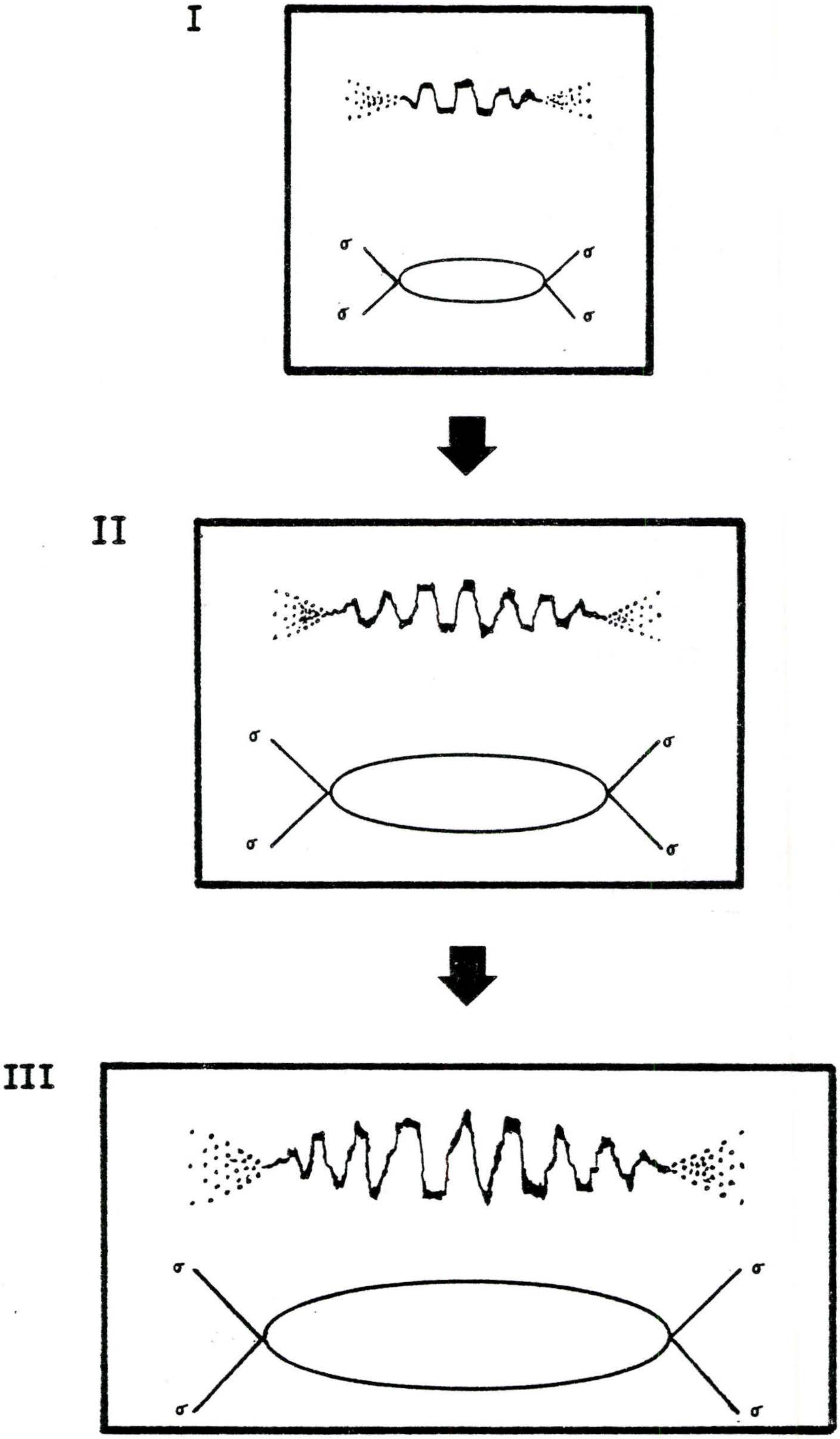
I
σ
σ
σ
σ
II
σ
σ
σ
σ
III
σ
σ
σ
σ

dolomite within the suture enables the rock to respond to this localized increase in stresses by pressure dissolution. The result is pressure solution textures directly associated to the pattern of dolomite occurrence (Figure 54).

3.6.6 DOLOMITE COALESCENCE

Dolomite crystals are observed to occur in mosaics adjacent to stylolites and within sutures (Figure 41,42). These consist of anhedral or subhedral crystals with little or no intervening calcite matrix adjacent to the stylolite and increasingly greater abundances of calcite further away. There are two ways in which to explain this fabric, growth coalescence (homogeneous nucleation) and solution coalescence (heterogeneous nucleation) after Schofield (1984).

Homogeneous nucleation requires that dolomite crystals nucleate homogeneously throughout the limestone matrix and grow simultaneously. Simultaneous growth will form compromise crystal boundaries as shown in Figure 55a and develop a dolomite mosaic.

Heterogeneous nucleation requires that crystals nucleate randomly throughout the limestone matrix and coalesce partly by growth of further dolomite or partly by coalescence via pressure-dissolution of the intervening

Figure 54 Schematic representation of secondary pressure solution responses in the immediate vicinity of stylolite sutures. Stage I: a stylolite that has grown by pressure dissolution at the sockets encounters a laminar concentration of dolomite crystals. Stage II: continued growth promotes the development of secondary stresses centered about concentrations of dolomite crystals (shown a dashed-line shadows) and the penetration of particles (cements) by dolomite crystals in the immediate vicinity of a suture. Stage III: the result of secondary stress development through continued growth may be seen as bridging stylolites and volume lost at particles (cements) which originated as a non-seam solution response.

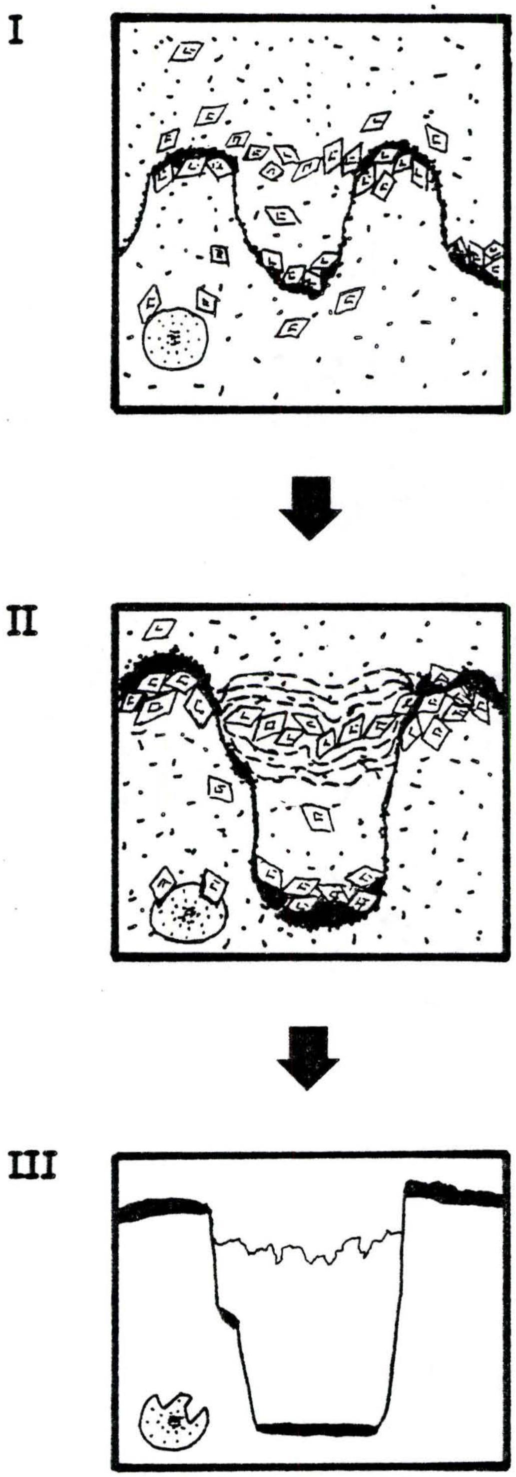
I
II
III

Figure 55 Schematic diagrams illustrating the formation of a dolomite mosaic. 5a) Growth coalescence of zones in adjoining crystals leads to a zonal pattern wherein a given compositional zone may be traced continuously around several crystals. 55b) Solutions coalescence of several zoned crystals; due to the solution and removal of intervening matrix. This results in the juxtaposition of non-correlative zones between crystals, and zones which cannot be traced continuously (after Schofield 1984).

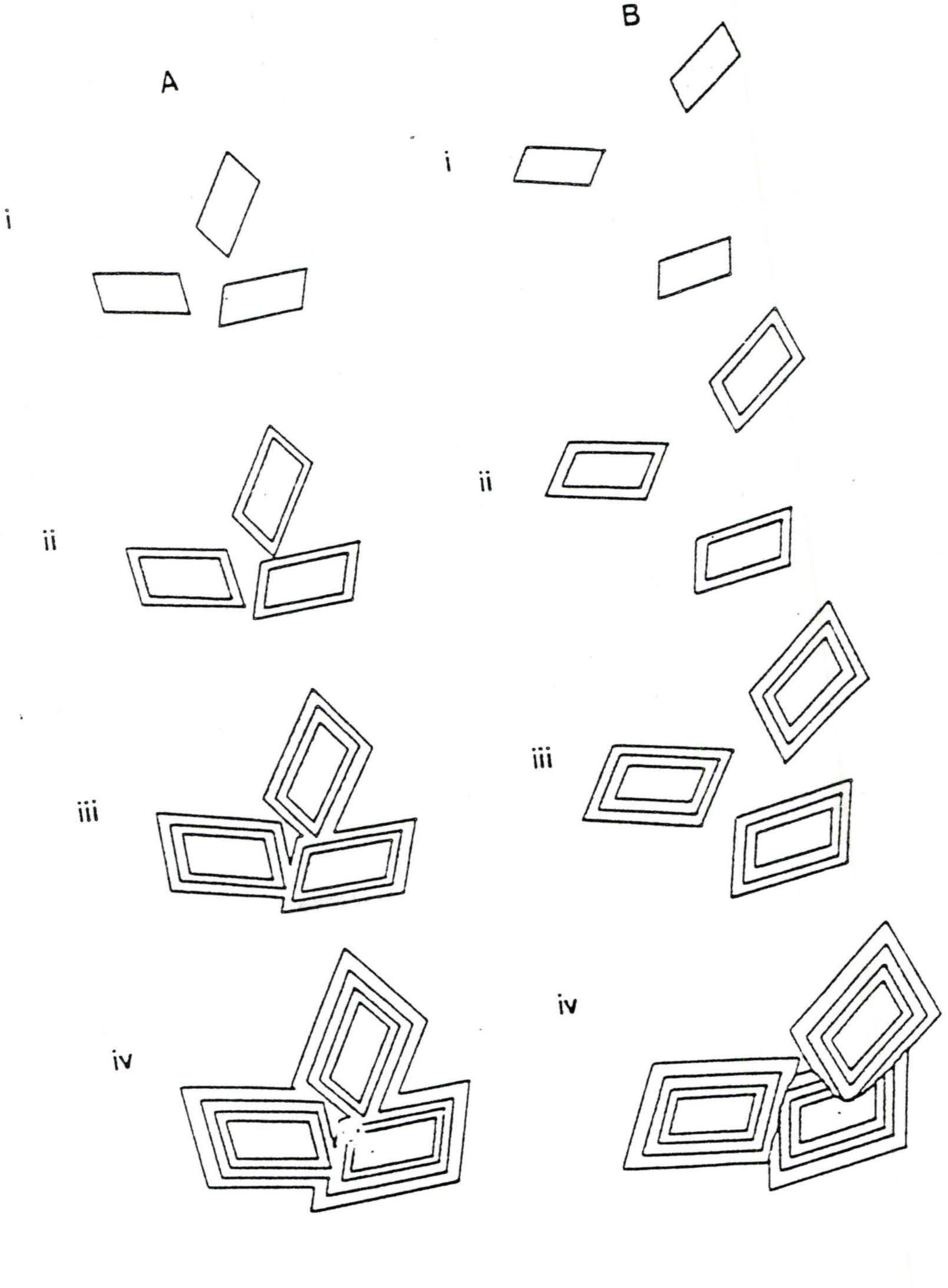
A
B
i
i
ii
ii
iii
iii
iv
iv

calcite (Figure 55b). This form of non-seam solution proceeds by migration of a thin fluid-film away from these sites.

Recognition of which mechanism was operative requires a minimum of three zones that can be identified in all crystals in the mosaic. Growth coalescence textures should show a minimum of one zone that can be traced continuously throughout a thin section. Solution coalescence textures should show zone-mismatches as dolomite crystals abutted together by crystal-contact pressure solution (Schofield 1984).

Cathodoluminescent study of better examples of "original" dolomite shows only two zones (Chapter 6, Section 6.5.2), thus interpretation of the textures are tenuous. Nevertheless, both growth and solution coalescence textures can be recognized under CL conditions (Chapter 6, Figure 84). Schofield (1983) states that this would be expected from a solution-coalesced dolostone, and that the process occurs during dolomitization.

On the last point, there is evidence suggesting differently. For example, CL studies show that dolomite mosaics are more recrystallized nearer a stylolite (Chapter 6 Figure 85) and intervening calcite is seen to increase in abundance away from a stylolite. This suggests that earlier formed dolomite recrystallized due to increased stresses associated with the accumulation of it at a stylolite surfaces and that these same stresses resulted in the dissolution of intervening calcite nearest the stylolite (Figure 56). Coincidentally, transport of the dissolved calcite by diffusion away from the stylolite can account for the dedolomite textures seen in the vicinity of some seams.

3.6.7 AMALGAMATION OF STYLOLITES

The truncation of smaller stylolites by bigger ones (Figure 25a) may be interpreted as two episodes to stylolitization, but it is difficult to explain anastomosed textures (Figure 25b) in the same manner. In light of the Lockport Formation study (Chapter 2) it seems easiest to explain these textures by amalgamation of stylolites, not microstylolites.

Stylolites that originally grew near one another may at some point in their growth history interfere with one another. It is at this point that the amalgamation mechanism is "born". With continued growth, the stylolites will amalgamate together (given the opportunity) and the resultant morphology of the stylolite will be a combination of constructive and destructive growth interference (Figure 57). In this manner, it is possible to account for the truncated (branched) and anastomosed textures seen, and the

Figure 56 Schematic representation of solution coalescence of dolomite crystals adjacent to a stylolite. Stage I: a stylolite that has grown in a dolomitic matrix. Stage II: continued growth via pressure-dissolution at the sockets accumulates dolomite crystals at the surface. Accumulation proceeds through solution coalescence: Stage III: continued growth of the above stylolite results in greater dolomite accumulations (through solution coalescence adjacent to the surface) and ultimately recrystallization.

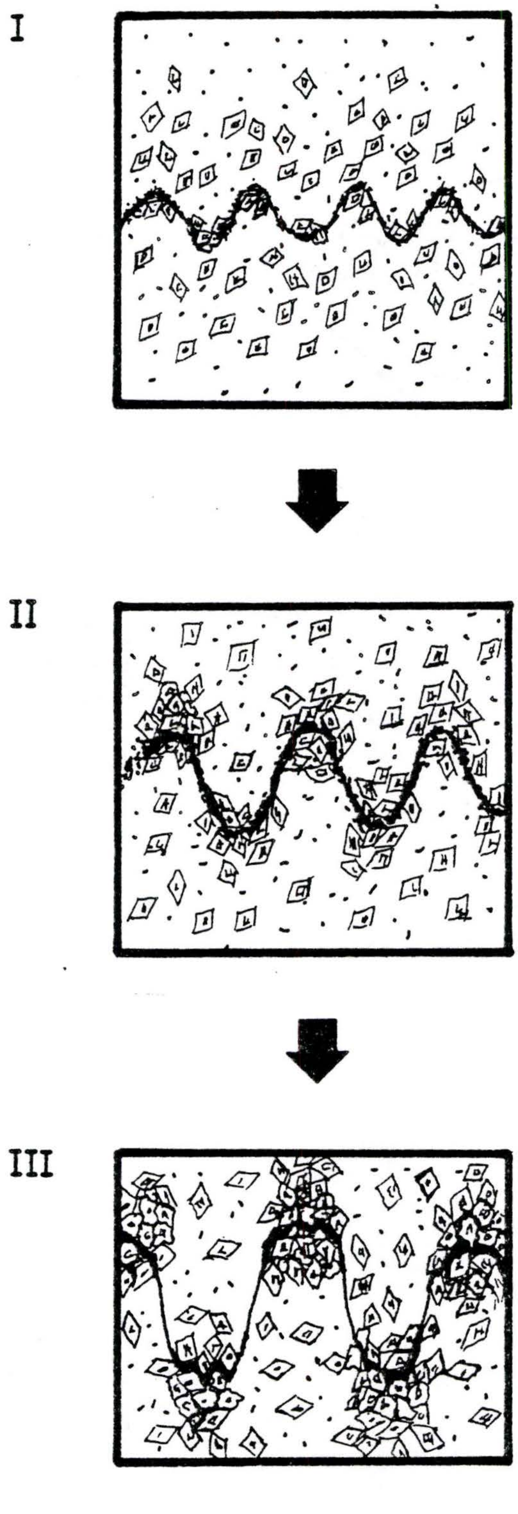
I
II
III

Figure 57 Schematic representation of amalgamation of two stylolites resulting in changes to suture morphology. Stage I: two sutured stylolites displaying a variably peaked and columnar suturing. Stage II: continued pressure solution results in stylolite growth. The seams are now closer together. Stage III: continued growth results in merging of the seams. The resultant morphology is determined by the phase relationships of the amalgamating seams. Through destructive interference undulatory sections may develop. Anastomosed portions are the result of incomplete amalgamation.

I

II

III

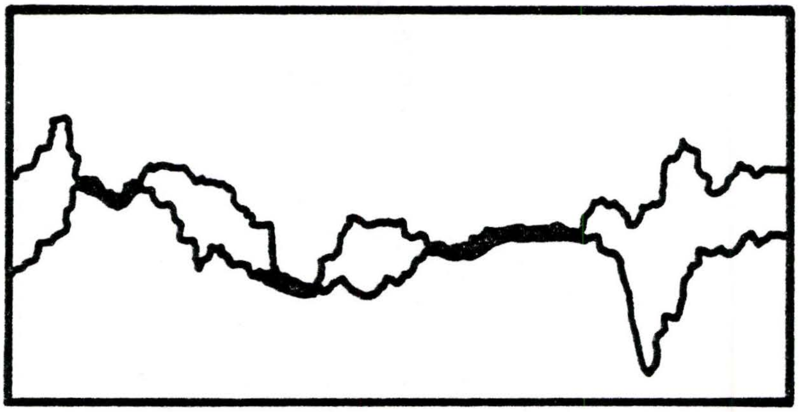

presence of undulatory non-sutured lengths seen in larger stylolites.

3.7 SUMMARY

Stylolitization of the Nisku Formation Zeta Lake Member is seen as limestone response to stress inhomogeneities created by concentrations of dolomite crystals. During burial and after the onset of dolomitization the matrix of the rock is susceptible to pressure solution about concentrations of dolomite. At these sites calcite responds to dolomitic stress perturbations by passing into solution due to the difference in the mechanical properties of the two phases. The process itself is considered to be a more extreme form and extension of neomorphism, the difference being that after calcite passes into solution, it migrates away from the site before being precipitated from the fluid-film. The presence of microspar and partial obliteration of microfossil structures confirms that neomorphism was active up to and possibly related to pressure solution. Maintenance of this process requires that diffusing fluid-films gain access to open pore systems which enhance material transfer by fluid flow.

Formation of a stylolite occurs with continued pressure solution and the lateral propagation of the dissolution surface along the stress anisotropy. This is easiest seen at abrupt boundaries between dolomite concentrations and matrix micrite and microfossils. More irregular concentrations of dolomite result in the formation of irregular incipient stylolites and microstylolites. Early in the development of a stylolite, its morphology is strongly influenced by the dolomite which caused it form. As the stylolite grows, dependency on dolomite is lost and the evolving stylolite may respond to other "environmental" parameters that influence its growth pattern. The result is seen as fewer dolomite-stylolite associations with increasing size of the seam.

Concommittant with change to the growing stylolite due to changing "environmental" parameters, may be change in the growth of the seam through amalgamation of nearby stylolites, and secondary responses to pressure solution within the interior of individual sutures. The results are seen as a more variable morphology of the stylolite and the development of bridged structures or irregular pressure solution textures within sutures.

Accumulation of dolomite at stylolite surfaces by pressure solution is believed to cause solution-coalescence of the dolomite. Solution-coalescence subsequently results in the recrystallization of the dolomite, tending towards crystalline mosaics of dolomite that show a homogeneous luminescent signature. During the process of solution-coalescence, intervening calcite is removed by non-seam solution, resulting in lower abundances of matrix calcite near stylolites. Diffusion of calcite from the stylolite surface sometimes has produced dedolomite textures.

Bridged structures and irregular pressure solution fabrics, as well as solution-coalescence of dolomite, imply that a stylolite, as it evolves, is capable of generating secondary pressure solution responses adjacent to the dissolution surface.

In summary, the process of dolomitization-stylolitization is responsible for the formation of these stylolites. But as they evolve and grow, changes due to differing "environmental" parameters, amalgamation, secondary responses, and solution-coalescence may subsequently alter the growth of the stylolite, such that its mechanism of formation is difficult to recognize. Figure 58 is the schematic of how a stylolite develops when formed by dolomitization-stylolitization.

Figure 58 Schematic representation of the dolomitization-stylolitization mechanism. Stage I: initial response is non-seam solution recognized by created porosity and fossil particle penetration. Stage II: evolution of non-seam solution to form stylolites by pressure-dissolution at abrupt dolomite boundaries, in dolomitic matrix, and by amalgamation of microstylolites. Stage III: continued stylolite growth may result in; a) shearing of socket walls and deeper penetration by dolomite crystals, b) accumulation of dolomite adjacent to stylolites by solution coalescence, and ultimately, recrystallization due to high stresses adjacent to the surface, c) secondary pressure solution responses due to high stresses at the stylolite surface results in bridging stylolites and non-stylolitic pressure-dissolution features, d) amalgamation of two stylolites that grow near one another. Stage IV: lateral propagation of the stylolite that occurs throughout its growth history.

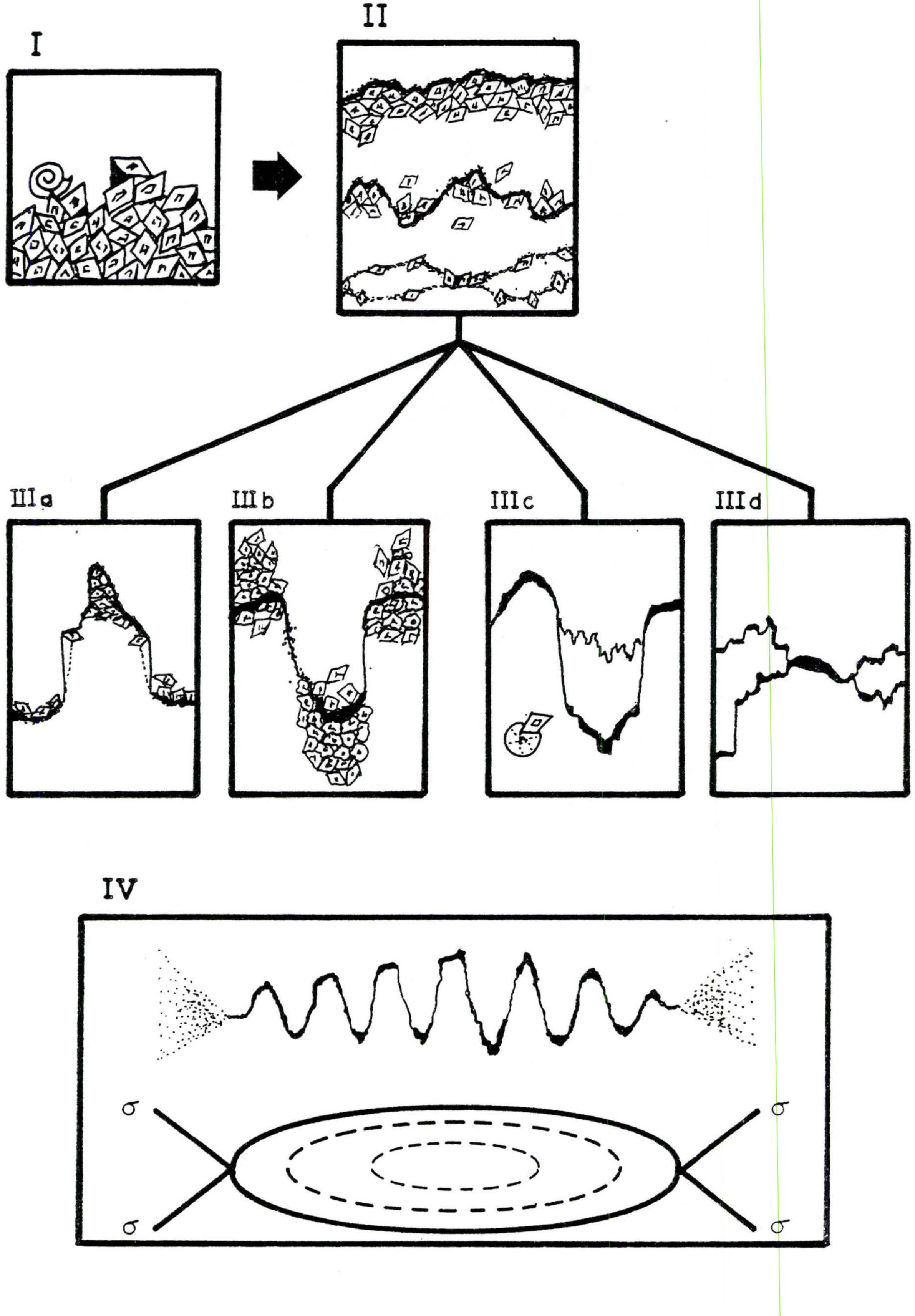
I
II
IIIa
IIIb
IIIc
IIId
IV
σ
σ
σ
σ

CHAPTER 4

PERMEABILITY BARRIERS

4.1 INTRODUCTION

Stylolites, being the product of a pressure-dissolution process, accumulate insoluble materials at their surface. Commonly this material is a residual film rich in clays. As a stylolite grows, more insoluble material is accumulated. It is because of this simple process that stylolites are thought to behave as permeability barriers. Flow across them is inhibited owing to their clay content and maturity. Maturity in this sense can be judged by the scale of the feature. For example, a stylolite with a 4 centimetre amplitude is much more mature than a stylolite with 250 micron amplitude. Thus, the more mature that a stylolite is, the more it should behave as a permeability barrier.

Already there are studies that show a close spatial relationship exists between the occurrence and amplitude of stylolites and the distribution of low permeability, low porosity zones. Dunnington (1967) and Wong and Oldershaw (1981) have shown that where stylolites occur there is an increase in the measured porosity and permeability of the adjacent sediments. In both studies the vertical distance over which stylolites influenced permeability and porosity was measurable in centimetres.

One is led to believe that stylolites behave as permeability barriers due to the accumulation of insoluble materials and a locally increased degree of cementation. It is a most convincing argument.

The purpose of this study is to look at one property of stylolites i.e. stylolites as vertical permeability barriers. Using drill core analyses, vertical permeability (Kvert) values for stylolite-bearing drill plugs will be compared to those for plugs without stylolites.

This is an entirely statistical study; it does not include any petrological aspect. Kvert values are compared as mean values i.e. on the average. One must realize that "the purpose of an average is to represent a group of individual values in a simple and concise manner so that the mind can get a quick understanding of the general size of the individuals in the group, undistracted by fortuitous and irrelevant variations" (Moroney, M.J., 1951 p. 34).

4.2 VERTICAL PERMEABILITY AND POROSITY PLOTS

Figure 59a, 59b, 59c, 59d, represents the vertical permeability and porosity profile of the Zeta Lake Member relative ot the drill plugs, main pore types and stylolite scales.

There appears to be no direct relationship between stylolite scale, main pore type, vertical permeability and porosity values. High and low Kvert values can be found in plugs with micron- or centimetre-scale stylolites regardless of the main pore type. Similar patterns are observed for porosity values, and for non-stylolitic plugs.

These profiles suggest that an ordered relationship is lacking. Stylolites are not always associated with low vertical permeability and porosity values and non-stylolitic plugs are not always associated with higher values.

In an effort to determine whether or not stylolites do behave as permeability barriers, the following statistical analysis was performed.

4.3 PROCEDURE

For a given well, stylolite-bearing drill plugs are marked and the scale of the feature noted (micron-scale through centimetre-scale). Using drill core analyses, frequency distribution plots are generated for all drill plugs (Combined Data), non-stylolitic plugs (No Seams), and

Figure 59a Vertical permeability and porosity plot for drill plugs 39 to 123, relative to stylolite scale and main pore type (Fossil = Fo, Large Vug = Lv, Fracture = Fr). For stylolite scale, open bar = 1 scale of occurrence, solid/open bar = 2 scales of occurrence, open/solid/open bar = 3 scales of occurrence.

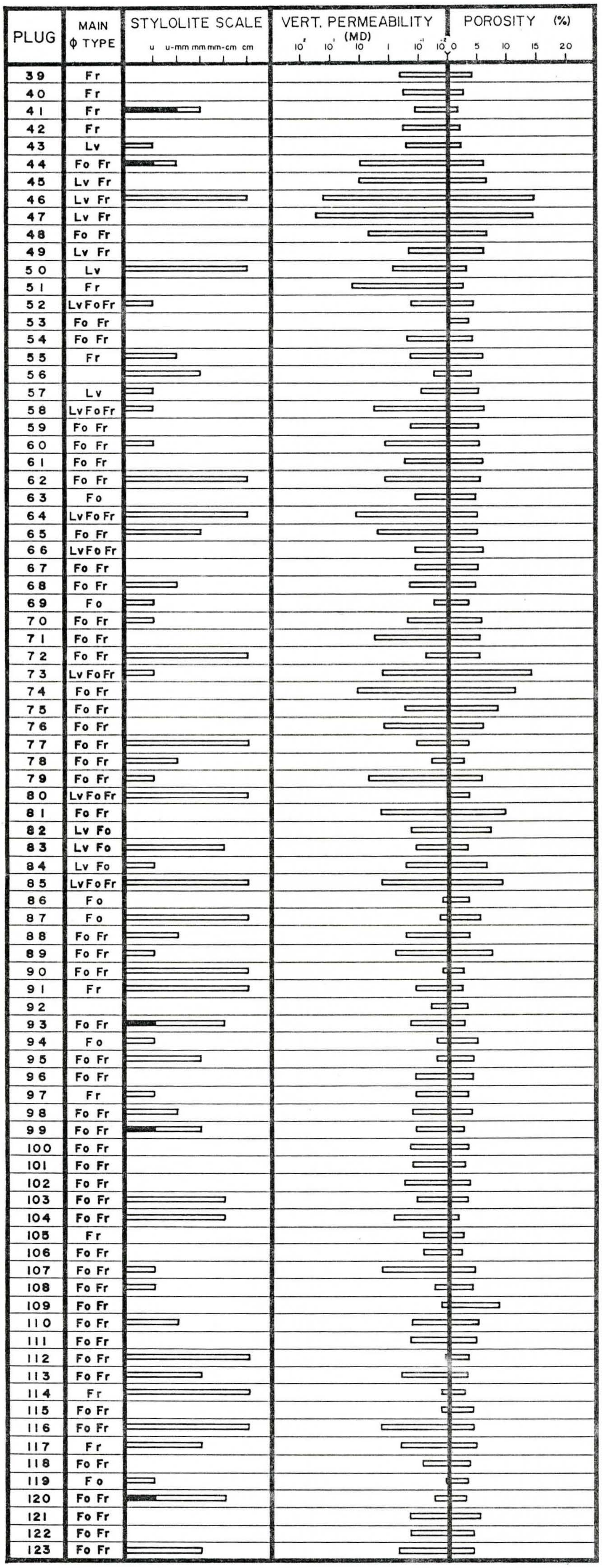

PLUG	MAIN ϕ TYPE
39	Fr
40	Fr
41	Fr
42	Fr
43	Lv
44	Fo Fr
45	Lv Fr
46	Lv Fr
47	Lv Fr
48	Fo Fr
49	Lv Fr
50	Lv
51	Fr
52	Lv Fo Fr
53	Fo Fr
54	Fo Fr
55	Fr
56	
57	Lv
58	Lv Fo Fr
59	Fo Fr
60	Fo Fr
61	Fo Fr
62	Fo Fr
63	Fo
64	Lv Fo Fr
65	Fo Fr
66	Lv Fo Fr
67	Fo Fr
68	Fo Fr
69	Fo
70	Fo Fr
71	Fo Fr
72	Fo Fr
73	Lv Fo Fr
74	Fo Fr
75	Fo Fr
76	Fo Fr
77	Fo Fr
78	Fo Fr
79	Fo Fr
80	Lv Fo Fr
81	Fo Fr
82	Lv Fo
83	Lv Fo
84	Lv Fo
85	Lv Fo Fr
86	Fo
87	Fo
88	Fo Fr
89	Fo Fr
90	Fo Fr
91	Fr
92	
93	Fo Fr
94	Fo
95	Fo Fr
96	Fo Fr
97	Fr
98	Fo Fr
99	Fo Fr
100	Fo Fr
101	Fo Fr
102	Fo Fr
103	Fo Fr
104	Fo Fr
105	Fr
106	Fo Fr
107	Fo Fr
108	Fo Fr
109	Fo Fr
110	Fo Fr
111	Fo Fr
112	Fo Fr
113	Fo Fr
114	Fr
115	Fo Fr
116	Fo Fr
117	Fr
118	Fo Fr
119	Fo
120	Fo Fr
121	Fo Fr
122	Fo Fr
123	Fo Fr

Figure 59b Vertical permeability and porosity plot for drill plugs 124 to 207, relative to stylolite scale and main pore types. Same legend as in Figure 59a.

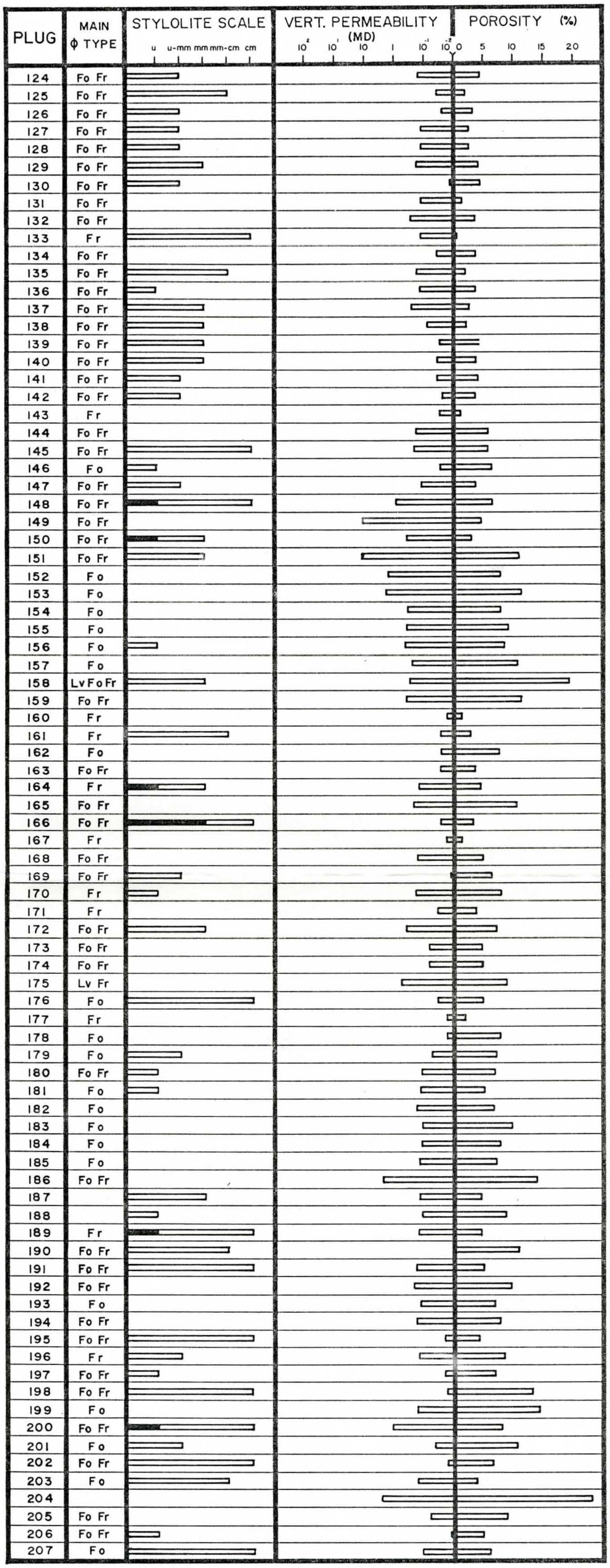

PLUG	MAIN φ TYPE
124	Fo Fr
125	Fo Fr
126	Fo Fr
127	Fo Fr
128	Fo Fr
129	Fo Fr
130	Fo Fr
131	Fo Fr
132	Fo Fr
133	Fr
134	Fo Fr
135	Fo Fr
136	Fo Fr
137	Fo Fr
138	Fo Fr
139	Fo Fr
140	Fo Fr
141	Fo Fr
142	Fo Fr
143	Fr
144	Fo Fr
145	Fo Fr
146	Fo
147	Fo Fr
148	Fo Fr
149	Fo Fr
150	Fo Fr
151	Fo Fr
152	Fo
153	Fo
154	Fo
155	Fo
156	Fo
157	Fo
158	Lv Fo Fr
159	Fo Fr
160	Fr
161	Fr
162	Fo
163	Fo Fr
164	Fr
165	Fo Fr
166	Fo Fr
167	Fr
168	Fo Fr
169	Fo Fr
170	Fr
171	Fr
172	Fo Fr
173	Fo Fr
174	Fo Fr
175	Lv Fr
176	Fo
177	Fr
178	Fo
179	Fo
180	Fo Fr
181	Fo
182	Fo
183	Fo
184	Fo
185	Fo
186	Fo Fr
187	
188	
189	Fr
190	Fo Fr
191	Fo Fr
192	Fo Fr
193	Fo
194	Fo Fr
195	Fo Fr
196	Fr
197	Fo Fr
198	Fo Fr
199	Fo
200	Fo Fr
201	Fo
202	Fo Fr
203	Fo
204	
205	Fo Fr
206	Fo Fr
207	Fo

Figure 59c Vertical permeability and porosity plots for drill plugs 208 to 292, relative to stylolite scale and main pore type. Same legend as in Figure 59a.

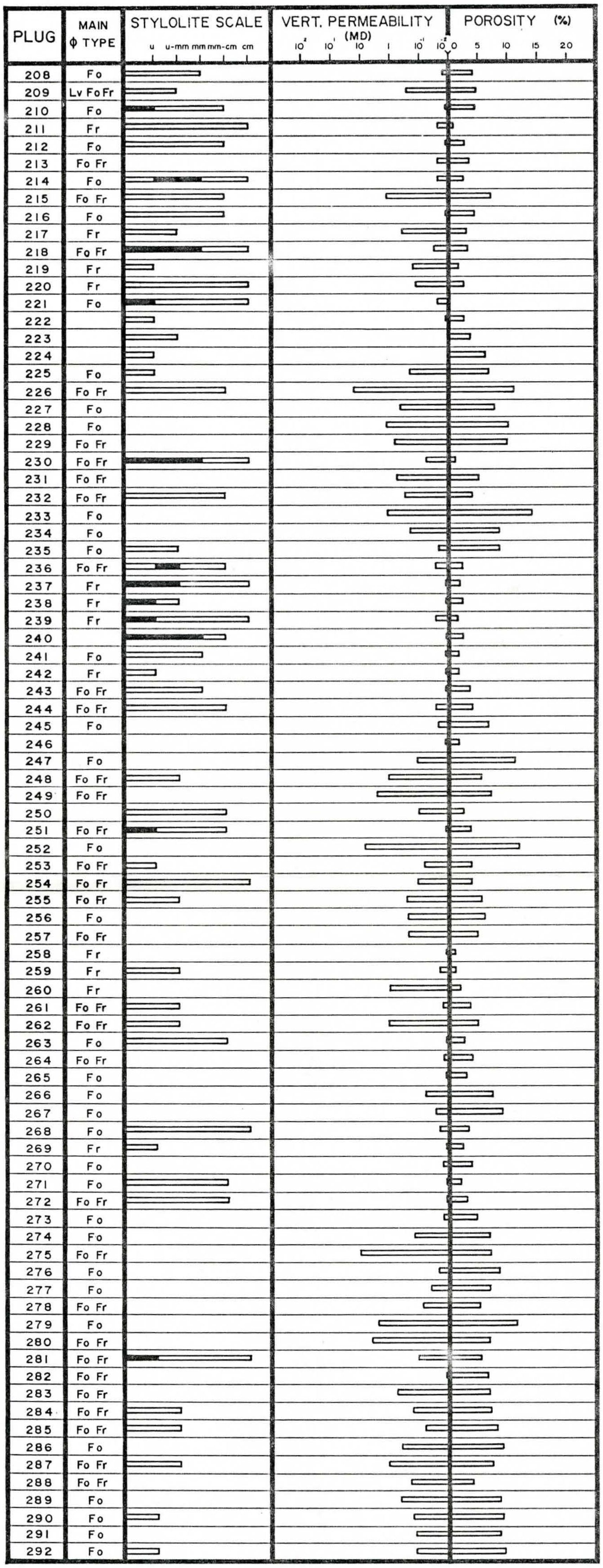

PLUG	MAIN φ TYPE
208	Fo
209	Lv Fo Fr
210	Fo
211	Fr
212	Fo
213	Fo Fr
214	Fo
215	Fo Fr
216	Fo
217	Fr
218	Fo Fr
219	Fr
220	Fr
221	Fo
222	
223	
224	
225	Fo
226	Fo Fr
227	Fo
228	Fo
229	Fo Fr
230	Fo Fr
231	Fo Fr
232	Fo Fr
233	Fo
234	Fo
235	Fo
236	Fo Fr
237	Fr
238	Fr
239	Fr
240	
241	Fo
242	Fr
243	Fo Fr
244	Fo Fr
245	Fo
246	
247	Fo
248	Fo Fr
249	Fo Fr
250	
251	Fo Fr
252	Fo
253	Fo Fr
254	Fo Fr
255	Fo Fr
256	Fo
257	Fo Fr
258	Fr
259	Fr
260	Fr
261	Fo Fr
262	Fo Fr
263	Fo
264	Fo Fr
265	Fo
266	Fo
267	Fo
268	Fo
269	Fr
270	Fo
271	Fo
272	Fo Fr
273	Fo
274	Fo
275	Fo Fr
276	Fo
277	Fo
278	Fo Fr
279	Fo
280	Fo Fr
281	Fo Fr
282	Fo Fr
283	Fo Fr
284	Fo Fr
285	Fo Fr
286	Fo
287	Fo Fr
288	Fo Fr
289	Fo
290	Fo
291	Fo
292	Fo

Figure 59d Vertical permeability and porosity plots for drill plugs 293 to 377, relative to stylolite scale and main pore type. Same legend as in Figure 59a.

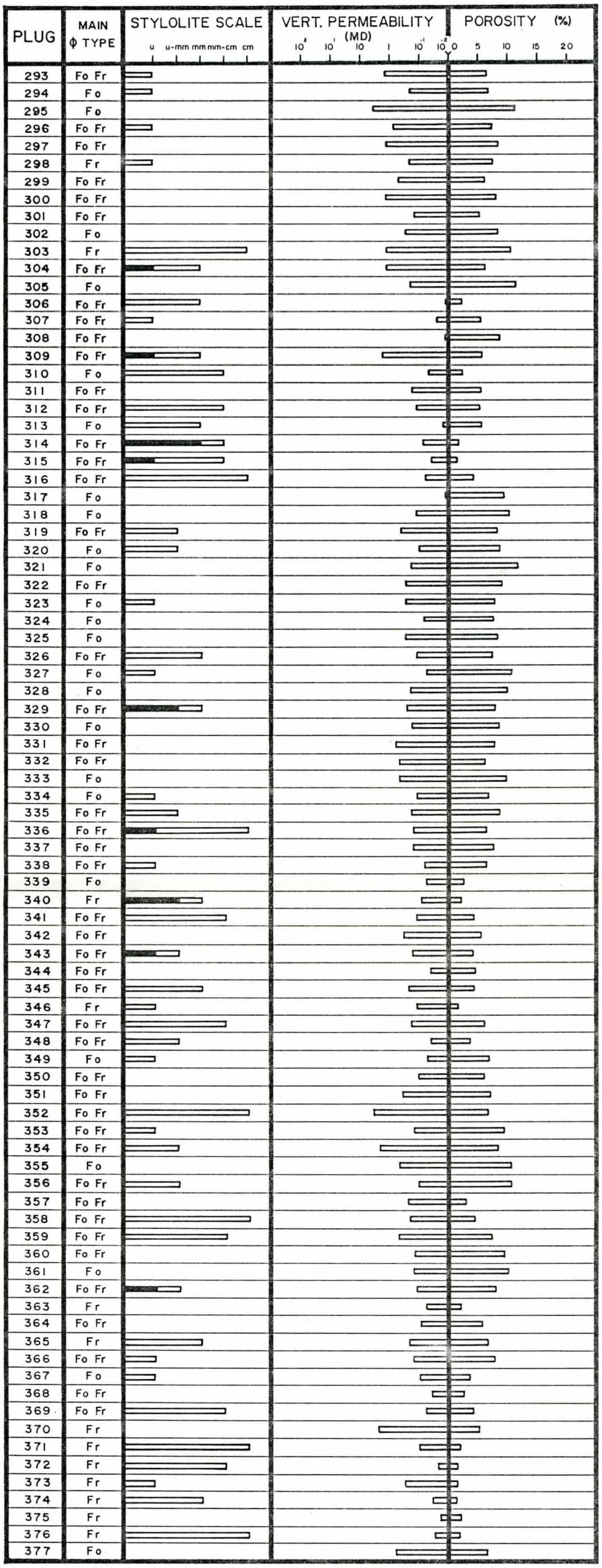

PLUG	MAIN φ TYPE
293	Fo Fr
294	Fo
295	Fo
296	Fo Fr
297	Fo Fr
298	Fr
299	Fo Fr
300	Fo Fr
301	Fo Fr
302	Fo
303	Fr
304	Fo Fr
305	Fo
306	Fo Fr
307	Fo Fr
308	Fo Fr
309	Fo Fr
310	Fo
311	Fo Fr
312	Fo Fr
313	Fo
314	Fo Fr
315	Fo Fr
316	Fo Fr
317	Fo
318	Fo
319	Fo Fr
320	Fo
321	Fo
322	Fo Fr
323	Fo
324	Fo
325	Fo
326	Fo Fr
327	Fo
328	Fo
329	Fo Fr
330	Fo
331	Fo Fr
332	Fo Fr
333	Fo
334	Fo
335	Fo Fr
336	Fo Fr
337	Fo Fr
338	Fo Fr
339	Fo
340	Fr
341	Fo Fr
342	Fo Fr
343	Fo Fr
344	Fo Fr
345	Fo Fr
346	Fr
347	Fo Fr
348	Fo Fr
349	Fo
350	Fo Fr
351	Fo Fr
352	Fo Fr
353	Fo Fr
354	Fo Fr
355	Fo
356	Fo Fr
357	Fo Fr
358	Fo Fr
359	Fo Fr
360	Fo Fr
361	Fo
362	Fo Fr
363	Fr
364	Fo Fr
365	Fr
366	Fo Fr
367	Fo
368	Fo Fr
369	Fo Fr
370	Fr
371	Fr
372	Fr
373	Fr
374	Fr
375	Fr
376	Fr
377	Fo

all stylolite-bearing plugs (All Seams). A restriction is applied to use only plugs containing one scale of stylolite, not two or more different scales. A second set of frequency distribution plots are constructed using a Ln transformation to transform the lognormal distribution observed to a normal distribution. Relative cumulative frequency plots indicate to what degree the Ln transformations approximate normality.

Having transformed the Kvert data to Ln values, mean and standard deviation values can be calculated for a first distillation scheme i.e. those plugs with No Seams, or micron-scale, micron to millimetre-scale, millimetre-scale, millimetre to centimetre-scale, and centimetre-scale seams. These calculated mean values are compared graphically and mathematically using Confidence Intervals and a T-test, respectively. The purpose of the comparison is to determine if the observed difference of means between non-stylolitic and stylolitic plugs is significant or if it has just occurred by chance.

The data are then distilled a second time to look even closer at the behaviour of stylolites as permeability barriers. Retaining the classification scheme of the first distillation, the data are now grouped by the presence of the main pore types. Once again, means and standard deviations are calculated for each class in each grouping.

Mean values are compared using T-tests to determine the significance of such.

Appendix A contains the equations used to calculate the parameters and perform the statistical tests.

4.4 SELECTION OF DATA

The data presented herein are from the well Texaco Bigoray 6-12-52-9W5. Of the 376 drill plugs analysed, plugs 2-38 represent the Wolf Lake Member tidal flat sediments. Plugs 39-377 represent the Zeta Lake Member reefal carbonates.

For the purpose of this study plugs 2-38 were omitted. The study is restricted entirely to the reefal carbonates. The reason for this omission is two fold. First, the style of pressure solution seen in the Wolf Lake Member differs appreciably from that observed in the Zeta Lake Members. Secondly, the tidal flat sediments are immensely different in their lithology. Hence, the behaviour of stylolites as permeability barriers in these sediments may not be comparable to those found in the reefal carbonates.

Of the remaining 338 plugs, 41 were not used. Either they had more than one scale of stylolite in them, or there were no Kvert data available for these plugs. Hence, 297 drill plugs representing the reef carbonates were used in this study.

4.5 FREQUENCY DISTRIBUTIONS

Three frequency distributions were initially plotted for the Zeta Lake Member data (plugs 39-377). The Combined Data plot represents the distribution of Kvert values for all 297 samples. The Kvert distribution for non-stylolitic drill plugs is shown in the No Seam plot and that for all scales (micron through centimetre) of stylolites is shown in the All Seam plot. These plots are labelled Figures 60, 61, and 62 respectively.

The first thing to strike the observers eye is the marked lack of symmetry of each plot. All three plots are very positively skewed. Calculated values of skewness for each plot are very similar, being near-equal to .11 (Table 5). The Combined Data plot (Figure 60) shows the overall distribution of Kvert values for all plugs being considered. The most frequent or most common class interval is that for .01 to.19 millidarcies (md), the mode being equal to .15 md. For this distribution the question that arises is "How does the presence of stylolites influence this distribution?"

To answer this question we look to the No Seam and All Seam plots (Figure 61,62). The No Seam plot has the

Figure 60 Vertical permeability (Kvert) frequency distribution plot for Combined Data. Class intervals are listed below in millidarcies (md). n = 297. Mean = 3.37 md. Standard deviation = 30.33 md. Skewness = .106. Mode = .147 md.

A	<0.01	T	3.60 - 3.79
B	0.01 - 0.19	U	3.80 - 3.99
C	0.20 - 0.39	V	4.00 - 4.19
D	0.40 - 0.59	W	4.20 - 4.39
E	0.60 - 0.79	X	4.40 - 4.59
F	0.80 - 0.99	Y	4.60 - 4.79
G	1.00 - 1.19	Z	4.80 - 4.99
H	1.20 - 1.39	AA	5.00 - 5.19
I	1.40 - 1.59	BB	5.20 - 5.39
J	1.60 - 1.79	CC	5.40 - 5.59
K	1.80 - 1.99	DD	5.60 - 5.79
L	2.00 - 2.19	EE	5.80 - 5.99
M	2.20 - 2.39	FF	6.00 - 6.19
N	2.40 - 2.59	GG	6.20 - 6.39
O	2.60 - 2.79	HH	6.40 - 6.59
P	2.80 - 2.99	II	6.60 - 6.79
Q	3.00 - 3.19	JJ	6.80 - 6.99
R	3.20 - 3.39	KK	>7.00
S	3.40 - 3.59		

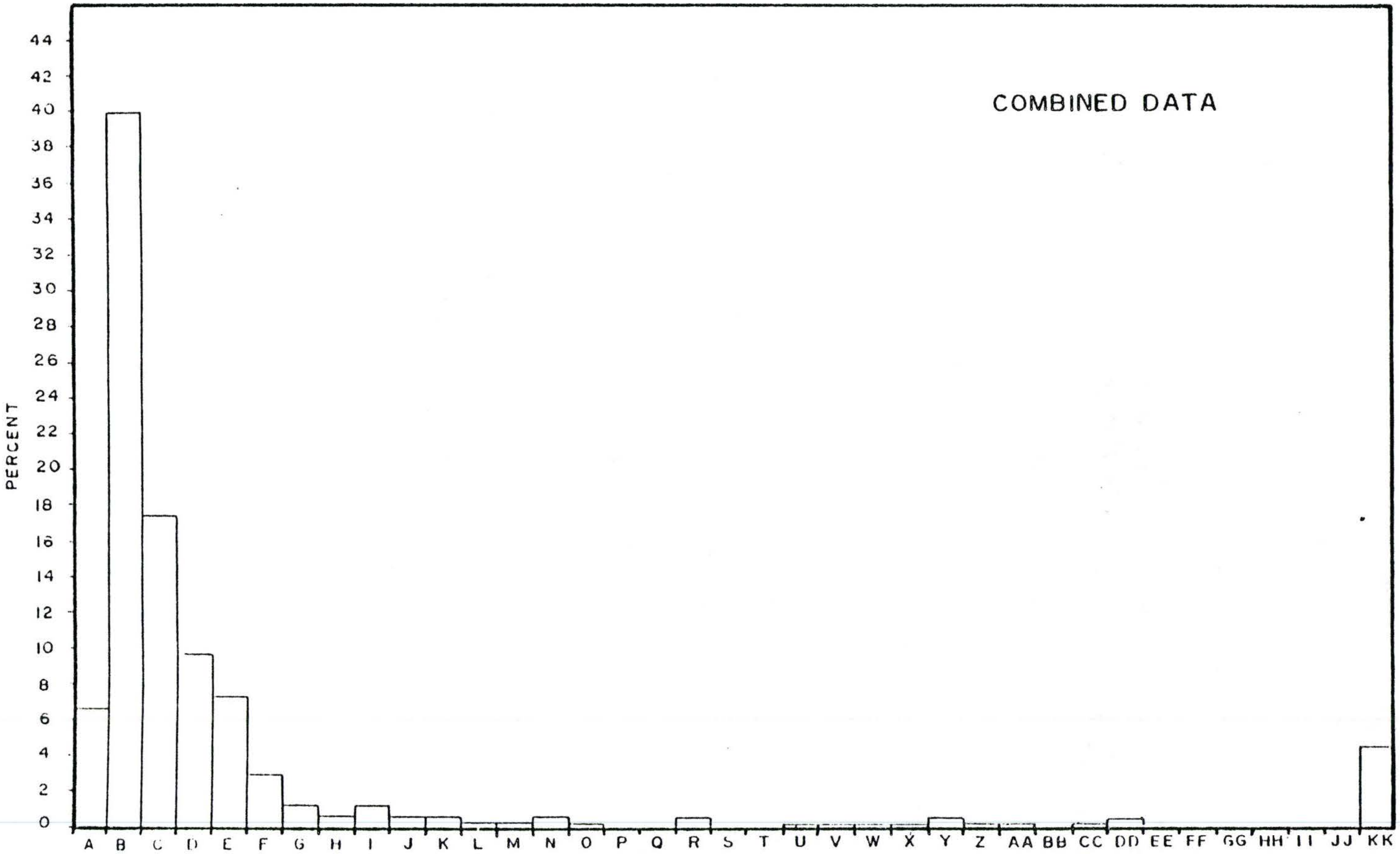
COMBINED DATA
PERCENT
44
42
40
38
36
34
32
30
28
26
24
22
20
18
16
14
12
10
8
6
4
2
0
A
B
C
D
E
F
G
H
I
J
K
L
M
N
O
P
Q
R
S
T
U
V
W
X
Y
Z
AA
BB
CC
DD
EE
FF
GG
HH
II
JJ
KK

Figure 61 Vertical permeability (Kvert) frequency distribution plot for No Seams data. Class intervals are as listed in Figure 60.
n = 140. Mean = 4.59 md. Standard deviation = 39.64 md. Skewness = .112. Mode = .164 md.

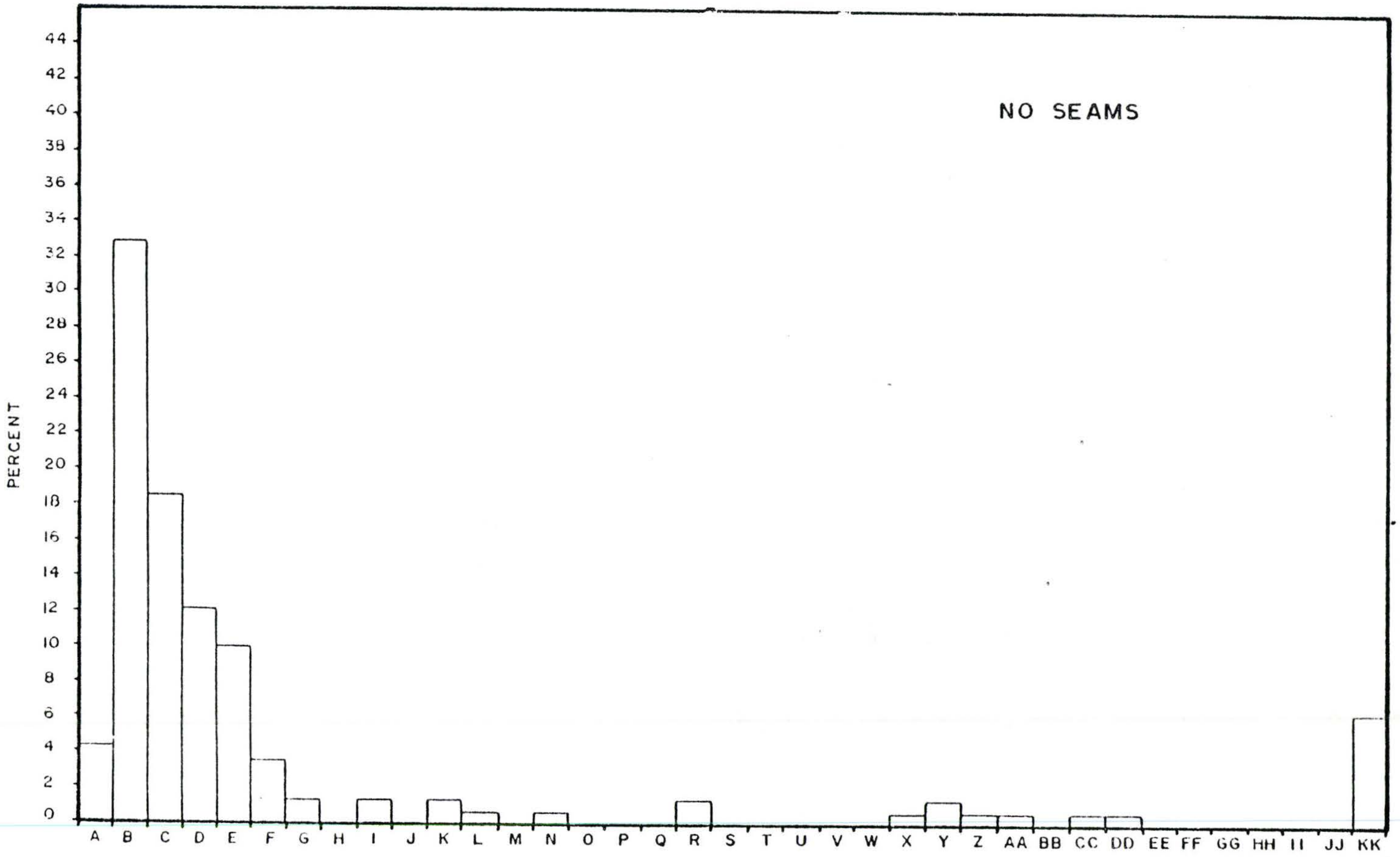
NO SEAMS
PERCENT
44
42
40
38
36
34
32
30
28
26
24
22
20
18
16
14
12
10
8
6
4
2
0
A
B
C
D
E
F
G
H
I
J
K
L
M
N
O
P
Q
R
S
T
U
V
W
X
Y
Z
AA
BB
CC
DD
EE
FF
GG
HH
II
JJ
KK

Figure 62 Vertical permeability (Kvert) frequency distribution plot for All Seams data. Class intervals are as listed in Figure 60.

n = 157. Mean = 2.25 md. Standard deviation = 18.40 md. Skewness = .115. Mode = .134 md.

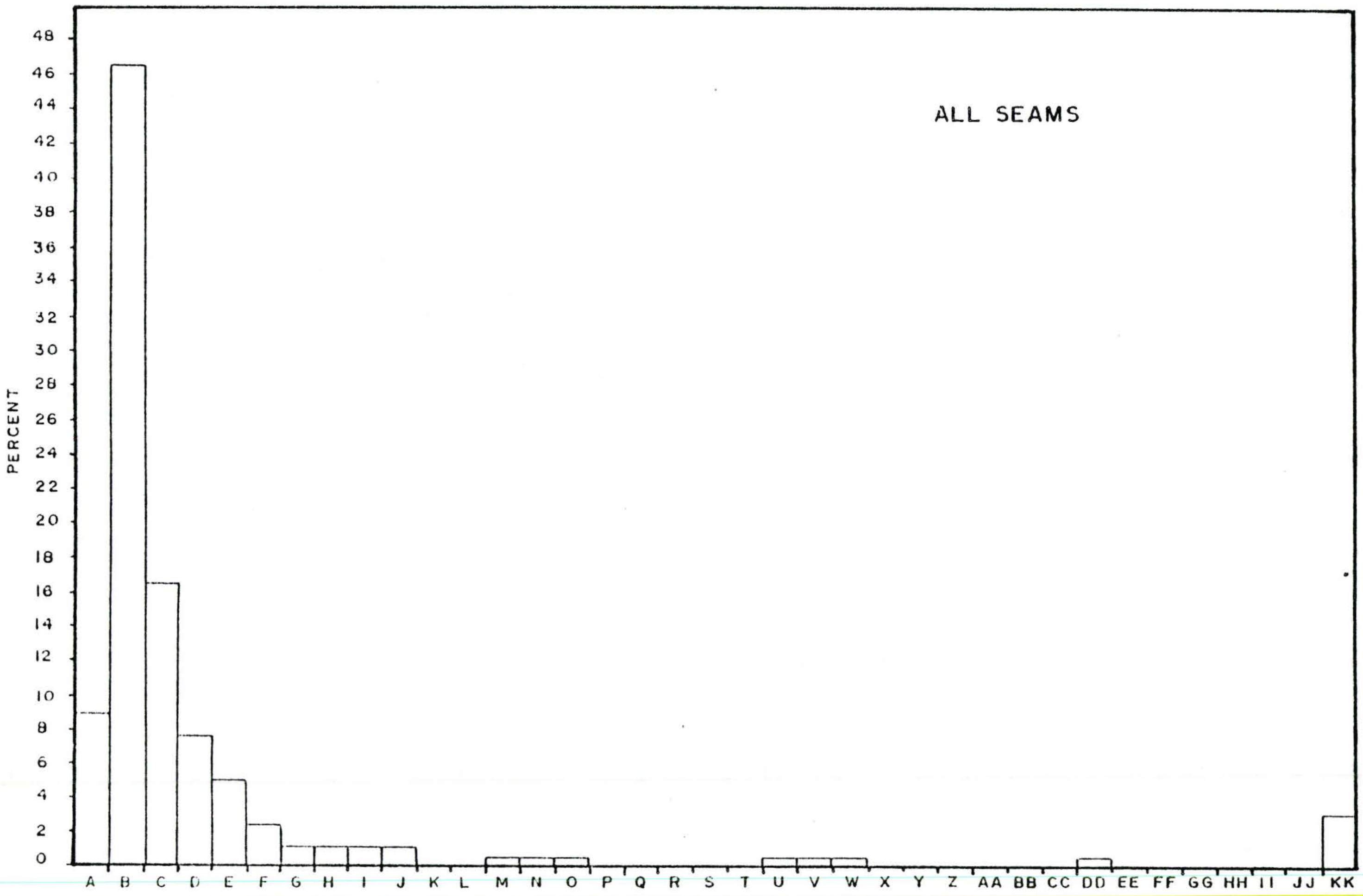
ALL SEAMS
PERCENT
48
46
44
42
40
38
36
34
32
30
28
26
24
22
20
18
16
14
12
10
8
6
4
2
0
A B C D E F G H I J K L M N O P Q R S T U V W X Y Z AA BB CC DD EE FF GG HH II JJ KK

same most frequent class interval as the one for Combined Data, the mode being .16 md. Both No Seam and All Seam plots are very peaked, the latter more than the former. This more peaked character of the All Seam plot shows up in the first two class intervals (<.01, .01 to .19 md.), where 55% of the Kvert values occur. In the No Seam plot 37% of Kvert values occur in these class intervals, these being less frequent than those for the All Seam data. Beyond these intervals roles reverse i.e. the No Seam data is more frequent than that for All Seams, to a maximum of 5% of occurrences per class interval.

These two plots reveal that the majority (55%) of stylolite-bearing plugs have Kvert values less than .20 md, and the majority of non-stylolitic plugs (55%) are less than .40 md. But the influence of stylolites appears not to be too significant. Both plots have greater than 80% of Kvert values less than 1.0 md. Also, they are near-equally skewed and have near-equal modes (Table 5).

To further this study the positive skewness of these distributions must be corrected to a more normal one using a Ln transformation. The transformed distributions are shown in Figures 63, 64 and 65. Plotting this transformed data on normal probability paper as relative cumulative frequency curves will indicate how near to normal this data are distributed (Figures 66,67 and 68). Although a straight

TABLE 5: FREQUENCY HISTOGRAM PARAMETERS

	Combined Data	No Seams	All Seams
$\bar{x}$	3.37 md	4.59 md	2.25 md
Sx	30.33 md	39.64 md	18.40 md
Mode	.147 md	.164md	.134 md
Skewness	.106	.112	.115

Figure 63 Frequency distribution of Ln transformation values for Combined Data vertical permeability data. Class intervals are as listed below . n = 297.

A	-4.99 to -4.50	M	1.00 to 1.49
B	-4.49 to -4.00	N	1.50 to 1.99
C	-3.99 to -3.50	O	2.00 to 2.49
D	-3.49 to -3.00	P	2.50 to 2.99
E	-2.49 to -2.50	Q	3.00 to 3.49
F	-2.49 to -2.00	R	3.50 to 3.99
G	-1.99 to -1.50	S	4.00 to 4.49
H	-1.49 to -1.00	T	4.50 to 4.99
I	-0.99 to -0.50	U	5.00 to 5.49
J	-0.49 to -0.01	V	5.50 to 5.99
k	0.00 to 0.49	W	6.00 to 6.49
L	0.50 to 0.99		

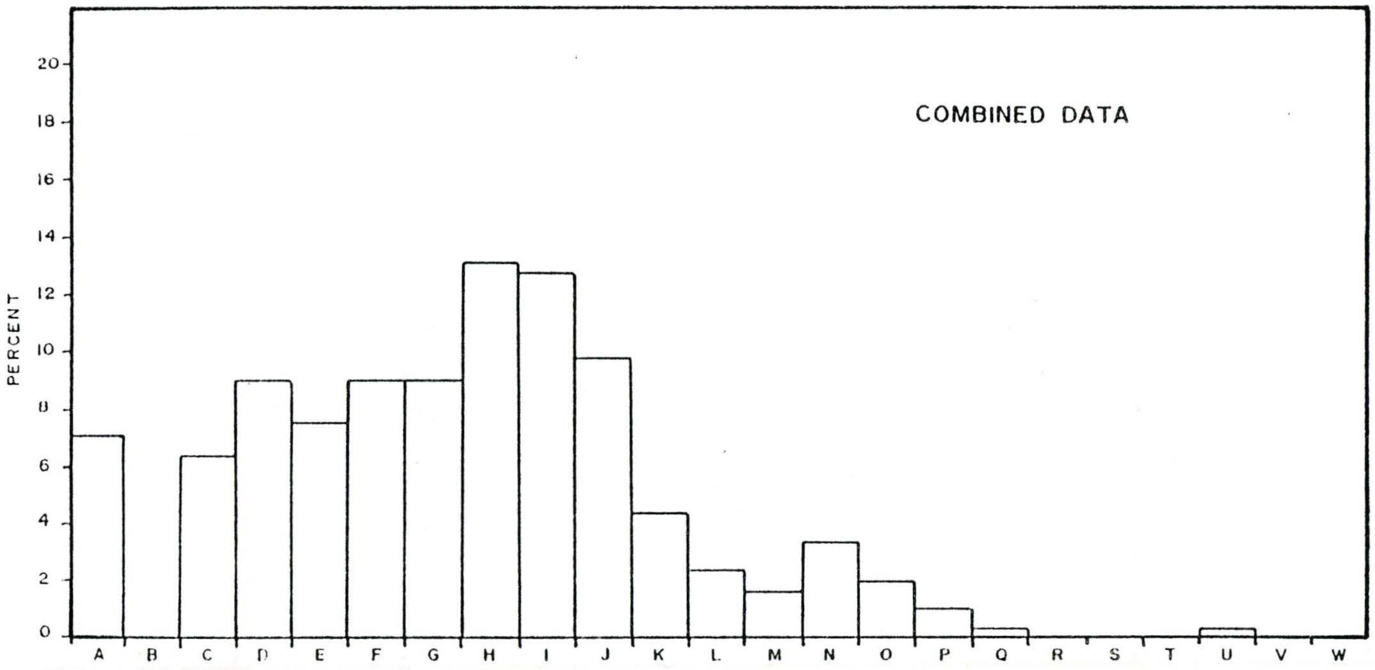
COMBINED DATA
PERCENT
0
2
4
6
8
10
12
14
16
18
20
A
B
C
D
E
F
G
H
I
J
K
L
M
N
O
P
Q
R
S
T
U
V
W

Figure 64 Frequency distribution of Ln transformation values for No Seams vertical permeability data. Class intervals are as listed in Figure 63. n = 140.

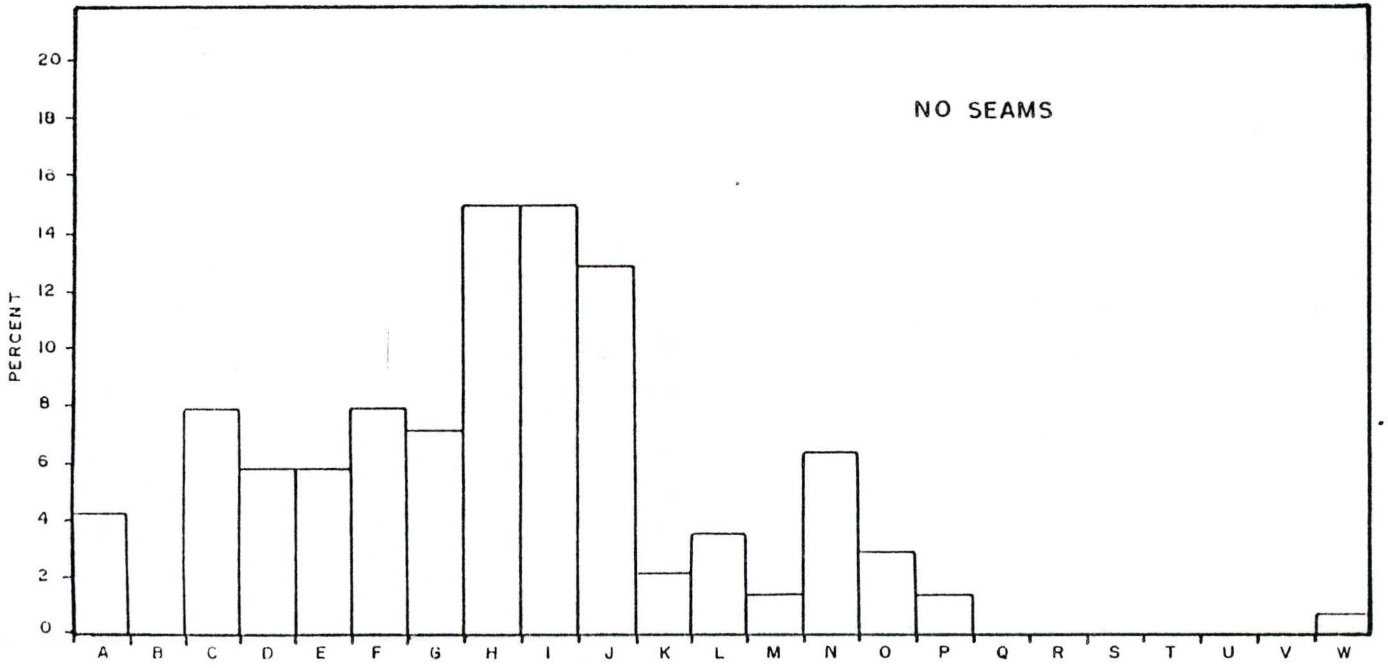
NO SEAMS
PERCENT
0
2
4
6
8
10
12
14
16
18
20
A
B
C
D
E
F
G
H
I
J
K
L
M
N
O
P
Q
R
S
T
U
V
W

Figure 65 Frequency distribution of Ln transformation values for All Seams vertical permeability data. Class intervals are as listed in Figure 63. n = 157.

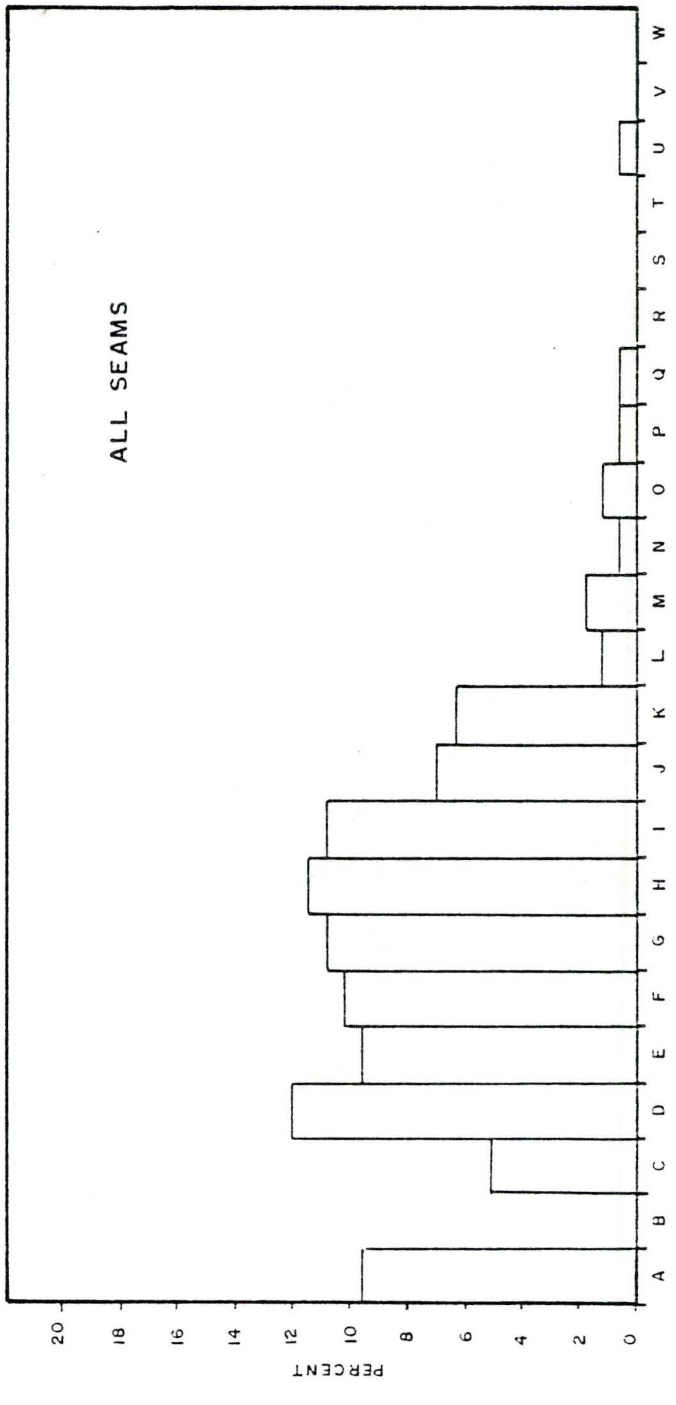
ALL SEAMS
PERCENT
0
2
4
6
8
10
12
14
16
18
20
A
B
C
D
E
F
G
H
I
J
K
L
M
N
O
P
Q
R
S
T
U
V
W

Figure 66 Relative cumulative frequency curve for Ln transformation Combined Data vertical permeability data. Same legend as in Figure 63.

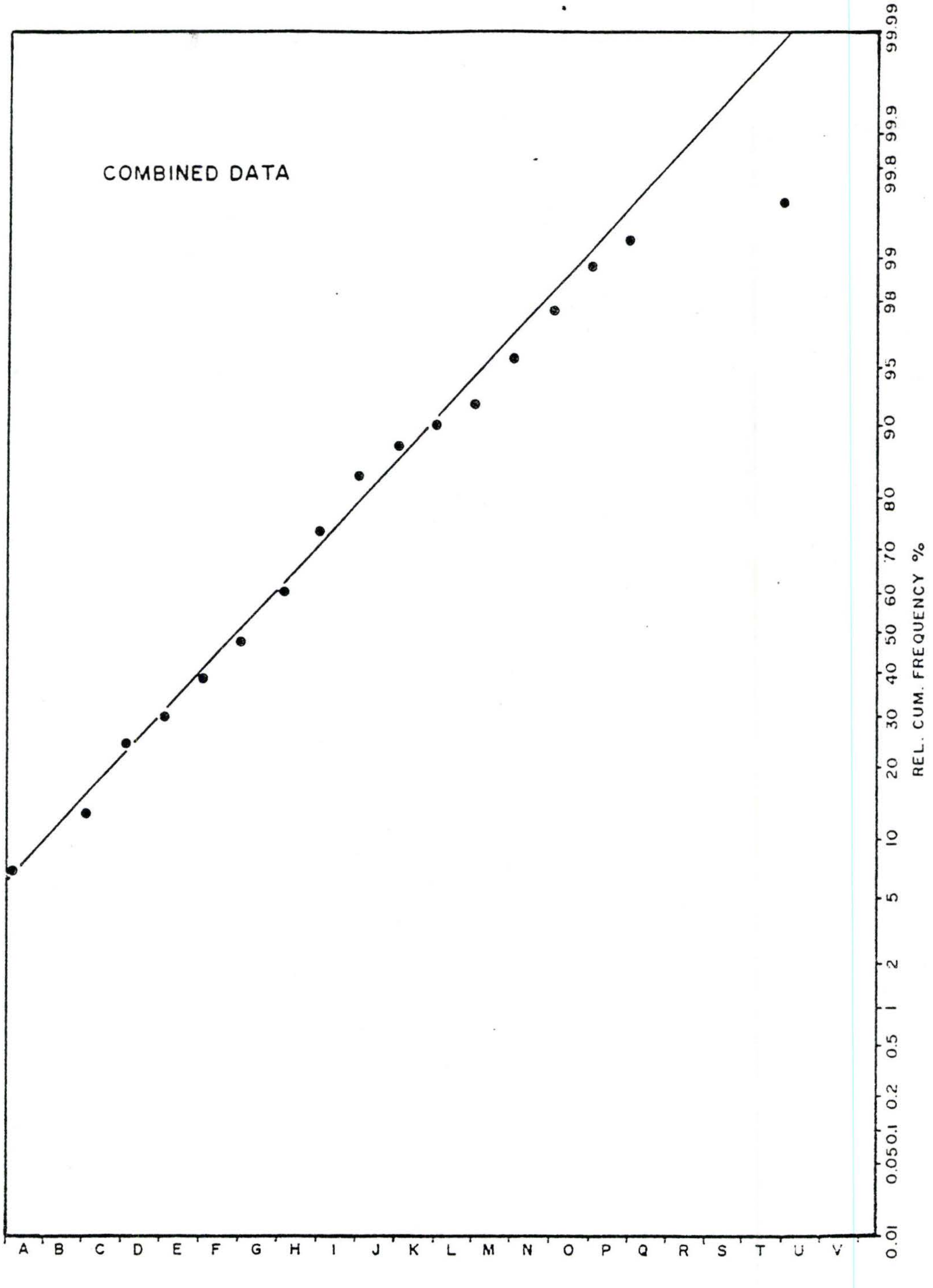
COMBINED DATA
A
B
C
D
E
F
G
H
I
J
K
L
M
N
O
P
Q
R
S
T
U
V
0.01
0.05
0.1
0.2
0.5
1
2
5
10
20
30
40
50
60
70
80
90
95
98
99
99.8
99.9
99.99
REL. CUM. FREQUENCY %

Figure 67 Relative cumulative frequency curve for Ln transformation No Seams vertical permeability data. Same legend as in Figure 63.

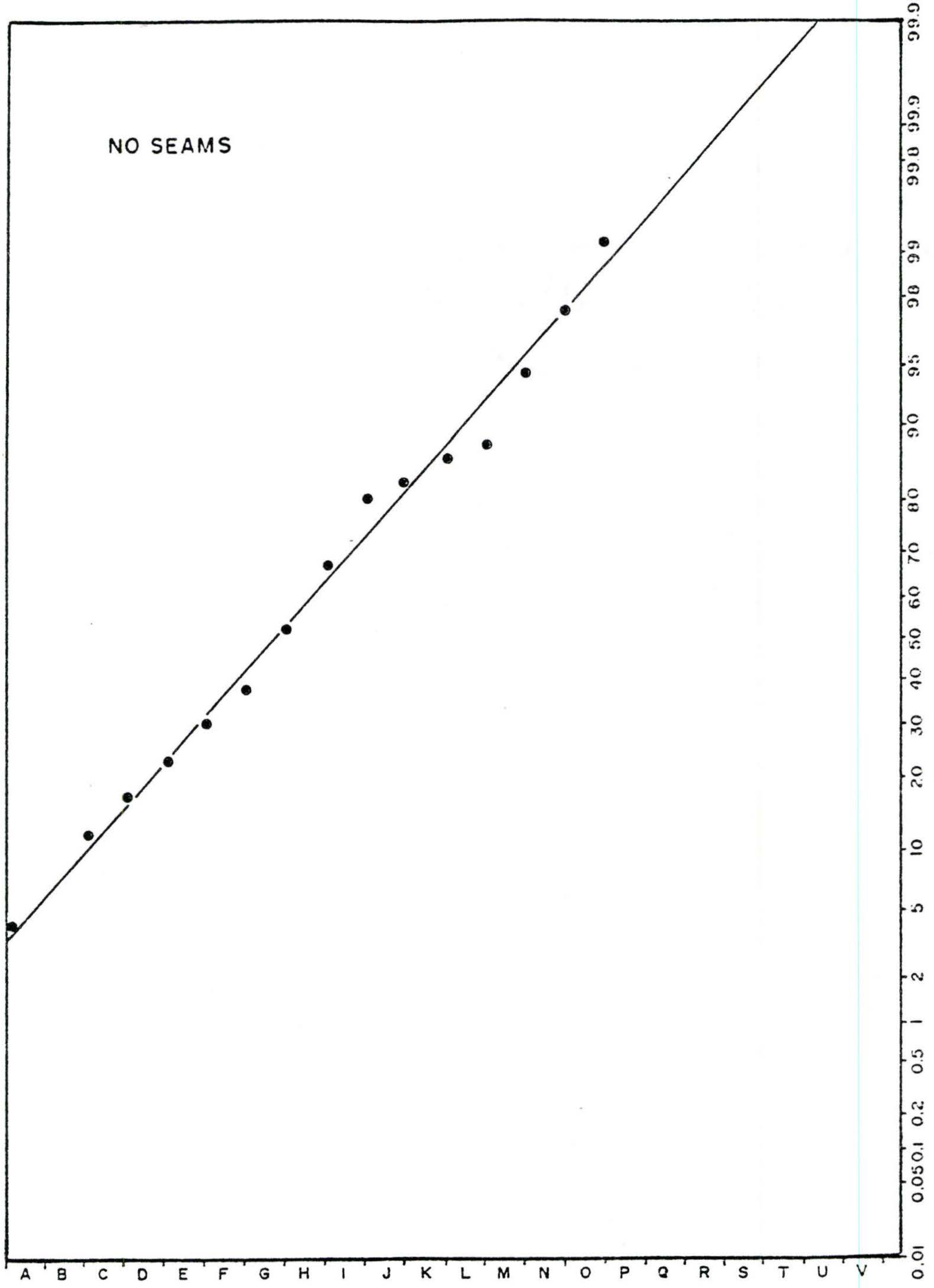
NO SEAMS
REL. CUM. FREQUENCY %
0.01
0.05
0.1
0.2
0.5
1
2
5
10
20
30
40
50
60
70
80
90
95
98
99
99.8
99.9
99.99
A
B
C
D
E
F
G
H
I
J
K
L
M
N
O
P
Q
R
S
T
U
V

Figure 68 Relative cumulative frequency curve for Ln transformation All Seams vertical permeability data. Same legend as in Figure 63.

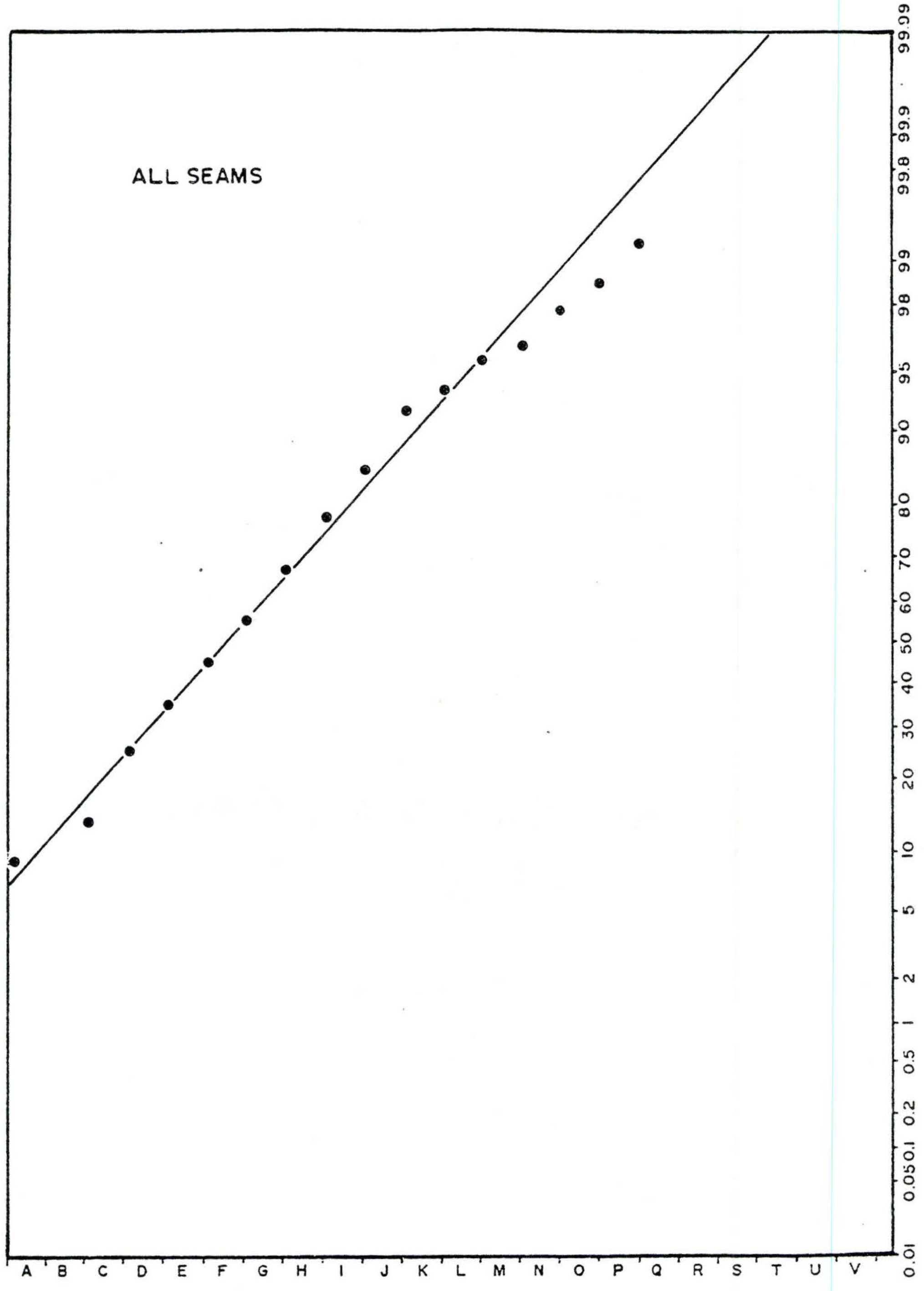
ALL SEAMS
A
B
C
D
E
F
G
H
I
J
K
L
M
N
O
P
Q
R
S
T
U
V
REL. CUM. FREQUENCY %
0.01
0.05
0.1
0.2
0.5
1
2
5
10
20
30
40
50
60
70
80
90
95
98
99
99.8
99.9
99.99

line fitted by eye does not exactly fit the data, it is sufficient to indicate that the data are distributed normal enough to satisfy the forthcoming tests of significance.

4.6 THE FIRST DISTILLATION-STYLOLITES BY SCALE

All stylolite-bearing drill plugs are classified as to the scale of the feature in them. The classification is based upon the amplitude of the stylolite i.e. micron-, micron to millimetre-, millimetre-, millimetre to centimetre-, centimetre-scale. Presumably, the greater the amplitude of the stylolite, the more mature it is. The more mature it is, then the more it should behave as a permeability barrier owing to greater accumulations of insoluble materials.

Once classified, means and standard deviations were calculated for the non-stylolitic and stylolitic plugs using the transformed Kvert values (Table 6). Initial examination implies that there is a decreasing trend with greater amplitude followed by an increase at the centimetre-scale class. Is this significant or does it just arise by chance? If this decreasing trend is significant, then it suggests that stylolites do act as barriers to flow, at least up to millimetre to centimetre-scale.

TABLE 6: FIRST DISTILLATION DATA

Ln (Kvert) And [Ln^{-1} (Kvert)] Values. Kvert in millidarcies.

	n	$\bar{x}$	Sx
No Seams	140	-1.16 [0.31]	1.82 [6.17]
Micron-Scale	48	-1.64 [0.19]	1.59 [4.90]
Micron To Millimetre-Scale	35	-1.74 [0.18]	1.42 [4.14]
Millimetre-Scale	24	-1.84 [0.16]	1.89 [6.62]
Millimetre To Centimetre-Scale	23	-2.10 [0.12]	1.92 [6.82]
Centimetre-Scale	27	-1.61 [0.20]	2.18 [8.85]
All Seams	157	-1.76 [0.17]	1.75 [5.75]

4.6.1 COMPARISON OF MEANS; VERTICAL PERMEABILITY VALUES I

Having calculated mean Kvert values for the above classification, it is necessary to test the significance of the trend observed in Table 6. To do this, the mean Kvert values of each class are individually compared to the mean Kvert value for the No Seam data. It is assumed that the No Seam data represent those plugs not directly affected by stylolitization; therefore they can be used as the control. By doing the comparison in this manner, it will tell us if the lower mean Kvert values for stylolitic plugs are significant of an actual difference or just an artifact of calculations.

Confidence Intervals afford a method by which one can graphically express this comparison. A Confidence Interval is an expression of the "standard error of the means" which may be regarded as a standard error of estimate (error bars) of the mean values calculated. Knowing a mean Kvert value for a stylolitic class and the corresponding confidence interval, if the mean of the control (No Seams) lies within two standard errors of the stylolitic mean, then the difference is not significant. But if the control mean lies beyond two standard errors, then this is probably a significant difference.

Expressing this argument differently, there is a 95% probability that the control mean will lie within two standard errors of the stylolitic mean if they both come from the same population. If the control mean lies beyond this confidence interval then it is significant at the 5% level i.e. there is 1 chance in 20 that this will occur by chance, but 19 in 20 that this difference between means is probably significant of a real difference. Furthermore, if the control mean lies beyond three standard errors of the stylolitic mean, then it is definitely significant at the 1% level i.e. there is 1 chance in 100 that this difference occurs by chance, and 99 times in 100 that it is definitely significant of a real difference. Table 7 lists the calculated Confidence Intervals at 2 and 3 times the standard errors of the stylolitic means. Figure 69 is the graphical presentation of this comparison.

Figure 69 reveals that at the 5% probability level (+/- 2 Std. Err. of Means) the difference that exists between No Seams and micron-, micron to millimetre-, millimetre-, and centimetre-scale seams is less than the error in its mean Kvert value. At the 1% level (+/- 3 Std. Err. of Means) the difference that exists between No Seam and all classes of stylolites does not exceed any of the errors in the individual mean Kvert values.

Significance is established for millimetre to centimetre-scale seams. The difference between these and No Seams is probably significant at the 5% level but not at the

TABLE 7: CONFIDENCE INTERVALS FOR FIRST DISTILLATION

	2 Std. Errors Of The Mean	3 Std. Errors Of The Mean
No Seams	.31	.46
Micron-Scale	.53	.79
Micron To Millimetre-Scale	.62	.92
Millimetre-Scale	.74	1.11
Millimetre To Centimetre-Scale	.76	1.14
Centimetre-Scale	.70	1.05
All Seams	.29	.44

Figure 69 Confidence Intervals of the first distillation: stylolites by scale compared to No Seams data. Solid line = +/- 2 Std. Err. of Means. Dashed line = +/- 3 Std. Err. of Means.

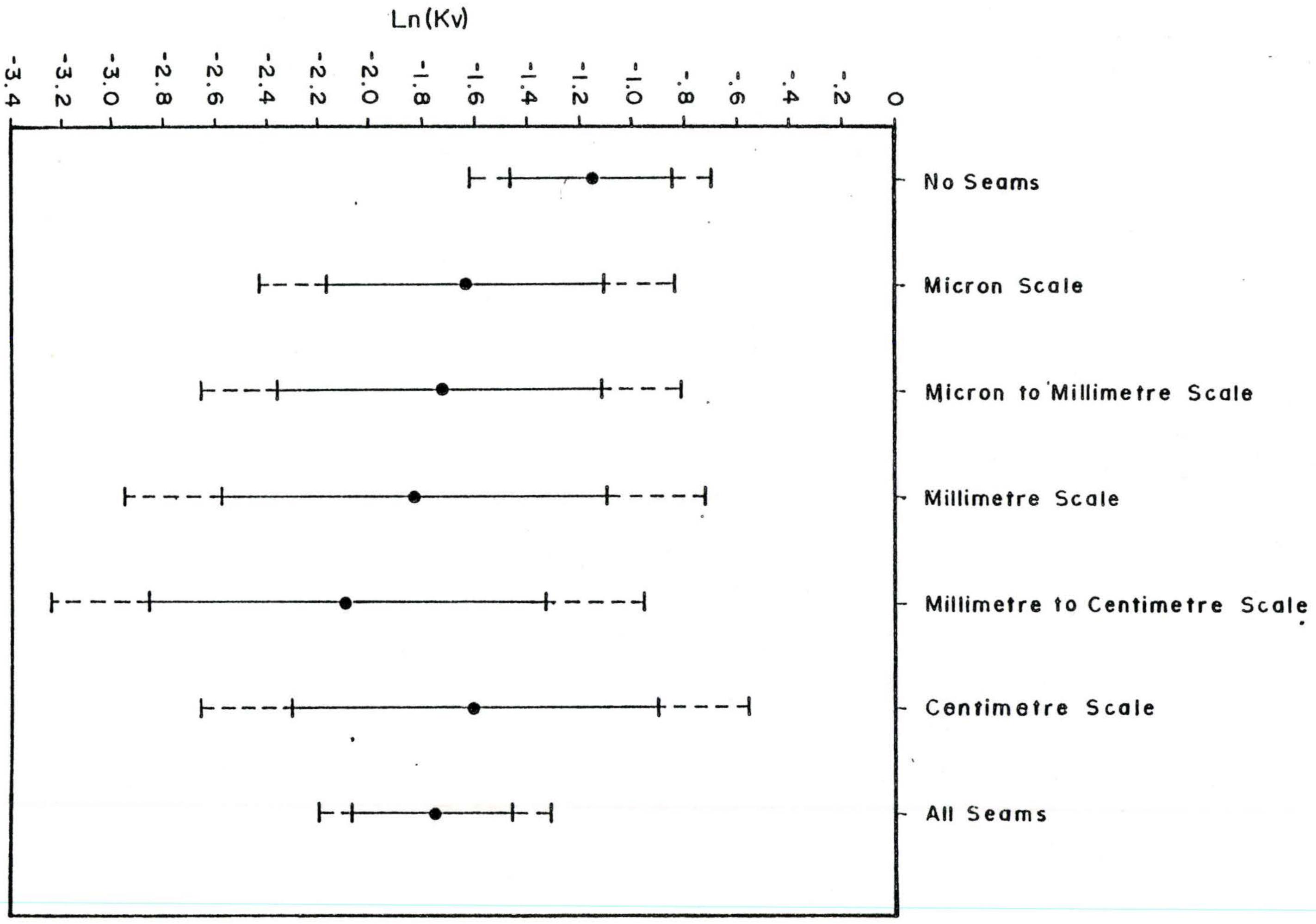
Ln(Kv)
-3.4
-3.2
-3.0
-2.8
-2.6
-2.4
-2.2
-2.0
-1.8
-1.6
-1.4
-1.2
-1.0
-.8
-.6
-.4
-.2
0
No Seams
Micron Scale
Micron to Millimetre Scale
Millimetre Scale
Millimetre to Centimetre Scale
Centimetre Scale
All Seams

1% level (i.e. the difference between the means is greater than the error at two standard errors of mean but less than that at three standard errors). On the plot of Confidence Intervals this is the class with the lowermost mean Kvert value and the greatest error bars.

The probable significance of the difference between millimetre to centimetre-scale seams and No Seams suggests that this scale of stylolite is the most effective permeability barrier. But this is only for separate classes of stylolites. The question that now arises is "How do stylolites behave as permeability barriers when one considers them as a whole i.e. all stylolites as one class?"

If we take all the stylolitic plugs used in the first distillation as one class and proceed as before, then the difference shows up as being definitely significant. The mean of the No Seam data lies beyond three standard errors for the All Seam data mean. This suggests that stylolites as a whole do behave as vertical permeability barriers (Figure 69). But the difference is not that great because the error bars for No Seam mean overlap those for the All Seam mean. Because of this overlap the significance of the difference becomes a questionable beyond the 5% level of significance. The actual difference is equal to .14 md. Similar results as these for Confidence Intervals were found using T-tests as comparisons of means. Like the

Confidence Intervals, these tested the significance of the difference between the No Seam mean and those for the stylolite classes. Results are shown in Table 8.

To explore this further a closer look at the millimetre to centimetre-scale class is called for. What makes this scale of stylolite have such a low mean Kvert value and be the only scale to show a significant difference? Is it due to an actual property of the feature (e.g. thickest accumulation of insolubles) or is it because of the small sample size involved (n=23)? Furthermore, why do centimetre-scale stylolites have a higher mean Kvert value than all other classes?

4.7 THE SECOND DISTILLATION-STYLOLITES BY SCALE AND MAIN PORE TYPES

The analysis of stylolites by scale and their role as permeability barriers needs further refinement. In the first distillation all that was considered was the scale of the stylolite and nothing else. In this distillation the main pore types are considered in conjunction with the scale of the stylolite.

From drill core analyses, three main pore types were considered: large vugs (lv), fossils (fos), and fractures

TABLE 8: SUMMARY OF T-TEST RESULTS FOR FIRST DISTILLATION

Comparison Being Made To No Seams	Calculated "t" Ratio And df	"t" Ratio To Exceed 5% Level	"t" Ratio To Exceed 1% Level	Significance
Micron-Scale	1.83 186 df	1.95	2.65	Not at 5% level
Micron To Millimetre-Scale	1.86 173 df	1.95	2.65	Not at 5% level
Millimetre-Scale	1.83 162 df	1.95	2.65	Not at 5% level
Millimetre To Centimetre-Scale	2.48 161 df	1.95	2.65	Significant at 5% level Not at 1% level
Centimetre-Scale	1.28 165 df	1.95	2.65	Not at 5% level
All Seams	4.13 295 df	1.90	2.60	Significant beyond 1% level

(frac). The question that arises is "How do the presence of these pore types affect the behaviour of a stylolite as a permeability barrier?"

Table 9 shows the main pore types considered and the combinations of these pore types found in drill plugs. As before, plugs are classified by the absence/presence of stylolites and the scale of the feature. For the 7 possible combinations of pore types only 3 are useful for purposes of comparison, the reason being the number of plugs containing these pore types and combinations thereof. Groups A, B, and D have sufficiently high numbers of occurrence to carry out this comparison. The remaining groups (C,E,F,G,) are not useful due to their low numbers of occurrence.

As before, working with the Ln(Kv) transformations, the means and standard deviations are calculated for each class in all three groups (Table 10). These calculated values will be compared as mean values of the vertical permeability for each class within their respective groupings.

4.7.1 COMPARISON OF MEANS; VERTICAL PERMEABILITY VALUES II

Having calculated mean Kvert values it is now necessary to determine whether the difference between the mean value for non-stylolitic and stylolitic classes is significant of a real difference. The comparison of means

TABLE 9: SECOND DISTILLATION

Main Porosity Types To Be Considered and Number Of Plugs In Each Grouping

Groupings	No Seams	micron scale	micron to millimetre scale	millimetre scale	millimetre to centimetre scale	centimetre scale	total number
Group A fos	50	15	4	3	6	5	83
Group B fos + frac	65	17	26	15	13	12	148
Group C fos + lv	1	1	0	0	1	0	3
Group D frac	15	8	4	3	2	7	39
Group E frac + lv	4	0	0	0	0	1	5
Group F lv	0	2	0	0	0	0	2
Group G lv + frac + fos	1	3	1	1	0	3	9

TABLE 10: SECOND DISTILLATION DATA

Ln (Kvert) And [Ln^{-1} (Kvert)] Values. Kvert in millidarcies.

	No Seams			Micron-Scale		
Group	n	$\bar{x}$	Sx	n	$\bar{x}$	Sx
A Fossils	50	-1.34 [0.26]	1.59 [4.90]	15	-2.00 [.14]	1.14 [3.13]
B Fossils & Fractures	65	-1.04 [0.35]	1.66 [5.26]	17	-1.31 [0.27]	1.75 [5.75]
D Fractures	15	-1.80 [0.17]	2.09 [8.08]	8	-2.12 [0.12]	1.61 [5.00]

	Micron to Millmetre-Scale			Millimetre-Scale		
Group	n	$\bar{x}$	Sx	n	$\bar{x}$	Sx
A Fossils	4	-2.66 [0.07]	.42 [1.52]	3	-4.14 [0.02]	.40 [1.49]
B Fossils & Fractures	26	-1.65 [0.19]	1.54 [4.66]	15	-1.49 [0.23]	2.02 [7.54]
D Fractures	4	-1.62 [0.20]	1.15 [3.16]	3	-1.39 [0.25]	1.25 [3.49]

(cont'd)

TABLE 10; SECOND DISTILLATION DATA

Ln (Kvert) And [Ln^{-1} (Kvert)] Values. Kvert in millidarcies. (cont'd)

	Millimetre to Centimetre-Scale			Centimentre-Scale		
Group	n	$\bar{x}$	Sx	n	$\bar{x}$	Sx
A Fossils	6	-3.73 [0.02]	1.43 [4.18]	5	-2.69 [0.07]	.73 [2.08]
B Fossils & Fractures	13	-1.19 [0.30]	1.88 [6.55]	12	-1.96 [0.14]	1.64 [5.16]
D Fractures	2	-3.11 [0.04]	.16 [1.17]	7	-2.21 [0.11]	1.23 [3.42]

is done using a T-test. This enables one to determine if the difference between two classes (stylolitic and non--stylolitic) is significant of a difference between the parent sources. The results are shown in Table 11.

From Table 11 the observed difference between non-stylolitic and stylolitic classes is significant for the Group A millimetre- and millimetre to centimetre-scale seams at the 1% level. For all other classes in this group and Groups B and C, the difference that exists is not significant. Significance was tested at a minimal 5% level i.e. a 95% probability that the observed difference is a real one and not one that occurs by chance.

There is some semblance of similarity between the Group A results and those of the first distillation. In the first distillation the millimetre to centimetre-scale of stylolites showed up as being probably significant of a difference when compared to No Seam data at a 5% level of probability. For the Group A data the mean Kvert for the intermediate scales of stylolites (millimetre- and millimetre to centimetre-) is definitely different from the No Seam mean Kvert value at a 1% level. This suggests that intermediate scales of stylolites behave as effective permeability barriers in these reefal carbonates and that centimetre-scale stylolites do not.

TABLE 11: SUMMARY OF T-TEST RESULTS FOR SECOND DISTILLATION

Group	Calculated "t" Ratio And Degrees of Freedom	"t" Ratio To Exceed 5% Level	"t" Ratio To Exceed 1% Level	Significance
Micron-Scale to No Seams:				
A	1.47 63 df	1.97	2.68	Not at 5% level
B	.59 80 df	1.95	2.65	Not at 5% level
D	.36 21 df	2.08	2.83	Not at 5% level
Micron to Millimetre-Scale To No Seams:				
A	1.63 52 df	1.98	2.70	Not at 5% level
B	1.61 89 df	1.95	2.65	Not at 5% level
D	.16 17 df	2.11	2.90	Not at 5% level
Millimetre-Scale To No Seams:				
A	2.98 51 df	1.98	2.70	Significant at 1% level
B	.90 78 df	1.96	2.66	Not at 5% level
D	.31 16 df	2.12	2.92	Not at 5% level

(cont'd)

TABLE 11; SUMMARY OF T-TEST RESULTS FOR SECOND DISTILLATION

(cont'd)

Group	Calculated "t" Ratio And Degrees of Freedom	"t" Ratio To Exceed 5% Level	"t" Ratio To Exceed 1% Level	Signifance
Millimetre to Centimetre-Scale To No Seams:				
A	3.46 54 df	1.96	2.68	Significant at 1% level
B	.29 76 df	1.97	2.67	Not at 5% level
D	.83 15 df	2.13	2.95	Not at 5% level
Centimetre-Scale To No Seams:				
A	1.85 53 df	1.96	2.68	Not at 5% level
B	1.74 75 df	1.97	2.67	Not at 5% level
D	.46 20 df	2.09	2.85	Not at 5% level

Group B and D results indicate no significant difference between stylolitic and non-stylolitic mean Kvert values. What is the reason for this? The common denominator of these two groups is the presence of fractures (as described in drill core descriptions). This suggests that fractures counteract stylolites by improving the vertical permeability of stylolitic rock.

4.8 DISCUSSION

Having seen vertical permeability frequency histograms for Combined Data, No Seams, and All Seams, one might be struck by the similarity of the three plots. They all have the same most frequent class interval, .01 to .19 md and approximately the same lack of symmetry (Sk = .11). The first hint that stylolites might behave as permeability barriers shows up when modes are compared i.e. .16 md for No Seams and .13 md for All Seams. Further evidence of permeability reduction is seen in the All Seam plot where the major distribution lies in the lowermost class intervals. However, both the No Seams and All Seams plots have greater than 80% (81.4% and 87.3% respectively) of the Kvert distribution lower than 1.0 md.

It appears that stylolites do reduce the vertical permeability of this rock but that they do not "drastically" alter it. The fact that the No Seam and All Seam plots are similarly skewed and have the same most frequent class interval attest to the lack of a "drastic" alteration.

All Seam data are classified by scale (micron through centimetre) to determine whether larger stylolites, thus the more mature ones, behave as more effective permeability barriers relative to smaller ones. Each class of stylolite is compared to the No Seam data using tests of significance with the No Seam data as the control. It is assumed that the stylolitic drill plugs would have had vertical permeability characteristics similar to non-stylolitic plugs were they not affected by stylolitization. Working with mean Kvert values allows one to look at representative values for each class and provides a basis for comparison.

Mean vertical permeability values for each class are successively lower as one goes from micron- to millimetre to centimetre-scale stylolites and then increases for centimetre-scale. This decreasing trend suggests that the increased accumulation of insoluble material as a stylolite matures (grows) reduces the vertical permeability i.e. the more mature stylolites are the more effective permeability barriers. But why do centimetre-scale stylolites have a higher mean vertical permeability than all other scales of stylolites?

The most feasible explanation can be attributed to the shearing action of a stylolite column in its socket as it grows, thus producing striations and thin "stretched-out" accumulations of insolubles along the sides of the column. These features are most commonly observed in centimetre-scale stylolites. As a stylolite grows insoluble materials increasingly accumulate. It is this accumulation of insolubles that acts as the permeability barrier along the stylolite surface. The data (Table 6) suggest that between micron- and millimetre to centimetre-scales, insolubles increasingly accumulate. At some point between millimetre to centimetre-scale and centimetre-scale in a stylolites growth history, the shearing process becomes so great that it extensively thins the accumulated insoluble material along the sides of individual columns, thus creating "holes" in the insoluble film. These "holes" counteract the behaviour of stylolites as permeability barriers, thus increasing the vertical permeability of the stylolitic rock.

It is necessary to statistically compare the mean Kvert values of the stylolitic classes to the No Seam data to determine how significant the permeability reduction actually is. Both Confidence Intervals and T-tests show similar results. Only millimetre to centimetre-scale stylolites differ significantly from the No Seam data, i.e. one time in twenty that it will occur by chance. All the other scales of stylolite classes do not differ significantly from the No Seam data i.e. more than one time in twenty the difference observed will occur by chance. It is suggested at this point that the probable significant difference of the millimetre to centimetre-scale stylolite class reflects the increasingly greater accumulation of insoluble materials in maturing stylolites. Furthermore, the lack of a significant difference for the centimetre-scale class might reflect the shearing action mentioned earlier.

If all the stylolites are compared as a whole to the No Seam data then the observed difference between the mean Kvert values is definitely significant. This suggests that all the stylolites do behave as effective permeability barriers (but remember that the main contributor to this result is the millimetre to centimetre-class). These results support the ideas brought forth earlier when discussing the frequency histograms, that stylolites do reduce the vertical permeability of the rock, but not drastically.

Grouping of the stylolite classes by the presence of main pore types affords a closer look at how stylolites behave as permeability barriers. When stylolites occur together with fossil porosity in the same drill plug, T-tests indicate that the intermediate scales (millimetre-,

millimetre to centimetre-) of stylolites have a definite significant difference when compared to the No Seam data. The remaining classes do not differ significantly from the No Seam data. As observed in the first distillation, all the stylolite classes have a lower mean Kvert that the No Seam data and the mean for the centimetre-scale class is higher than that for intermediate scales.

These results suggest three things: first, that millimetre- and millimetre to centimetre-scale stylolites reflect the increasing accumulation of insoluble materials and are the most effective permeability barriers in carbonate with fossil porosity; second, that centimetre-scale stylolites elevate the previously reduced vertical permeability of the rock due to the shearing effect; third, stylolites do behave as permeability barriers, but the difference is only significant for the intermediate scales.

Stylolites occurring with fractures or fossils and fractures show dissimilar results. Using T-tests, no significant differences were found to exist between the mean Kvert values of each individual stylolite class and the No Seam class. Most stylolite classes have a mean vertical permeability lower than their No Seams class does, but there is not the decreasing then increasing pattern as observed before. In some cases the mean Kvert for the stylolite class approaches or exceeds that for the No Seams class. Any systematics that were observed earlier are now absent.

As a possible explanation it seems reasonable to look to the common denominator between these two groupings, the presence of fractures. In drill core, fractures were observed propagating from and cross-cutting stylolites of all scales. These fractures vary in length from less than 1 centimetre to upwards of 14 centimetres and usually occur several at a time. Knowing that this relationship exists, it is suggested that fractures may disrupt the behaviour of stylolites as permeability barriers by providing alternative avenues of vertical flow.

4.9 SUMMARY

Statistical analysis of vertical permeability data indicates that stylolitic drill plugs do have reduced vertical permeabilities and that intermediate scale stylolites are statistically the most effective permeability barriers. The first distillation of data shows these to be millimetre to centimetre-scale stylolites regardless of pore types. The second distillation of data indicates that millimetre- and millimetre to centimetre-scale stylolites are the most effective permeability barriers only when associated with fossil porosity (Group A). The presence of fractures disrupts the decreasing then increasing trend observed in the first distillation and associated with fossil porosity, such that the resulting pattern is erratic (Table 10).

Small scale stylolites (micron to millimetre-) have mean Kvert values similar to that for centimetre scale stylolites in the first distillation and for Group A of the second distillation. For the micron to millimetre-scale stylolites this reflects relatively lower accumulations of insoluble material along the stylolite surface resulting in a lesser degree of permeability reduction. A similar mean Kvert value for centimetre-scale stylolites cannot be explained in this manner. The shearing action of a stylolite column against its socket walls essentially thins the accumulated insoluble material between the socket and column. This results in less permeability reduction due to decreased thicknesses of insoluble material at these interfaces.

This analysis relates vertical permeability reduction to the scale of individual stylolites. It implies that as a stylolite grows it will increasingly reduce Kvert through to intermediate scales then return to values equivalent to those for early stages of growth at centimetre-scale. Whether this pattern is ubiquitous for all stylolitic carbonates is unknown. It may only apply to reefal carbonates such as these.

CHAPTER 5

CATHODOLUMINESCENCE

5.1 INTRODUCTION

Cathodoluminescence (CL) refers to the emission of light from a crystalline substance when it is bombarded with a low-energy electron beam. The phenomenon has been known for over 100 years, yet it is only within the last 20 years that its potential as a petrologic tool has been realized.

Geological applications of cathodoluminescence were initially made with an electron microprobe analyser (Long and Agrell 1965, Smith and Stenstrom 1965). This proved to be of limited use as a petrologic tool but soon afterward the first microscope-attached instrument was developed (Sippel and Glover 1965). Since then the CL technique has become widely used in the examination of geological materials.

The most widespread use of this technique has been in the study of carbonates. Growth structures and fabrics are revealed that are invisible with a petrographic microscope. Staining may reveal similar features but cathodoluminescence yields more information. A decade ago the principle of "cement stratigraphy" was introduced (Meyers

1974, 1978) and has since proved to be invaluable in understanding paleoaquifer systems. Geochemical interpretation of CL zones and sequences has lead to a better understanding of the chemical nature of the pore waters that have passed through the rock. However, our present state of knowledge of the relationship between CL signatures and the precipitational environments of carbonates is in an adolescent stage, yet to be refined upon maturing.

5.2 CAUSES AND CONTROLS OF CATHODOLUMINESCENCE IN CARBONATES

Carbonate luminescence has been related to a multitude of factors, among which are: distorted crystal surfaces and cracks, distorted internal structure between mosaic crystals and intergrown crystals, omission defects in lattice sites, inhomogeneities of composition in different parts of a crystal, impurities in surface, lattice, and interstitial sites, charge displacements resulting from abnormally ionized atoms and/or separated cation/anion pairs. These are lesser causes which are more suitably addressed by Nickel (1978) and Marfunin (1979).

The main cause of carbonate cathodoluminescence is attributed to the presence of trace elements in the crystalline solid. These elements either promote or suppress the emission of light from a crystal when excited by an electron beam. Conveniently, they are grouped as activators or quenchers. Early investigations via microprobe analysis showed divalent manganese, Mn^{2+}, to be the main activator (Long and Agrell 1965, Sippel and Glover 1965, Smith and Stenstrom 1965) largely because it is the most abundant element having such abilities (Sommer 1972a). To a lesser degree, Pb^{2+}, is also considered to behave as an activator (Long and Agrell 1965).

Quenchers are those elements that suppress active luminescence. The main quencher is recognized as ferrous iron, Fe^{2+}, once again due to its abundance. The ability to quench luminescence has also been attributed to Ni^{2+} and Co^{2+}, however these elements are not as abundant as Fe^{2+} in quenched luminescent samples. Carbonate cathodoluminescence therefore has been considered to be dependent upon manganese and iron concentrations by many investigators (Sommer 1972a, 1972b, Carpenter and Oglesby 1976, Nickel 1978, Pierson 1981, Frank 1981, Richter and Zinkernagel 1981, Frank et al. 1982, Fairchild 1983, James and Choquette 1984, Schofield and Adams 1986).

Within the last decade, investigators have attempted to determine what controls the cathodoluminescent intensity of calcite and dolomite. Carpenter and Oglesby (1976) suggested that CL intensity was proportional to Mn^{2+} concentrations and inversely proportional to Fe^{2+} concentrations in the crystalline solid. Concentration ratios are visible as variable CL intensities of carbonates. Pierson (1981) studied the control of these elements on the CL of dolomite. He suggested that the intensity of luminescence is not proportional to Mn^{2+} concentrations but that Fe^{2+} begins to quench the Mn-induced luminescence as it reaches 10,000 ppm. Beyond 15,000 ppm Fe^{2+}, CL is totally extinct, regardless of the Mn^{2+} concentration.

The studies of Frank (1981) and Frank et al. (1982) propose that CL intensities are controlled by Fe/Mn ratios for both calcite and dolomite and not absolute concentrations. The graph of Figure 70 illustrates this relationship for calcite.

Fairchild (1983) does not dispute this proposal but notes that there are differences in the limits of the Fe/Mn ratios between luminescent and non-luminescent samples in these studies.

Instead of relating the dependence of luminescent intensities to Fe/Mn ratios, Fairchild (1983) prefers the idea of a "Fe-quenching" line (Figure 71). Above a certain concentration of Fe, luminescence is quenched. This is shown for dolomite (Figure 71a). There are insufficient data to show this for calcite (Figure 71b). However, closer examination of the dolomite data (Figure 71a) shows that boundaries similar to Frank et al. (1982) (Figure 70) may be

Figure 70 Relationship between concentration of $FeCO_3$ and $MnCO_3$ (mole %) and luminescence in calcite. Data suggest that the ratio Fe/Mn, not the absolute amounts of either cation, controls the luminescent intensity displayed by calcite. Arrows indicate $FeCO_3$ or $MnCO_3$ concentrations less than 0.05 mole percent (from Frank et al., 1982).

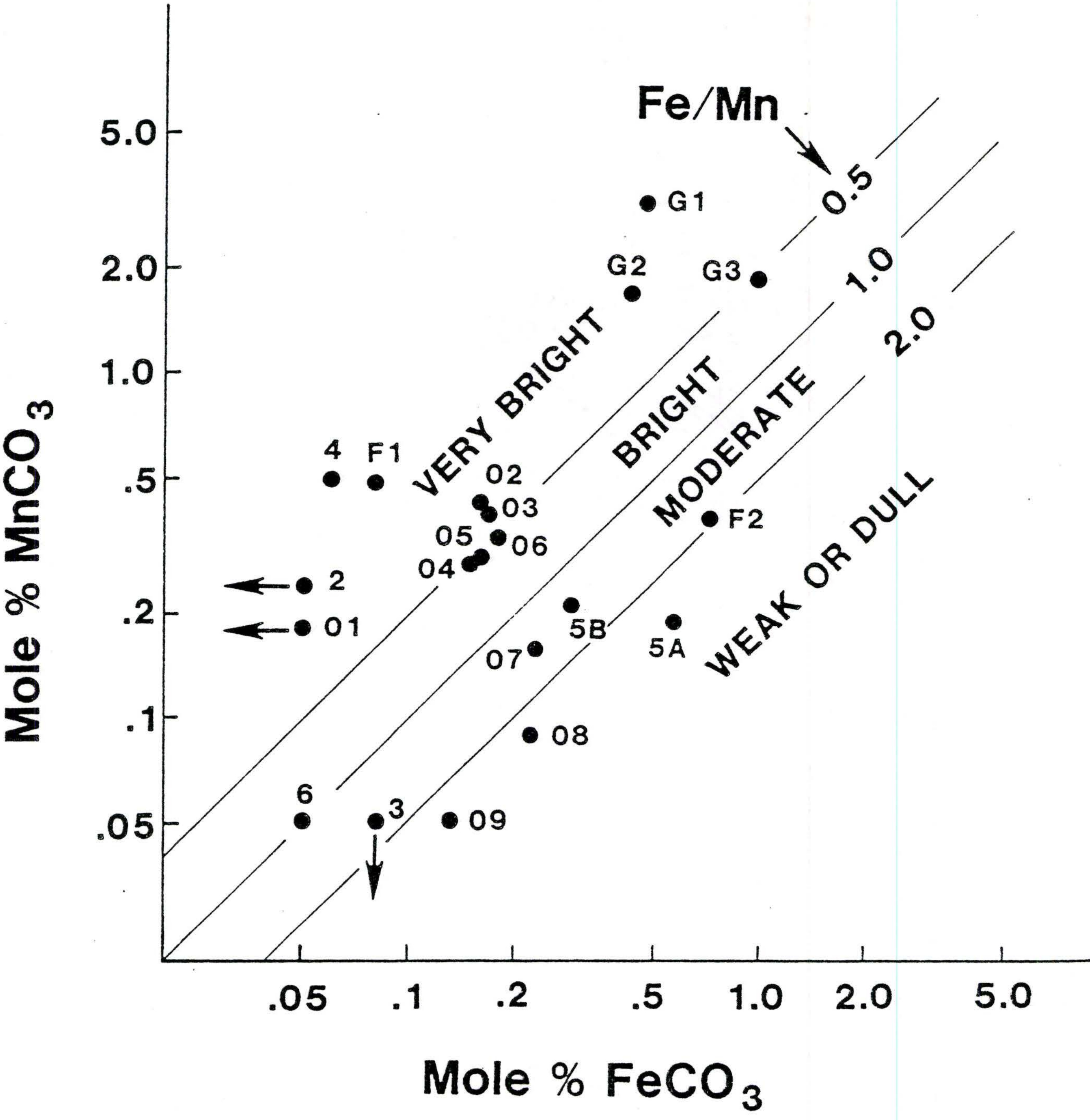
Fe/Mn
0.5
1.0
2.0
VERY BRIGHT
BRIGHT
MODERATE
WEAK OR DULL
G1
G2
G3
4
F1
02
03
05
06
04
2
01
5B
5A
F2
07
08
6
3
09
5.0
2.0
1.0
.5
.2
.1
.05
Mole % MnCO3
.05
.1
.2
.5
1.0
2.0
5.0
Mole % FeCO3

Figure 71 Relationship between Fe-Mn chemistry (weight %) and luminescence for carbonates of the Bonahaven Formation. 71a) Data for dolomite samples. 71b) Data for calcite samples. From Fairchild 1983.

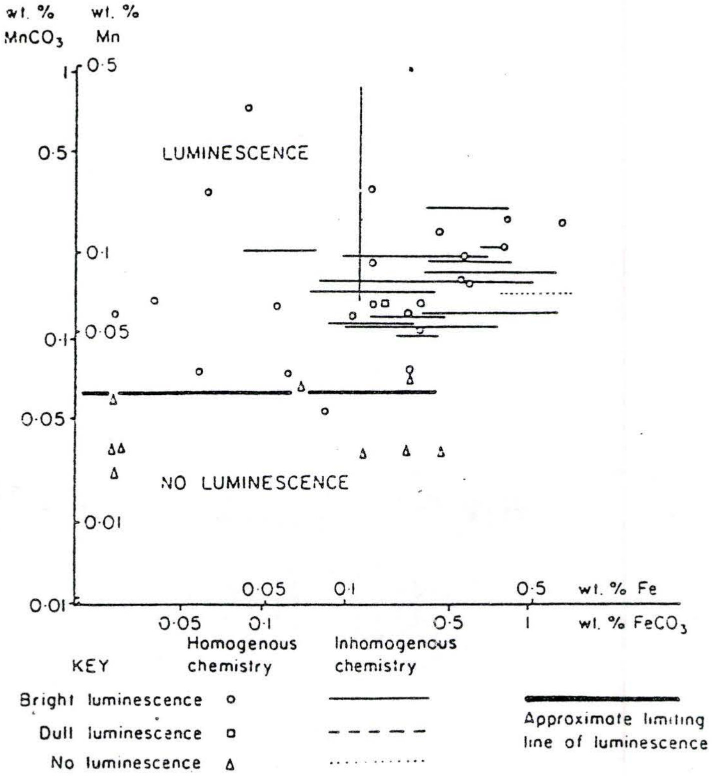
wt. %
MnCO₃
wt. %
Mn
1
0·5
0·1
0·05
0·01
0·5
0·1
0·05
0·01
LUMINESCENCE
NO LUMINESCENCE
0·05
0·1
0·5
wt. % Fe
0·05
0·1
0·5
1
wt. % FeCO₃
KEY
Homogenous chemistry
Inhomogenous chemistry
Bright luminescence ○
Dull luminescence □
No luminescence △
Approximate limiting line of luminescence

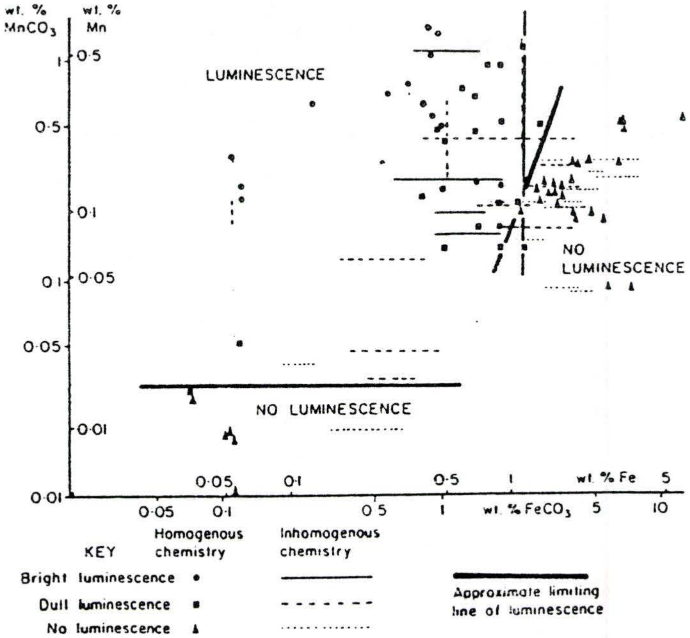
wt. %
MnCO₃
wt. %
Mn
1
0·5
0·1
0·05
0·01
0·5
0·1
0·05
0·01
LUMINESCENCE
NO LUMINESCENCE
NO LUMINESCENCE
0·05
0·1
0·5
1
wt. % Fe
5
0·05
0·1
0·5
1
wt. % FeCO₃
5
10
KEY
Homogenous chemistry
Inhomogenous chemistry
Bright luminescence ●
Dull luminescence ■
No luminescence ▲
Approximate limiting line of luminescence

drawn at 45° to the axes as shown. A similar criticism may be drawn for the calcite data (Figure 71b).

Table 12 is a compilation of data available in the literature showing Fe/Mn ratios as related to CL intensity for calcites and dolomites. For calcite, bright luminescence is exhibited for those samples having a Fe/Mn ratio less than 1. Dull luminescence is exhibited in samples with an Fe/Mn ratio between 1 and 3. No luminescence is found in samples with an Fe/Mn ratio greater than 3. Of course there are exceptions. For dolomite, boundaries are not so easily defined. As the ratio becomes greater, luminescence decreases. An approximation of a Fe/Mn ratio limit between luminescence and no-luminescence is hard to make. It was suggested by Fairchild (1983) that the differences in the limiting ratios are real, not due to differences in techniques, and likely due to behavioural differences between different sample suites.

Concommittant with the investigations of CL controls was the determination of minimal amounts of Mn^{2+} and Fe^{2+} required to activate or quench luminescence in calcite and dolomite. Pierson (1981) reported that Mn^{2+} concentrations as low as 100 ppm were found in brightly luminescing samples. Previously, Meyers (1974) had suggested that this minimum was close to 1000 ppm. Frank et al. (1982) stated that less than 300 ppm Mn^{2+} induce luminescence assuming

TABLE 12: VARIATION IN LUMINESCENT INTENSITY OF CALCITE AND DOLOMITE WITH IRON AND MANGANESE CONCENTRATION

Reference	$FeCO_3$	$MnCO_3$	Fe/Mn	Luminescence
Long and Agrell (1965) wt % Fe, Mn calcite	0.1	1.0	0.1	"Bright Lum."
	1.0	0.1	10	"Non-lum."
Martin and Zeegers (1969) wt % Fe, Mn calcite	-	0.36	-	"le niveau supereur"
	-	0.14	-	"le niveau moyen"
	-	0.03	-	"le niveau inferieur"
Sommer (1972b) ppm Fe, Mn aragonite shell	500	850	.59	"high intensity"
	500	000	-	"non-lum."
	430	660	.65	"very-bright"
Oglesby (1976) mole % calcite	<0.05	0.18	<0.28	"very bright"
	0.16	0.42	-0.38	"bright to very bright"
	0.17	0.38	-0.45	"bright to very bright"
	0.15	0.28	-0.54	"bright to very bright"
	0.16	0.29	-0.55	"bright to very bright"
	0.18	0.33	-0.55	"bright to very bright"
	0.23	0.16	-1.4	"dull"
	0.22	0.09	-2.4	"dull"
	0.13	0.05	-2.6	"dull"
	<.05	<.05	-	"non-lum"
George (1977) mole % calcite	0.47	3.04	0.15	"very bright"
	0.42	1.69	0.25	"very bright"
	0.97	1.85	0.52	"bright"
Meyers (1978) mole % calcite	0.15	0.05	3.0	"non-lum."
	2.20	0.35	.57	"bright to moderate"
	0.20	0.10	2	"non-lum"
	0.50	0.08	6.67	"dull-lum"

(cont'd)

TABLE 12; VARIATION IN LUMINESCENT INTENSITY OF CALCITE AND DOLOMITE WITH IRON AND MANGANESE CONCENTRATION

(cont'd)

Reference	$FeCO_3$	$MnCO_3$	Fe/Mn	Luminescence
Ebers and Kopp (1979) wt % Fe, Mn dolomite	0.3	0.05	6	"bright-red"
	0.6	<.02	<30	"med-darkred"
Fox (1979) mole % calcite	0.08	0.48	0.17	"bright"
	0.72	0.38	1.9	"dull"
Frank (1981) mole % dolomite	1.40	0.14	10.0	none
	1.40	0.96	1.5	Moderate
	1.42	0.19	7.5	Weak
	3.48	0.45	7.7	None
	4.56	0.35	13.0	None
	2.18	0.16	13.6	None
	1.28	0.27	4.7	Weak
Fairchild (1983) wt %			.5-1.0	bright dolo.
			1.0-2.4	dull "
			2.0-20	non-lum "
			.85-5	bright calcite
			1.5	dull "
			.66-12.5	non-lum "
Schofield and Adams (1986) Mole %	12.5	.05	2.5	red dolomite

(modified from Frank et al. (1982))

Fe^{2+} is absent. Richter and Zinkernagel (1981) reported that calcite and dolomite require 20-40 ppm Mn^{2+} to luminesce; however, the equipment they used differed from the majority of other workers. Fairchild (1983) presented the best summary. For calcite, activation occurs at Mn^{2+} concentrations of <200 ppm to 600 ppm, whereas for dolomite activation occurs at 150 to 300 ppm (see limiting lines Figure 71).

Fe-quenching in calcites and dolomites is not as well understood. Frank (1981) and Frank et al. (1982) suggested that calcites and dolomites will luminesce regardless of the amount of Fe^{2+} present as long as there is sufficient Mn^{2+} present. This relates to the dependency of CL intensity on the Fe/Mn ratio. On the other hand, Pierson (1981) prefers critical concentrations of Fe^{2+} regardless of the Mn^{2+} concentration. Fairchild (1983) states that luminescence persists in dolomites up to concentrations of 20,000 to 30,000 ppm Fe^{2+} but that this is partly dependent upon Mn^{2+} content. For calcite this value was reported as 10,000 ppm Fe^{2+}, but it was also noted that Fe-quenching may be different between different rock suites. These differences in quenching behaviour were suggested to be due to the presence of small and varying amounts of ferric iron, Fe^{3+}, in the calcite lattice. Marfunin (1979) reports that Fe^{3+} is a more effective quenching agent than Fe^{2+}.

In summary, there is a division in the present state of knowledge concerning CL intensity. One school of thought believes that CL intensities are controlled by the Fe/Mn ratios, whereas the second school believes that CL intensities are controlled by critical amounts of Fe^{2+} regardless of the amount of Mn^{2+} present. In what follows, it is accepted that the Fe/Mn ratio is the controlling factor.

Table 12 shows data taken from plots in Fairchild's (1983) paper that overlaps with data presented in paper by Frank (1981) and Frank et al. (1982). Though there is not an exact correlation between the data there is a trend that supports this belief.

5.3 GEOLOGICAL APPLICATIONS OF CATHODOLUMINESCENCE

Since Smith and Stenstrom (1965) first suggested the use of electron-excited luminescence as a petrologic tool, the list of geological applications has grown considerable. Table 13 presents a summary of applications taken from Nickel (1978). Though this list is by no means exhaustive, it gives the reader an idea as to how useful CL is to petrology.

For this study, cathodoluminescence has been used in several ways. First, it is used to reveal textures and fabrics otherwise invisible under normal petrographic conditions e.g. crystal growth zonations/textures, neomor-

TABLE 13: GEOLOGICAL APPLICATIONS OF CATHODOLUMINESCENCE

Category	Application
Characterization of Minerals	-clearly distinguish minerals, in mineral separation
	-control contamination
	-petrological application-identify twinning and microinclusions
	-matrix identification
Sedimentary Petrography	-identification of micro-grains
	-reveal original fabrics
	-reveal internal textures e.g. polycrystalline quartz is internally fractured
	-estimation of detrital/authigenic mineral ratios
	-identify allochems in highly altered carbonates
	-identify original facies
Compaction and Fracture Studies	-identify original grain contacts
	-distinguish between pressure solution and growth interference textures
	-establish fracture and cement generations
Diagenesis	-recognize zonal growth of cements
	-identify original vadose fabrics
	-recognize detrital versus authigenic minerals
	-establish cement stratigraphy i.e. mapping cement zones
	-relate Mn, Fe, Mg, Ca distributions to character of pore waters
	-reveal evidence of changing pore water chemistry
	-establish timing of precipitation, dissolution and coprecipitation of mineral phases

(cont'd)

TABLE 13; GEOLOGICAL APPLICATIONS OF CATHODOLUMINESCENCE (cont'd)

Category	Application
Provenance Studies	-identify clasts, original composition of clasts -identification of differing mineral characteristics related to two source areas -source rock evaluation
Geochemistry	-sample selection for isotope studies studies i.e. original versus recrystallized mineralogy -economic applications i.e. trends in trace elements -relate zonation in carbonates to former pore solution

(after Nickel 1978)

phic textures, compaction textures and features related to pressure solution. Secondly, cathodoluminescence has been used to establish a vertical cement stratigraphy in the Nisku Formation pinnacle reef studied. Lastly, it has been used to indicate the chemical nature of the pore waters responsible for precipitating pore-occluding cements, through geochemical interpretations of CL intensities.

5.3.1 CATHODOLUMINESCENT TEXTURES AND THEIR INTERPRETATIONS

One of the most significant features of CL petrology is the revelation of multiple zoned cement crystals. Zonation provides a complete growth history. It indicates, a variation in the water concentration of ions responsible for luminescence (mainly Mn^{2+}, Fe^{2+}) as they were incorporated into the growing crystal (Sippel and Glover 1965, Meyers 1978). Conversely, homogeneity in the luminescence of a crystal, (or within a crystal zone) implies precipitation from a chemically homogeneous pore fluid through that period of growth (Frank 1981).

Much information about the growth history of a cement can be extracted from the compositional zonation observed. Zonal contacts that are sharp and regular imply rapid changes in the composition of the pore fluid from which the zones precipitated. Zonal contacts that are not sharp, but gradational, result from gradual changes in pore water chemistry. Zonal contacts that are sharp, but irregular, have been interpreted by Meyers (1978) as micro-etching surfaces (i.e. dissolution unconformities) that reflect a period of dissolution between growth periods.

Zonal contacts may also be an indicator as to whether diffusional processes had been active. Meyers (1978) cites evidence for lack of diffusion as the sharpness of zonal boundaries, and the sharpness of luminescent veinlet boundaries cross-cutting non-luminescent cements. Active diffusional processes would have made these boundary contacts gradational. Gradational contacts observed in crystals may be due to precipitation in gradually changing pore waters. This does not apply to fracture contacts.

Crystal forms and growth morphologies as revealed by compositional zoning in porosity filling cements can yield important information about the diagenetic environment. Meyers (1974) has used the geometry of growth zones as revealed by CL to distinguish between vadose zone cementation and phreatic zone cementation. Walken and Berry (1984a) have distinguished four styles of syntaxial overgrowths, the morphologies of which appear to depend on three major factors: grain surface conditions, the surrounding pore conditions and the nature of diagenetic environment. Thus, interpretations that might otherwise be hard to make are aided by features defined under CL conditions.

Non-zonal luminescent patterns, those that are blotchy and have variable luminescent intensities, are characteristic of neomorphic replacements. Meyers (1974) interprets such patterns in marine cements to reflect the uptake of Mn^{2+} during recrystallization from aragonite to calcite. James and Klappa (1983) describe several types of fibrous calcite marine cements that display these luminescent properties. Relict needle-like cement fabrics have been recognized by Bathurst (1983) when examining neomorphic spar under CL conditions. These characteristic blotchy, variably luminescent patterns have been described by a number of authors in association with neomorphic products, whereas original cements whose luminescence have been described display some type of zonation or uniformity.

Cathodoluminescence can reveal vein structures and healed fracture surfaces that are otherwise undetectable due to their perfect optical continuity with the host. Direct correlation of such features with stylolite surfaces provides evidence of pressure solution generated cements. It can also indicate whether compositionally zoned crystals have been pressure-solved or grew together along growth compromise boundaries. Observation of these features enables one to establish timing relative to compactional processes.

5.3.2 CEMENT STRATIGRAPHY

Cement stratigraphy is an approach to carbonate cement studies utilizing compositional zonation as revealed by cathodoluminescence. Meyers (1974, 1978) applied this principle to his study of Mississippian carbonates in New Mexico. The concept is simple. Crystal zones can be correlated between samples within a measured section and between sections. Thus, it allows for these zones to be mapped petrographically , based upon their luminescent characteristics and relative positions.

In the correlation of zones it is assumed that they are always in the same order. If the general sequence is not complete, it is assumed that one zone is missing, not that one or more of the zones have changed characteristics to look like one of its neighbours. These assumptions imply that there may be cement unconformities within the compositional sequence.

Each zone is believed to represent a time correlative discrete episode of cementation, the equivalent of a time-stratigraphic unit. Zones are not believed to be diachronous, an interpretation that must be supported by regional petrographic evidence. Correlation must be first done within sections, then between sections. Regional correlations are based upon consistent similarity in ages, similarity of the sequence and the number of luminescent zones. It must be recognized that the synchroneity of time and regional consistency of ages of each zone provides the framework for regional correlations. Ebers and Kopp (1979) point out that any lack of correlation may be due to porosity occlusion early in the cementation history or a local interruption in the flow of pore fluids.

5.4 GEOCHEMICAL INTERPRETATIONS

Much effort has been made in the last decade to make geochemical interpretations from the luminescent color and intensity of carbonates, with regard to their precipitational environments. There is some concern as to whether such interpretations can be made with confidence (see Machel 1985) based upon the need to know whether Mn^{2+} and Fe^{2+} are the principle ions responsible for luminescence. All geochemical interpretations have been based upon the presence of these ions.

Meyers (1974) approached this problem by considering the conditions needed to incorporate Mn^{2+} into the calcite lattice. Based upon the concentration of Mn^{2+} needed to induce luminescence, the partitioning of Mn^{2+} between water and calcite, and the Mn^{2+}/Ca^{2+} activity ratios of natural waters, Meyers came to several conclusions.

Calcite precipitated from normal marine waters should contain 10-50 ppm Mn^{2+} or less. Earlier it was reported that luminescing calcites were found that contain <200 to 600 ppm Mn^{2+} (Fairchild 1983) with the exception of Richter and Zinkernagel (1981) who reported concentrations as low as 20-40 ppm. Meyers (1974) concluded shallow ground waters and surface meteoric waters as most likely to yield Mn^{2+} luminescing calcites (i.e. these waters would contain sufficient Mn^{2+}). Deep subsurface waters are less likely and sea water would be least likely.

Meyers (1974) also reported that marine waters and aerated surfaces waters would have all iron in the trivalent state (Fe^{3+}). Therefore ferroan calcite cannot precipitate from these waters. More likely candidates for a source of Fe^{2+} to quench luminescence would be shallow and deep subsurface waters.

Luminescent compositional zoning in carbonates is assumed to reflect variations in Mn^{2+} and Fe^{2+} incorporated into the crystal lattice. Meyers (1978) proposes two explanations for this. Variations of Eh in the presence of sufficient Mn^{2+} and Fe^{2+} would result in compositional zoning. The trace element-free zones represent oxidizing pore waters (Mn and Fe in their trivalent states), and the trace element-rich zones represent reducing pore waters. Or, under constant and reducing Eh conditions, variations in the $Fe/_{Ca}$ and $Mn/_{Ca}$ ratios due to a varying supply of Mn and Fe, would account for trace element-free and -rich zones.

Temperature and Ph conditions are considered by Meyers (1978) not to be important in causing Mn^{2+} and Fe^{2+} variations. The distribution coefficient for Mn^{2+} in calcite is not particularly temperature sensitive, and for his study the cements precipitated at a relatively constant and low temperature (~30°C, Meyers 1974). Also, modern shallow groundwaters in carbonate terrains have been reported to have relatively uniform pH values (pH=7-8) by several workers (see Meyers 1978, p. 376).

Carpenter and Oglesby (1976) proposed a theoretical model for the formation of successive zones of differing chemistry and luminescence in calcite. It is based upon the precipitation of calcite from aqueous solutions with the simultaneous removal of Mn^{2+} and Fe^{2+} from solution to the growing crystal. In this model, crystalline composition is controlled by Ca^{2+}/Mn^{2+} and Ca^{2+}/Fe^{2+} activity ratios in the ambient pore water. Mn^{2+} and Fe^{2+} activities are related to the pH, redox potential, and concentration of total sulfur. This implies that a homogeneously luminescent zone reflects a cementation period when these variables were essentially constant. Compositional zoning within a crystal then reflects a diagenetic sequence of these parameters, a cathodoluminescent signature.

This model was presented in a more refined state by Frank et al. (1982). In it Carpenter postulated four types of diagenetic environments. Each is characterized by differences in pe (Eh), Ph and total dissolved sulfur of pore-water (H_2S). The model predicts mineral assemblages, calcite composition, and calcite cathodoluminescence as a function of pH and pe related to each environment (see Figure 72). Manganese and iron are assumed to be available to the pore water.

Calcite that precipitates under various pe/pH conditions would exhibit distinct luminescent characteristics (Figure 72). A path defined by a pe/pH or pe only decrease would result in a sequence non-luminescent/bright/dull/bright/dead. This model makes it possible to relate calcite luminescence to environmental conditions. To accurately assess these conditions accessory minerals related to individual luminescent zones should be present, otherwise interpretations based solely upon luminescence are tenuous.

Grover and Read (1983) report a sequence of zoned cements very similar to that predicted by Carpenter and Oglesby (1976) and Frank et al. (1982). Their sequence of non-luminescent/bright/dull cements relates to an increasingly reducing pore water. The non-luminescent zone (low Mn content) probably precipitated from high pe, oxidizing waters. Under these conditions Mn is in an oxidized state (Mn^{3+}, Mn^{4+}) that inhibits its substitution for Ca^{2+} in calcite. Bright cement marks the reduction of

Figure 72 Predicted mineral assemblages, calcite composition, and calcite cathodoluminescence as a function of pH and pe (from Frank et al., 1982).

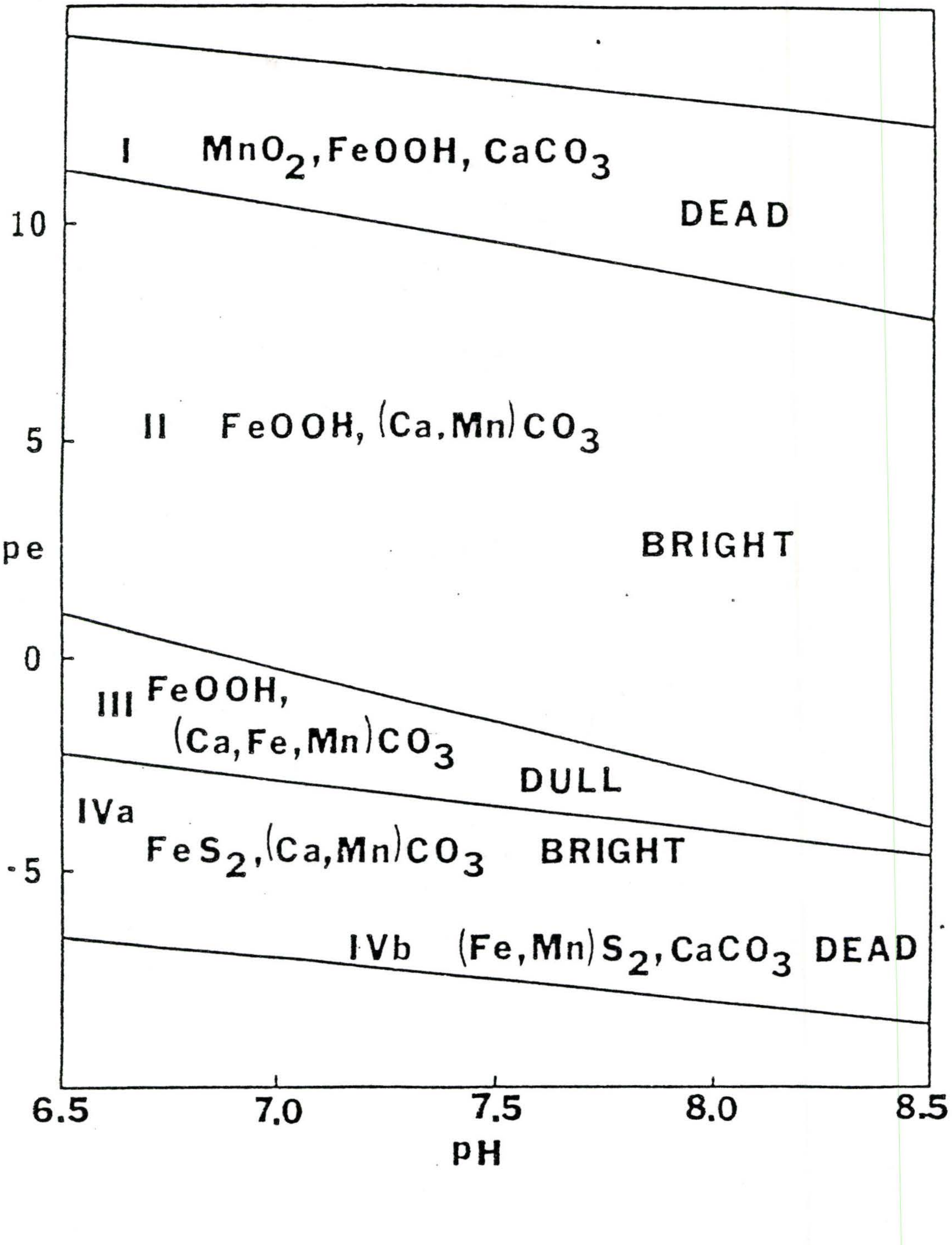
I MnO$_2$, FeOOH, CaCO$_3$
DEAD
II FeOOH, (Ca, Mn)CO$_3$
BRIGHT
III FeOOH, (Ca, Fe, Mn)CO$_3$
DULL
IVa FeS$_2$, (Ca, Mn)CO$_3$
BRIGHT
IVb (Fe, Mn)S$_2$, CaCO$_3$
DEAD
10
5
0
-5
pe
6.5
7.0
7.5
8.0
8.5
pH

Mn to its Mn^{2+} state and substitution into the calcite lattice due to a decrease in the redox potential of the pore fluid. The dull zone reflects a continued decrease in redox potential and marks the reduction of Fe to its Fe^{2+} state. Under these conditions both Mn^{2+} and Fe^{2+} are incorporated into the growing crystal resulting in a dull quenched luminescence.

Machel (1985) cautions against the use of pe(Eh)/pH diagrams for chemical interpretation of cathodoluminescent intensities. Other factors may be involved that are frequently neglected.

Trace elements other than Mn^{2+}, Fe^{2+} may interact with these ions, or be the elements responsible for the luminescence observed. Also, Mn^{2+} and Fe^{2+} concentrations in natural waters may vary due to trace element partitioning, or clay mineral/organic matter diagenesis, not just redox potential. Machels' argument for trace element partitioning is somewhat convincing and merits further thought. However, the argument for clay mineral/organic matter diagenesis is not convincing and requires further research.

Though Machel (1985) brings to light other factors to be considered, he proposes a model for the interpretation of precipitational environments from CL intensities (Figure

73). This model is similar to that Frank et al. (1982) (Figure 72), though it does not consider a system containing H_2S. Paths defined by a pe (Eh)/pH, or only a pe (Eh) decrease would result in zonation sequences of non-luminescent/bright/dull/extinct. Interpretation of the model does not require the presence of accessory minerals since the absence of sulfur species in the pore waters allows free Fe^{2+} to be incorporated into the growing crystal under reducing conditions. Were sulfur present (as sulfate), under reducing conditions pore waters might precipitate FeS_2, and the coeval calcite would be Fe^{2+} poor and brightly luminescent (environment 1Va, Figure 72).

The approaches are simplified. Accurate partition coefficients are not well known for Mn^{2+} and Fe^{2+} species over the range of diagenetic reactions, and the fields defined may vary somewhat due to other parameters. The obvious drawback to this modelling is the uncertainty as to the controls of luminescent intensities.

Figure 73 Predicted calcite or dolomite luminescence as a function of Eh and pH. The stippled area marks the field of Mn^{2+} - activated luminescence without Fe-quenching. Above this field are non-luminescent carbonates (non-lum) due to insufficient Mn^{2+} content. Below the stippled field are quenched (qu-lum) and extinct (ex-lum) carbonates due to increasing Fe^{2+} content. The lines A to C, and A′ to C′ record the luminescence sequences expected as a function of Eh and pH, or Eh only decrease. From Machel 1985.

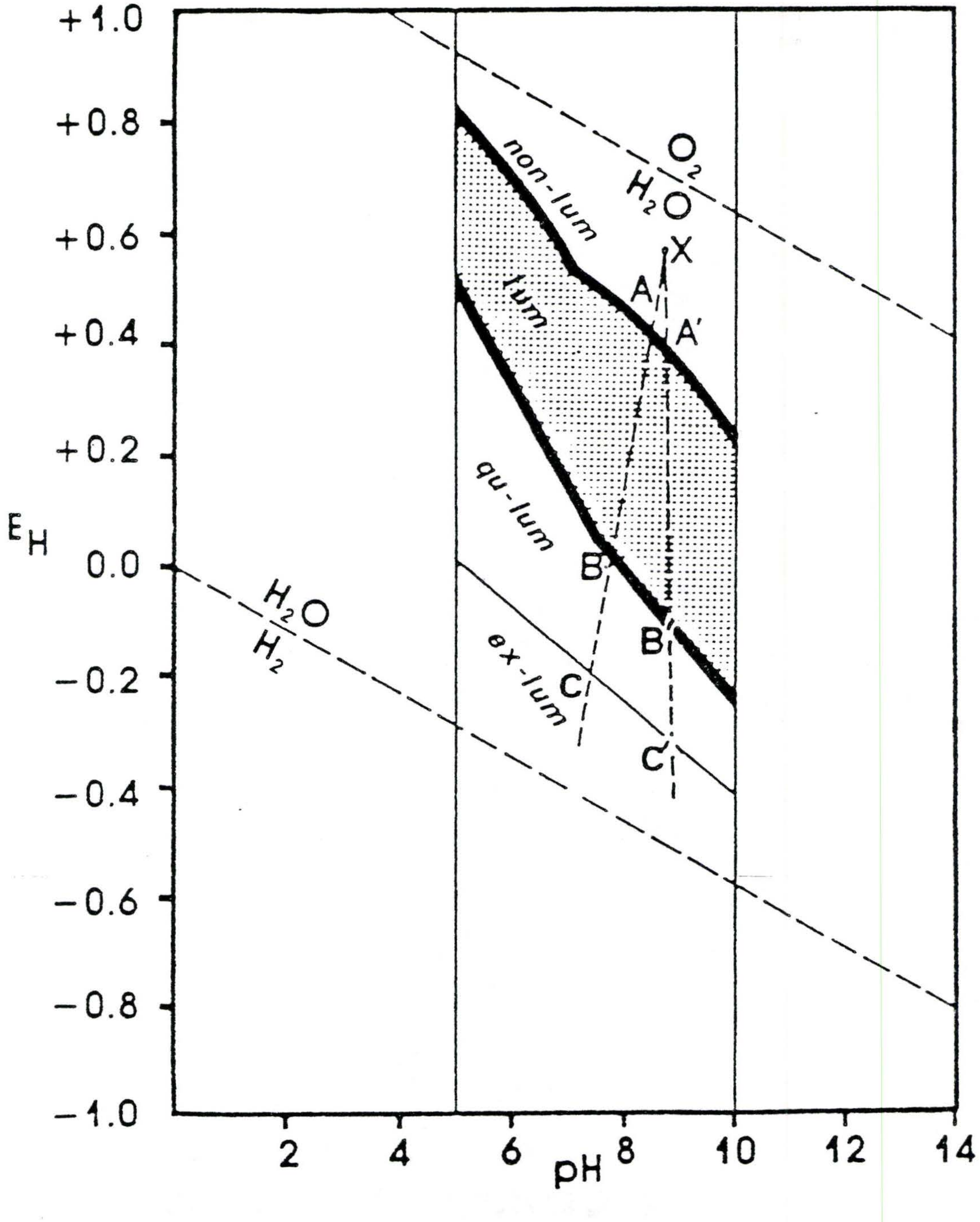
+1.0
+0.8
+0.6
+0.4
+0.2
0.0
−0.2
−0.4
−0.6
−0.8
−1.0
E H
2
4
6
8
10
12
14
pH
O_2
H_2O
H_2O
H_2
non-lum
lum
qu-lum
ox-lum
X
A
A'
B
B'
C
C'

CHAPTER 6

CATHODOLUMINESCENT OBSERVATIONS

6.1 INTRODUCTION

Cathodoluminescence, as discussed in the preceding chapter, can be used to reveal features otherwise invisible under normal petrographic conditions. The focus of this study is on those features directly or indirectly related to stylolites and ultimately to find evidence of pressure solution generated-cements. Appendix B defines the Luminoscope operating conditions and methods of photography.

Cathodoluminescent photographs included in the text do not accurately represent the true color and intensity as observed through the Luminoscope and originally photographed. For these reasons a duplicate set of color slides is available for examination.

6.2 CRITERIA FOR GENERATED-CEMENTS

For the pressure solution process to remain operative it is necessary that dissolved material be transported away from a stylolite, the site of dissolution. To find evidence of a generated-cement one must look towards the "plumbing" system utilized by the transport mechanism. "Plumbing" systems may be considered to have two forms;

those directly associated with stylolites, and those which are indirectly associated. Direct associations are those which one can recognize as being related to stylolites. Indirect associations are those which one must infer as being related to stylolites based upon characteristics found within the immediate vicinity.

The occurrence of fractures originating at a stylolite surface and propagating outwards from it is the only direct evidence of a stylolite-related plumbing system. These fractures are often wedge shaped and terminate at the stylolite at their wider end. These fractures are believed by Nelson (1981) to be extension fractures derived from the same compressive state of stress as the stylolite. Thus it seems logical that this type of fracture/stylolite association be direct lines of evidence for the plumbing system required.

Following this reasoning, it also seems logical that the cement which infills these fractures was supplied by dissolution along the stylolite surface, its nearest source, provided that the mineralogy is consistent with the rocks' matrix and constituents. We can assume then that this is pressure solution generated-cement.

There are no other direct links between pressure solution and cementation. Researchers must rely on spatial and temporal relationships to connect the two processes. Thus indirect evidence may be found in differing forms.

Wong and Oldershaw (1981) demonstrated increased porosity occlusion adjacent to stylolites. Using zoned calcite cements they illustrate a temporal relationship between stylolite growth and cement precipitation; such that "stratigraphically" younger cement zones predominate at greater distances from stylolitic tight zones. This close spatial relationship between zoned calcite cements and stylolites suggests a causative association. Furthermore, the temporal relationship indicates that calcite cements were precipitated immediately adjacent to stylolites, then proceeded outwards with continued stylolitization, as porosity was progressively filled.

Wanless (1979) believes that pressure solution can generate dolomite (pressure solution dolomitization) and suggests characteristics to distinguish precurser and post-pressure solution dolomite from dolomite formed during pressure solution. Precursor dolomite concentrated along stylolite seams should be similar in size, character, and abundance to dolomite found in adjacent limestones that have not undergone pressure solution. Dolomite rhombs restricted to areas of volume reduction by pressure solution that are different in character (size, zonation, ion content, clay inclusions) from rhombs found elsewhere, may have formed during or after pressure solution. Such rhombs grew during pressure solution if they display a slightly intergrown grain-supported framework due to selective pressure solution of the limestone. Dolomite that formed after pressure solution should not display such a fabric, but be more commonly intergrown.

Mattes and Mountjoy (1980) believed that dolomite precipitated along and adjacent to pressure solution surfaces. This dolomite mimics stylolite topography and decreases in density and maturity away from a stylolites.

Though both Wanless (1979) and Mattes and Mountjoy (1980) cite dolomite as the generated material, the characteristics and associations used for their reasoning can be applied to distinguish pressure solution generated material. Specifically, differences in size, zonation, chemistry, and fabric that are spatially or temporally related to stylolite occurrence can be used as indirect evidence of generated material. Individual characteristics may be subtle, but a combination of characteristics, especially if direct evidence is found and related to indirect evidence, should be sufficient proof of pressure solution generated-cements.

6.3 RECORDING OF LUMINESCENCE

The emitted luminescence was observed visually, without the aid of a spectrometer. Luminescence is described simplistically, following the standards set by other workers in this field. Thus calcite and dolomite luminescent intensities are describes as "bright", "dull", "very dull", and "non-luminescent" and/or the dominant color is noted. Following this scheme, a luminescent calcite zone might be described as "bright-orange luminescence" or a dolomite crystal might be referred to "red-", or "bright-red"luminescence.

6.4 OBSERVATIONS

Since two suites of samples were studied, cathodoluminescent observations will be reported for each.

6.4.1 LOCKPORT FORMATION OBSERVATIONS: GENERAL CHARACTERISTICS

The Lockport Formation dolomite is made up of two components, a finely crystalline dolomicrite and a medium crystalline xenotopic-hypidiotopic dolomite. Cathodoluminescent study of these samples reveals that dolomitization was extensive. No calcite or "invisible" particles were observed under CL conditions in all thin sections examined. Though the Lockport is a pure dolomite, the crystalline nature is poorly defined. Cathodoluminescence does not reveal any growth zonations, nor accentuate individual crystal boundaries. The luminescent character of the rock is mottled bright-red/dull-red for both the dolomicrite and the coarser xenotopic-hypidiotopic dolomite (Figure 74a,74b). Close examination of Figure 74b suggests that the bright-red luminescence pervades the dull-red interiors of the crystals in an irregular fashion. This is not as evident in the dolomicrite (Figure 74a) though the irregular pervasiveness of the bright-red luminescence can be seen.

Cathodoluminescence accentuates the porosity, seen as black patches. In dolomicrite samples porosity is very low (Figure 74a), essentially as pin-point intercrystalline pores of relatively uniform size. The coarser dolomite (Figure 74b) has a higher intercrystalline porosity associated with it. The distribution of pore sizes is variable from small pin-point pores to pores comparable in size to the crystalline components. Pore shape is variable as well, from equant to highly irregular.

6.4.2 DOLOMITE CEMENT

Dolomite cement does occur, but only very rarely. Figure 75 shows dolomite cement crystals that were found within intraskeletal pores of a pyritized bryozoan. These cement crystals are larger than xenotopic-hypidiotopic

Figure 74 Cathodoluminescent photographs of the general characteristics of Lockport Formation dolomite. 74a) Mottled bright-red is pervasive throughout photograph. 74b) Mottled bright-red/dull-red luminescence of xenotopic-hypidiotopic dolomite. Bright-red dolomite occurs at edges of crystals and as patches in crystal interiors. Porosity is black. Magnification 28x. Scale bar = 1 mm.

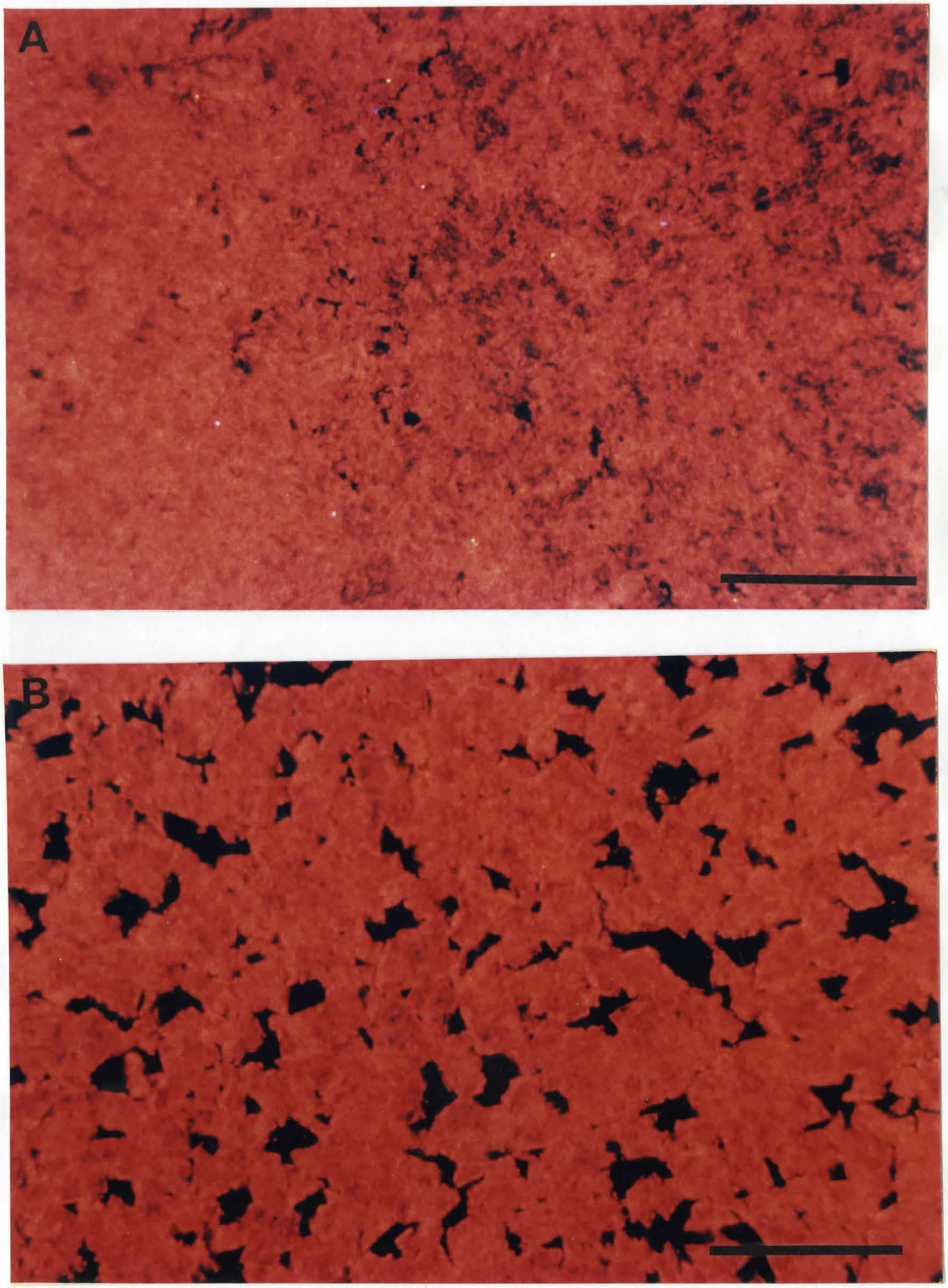
A
B

Figure 75 Cathodoluminescent photograph of zoned dolomite cement crystals found within intraskeletal pores of a pyritized bryozoan. Zonation is dull-red/bright-red repeated twice. Note how bright-red dolomite occurs as patches within crystal interiors. Magnification 28x. Scale bar = 1 mm.

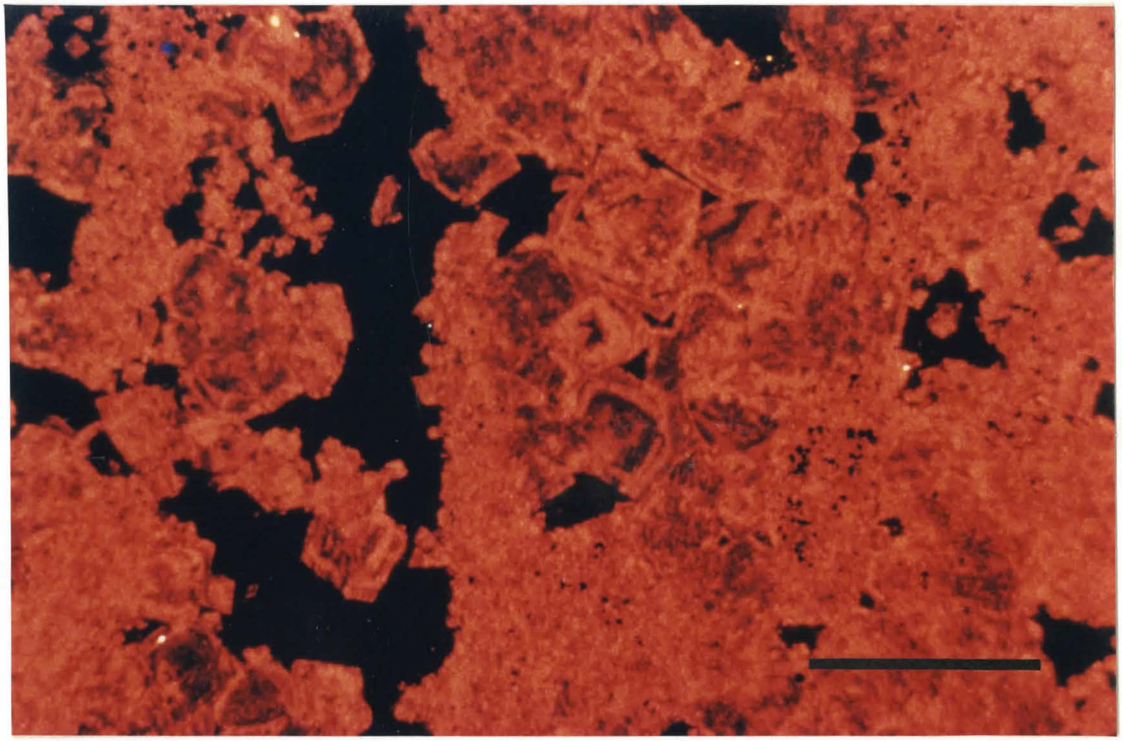

dolomite. They display a growth zonation sequence of dull-red/bright-red repeated twice. This zonation is not consistent between crystals nor are the zonal boundaries always sharp. Similar to Figure 74b, the bright-red luminescence is seen to pervade the dull-red interior of the crystals, disrupting the zonation seen.

6.4.3 POROSITY OCCLUSION

Porosity is occluded in the Lockport by the bright-red luminescent dolomite component. Though the rock has a mottled bright-red/dull-red luminescent character and the crystalline nature is poorly defined, pores are seen lined with bright-red dolomite (Figure 74b,76). Pore linings may show protruding euhedral crystal faces, or show an etched nature that sometimes exposes the mottled interior of the crystals. These bright red pore linings commonly have irregular boundaries that intrude crystal interiors or the boundary is sometimes planar yet diffuse. Figure 76a shows extremely variable pores and pore sizes partially occluded by bright-red dolomite. Very small pin-point pores are found in patches of diffuse bright-red dolomite. This is best observed in Figure 76b where this diffuse patches are enhanced in the mottled dolomicrite.

Figure 76 Cathodoluminescent photographs of porosity occlusion by bright-red dolomite. 76a) Pores lined with bright-red dolomite show euhedral faces. Note "bow tie" structure due to porosity occlusion in center of photograph. 76b) Pin-point porosity in dolomicrite that is enhanced by bright-red dolomite which lines pores and diffuses into "background" dolomite. Magnification 28x. Scale bar = 1 mm.

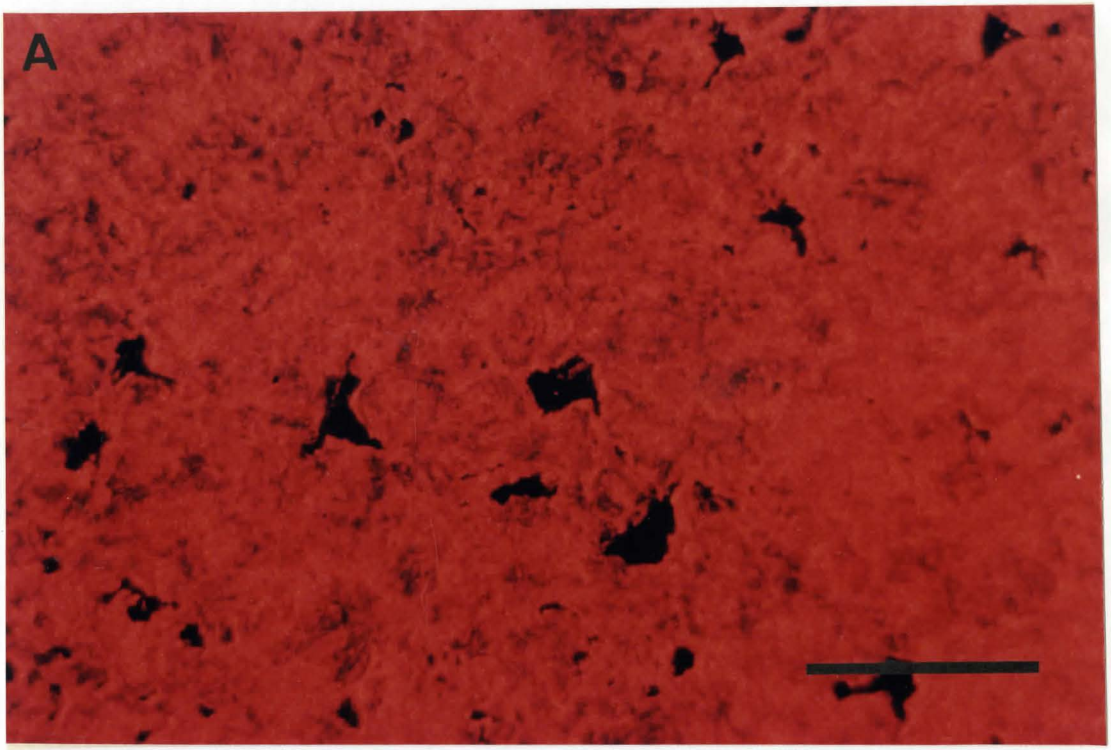
A

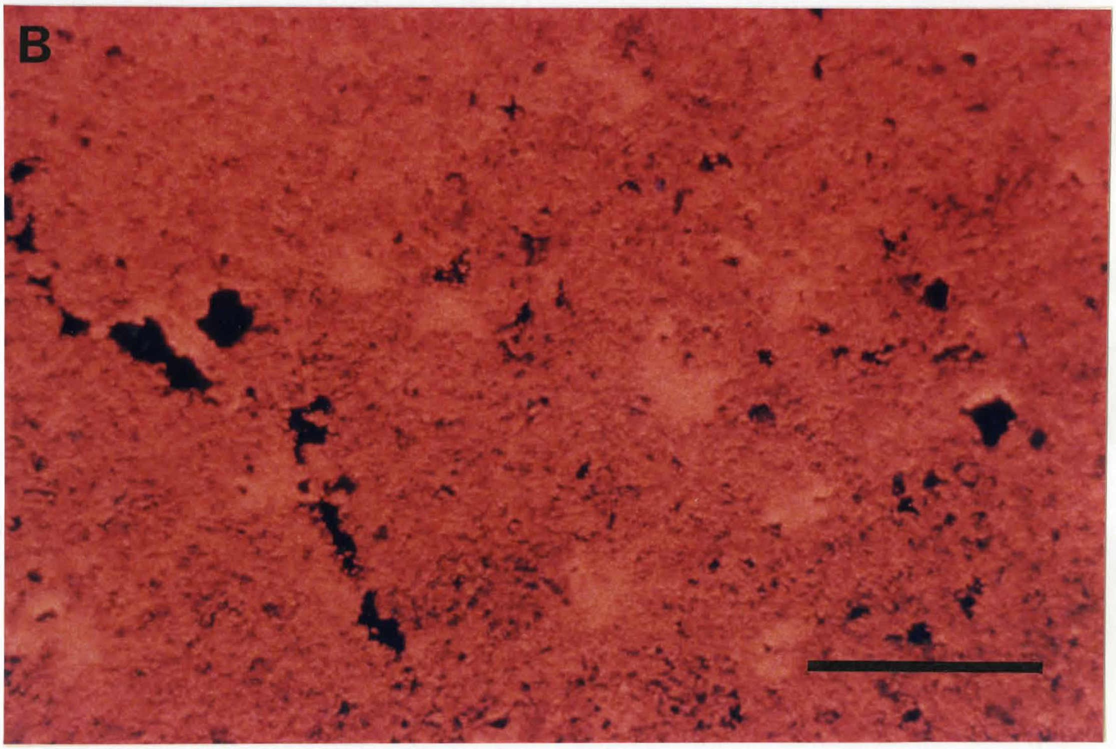
B

6.4.4 STYLOLITE RELATIONSHIPS

Stylolites of differing evolutionary stages occur throughout the Lockport. Of all the thin sections examined, only a few contained the stylolite/fracture associations described in the preceding section. As might be expected, these stylolites are late adolescent or mature stages of growth. Figure 77a shows a fracture that is partially filled by bright-red luminescent dolomite. The gap of this fracture is wider near the stylolite than away from it, though it does not originate right at the stylolite. Close examination of the bright-red infilling reveals that the cement is not in sharp contact with the fracture walls, but is diffuse. Porosity in this sample is very low, yet the few small pores that can be observed commonly show diffuse bright-red associations. Note how the mottled texture in this example resembles isolated "islands" of dull-red separated by an irregular network of bright-red luminescence.

When a growing stylolite encounters a pre-existing channel/fracture/pore, with continued growth, it may extend into this space. Figure 77b displays this texture. The fracture in this sample does not show any infilling by bright-red dolomite. This may be real or may be an artifact of the grinding process involved in making the thin section. This is unknown. However, an interesting feature

Figure 77 Cathodoluminescent photographs of stylolite-related features. 77a) Fracture that originates near a stylolite (top right) is partially infilled by bright-red dolomite. Contact between the host and infilling dolomite is diffuse, not sharp. 77b) Bright-red dolomite in a diffuse patch where a stylolite has extended into an open fracture (left center of photograph). Porosity adjacent to this area shows bright-red crystals growing into open space. Magnification 28x. Scale bar = 1 mm.

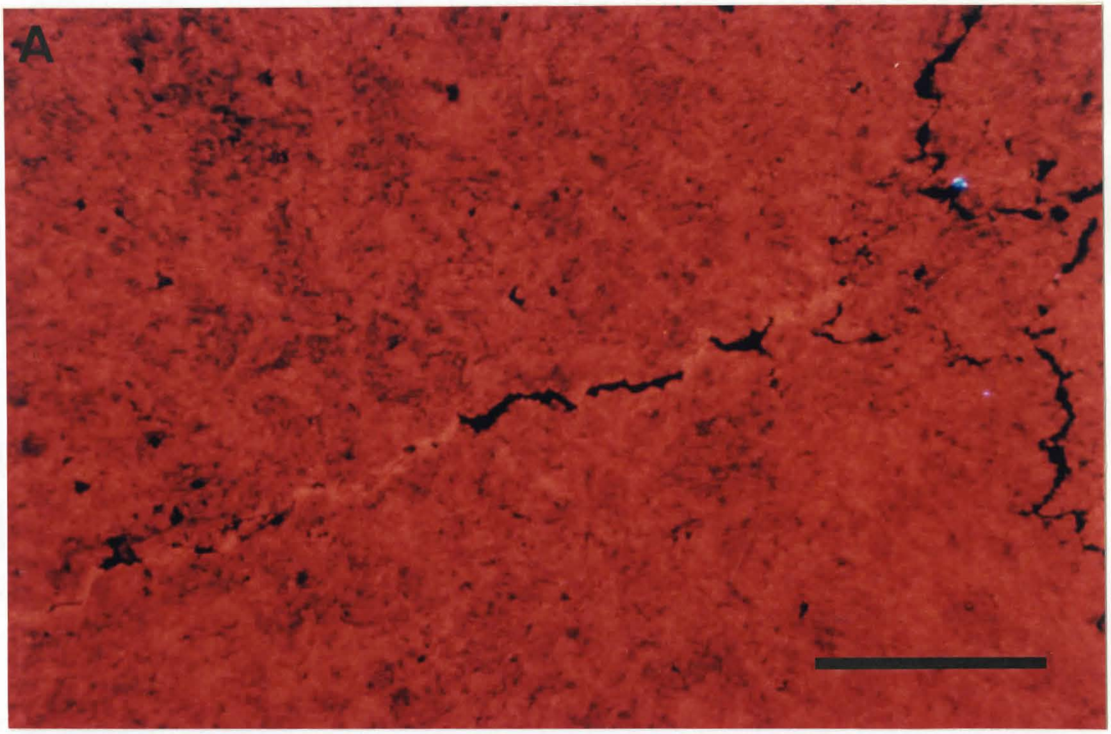
A

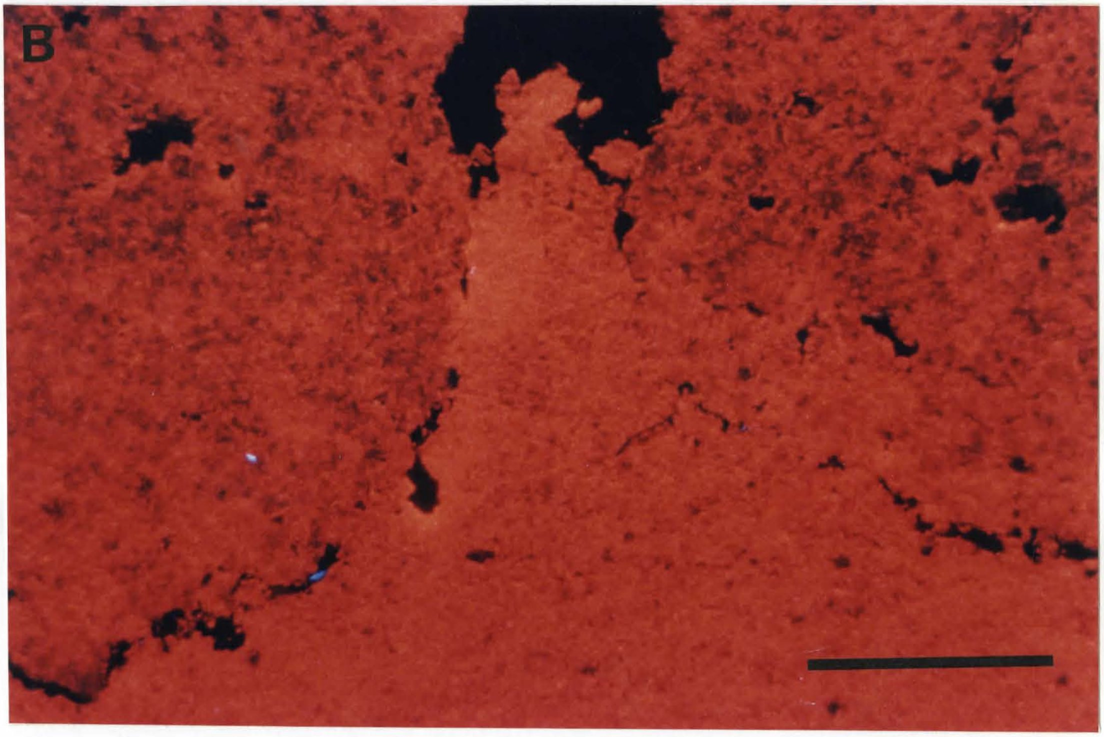
B

of this (extrusive) texture is the concentration of bright-red luminescence at the stylolite surface extending into the space. Though the dolomite on one side of the stylolite is brighter than that on the other side, this concentration is recognizable by its greater intensity. Additionally there is a minute euhedral bright-red crystal growing into a pore within this concentration. Porosity is very low in this sample and most pores show a bright-red infill.

Real appreciation of the cathodoluminoscope comes when one observes textures such as those in Figure 78. Microscopic veinlets propagating outwards from a stylolite and dissipating into the dolomicrite strongly suggests pressure solution generated-cement. In Figure 78a these veinlets contain bright-red luminescent cement. The texture is very subtle due to its scale (approximately 1 centimetre in length) and the diffuse nature of the texture as the bright-red cement dissipates into the dolomicrite.

Larger bright-red veinlets were found in these samples propagating away from stylolites as in Figure 78a. Figure 78b shows a veinlet that originated at a mature stylolite only a few millimetres away. In this photo, the veinlet branches and connects pores partially filling them with bright-red dolomite. The finer branches dissipate outward as in Figure 78a, becoming diffuse.

Figure 78 Cathodoluminescent photographs of stylolite-related veinlets. 78a) Two faintly visible bright-red veinlets propagating away from stylolite at left of photograph and dissipating into dolomicrite. 78b) Bright-red dolomite veinlet that originated at a stylolite several millimetres away. From left to right, the veinlet branches and connects pores, then dissipates into dolomicrite. Magnification 28x. Scale bar = 1 mm.

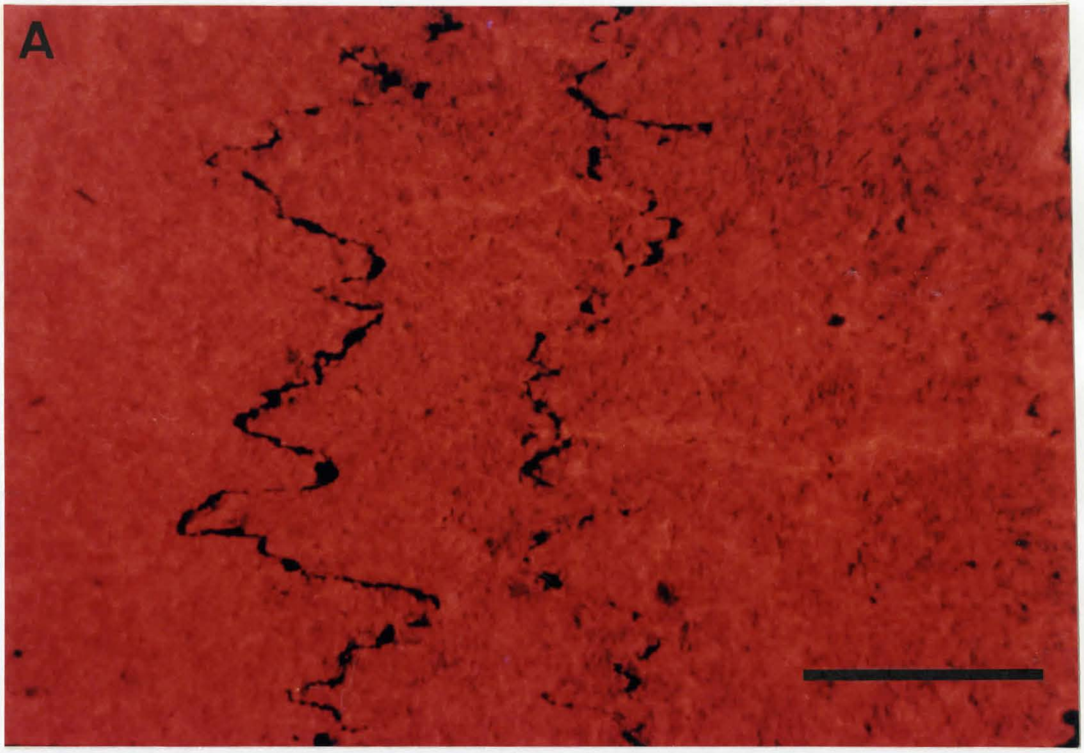
A

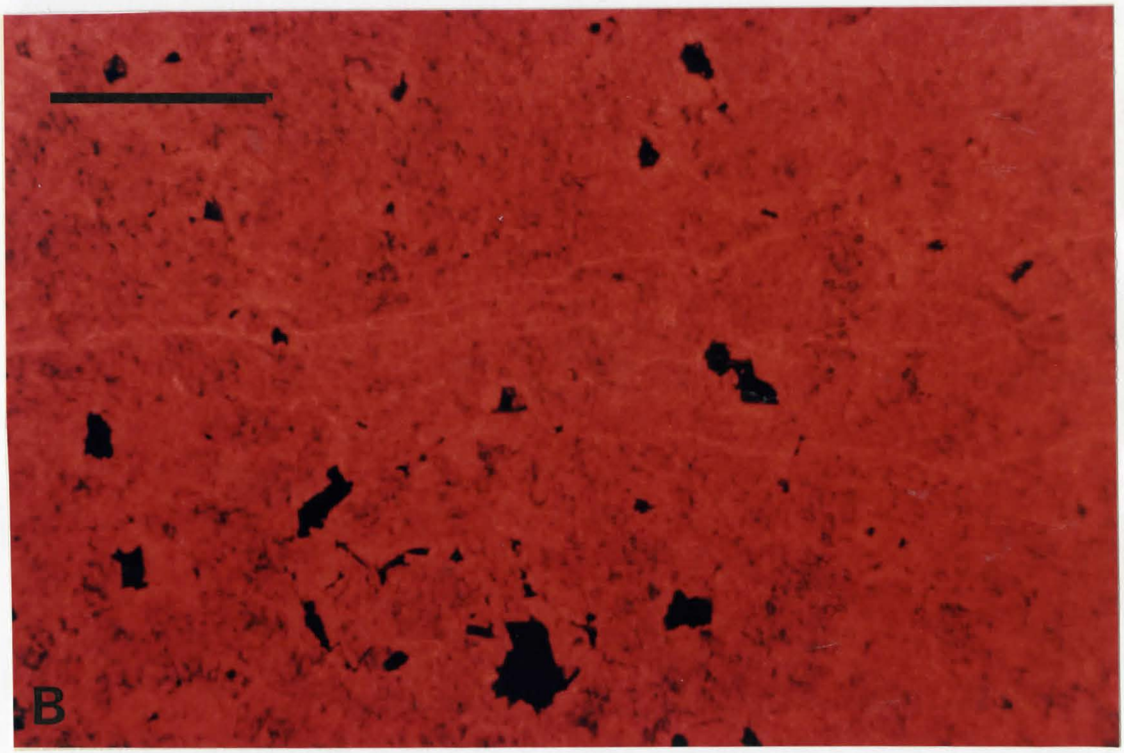
B

6.4.5 SUMMARY LOCKPORT FORMATION

Bright-red luminescent dolomite is found in three modes of occurrences. It lines pores, partially-to-nearly occluding them. It is pervasive in the background dull-red luminescent dolomite and rare zoned dolomite cements, in irregular and diffuse patterns. This results in a variable bright-red luminescent intensities of the rock as a whole. It is found associated with fractures and in veinlets (the latter definitely originate at stylolites) where it is observed to have diffuse (not sharp) boundaries against the "wall-rock".

6.5 NISKU FORMATION OBSERVATIONS: ZETA LAKE MEMBER

Since pressure solution is a process that is initiated during burial in the mesogenetic environment, it follows that its products (if any) should be found in the (later) cements that occlude porosity. With this reasoning in mind, petrographic observation suggests that calcite spar mosaics, matrix dolomite, and Fe-dolomite be selected as the targets for this study.

6.5.1 CALCITE SPAR AND Fe-DOLOMITE

Porosity occlusion in the Zeta Lake Member during burial was by precipitation of a non-ferroan, zoned luminescent, clear calcite spar. The basic zonation is non-luminescent/bright/dull with variations upon this theme. Zoned calcite spar succeeds an earlier non-ferroan calcite mosaic that has a distinct mottled dull luminescence. This earlier mosaic is found lining the walls of intraskeletal pores (Figure 79a) and as euhedral extensions of fibrous calcites (Figure 79b). Zoned calcite succeeds mosaic calcite as overgrowths and as scalenohedral crystals growing into pores (Figure 79a,79b).

Where the earlier mosaic is absent, zoned calcite may occur as idiotopic growths nucleating on micrite (Figure 80a), scalenohedral crystals on micrite (Figure 80b), or as idiotopic overgrowths on particles (Figure 81). It also succeeds an earlier thin dogtooth spar and fibrous calcite, as scalenohedral crystals and euhedral extensions, respectively.

Zonations help establish temporal relationships relative to dolomitization. In Figure 81 a red-luminescent dolomite cement protrudes into the pore being filled by the zoned calcite. Precipitation of this dolomite cement followed the growth of the non-luminescent zone, but preceded the growth of the bright zone. In Figure 80a and 80b, the precipitation of the dull zone was followed by the precipitation of Fe-dolomite, the dull maroon crystals with red cores.

Figure 79 Cathodoluminescent photograph of zoned non-ferroan calcite spar. 79a) Zoned calcite spar succeeding an earlier mottled dull mosaic calcite in an intraskeletal pore. Basic zonation is non-luminescent/bright/-dull. 79b) Zoned calcite spar that has grown as euhedral extensions of fibrous calcite crystals. Calcite spar shows same basic zonation as above. Fibrous calcite displays a random pattern of luminescence. Magnification 28x. Scale bar = 1 mm.

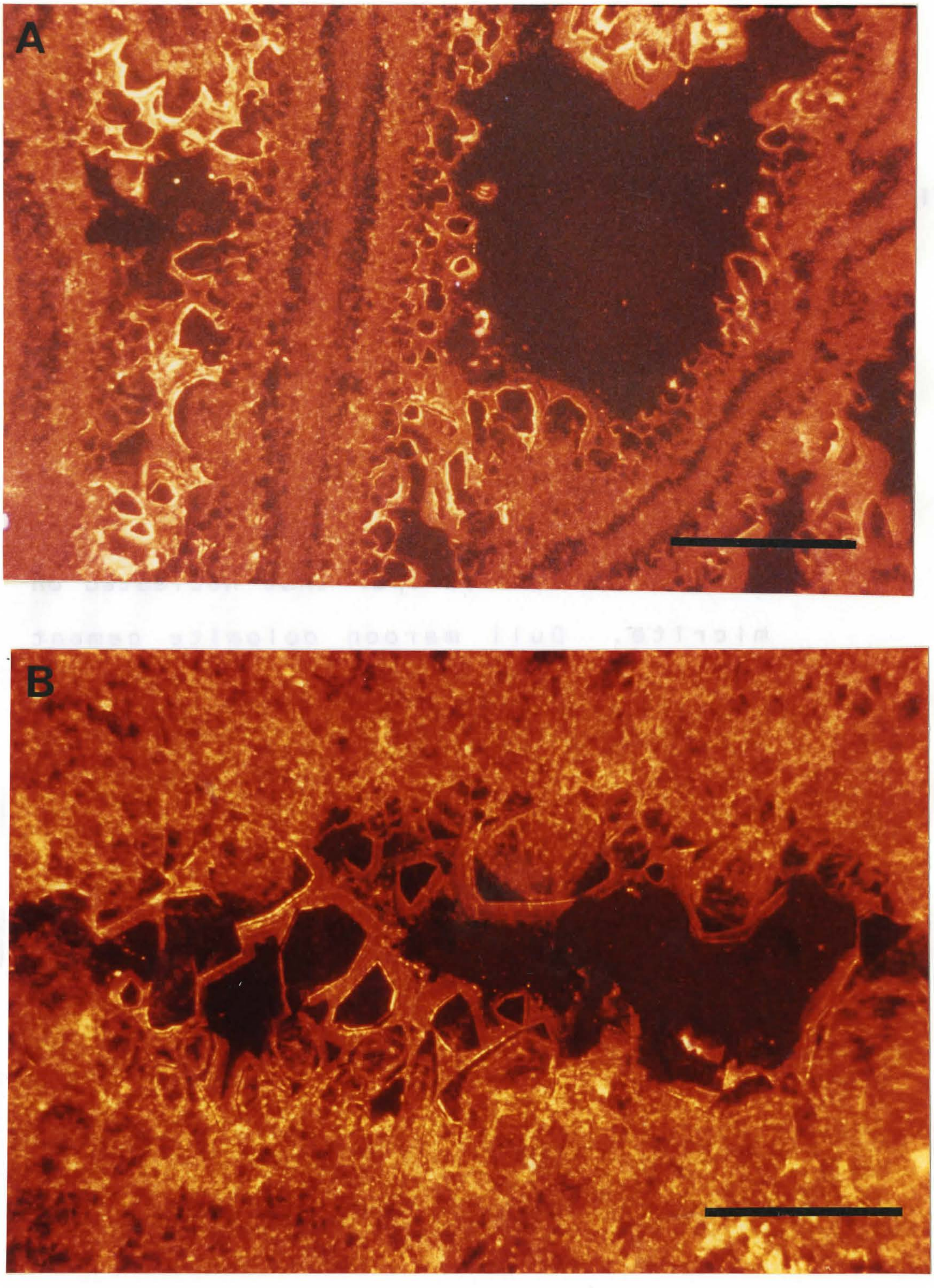
A
B

Figure 80 Cathodoluminescent photographs of zoned calcite spar that nucleated on micritic substrates. 80a) Zoned calcite that shows an idiotopic growth pattern succeeded by dull maroon dolomite cement (left center of photograph). Micritic substrate is dull luminescent. 80b) Zoned scalenohedral crystal of calcite spar that nucleated on micrite. Dull maroon dolomite cement succeeded dull calcite precipitation. Magnification 28x. Scale bar = 1 mm.

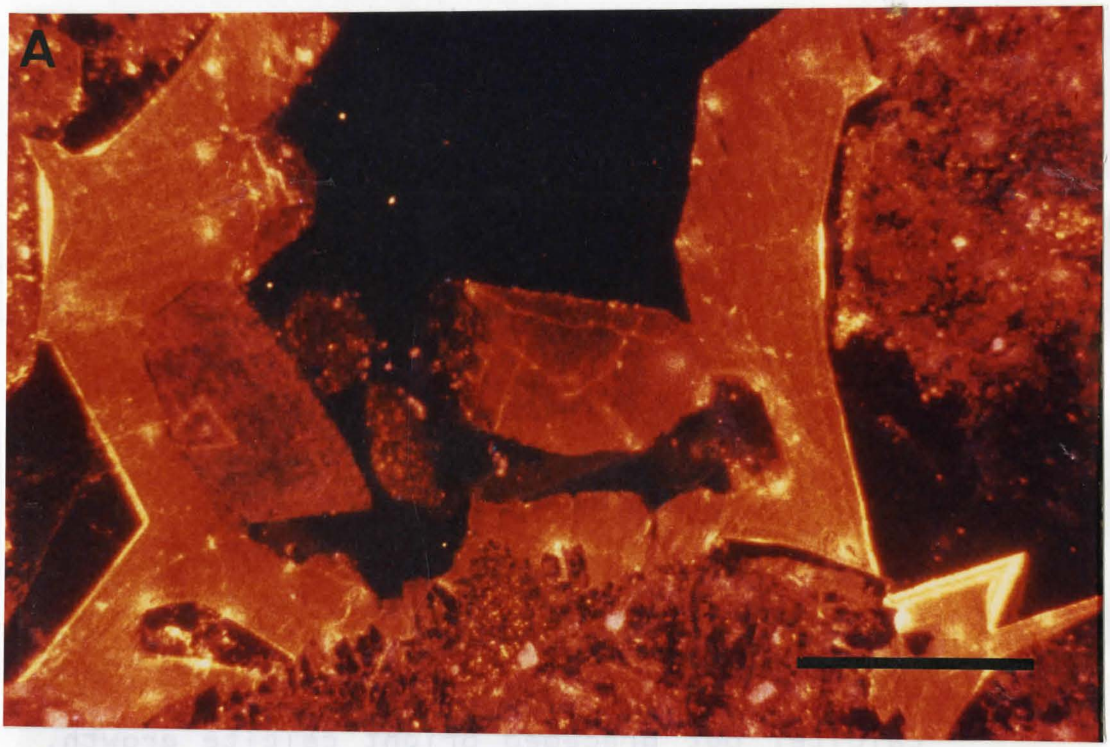
A

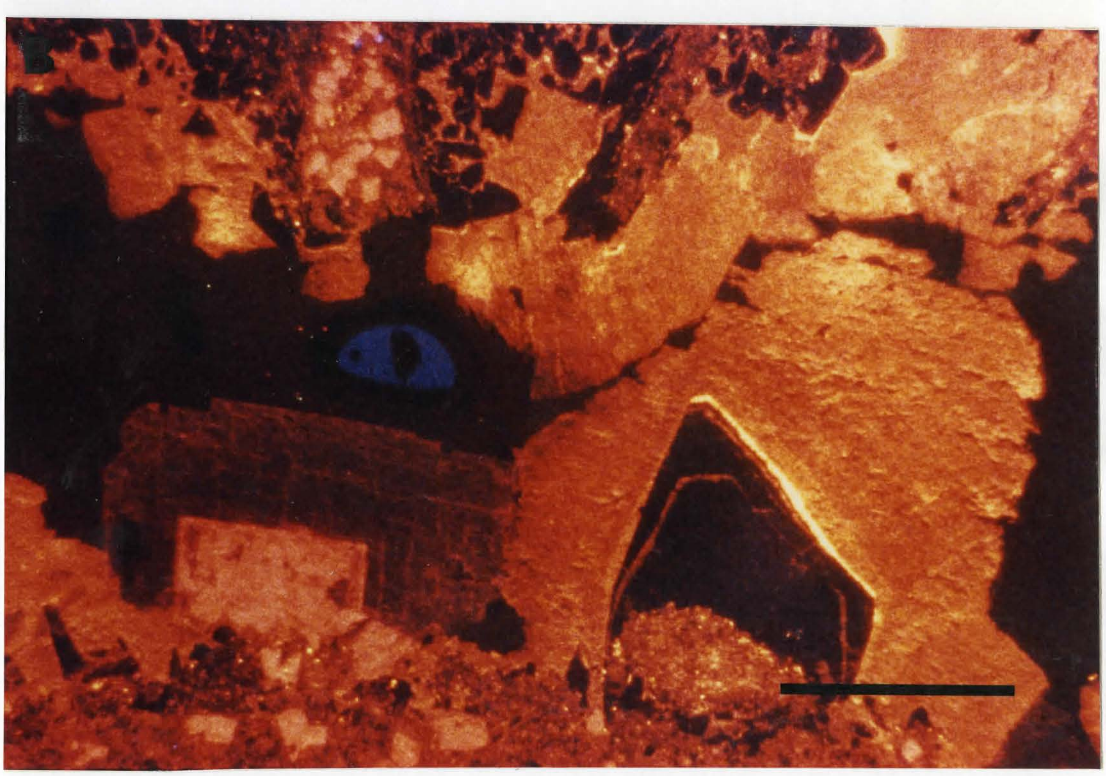
B

Figure 81 Cathodoluminescent photograph of zoned syntaxial overgrowth on crinoidal particle. Particle shows a random luminescence. Evidence of an early cement is seen as an etched, brighter, patchy luminescent "rind" between particle and overgrowth. Red-luminescent dolomite cement crystals (top left of photograph) succeeded non-luminescent calcite, but preceded bright calcite growth. Magnification 28x. Scale bar = 1 mm.

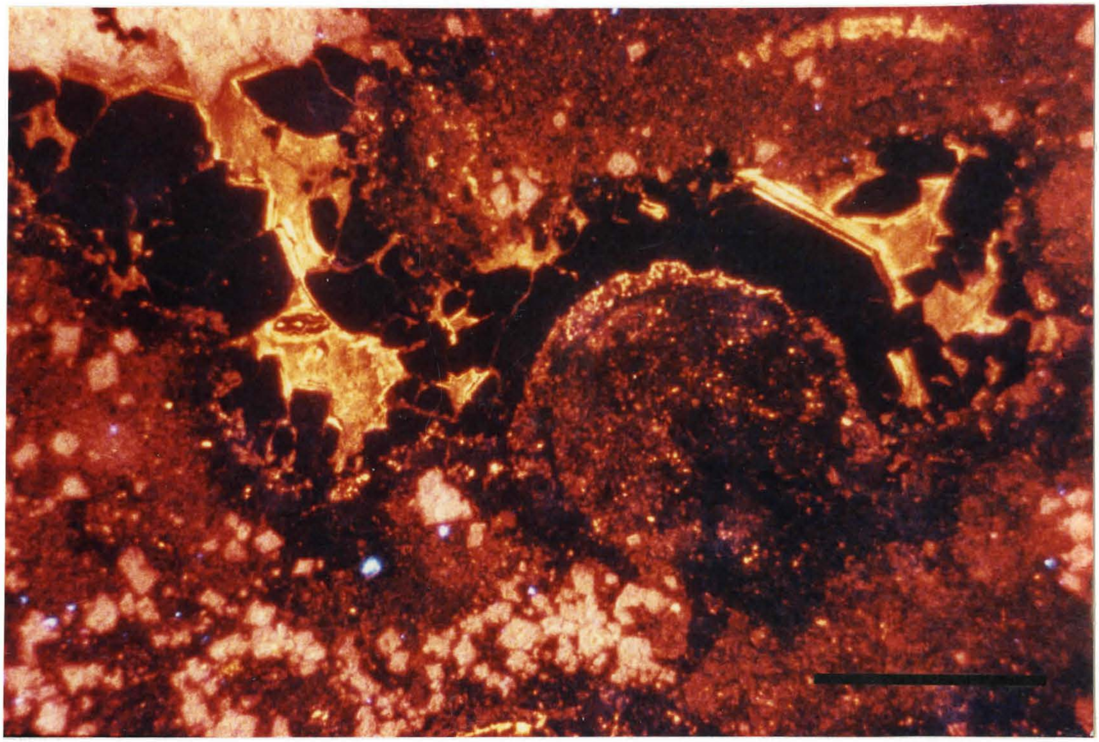

Figure 82 Cathodoluminescent photograph of subzoned calcite spar crystals that occlude porosity after bright calcite. Growth patterns of scalenohedral shape appear discontinuous relative to pore lining crystals. Magnification 28x. Scale bar = 1 mm.

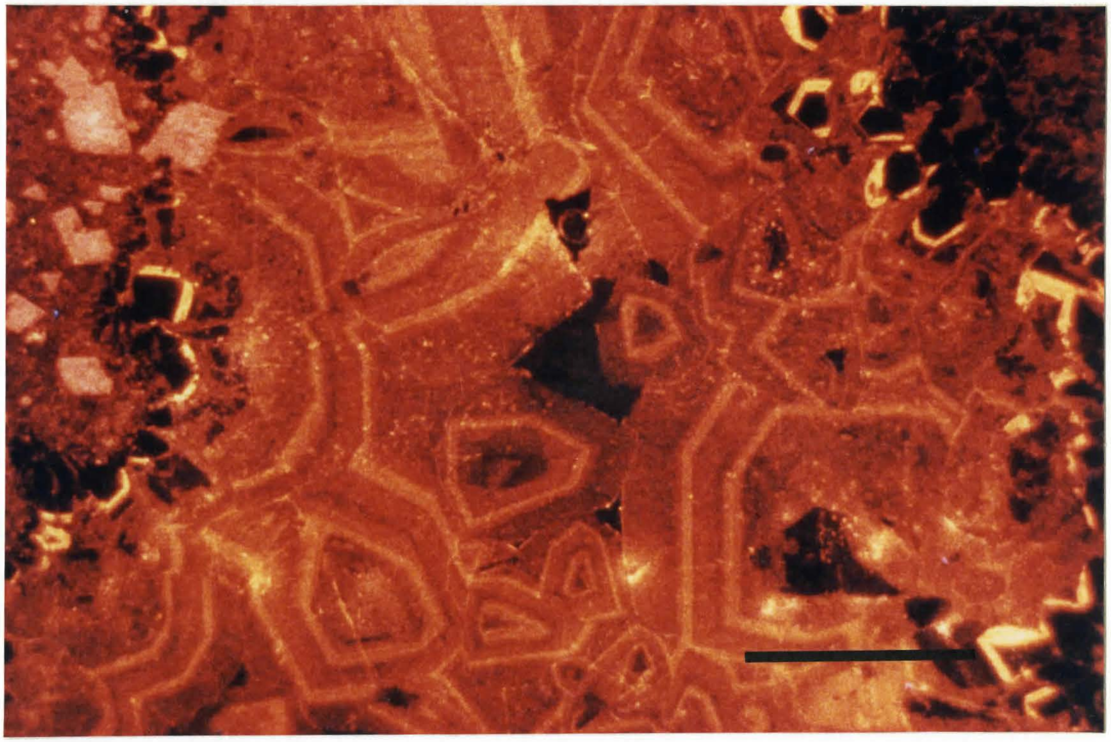

Calcite dissolution textures were observed in some of the thin sections studied. Extreme dissolution is observed in Figure 83a where the etched and pitted topography of the non-luminescent zone is enhanced primarily by the mimicking character of the bright zone and succeeding subzones. More subtle indications of calcite dissolution can be seen in Figure 83b where several pore lining crystals show undulatory growth zones. Walken and Berry (1984a) believe this pattern to result from the removal of crystal faces through dissolution. The significance of this texture will be discussed in the next chapter.

6.5.2 MATRIX DOLOMITE

Dolomitization of the Zeta Lake Member resulted in the replacement of micrite by dolomite. Zonation is not abundant in the matrix dolomite. Rarely are crystals observed that show as well-defined zonation as in Figure 84. Two zones are evident, a bright red interior and a dull red exterior. Of particular note is that clusters of crystals appear coalesced into tight groupings. Coalescence can be attributed to either growth coalescence or solution coalescence through pressure solution (Chapter 3). Zonation of crystals helps to determine whether coalescence is due to the former or the latter, analagous to growth interference and pressure solution contacts, respectively. Close

Figure 83 Cathodoluminescent photographs of dissolution textures revealed by growth patterns. 83a) Extreme dissolution of non-luminescent calcite enhanced by the mimicking character of the bright zones. 83b) More subtle dissolution textures shown as undulatory bright zones that mimic the topography of the earlier non-luminescent zones (left and lower portions of the photograph). Subsequent growth zones show euhedral faces. Magnification 28x. Scale bar = 1 mm.

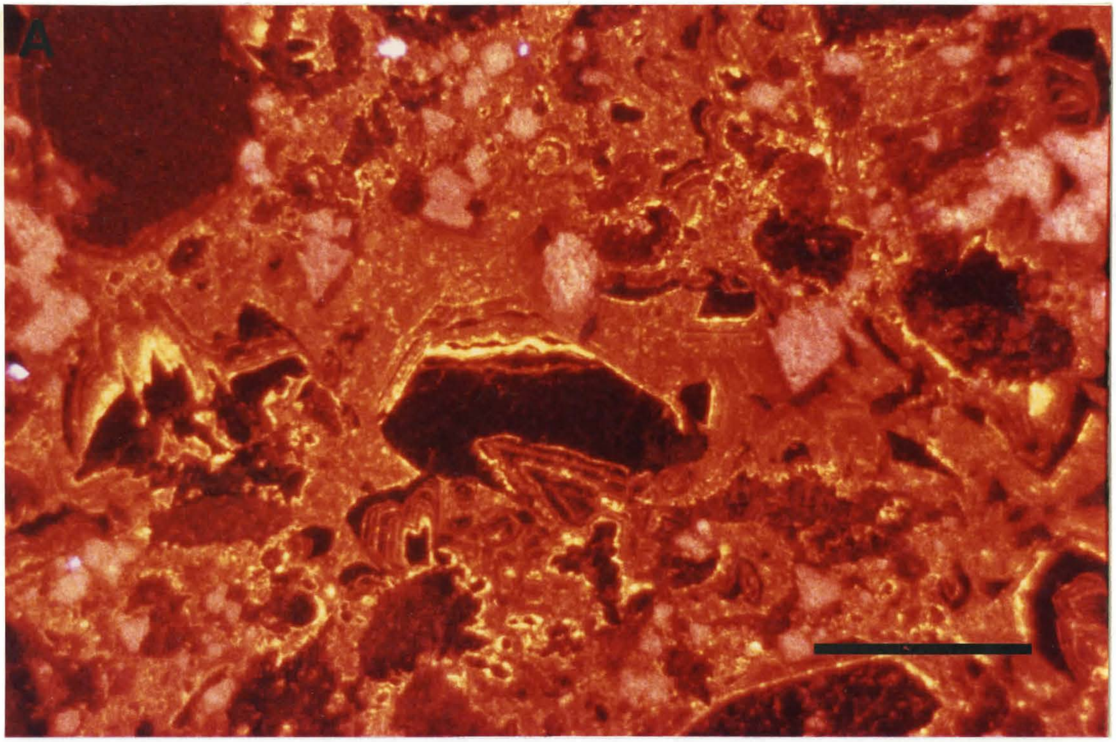
A

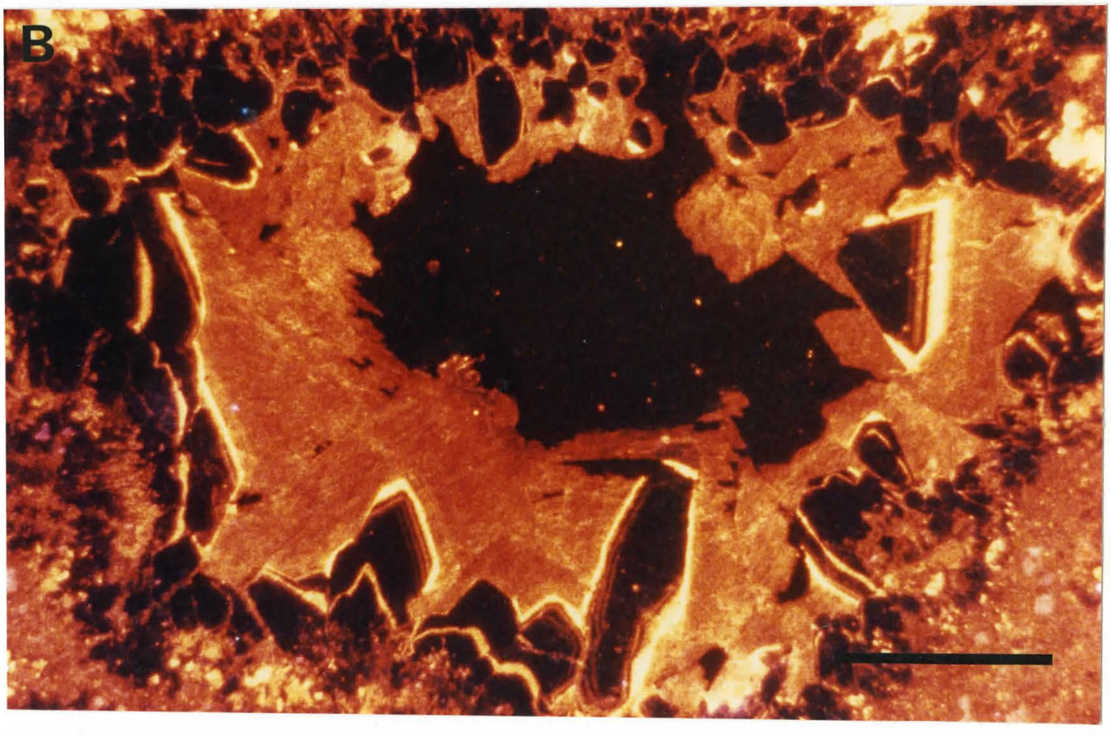
B

Figure 84 Cathodoluminescent photograph of rare zonation seen in matrix dolomite crystals. Bright-red interiors are succeeded by a dull-red zone. Close examination of clusters of dolomite crystals suggests that both growth and solution coalescence were once active. Magnification 28x. Scale bar = 1 mm.

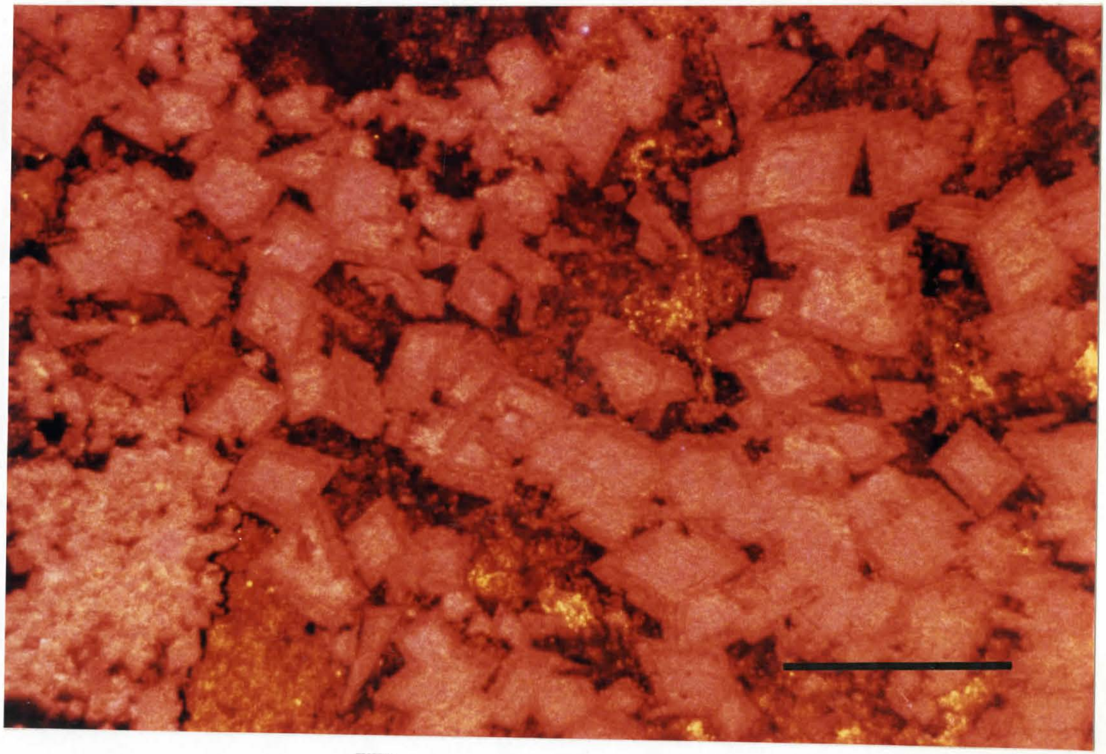

examination of Figure 84 suggests that both styles of coalescence can be found.

Matrix dolomite is seen accumulated along stylolite surfaces analagous to an insoluble residue. The zonation seen in dolomite crystals in interstylolitic regions is progressively lost nearer the stylolite. Figure 85a, 85b, and 85c records a traverse over 1.5 centimetres towards a stylolite. In figure 85a the zonation that is observed fades through Figure 85b and is essentially gone in Figure 85c.

6.5.3 COMPACTION TEXTURES

Compaction-related features are associated with dull luminescent calcite. In Figure 86a dull calcite heals broken crystals in a "collapsed" pore. The broken crystals display a repetitious non-luminescent/bright zonation and dull calcite fills the interstices between them. For fracturing of the interior crystals to have occurred the matrix must have been lithified. The calcrete crust that rims the pore exterior suggests that it was.

Figure 86b shows a fractured non-luminescent/bright crystal. The fracture is healed by dull calcite which also occludes the remaining porosity. It seems likely that this fracture may have been the conduit for dull calcite that fills the pore, though because it is so minute it is

Figure 85 Cathodoluminescent photographs showing more "homogeneous" luminescence of dolomite crystals nearer a stylolite. The zonation seen in 85a fades in 85b and is essentially gone in 85c adjacent to the stylolite surface. Note the decrease in the abundance of matrix calcite nearer the stylolite. Read each photo right to left. Magnification 28x. Scale bar = 1 mm.

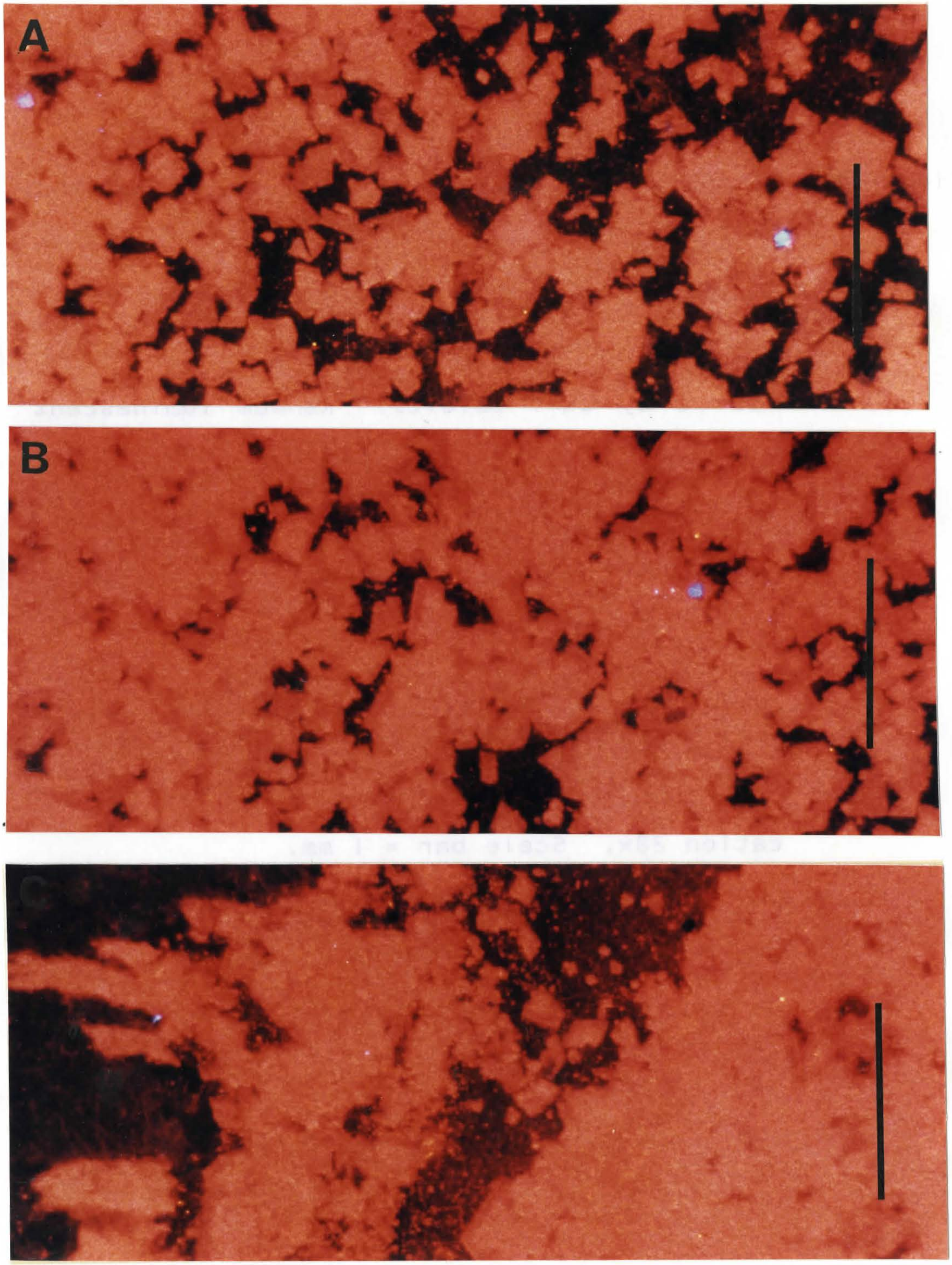
A
B
C

Figure 86 Cathodoluminescent photographs of fractured zoned calcite crystals. 86a) A collapsed pore in which pore-lining non-luminescent/ bright (repetitious) crystals are broken and healed by dull calcite. Random luminescent "rind" encircling the pore is suggestive of a calcrete crust. 86b) Fractured non-luminescent/bright crystal that is healed by dull calcite. Careful examination of the fracture suggests that it originates in the region of the linear arrangement of dolomite crystals (left side of photograph). Magnification 28x. Scale bar = 1 mm.

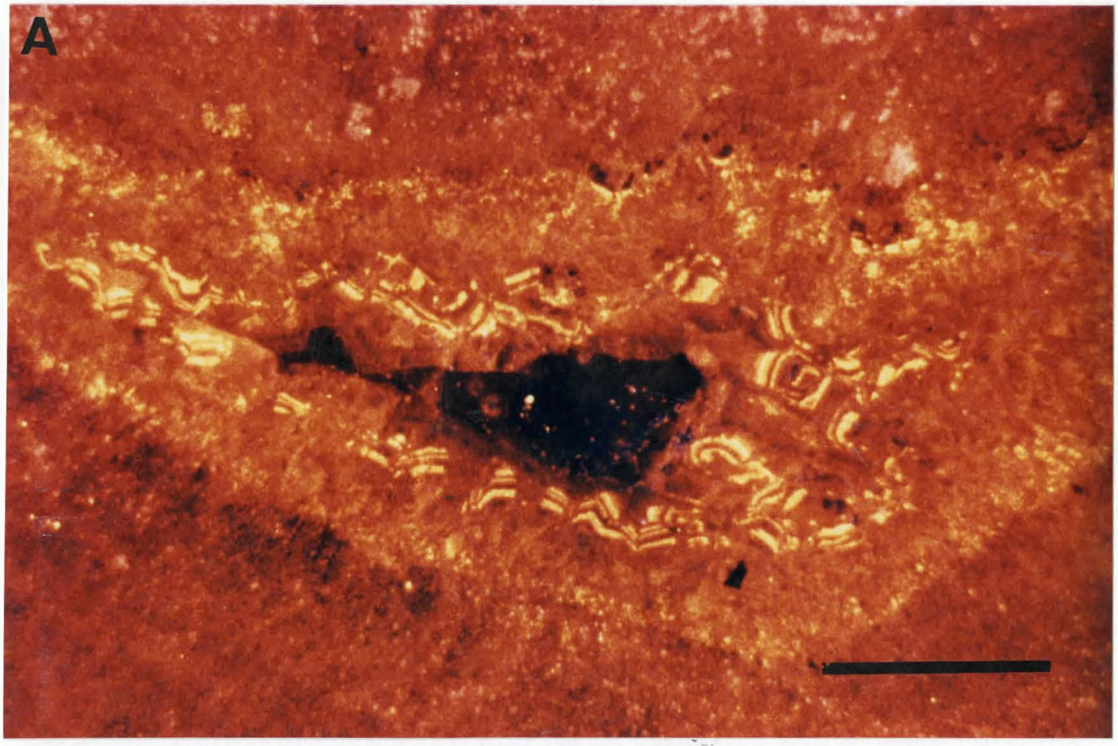
A

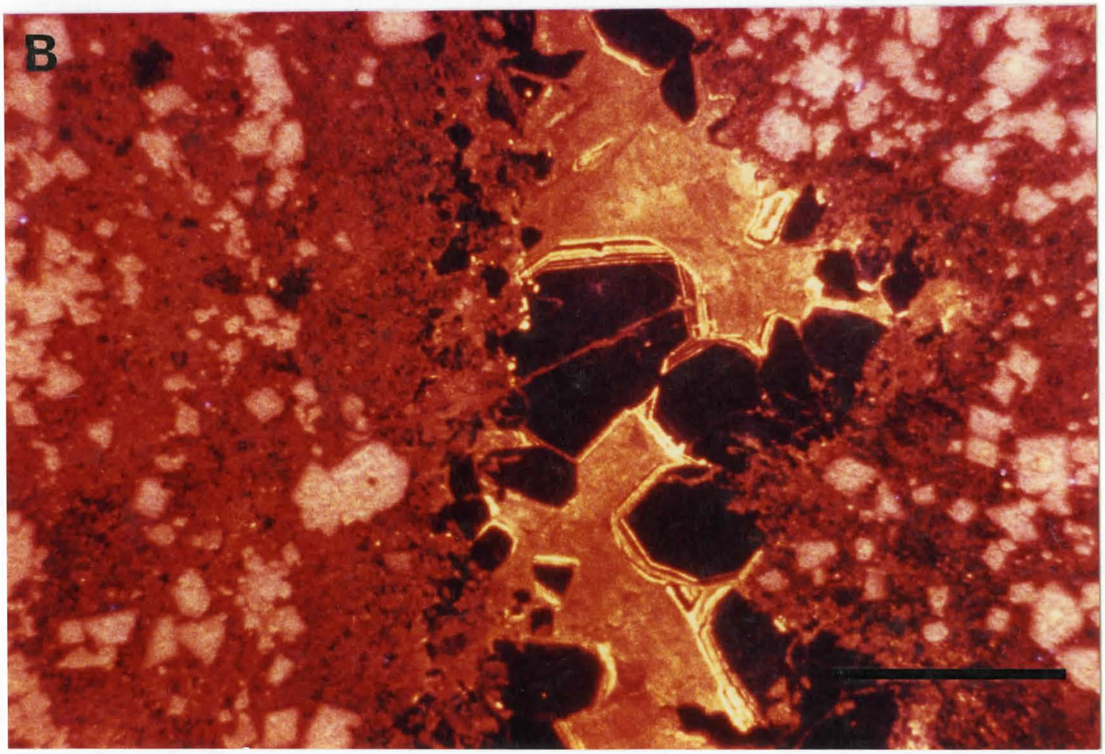
B

difficult to trace it across the bright repetitious zone. Close examination of the fracture suggests that it originates in the region of dolomite crystals arranged in a linear manner. In plane polarized light this was observed to be a microstylolite.

Compaction has resulted in fracturing and sometimes displacement of fossil fragments. Figure 87a and 87b show fractured coral skeletons in which the fractures and some intraskeletal pores are filled with dull calcite. There is no zoned calcite in these fractures or on any broken surface, so fracturing and infilling must have occurred after non-luminescent and bright calcite precipitation.

In Figure 87a the stylolite seen penetrating the coral skeleton is suggestive of compactive pressures that may have also been responsible for the fracturing and displacement of the skeleton. It is difficult to relate these two processes, though in this example, it seems likely due to the close spatial relationship.

Tracing the fracture out of the skeleton in Figure 87b, one can see that its boundaries are no longer sharp, but hard to distinguish from the matrix. This is commonly the case where fractures are infilled by dull calcite can only be recognized in the matrix by tracing a line of broken particles.

Figure 87 Cathodoluminescent photographs of fractured coral skeletons that have been healed by dull calcite. 87a) The stylolite that penetrates the coral (top right corner, defined by penetrating dolomite rhombs) is suggestive of compactive pressures that may have caused fracture and displacement of the coral. 87b) Tracing the fracture out of the coral, it is difficult to distinguish the matrix from the dull calcite that fills the fracture and intraskeletal porosity. Magnification 28x. Scale bar 1 mm.

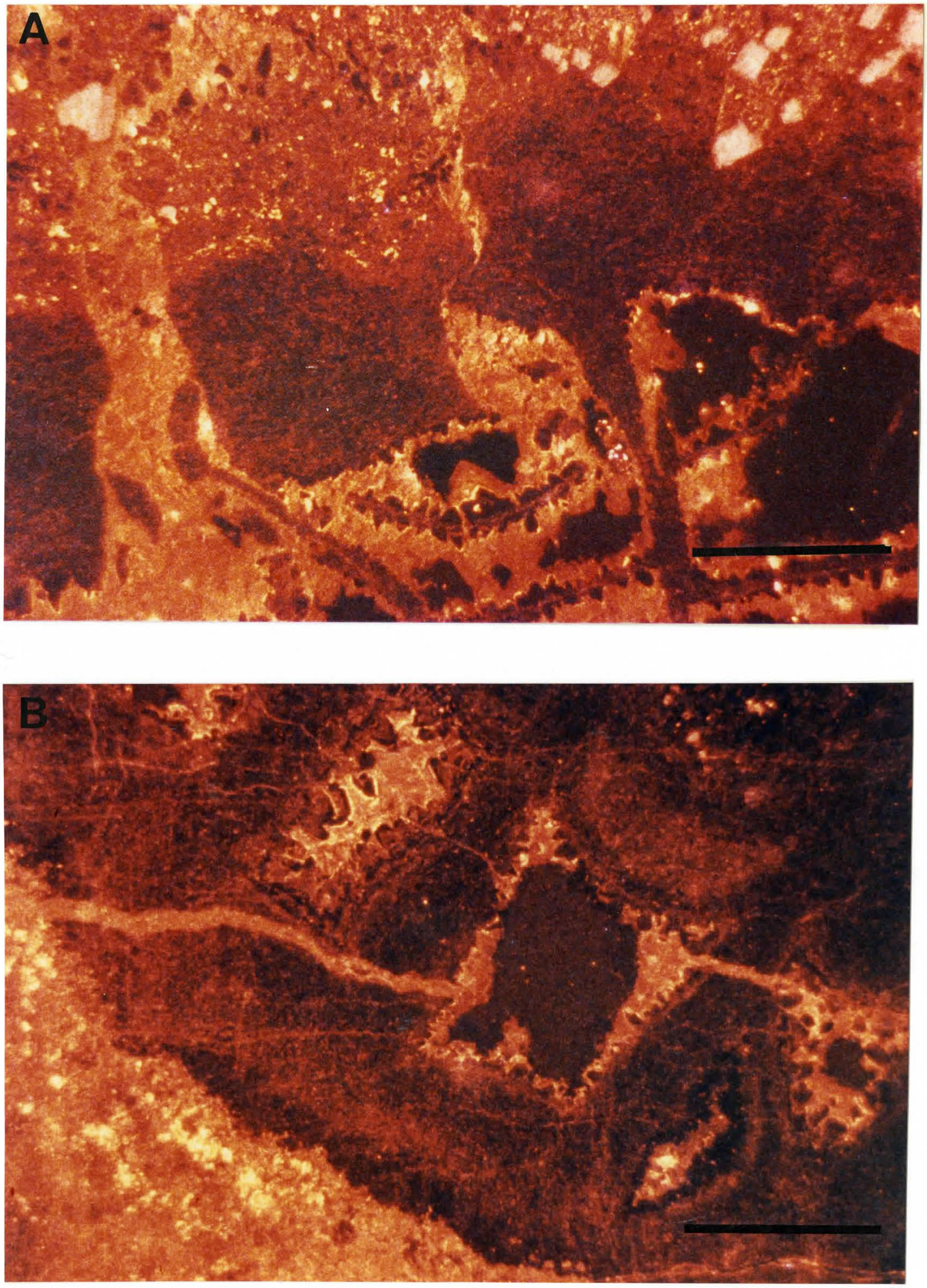
A
B

6.5.4 STYLOLITE RELATIONSHIPS

As in the Lockport Formation, veinlets are observed to originate at stylolites and propagate away from them. The veinlet pair shown in Figure 88a are made up of dull calcite. These veinlets were traced out for 2 centimetres, where one was seen to cross-cut non-luminescent crystals and enter a pore filled with a dull calcite which was indistinguishable. These veinlets are so fine that they are best visible cutting across matrix dolomite where the contrast accentuates them.

Veinlets are also found in dense concentrations that originate at a highly irregular suture (Figure 88b). Similarly, the veinlets are made up of dull calcite. Their length is approximately 3 millimetres and they cannot be traced out into any pores, only into matrix dolomite and micrite.

Dull calcite is not the only material found infilling veinlets. Where dolomite concentrations are high, dull maroon luminescent dolomite veinlets have been found (Figure 89). Unlike the dull calcite veinlets these veinlets are in optical continuity with their dolomite hosts. Their luminescence resembles that of the Fe-dolomite described earlier.

These veinlets do not extend very far, commonly several millimetres or less, nor are they seen to enter any

Figure 88 Cathodoluminescent photographs of dull calcite veinlets that originate at a stylolite. 88a) Two veinlets cross-cutting red luminescent dolomite that originate at an undulatory section of a stylolite. 88b) Numerous veinlets originating at an irregular stylolite suture and cross-cutting dolomite. Magnification 28x. Scale bar = 1 mm.

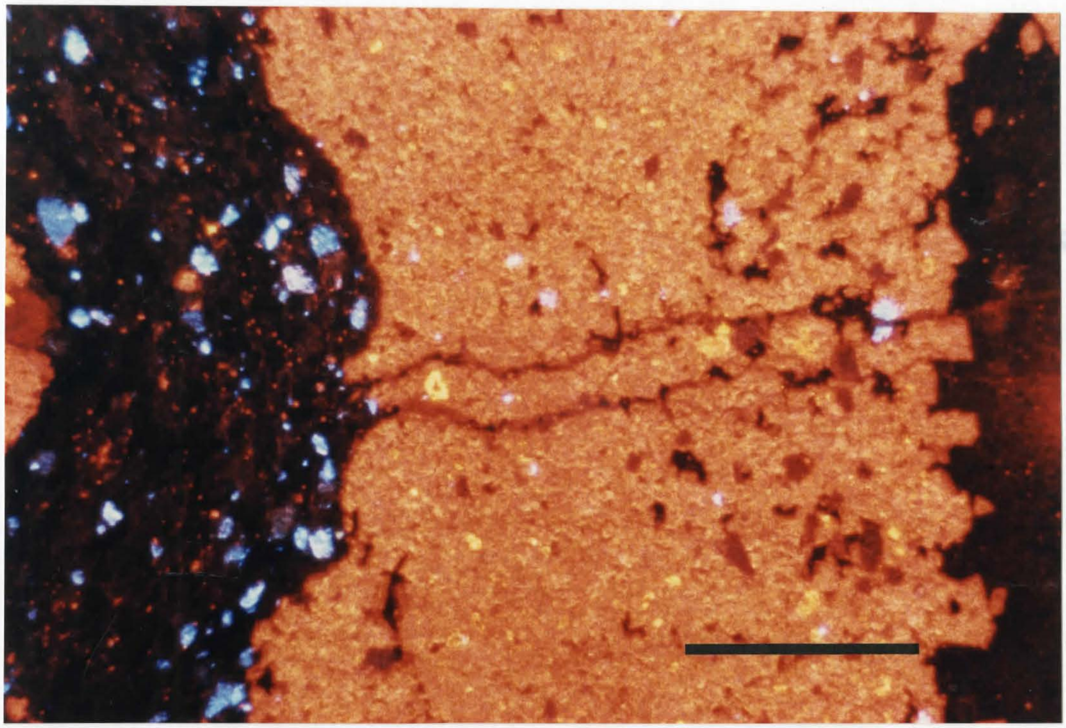

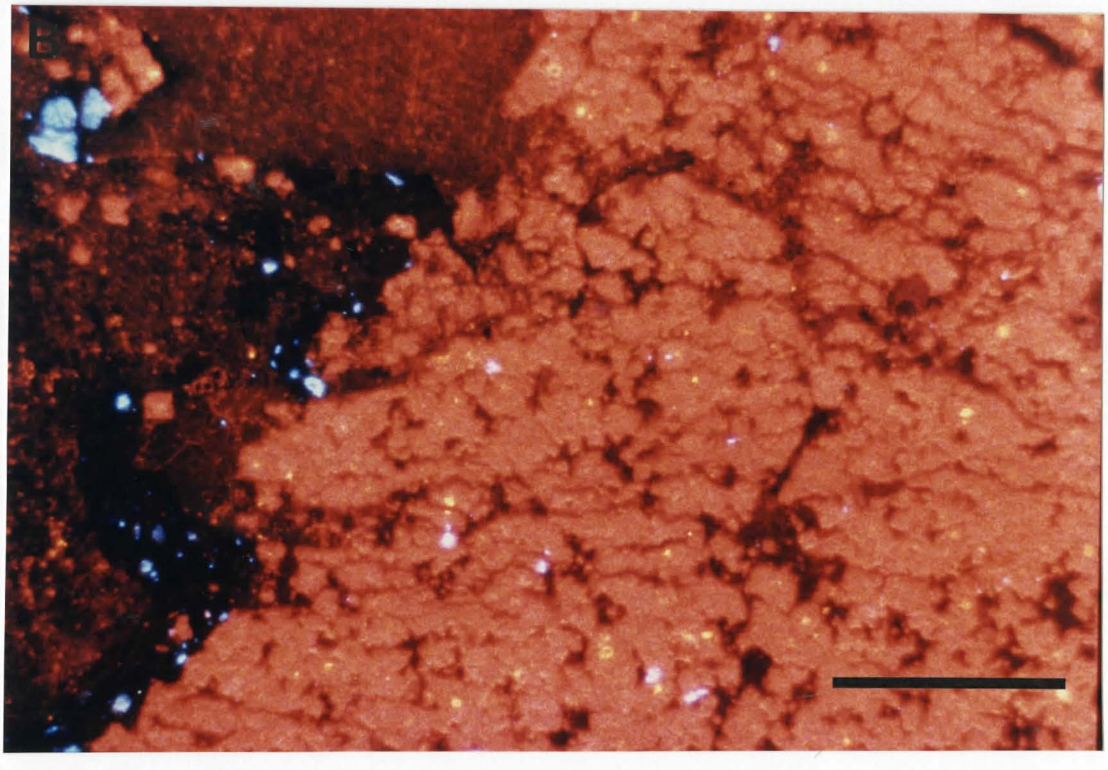
B

Figure 89 Cathodoluminescent photograph of a stylolite suture with dull maroon dolomite veinlets in its interior. Note the absence of matrix calcite within the suture. Magnification 28x. Scale bar = 1 mm.

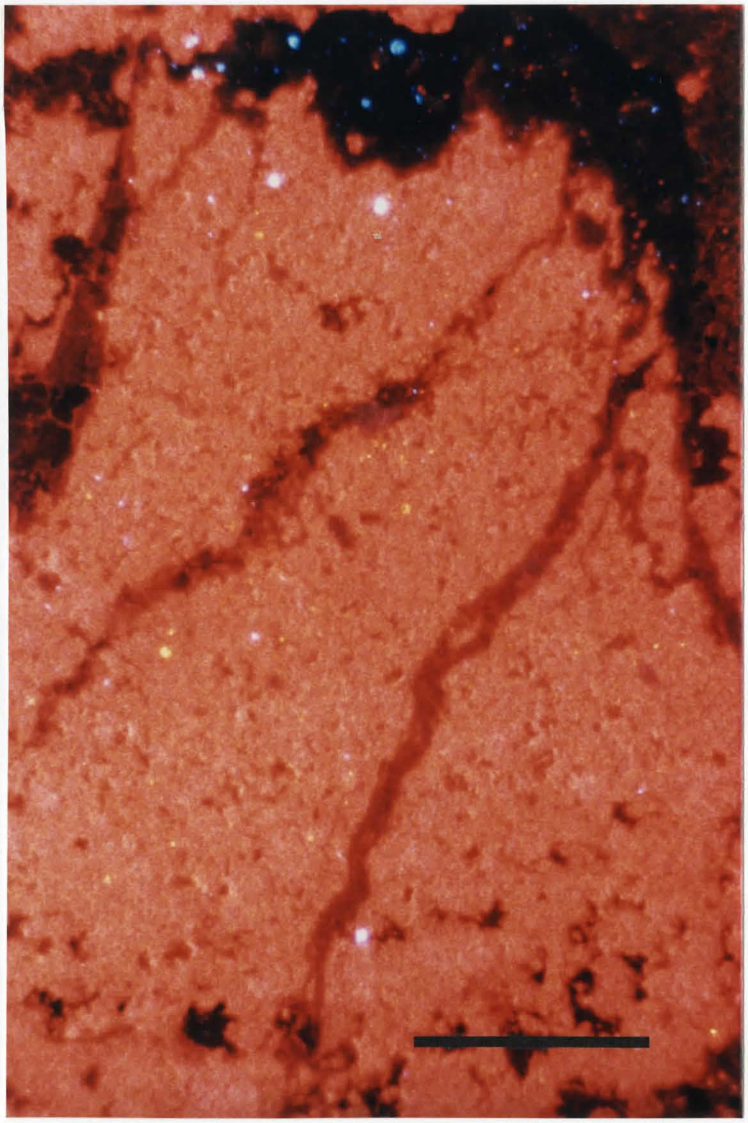

pores. They have been found related to brecciated matrix dolomite, suggesting that the brecciated matrix dolomite has been healed by this dull maroon dolomite. Otherwise the veinlets just die out.

Dull calcite has been found in porosity created by stylolitization, or more precisely, the stylolite it is associated with. A penetrating stylolite column may create porosity by shearing the socket walls with a projection from itself (e.g. dolomite crystals). Porosity may also be created by extensional separation of the socket and column walls. Dull calcite has been observed in these secondary pores, either partially or completely filling them. Figure 90 shows this relationship which suggests the dull calcite post-dates this particular stylolite.

6.5.5 SPATIAL RELATIONSHIPS AND REPLACEMENT TEXTURES

Dedolomitization textures have been found in close proximity to stylolites in variable concentrations. Dedolomitization is observed as the replacement of dolomite crystal cores by dull luminescent calcite. Figure 91 shows a spectacular example of this seen only 2 millimetres away from a stylolite. Replacement is extensive. All crystals have been dedolomitized to some degree. Interestingly, the outer dolomite zone appears resistant to calcification. Replacement commonly stops abruptly at the zonal boundary.

Figure 90 Cathodoluminescent photograph of dull calcite infilling porosity created by the shearing of the socket walls. Magnification 28x. Scale bar = 1 mm.

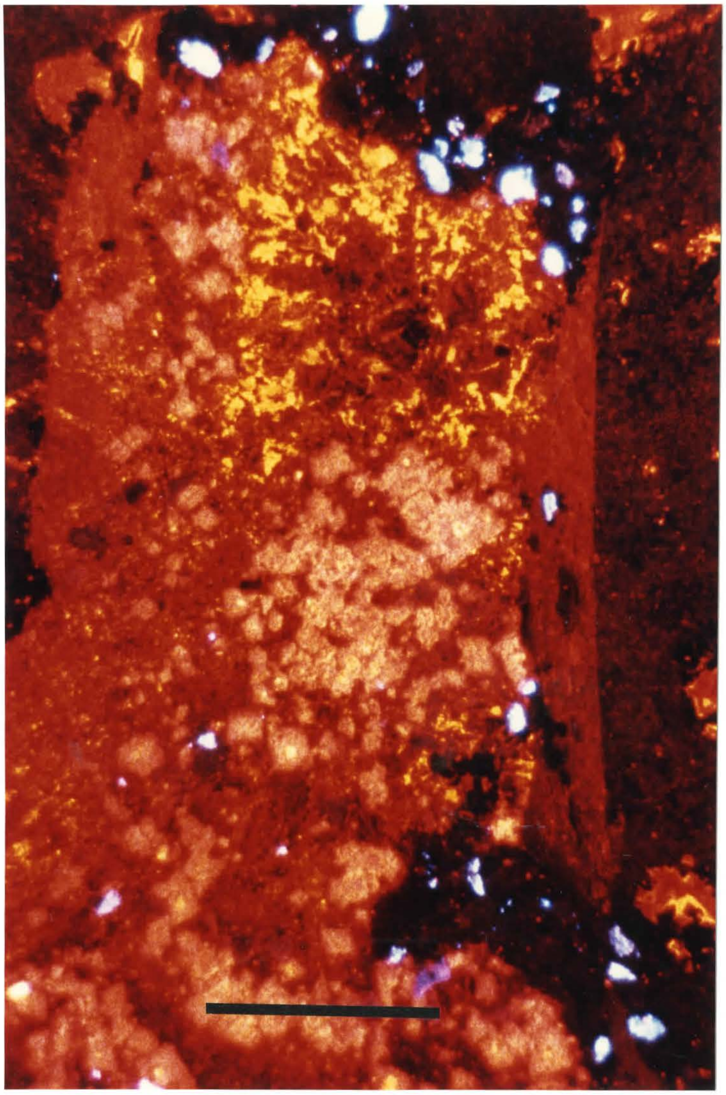

Figure 91 Cathodoluminescent photograph of extensive dedolomitization of matrix dolomite by dull calcite. The interiors of the dolomite rhombs have been replaced by dull calcite while the outer zones remained resistant to calcification. Magnification 28x. Scale bar = 1 mm.

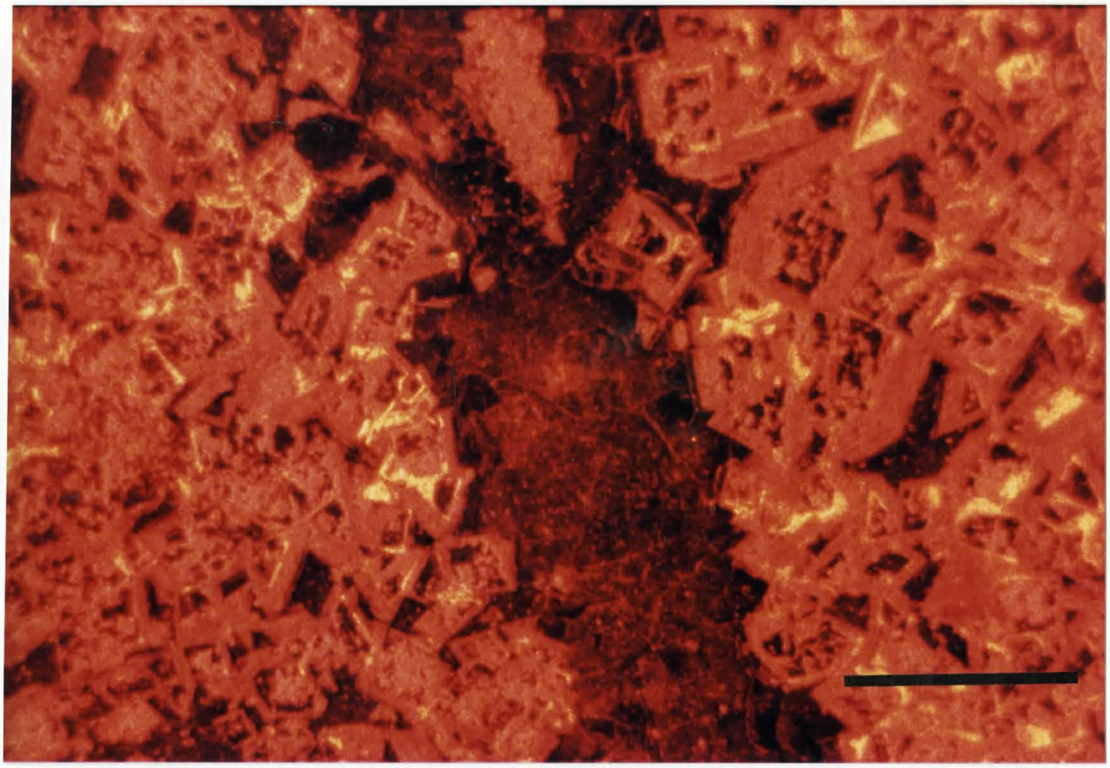

Dedolomitization is observed in both matrix dolomite and red-luminescent dolomite cements. Figure 92a shows a dolomite cement crystal extensively replaced by dull calcite and partial replacement of the finer matrix dolomite in the immediate vicinity. As described earlier, the dolomite cement precedes the precipitation of bright calcite. Yet dedolomitization is by dull calcite, not bright calcite (which succeeds the dolomite cement). Figure 92b shows similar relationships. The pore lining dolomite crystals have been partially replaced, but the larger zoned dolomite crystals have not. These crystals appear to pre-date the bright luminescent zone similar to the dedolomitized crystals, yet they are not replaced by dull calcite.

Dull calcite is also observed to replace earlier non-luminescent and bright calcite. Where the nucleating crystals are in contact with a micritic substrate. In Figure 93a dull calcite pervades the non-luminescent cores of crystals lining the pore, apparently from the micrite towards the pore interior. The texture does not resemble any cement fabric or growth zonation, nor is it likely to be an extremely delicate structure. Crystals in the interior of pores, not nucleated on micrite, appear unaffected.

Dull calcite may obliterate earlier zonal sequences. Figure 93b shows relict zonations visible through the dull calcite that pervades the interior of these

Figure 92 Cathodoluminescent photographs of dedolomitization of matrix dolomite and red-luminescent dolomite cement crystals. 92a) Dolomite cement preceded bright calcite precipitation. Dolomite crystal in center of photograph and matrix dolomite are partially replaced by dull calcite. Dull calcite occludes porosity after bright calcite. 92b) Large pore infilled by zoned calcite. Red dolomite crystals lining pore are partially replaced by dull calcite (top left of photograph). Magnification 28x. Scale bar = 1 mm.

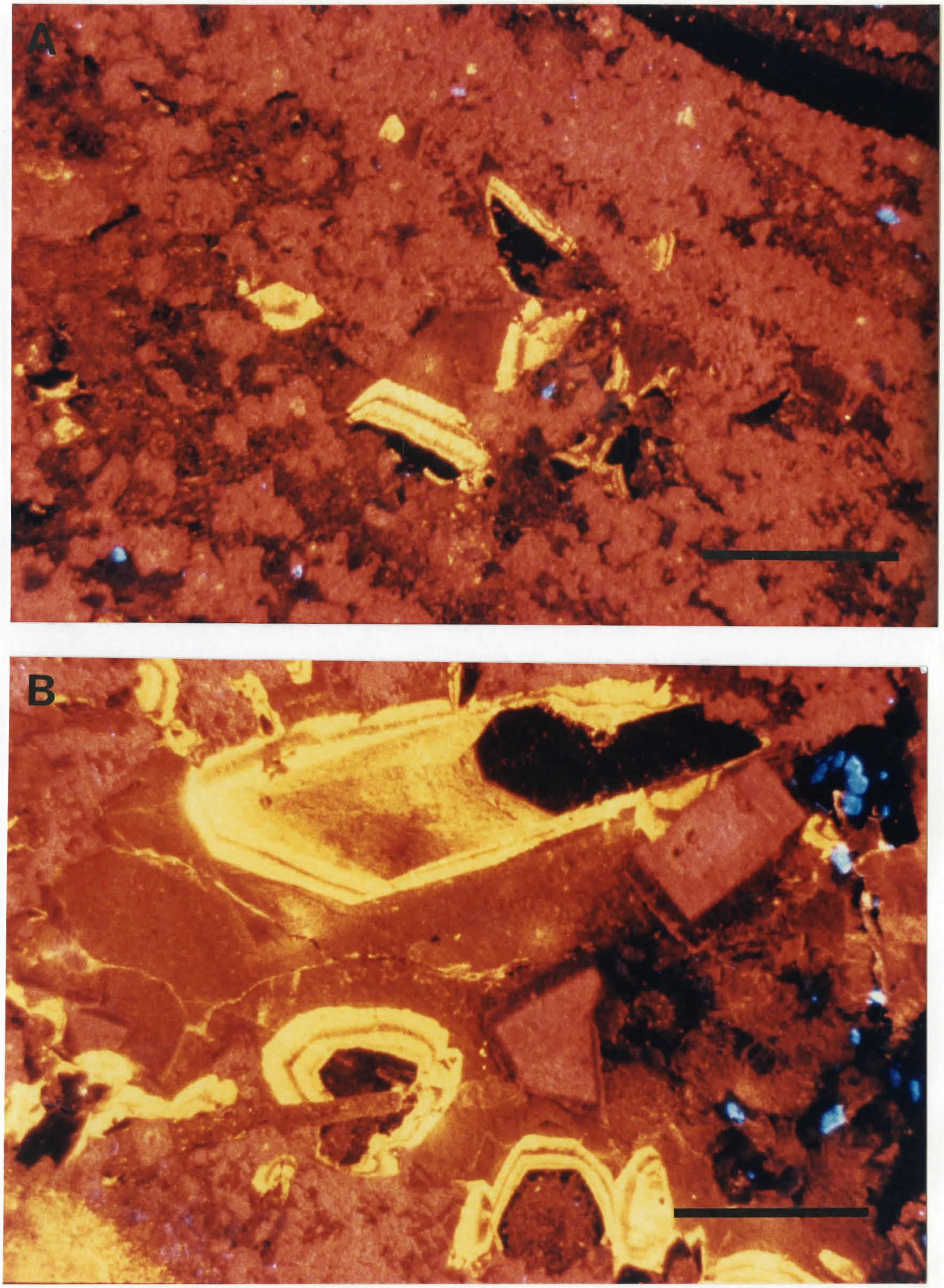
A
B

Figure 93 Cathodoluminescent photographs showing dull calcite replacing non-luminescent calcite crystal interiors. 93a) Crystals that nucleated on micrite (dull luminescent) have had their cores partially replaced by dull calcite. Those that are found in the pore interior have not. 93b) Dull calcite has nearly obliterated the zonation seen with non-luminescent crystals. Magnification 28 x. Scale bar = 1 mm.

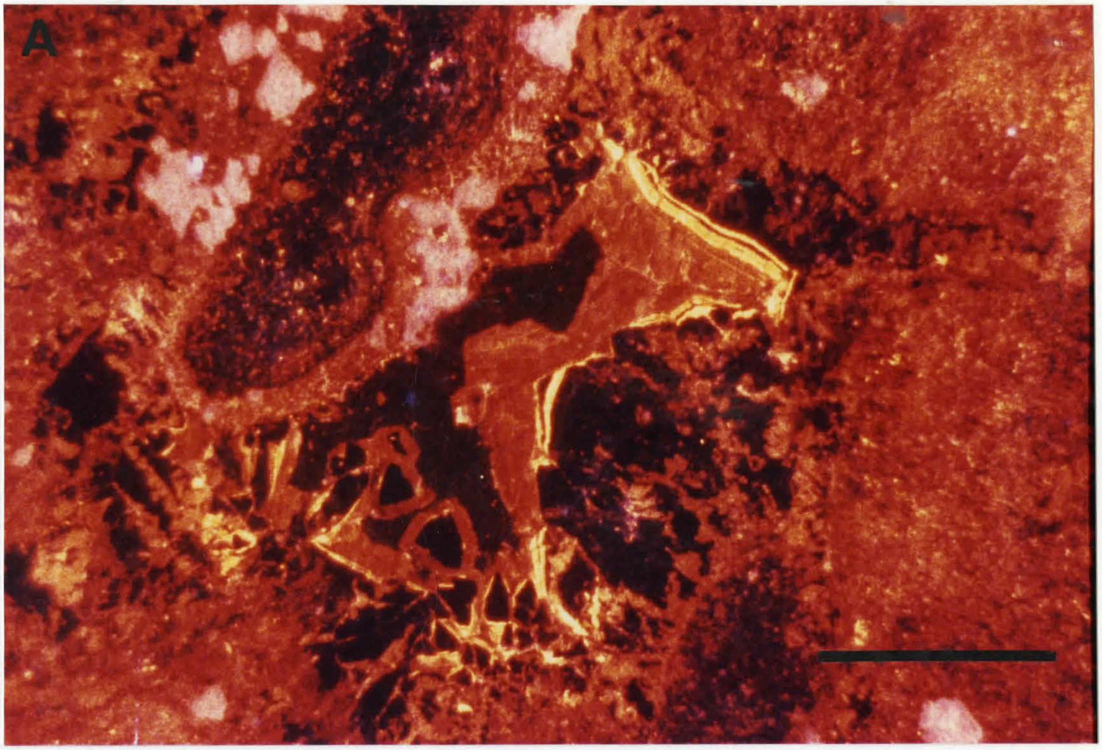
A

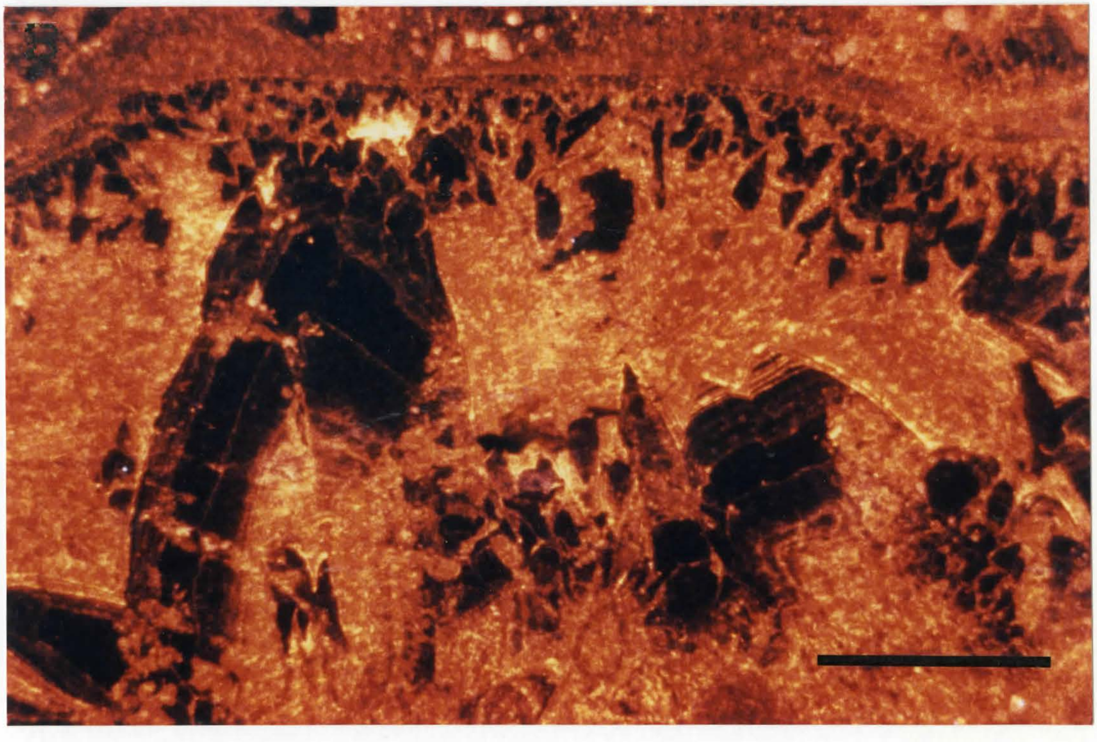
B

crystals. Note that the luminescence of this pervading calcite is indistinguishable from the pore occluding dull calcite and that the micritic matrix has a very similar luminescence in both samples.

This texture is not confined only to the cores of crystals but may also disrupt entirely filled pores as seen in Figure 94a. In this photo the dull calcite pervades not only non-luminescent cores, but also disrupts the bright zonation in the pore interior.

This texture con be related spatially to pressure solution sites. Figure 94b shows a highly repetitious non-luminescent, bright luminescent sequence, pervaded by dull luminescent calcite. Relict zonations are visible through the dull calcite. Penetrating, not replacing, this zonal sequence are clusters of dolomite rhombs and a stylolite suture (not well defined in luminescence). Porosity is exceptionally tight in this example as the rock is primarily micritic.

Figure 94 Cathodoluminescent photographs showing dull calcite partially replacing earlier non-luminescent/bright/dull crystals. 94a) Dull calcite has partially obliterated the non-luminescent/bright sequence in the completely occluded pore. 94b) Dull calcite that has partially obliterated this very repetitious non-luminescent/bright sequence. A suture of a stylolite penetrates this sequence at top center and dolomite crystals penetrate it at the bottom center. Magnification 28x. Scale bar = 1 mm.

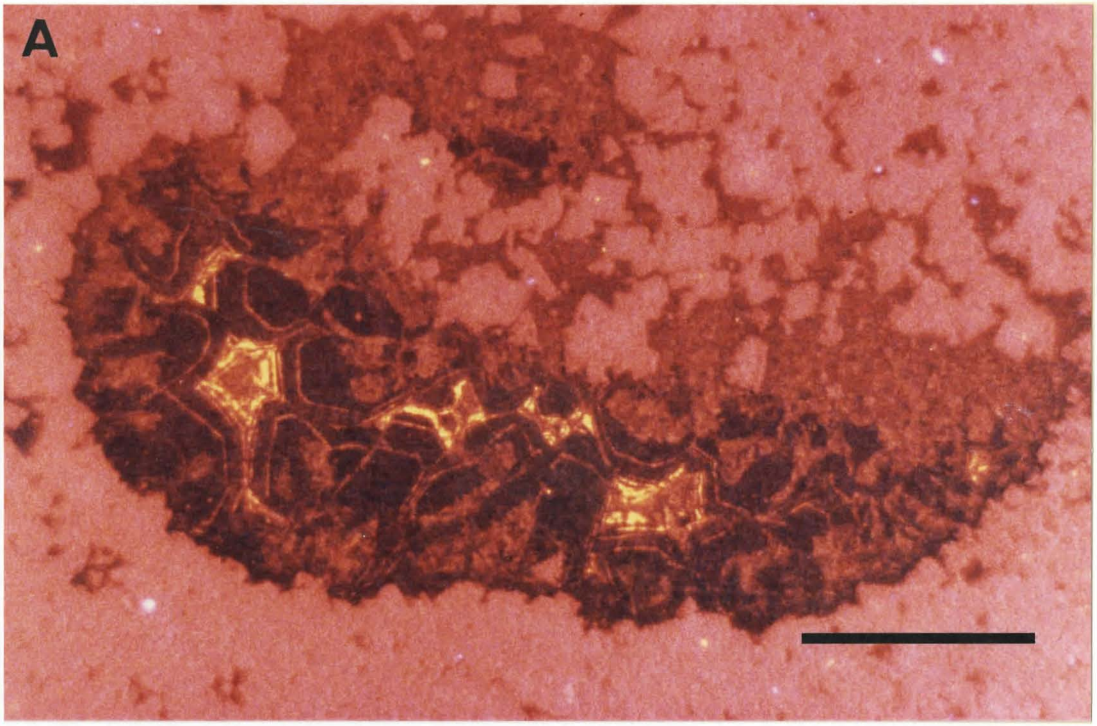
A

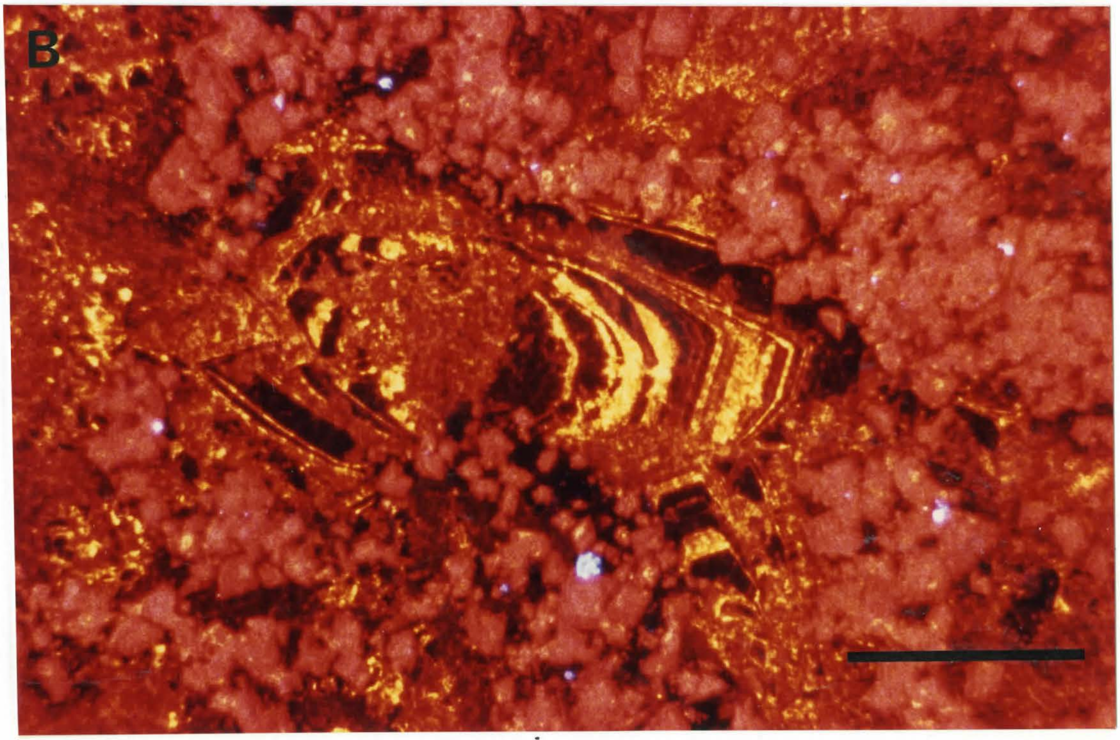
B

6.6 SUMMARY-NISKU FORMATION

Dull calcite is the last zone in a non-luminescent/bright/dull sequence. It has been found filling fractures and healing broken surfaces in which the early zones are absent. Some of this fracturing is spatially related to stylolitic surfaces.

Matrix dolomite shows signs of solution coalescence where zonation is visible. Typically, the zonation of matrix dolomite becomes less apparent closer to a stylolite, resulting from a "rearrangement" of its luminescent signature due to recrystallization.

Stylolite/fracture associations show veinlets of dull calcite propagating away from stylolites, sometimes entering pores filled with dull calcite. Commonly, these veinlets dissipate into the matrix. Veinlets of dull maroon dolomite, resembling the Fe-dolomite luminescence, have also been observed. These veinlets are not found often.

Dedolomitization is spatially related to stylolites. Both matrix dolomite and early dolomite cement is susceptible to dedolomitization. The interior of individual crystals are preferentially replaced by dull calcite. Based upon luminescent characteristics and zonal relationships this appears to be the same dull calcite associated with the zonal sequence of calcite spar.

Lastly, dull calcite is observed to pervade and obliterate interior zonations of calcite spar. It preferentially pervades crystals lining micritic pore walls and is spatially related to pressure solution sites.

6.7 INTERPRETATIONS

The search for pressure solution generated cement has been exhaustive. Observation of direct and spatial relationships enables the following interpretations to be made.

In both Lockport Formation and Zeta Lake Member samples, cathodoluminescence reveals veinlets and fractures originating at stylolites. The infill has the same luminescent characteristics as the last major phase of porosity-occluding cements. Furthermore, these features have been observed to invade pore spaces in which one cannot distinguish between vein/fracture material and pore occluding cement. These textures and characteristics lead to the interpretation that a) Lockport Formation stylolites generate bright-red dolomite, and b) Zeta Lake Member stylolites generate dull calcite and sometimes dull maroon dolomite.

In the Zeta Lake Member, dolomite veinlets have luminescent characteristics similar to those of Fe-dolomite seen in pores. These veinlets are believed to be a possible source of material for this dolomite, hence, they are post-dull calcite in origin. This suggests that the dolomite that infills them is a late pressure solution generated cement.

In the Zeta Lake Member, the dull calcite heals fractured and broken surfaces some of which are spatially related to stylolites. These breakage textures are interpreted as pressure solution-induced, hence there is a temporal relation between dull calcite generation and healing associated with stylolites, i.e. stylolitization fractured the particles and the generated cement subsequently healed them. The scarcity of skeletal particles in the Lockport Formation does not permit this interpretation to be made.

Of the thin sections examined, less than 15% showed direct stylolite/fracture associations. This lack of direct evidence strongly suggests that the transport was not only along fractures but also along a system whose existence is not as easily detected. Similarities in luminescence of generated cements (bright-red dolomite - Lockport, dull calcite - Zeta Lake) and material that pervades the matrix and earlier cement crystals is taken as evidence of a diffusion transport mechanism. Diffusion transport is believed to have been active as an intracrystalline mechanism in the Lockport and within the micritic matrix of the Zeta Lake.

In the Lockport Formation, the pervasive mottling of the bright-red dolomite in the interior of dull-red dolomite crystals, and the dissipation of veinlets into dolomite crystals supports diffusion transport. For the Zeta Lake Member, the partial obliteration of crystal interiors which nucleate on micritic substrate suggests diffusion from the matrix, through crystals, outward into pores. Similarly, dissipation of veinlets into the micritic matrix, suggests diffusion was active. Where diffusion textures are evident the micritic matrix is dominantly dull luminescent, often indistinguishable from dull calcite that occludes porosity. These textures, relationships, and characteristics all support the interpretation of diffusion transport.

Diffusion transport also serves to explain the dedolomitization of matrix dolomite and early dolomite cements by dull calcite. Dull calcite diffusing away from an active stylolite by migrating thin fluid-films was able to calcitize dolomite due to the stressed state of these crystals proximal to the stylolite. Further away from this stressed region, dolomite became less susceptible to calcitization as stresses progressively decreased, confining diffusion transport to the micritic matrix.

Coalescence and recrystallization of matrix dolomite nearer to stylolites suggests that stresses were higher near stylolites than further away. Rearrangement of the luminescent nature of matrix dolomite is interpreted as a localized stress-induced effect and not a product of pressure solution-generated material analagous to Wanless (1983) and Mattes and Mountjoy (1981).

CHAPTER 7

PRECIPITATIONAL ENVIRONMENTS, CEMENT STRATIGRAPHY, AND GEOCHEMICAL INTERPRETATIONS-NISKU FORMATION

7.1 INTRODUCTION

The last three cementing materials in the Nisku Formation Zeta Lake Member are, in order , non-ferroan calcite spar, Fe-dolomite, and anhydrite. The most abundant, and that which is of interest to this research, is calcite spar. Watts (1984) has interpreted this cement to have formed during shallow to intermediate burial. It can be related to vadose/phreatic, deep phreatic, and shallow subsurface origins.

In an effort to better understand the origin of this calcite cement, luminescent zonations were mapped and geochemical interpretations based upon these luminescent sequences were made.

7.2 COMPOSITIONAL ZONING OF CALCITE SPAR CEMENTS

Distinctive luminescent zonations are seen in calcite spar cements. It is the last zone of this cement which previously (Chapter 6) has been interpreted to be of pressure solution origin. Identical and near-identical sequences are found in primary fenestral pores, intraskeletal spaces, brachiopod interiors, mollusc molds, and within crinoid syntaxial overgrowths. Limited powers of magnification prevent recognition of such sequences in the micritic matrix, though luminescent intensities similar to those in the cements are seen.

Following Meyers (1974), luminescent intensities are here interpreted in terms of relative Mn^{2+} and Fe^{2+} concentrations.

Zone 1 is the oldest cement. It is non-luminescent, Mn^{2+}-poor and Fe^{2+}-free. Luminescence may be uniform or contain thin bright or dull bands towards its outer boundary. Bands may occur only once or be repeated several times. This early, non-luminescent generation commonly shows regularly developed euhedral morphologies. Absence of this form can be related to dissolution events.

Zone 2 is a thin zone of bright luminescent cement Mn^{2+}-rich and Fe^{2+}-free. The luminescent color varies from bright-yellow through bright-orange. The underlying morphology of zone 1 is mimicked by this cement. Bright cement may entirely or partially envelop the earlier generation zone 1, resulting in a continuous or discontinuous zonation. It accentuates crystal faces, irregular and fretted dissolution surfaces, and may show preferred growth directions. Thin banding of non-luminescent or dull luminescent cement may be found within this zone, repeated once, or several times.

Zone 3 is the youngest cement. It has a dull to very dull luminescence that internally is uniform or may be faintly to distinctly subzoned with brighter luminescence (Figure 82,83b). Thin band repetitions are not seen in this zone. It is interpreted as containing Fe^{2+} and moderate amounts of Mn^{2+}. This cement is not constrained by earlier cement morphologies. It may appear as a continuous or discontinuous growth after zone 2, or where absent, zone 1. Unlike the earlier zones, this cement may be found in the absence of the other two zones, primarily in fractures or intergranular pores.

All zonal boundaries are sharp, including those associated with thin bands. Subzones show more gradational to sharp boundaries.

Accessory minerals, oxides and sulfides are not seen associated with any of these zones.

7.3 PRECIPITATIONAL ENVIRONMENT INDICATORS

Features indicating a vadose zone origin are not found associated with calcite spar. Absent are gravitationally controlled forms (pendant textures) and grain-contact related forms (meniscus style cement). Crystal silt, which is thought to be characteristic of vadose diagenesis (Dunham 1969), though may be produced by boring sponges (Moore et al. 1976), is not seen related to any of the cement zones. Instead the features, textures, and relationships described earlier and zonal patterns discussed herein suggest that precipitation of this calcite took place in water-filled pores during progressive burial.

Forms and morphologies of the growth zones observed are analagous to those described by Meyers (1974) in the Lake Valley Formation calcarenites, New Mexico. Zonal sequences that display zonal thickening toward pore interiors, growth inhibition around grain (crystal) contacts, and/or pinching-out of zones towards grain contacts are indicative of precipitation in water-filled pores. These features can all be seen in Figure 81.

Exceptions to this pattern are seen in Figure 92a. This may be explained by preferred growth direction in water-filled pores (Meyers 1974) or by dissolution effects that disrupt zonal patterns. Meyers (1974) interpretations were based upon syntaxial overgrowth cements in calcarenites. These samples, mainly wackestones and packestones, contain an abundance of void-filling calcite spar and few overgrowths. It seems logical that zonal patterns observed within this pore-filling spar will be more typical of growth competition rather than the inhibition patterns best illustrated by zonal thickening. Nevertheless, the principles upon which Meyers (1974) interpretations were based may be applied here.

Zonal patterns seen in syntaxial overgrowths have also been studied and environmental interpretations were made from them (Walken and Berry 1984a). Spired overgrowths (figure 95a) with a persistent euhedral morphology imply nearly ideal growth conditions following nucleation on a structurally discontinuous fresh grain surface. Needle overgrowths (Figure 95b) reflect growth by displacement or replacement into interstitial carbonate mud. Entrainment of impurities prevents amalgamation of individual spires. Contouring overgrowths (Figure 95c) imply the existence of spire-inhibiting factors. Walken and Berry (1984a) interpret this pattern as either dissolution effects within the meteoric diagenetic environment or surface tension effects within the vadose zone. Idiomorphic overgrowths (Figure 95d) also reflect near-ideal growth conditions. Early spire development was probably unnecessary because of early cementation of the original pore system. The overgrowth nucleated on a smooth surface and not one that was rough and discontinuous.

The principles developed by Walken and Berry (1984a) are believed to be applicable not only to overgrowth phenomena, but also to pore occluding cements in general. It is believed that the degree of earlier substrate cementation will be reflected in the morphology of the zonal patterns observed.

Figure 95 Schematic representation of four distinct syntaxial overgrowth styles on echinoderm grain substrates. 95a) Spired overgrowth. 96b) Needle overgrowth. 95c) Contouring overgrowth. 95d) Idiomorphic overgrowth. All patterns represent growth in the c-axial direction. From Walken and Berry (1984a).

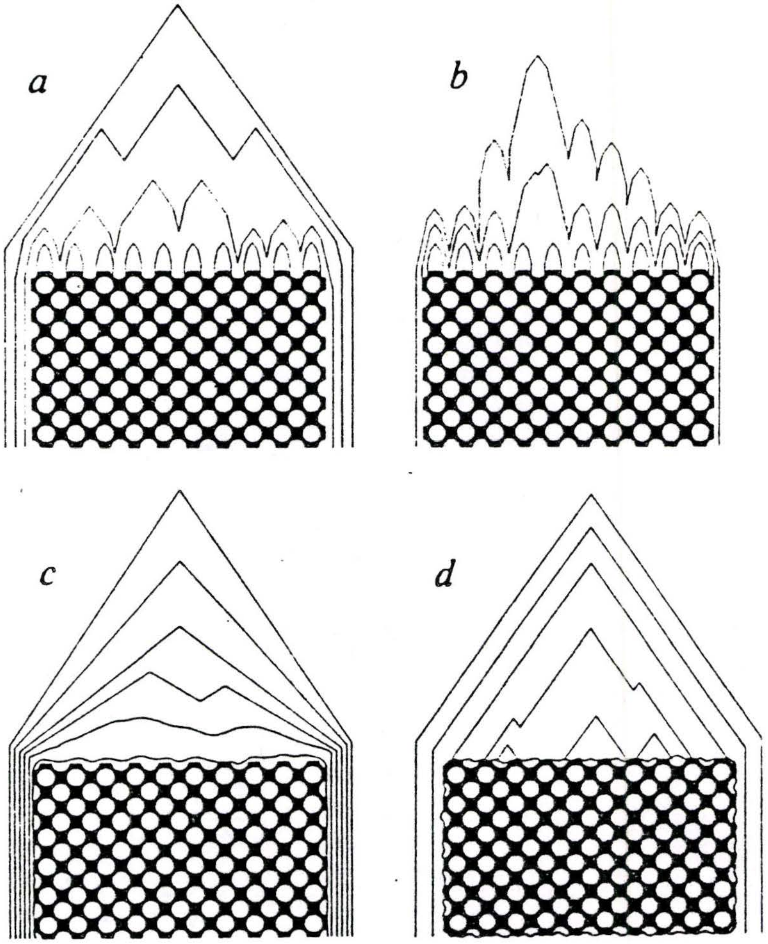
a
b
c
d

The persistent euhedral morphology of crystals nucleating on micritic pore walls (Figure 80b,81,82,86b) is interpreted as growth during near-ideal conditions on a partially cemented substrate suggested by a general absence of spired morphologies. Idiomorphic growth patterns as seen in Figures 80, 80a, and 81 suggests seeding on an early cement. Evidence of this may be seen in Figure 81, but may only be inferred for Figure 80a where the substrate is micritic and an early cement cannot be recognized. Where earlier cements are easily recognized (Figure 79a and 79b) zonal patterns are consistently euhedral and idiomorphic. Contouring overgrowths (Figure 83a,83b) are interpreted to result from dissolution effects.

Zonal patterns and their interpretations suggest that calcite spar growth occurred under near-ideal conditions on substrates that may have experienced variable degrees of earlier cementation. Subsequent to precipitation of the early zones, dissolution occurred in a meteoric environment. Dissolution textures are variably intense (Figure 83a,83b) and are not seen in all pores. This suggests restricted access of the fluids responsible for dissolution.

7.4 CEMENT STRATIGRAPHY

Mapping of zonal sequences in calcite spar uses the principles established by Meyers (1974, 1978). It is assumed that sequences are always in the same order, and that individual zones represent discrete episodes of cementation. Absence of a zone from the sequence implies the existence of a cement unconformity. Synchroneity or diachroneity of the cements cannot be established since only one borehole is studied. The vertical distribution of cement zones is shown in Figure 96.

Immediately obvious is the lack of any well-defined pattern in the distribution of zonal sequences. 76% of the samples show the basic zonation non-luminescent/bright/dull, 16% lack any bright association at all, and 8% have thin bright bands within the non-luminescent zone. Of all the samples, only two do not have a non-luminescent or bright zone. Conversely, 100% of the samples show a dull zone relation.

There appears to be no gross facies control over cement distribution and zonal sequences. Boundstones, packestones, and wackestones are individually and collectively equally variable. Closer examination of Figure 96 suggests that there might be a local facies control. Microfacies are indicated beside each sample location. Pack-

Figure 96 Vertical distribution of calcite spar cement zones in the Nisku Formation. NON LUM is non-luminescent cement. THIN BRI is thin bright bands of cement within the basic zonation. THIN NONL is thin non-luminescent bands. V. DULL is very dull cement. Note the absence of similarity in zonal sequences between samples at a facies scale. Similarity between sequences is difficult to recognize at a microfacies scale. Generally, zonal sequences are more complex and variable in local packestones textures than wackestones. Discontinuous zonation of bright cements is common to wackestones. Dull cement is ubiquitous throughout the formation. Each dot represents a single sample.

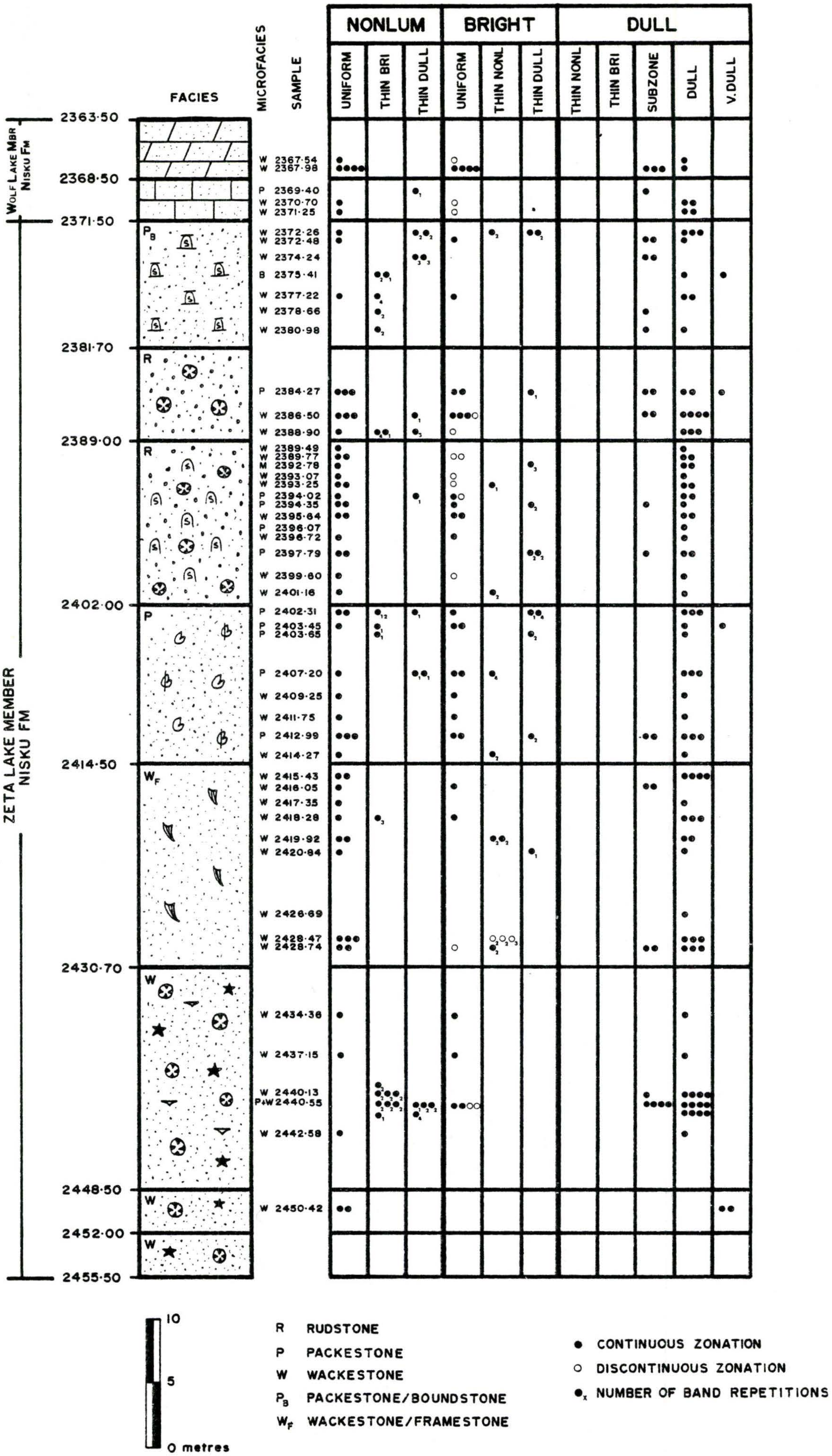
NONLUM
BRIGHT
DULL
UNIFORM
THIN BRI
THIN DULL
UNIFORM
THIN NONL
THIN DULL
THIN NONL
THIN BRI
SUBZONE
DULL
V. DULL
FACIES
MICROFACIES
SAMPLE
WOLF LAKE MBR NISKU FM
ZETA LAKE MEMBER NISKU FM
2363·50
2368·50
2371·50
2381·70
2389·00
2402·00
2414·50
2430·70
2448·50
2452·00
2455·50
W 2367·54
W 2367·98
P 2369·40
W 2370·70
W 2371·25
W 2372·26
W 2372·48
W 2374·24
B 2375·41
W 2377·22
W 2378·66
W 2380·98
P 2384·27
W 2386·50
W 2388·90
W 2389·49
W 2389·77
M 2392·78
W 2393·07
W 2393·25
P 2394·02
P 2394·35
W 2395·64
P 2396·07
W 2396·72
P 2397·79
W 2399·60
W 2401·16
P 2402·31
P 2403·45
P 2403·65
P 2407·20
W 2409·25
W 2411·75
P 2412·99
W 2414·27
W 2415·43
W 2416·05
W 2417·35
W 2418·28
W 2419·92
W 2420·84
W 2426·69
W 2428·47
W 2428·74
W 2434·36
W 2437·15
W 2440·13
P+W 2440·55
W 2442·58
W 2450·42
P_B
R
R
P
W_F
W
W
W
10
5
0 metres
R RUDSTONE
P PACKESTONE
W WACKESTONE
P_B PACKESTONE/BOUNDSTONE
W_F WACKESTONE/FRAMESTONE
● CONTINUOUS ZONATION
○ DISCONTINUOUS ZONATION
$●_x$ NUMBER OF BAND REPETITIONS

estones account for 24% of the samples, wackestones 75%. The remaining 1% represents a mudstone and boundstone.

Of the packestones examined, between 50% to 60% show bright thin banding in non-luminescent zones or the presence of subzones. Wackestones that show this complexity only account for between 20% to 25% of the samples. Similarly, nearly 60% of the packestones show non-luminescent thin bands in bright zones. Wackestones display this in only 20% of the samples. Thin bands of bright and non-luminescent cement seen in both non-luminescent and bright zones, respectively, account for 16% of the packestones and 3% of the wackestones.

The number of thin bands in a zone is variable. Commonly, these are between 1 and 4 repetitions within a single sample. A maximum number of 12 repetitions has been seen, though this is a rarity.

Discontinuous (partial) zonations are seen only in the bright zone, primarily the uniform bright cements. However, one sample did display this type of zonation in bright cements with thin non-luminescent bands. This type of zonation is rare. Patterns such as these may reflect an irregular growth form or dissolution surfaces.

Local packestone textures show a greater percentage of more complex zonation sequences than do wackestones. Wackestones are less complex, though they represent a greater fraction of the samples examined. It seems logical that packestones, with inherently higher porosities and permeabilities, be more sensitive to rapid changes in pore water chemistry. This "sensitivity" is reflected in the cements precipitated, and the zonal sequences seen.

The only cementation episode that is always seen is that represented by dull calcite. The lack of non-luminescent and bright zones seen in several samples suggests that local conditions were not suitable for the precipitation of the zones at that time.

7.5 GEOCHEMICAL INTERPRETATIONS

The luminescent intensities of cement zones were earlier related by their relative trace element concentrations (Mn^{2+} and Fe^{2+}), based upon the classic study of Meyers (1974) and many other workers. No attempt has been made in this study to determine actual trace element concentrations of individual luminescent zones. It is recognized that this is a significant drawback; however it is believed that the similarity of zonal sequences seen in this study, to those of other workers, makes the present approach useful, nonetheless.

The general sequence of zoned cements is similar to the theoretically predicted sequences of Frank et al. (1982) and Machel (1985). Both models relate zonal sequences to a change in redox potential and to a lesser extent pH. Application of these models suggests that these cements were precipitated under conditions of decreasing redox potentials. Sequences predicted by Frank et al. (1982) would require accessory minerals to confirm this interpretation, but the sequence of Machel (1985) supports a lowering of redox potential.

The general lack of luminescence in Zone 1 cements is believed to reflect the minimal uptake of manganese in an oxygenated environment (Meyers 1974, 1978). Decrease of the redox potential of pore fluids results in the reduction of manganese from its Mn^{3+} and Mn^{4+} states to divalent manganese, Mn^{2+} (Figure 97). This allows for the substitution of manganese for calcium in the calcite lattice and is marked by the precipitation of bright cement (Garrels and Christ 1965, Krauskopf 1979, Grover and Read 1983). Continued decrease of the pore fluid redox potential permits the incorporation of Fe^{2+} into calcite, resulting in the precipitation of dull cement.

The cement stratigraphy mapped in Figure 96 suggests a much more complex geochemical nature of the pore fluids. Thus bright and dull bands in the non-luminescent zone suggest intermittent introductions of variably reducing pore fluids into an oxygenated environment. Bright zones that contain thin non-luminescent and dull bands suggest inter-

Figure 97 Stability relation diagrams that show the redox potential and pH at which manganese and iron enter the carbonate phase. 97a) Stability relations among manganese compounds in water at 25°C and 1 atm total pressure. Total dissolved carbonate = 10^{-2}. Manganese enters the carbonate phase ($MnCO_3$) between Eh = +0.5 and -0.2 at pH = 7 to 12. 97b) Metastable iron hydroxides and siderite at 25°C and 1 atm total pressure. Boundaries between solids and ions at total activity of dissolved species 10^{-6}, and boundaries of $Fe^{3+}/Fe(OH)^{2+}/Fe^{2+}$ at activity ratios = 1. Total carbonate = 10^{-2} molal. Iron enters the carbonate phase between Eh = +0.1 and -0.5 and pH = 7 to 11. From Machel (1985), modified after Garrels and Christ (1965).

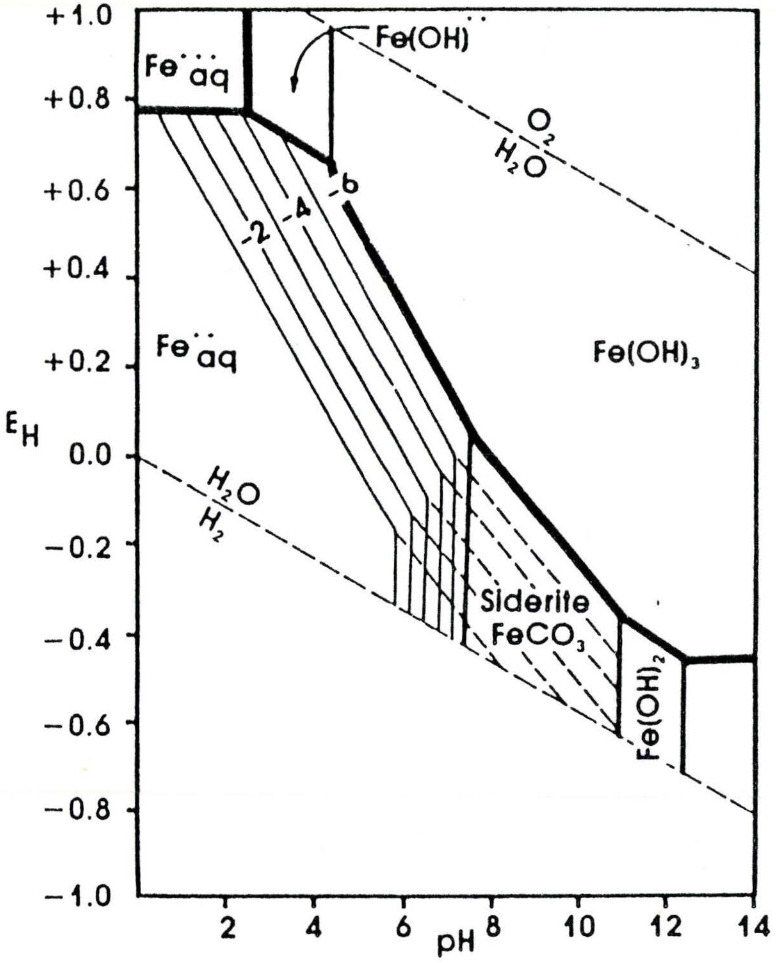
+1.0
+0.8
+0.6
+0.4
+0.2
0.0
−0.2
−0.4
−0.6
−0.8
−1.0
E_H
2
4
6
8
10
12
14
pH
$Fe^{\cdot\cdot\cdot}aq$
$Fe(OH)^{\cdot\cdot}$
O_2
H_2O
−2
−4
−6
$Fe^{\cdot\cdot}aq$
$Fe(OH)_3$
H_2O
H_2
Siderite
$FeCO_3$
$Fe(OH)_2$

A

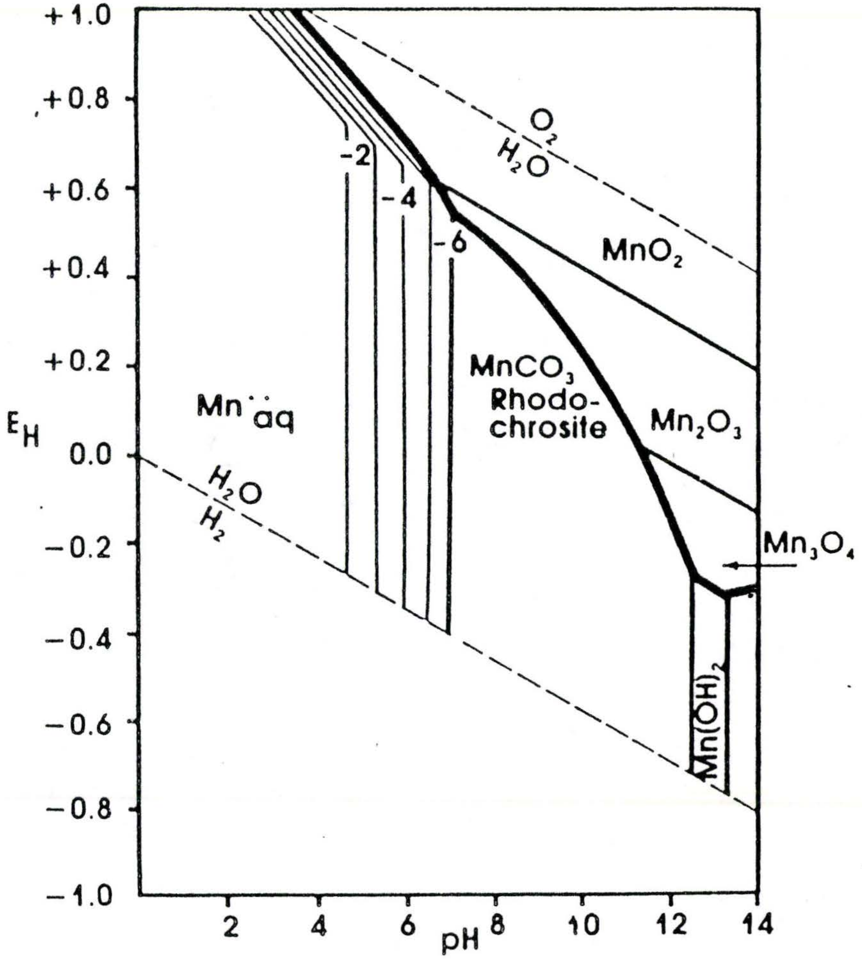
+1.0
+0.8
+0.6
+0.4
+0.2
0.0
−0.2
−0.4
−0.6
−0.8
−1.0
E_H
2
4
6
8
10
12
14
pH
O_2
H_2O
−2
−4
−6
MnO_2
$Mn^{\cdot\cdot}aq$
$MnCO_3$
Rhodo-
chrosite
Mn_2O_3
H_2O
H_2
Mn_3O_4
$Mn(OH)_2$

B

mittent introduction of oxygenated and further reduced porefluids, respectively, into and already reducing environment. Similarly, subzones in dull cements reflect minor increases in the redox potential of the pore fluids. The very dull cement observed in some samples likely reflects precipitation from fluids of the lowest redox potential before total luminescence extinction.

7.6 INTERPRETATIONS

The early history of calcite spar cements was inconsistent. Crystals nucleated under near-ideal conditions on earlier cements and micritic substrate in the phreatic environment. They precipitated from oxidizing pore-fluids that were subject to periodic influxes of more reducing waters. These cements were then subjected to partial dissolution by meteoric waters.

Bright cements, marking the reduction of manganese, were precipitated from pore-fluids that did not maintain a constant redox potential. Non-luminescent and dull bands suggest that there were minor influxes of oxygenated and more reducing waters. This episode was relatively short as evidenced by the thinness and partial development of some zones.

It was not until the precipitation of the dull cements that conditions became more stable. Unlike older cements, all samples examined contain the younger dull cement. Subzones, though they suggest minor increases in redox potential, do not reflect as drastic of changes as those implied in earlier zones. The faint to distinct patterns of subzones suggest gradual to sharp changes in pore water chemistry that ultimately precipitated uniform dull cement.

CHAPTER 8

STABLE ISOTOPE ANALYSIS-NISKU FORMATION

8.1 INTRODUCTION

Isotopic analysis of carbonate sediments and cements has become an important tool in diagenetic studies. The oxygen and carbon isotopic composition of carbonate mineral phases is often used to characterize pore waters and to unravel diagenetic histories.

In Chapter 6 and 7 the interpretations made suggested that dull calcite is pressure solution generated, and that it precipitated in a reducing environment. Transport of the solute to the precipitation sites was partially by diffusion through micrite. The oxygen and carbon isotopic composition of the main mineral phases (Zeta Lake Member) were determined, in the hope that the data would show some sign of the changes and products of pressure solution.

8.2 ISOTOPIC TERMINOLOGY

Carbon and oxygen isotopic compositions are expressed as per mil (parts per thousand) in del notation. For example:

$$\text{del } C^{13} = \frac{C^{13}/C^{12} \text{ sample} - C^{13}/C^{12} \text{ standard}}{C^{13}/C^{12} \text{ standard}} \times 1000$$

and in analagous fashion for O^{18}/O^{16}. The del value is the difference in isotopic ratio between a sample and a standard. A sample with a del O^{18} value of +10.0 per mil is enriched in O^{18} by 10 per mil, or 1 percent, relative to the standard.

For carbonates, the PDB standard is used for both carbon and oxygen isotopes. PDB was a Cretaceous belemnite from the Peedee Formation of Carolina. It is now entirely dissolved in phosphoric acid. Its isotopic composition, del $C^{13} = 0$, del $O^{18} = 0$, is close to that of many marine carbonates whose del values may be slightly positive or negative. A positive del value signifies enrichment in the heavy isotope relative to the standard. A negative del value signifies depletion in the heavy isotope relative to the standard. Subsequently, substances are referred to as "heavy" or "light" in carbon or oxygen, as the case may be (Hudson 1977).

8.3 SAMPLING

The samples collected were from the Zeta Lake Member, Nisku Formation. They represent marine sediments and cements, replacement dolomite, dull calcite spar, and late Fe-dolomite cement. These mineral phases were selected because they represent marine through burial diagenetic products, those before and those due to pressure solution.

Samples were collected as powder, drilled from the rock chip with a 0.7 millimetre drill bit, and stored in vials. Sampling sites were selected for homogeneity using thins sections, the cut-off rock chip, photo-maps, and cathodoluminescence. Only those samples which could be collected without fear of contamination from other mineral phases were chosen. For this reason there is no systematic distribution of samples, one cut-off chip may provide up to 3 individual samples. Zone 1 and 2 of calcite spar cements were not sampled, due to the extremely small scale of these zones.

Isotopic analysis was not done for the Lockport Formation. The extremely fine nature of the mineral phases made separation of them impossible. Only bulk rock analysis could be performed but these were considered to be unsuitable for this study.

Appendix C outlines the procedures used for preparation, collection, and analysis.

8.4 FUNDAMENTALS

The waters involved in the precipitation of individual carbonate phases determine their isotopic composition. For example, marine precipitates are often enriched in O^{18} and C^{13} relative to those of fresh and brackish waters.

In water, the H_2O molecule and dissolved CO_2 (HCO_3^-) are the main "reservoirs" of O^{18} and C^{13} isotopes. The isotopic composition of water is controlled by thermodynamic conditions, equilibrium exchange reactions between the water and rock, and external sources contributing CO_2. Temperature increases through burial result in water depleted in O^{18}. The content of C^{13} is also controlled by thermodynamic conditions, though to a lesser degree, such that one might only expect changes in large reservoirs (Walls et al. 1977).

The effect of rock/water interactions on isotopic composition of waters and precipitates is extremely variable. In carbonate rock, the carbonate ion (CO_3^{2-}) acts as both the O^{18} and C^{13} reservoir. Depending upon the degree of water/rock interaction, these reservoirs may be important contributors to the isotopic composition of waters. Consider oxygen reservoirs. In carbonate-meteoric phreatic systems, the rock contributes more oxygen than water ($O_R/O_W=1.479$ based upon relative molar abundances of oxygen in equal volumes of rock and water). In carbon reservoirs, even highly CO_2 charged waters, $CaCO_3$ contains $1.7x10^7$ times more C then in an equal volume of water (Meyers and Lohmann 1985).

As potential sources, rock reservoirs dominate over water reservoirs, based upon relative concentrations and relative sizes. Under conditions of dissolution the isotopic composition of the rock is proportionately mixed with that of the water. The resultant water composition is dependent upon the number of moles of O and C that each contribute and the concentration of their molecular species.

For example, oxygen is contained in H_2O and dissolved HCO_3^- species of water and rock reservoirs, respectively. For each mole of H_2O, one oxygen is available. Three oxygens are available for every mole of HCO_3^- released through dissolution. In pore waters, the concentration of HCO_3^- is small. Minor rock/water interaction (establishing equilibrium) will have a negligible effect on pore-water oxygen isotope composition. In cases of active dissolution a significant contribution of HCO_3^- could effectively change the oxygen isotopic composition of the pore-water and precipitates (Meyers and Lohmann 1985). The carbon isotopic composition also changes. HCO_3^- species are not abundant in pore water, so any significant contribution through dissolution will change the carbon isotopic signature, too.

Sources other than rock can supply waters with C^{13}. Light C^{13} isotopes may be derived from soil/gas CO_2 and the oxidation of marine organic matter in early meteoric pore-waters. Dissolved CO_2 from these sources is extremely light and may account for some large fluctuations in del C^{13} values of precipitates. Meyers and Lohmann (1985) report del C^{13}=-25 per mil for organic carbon. Walls et al. (1977) state only that soil/gas CO_2 is strongly depleted in C^{13}.

Organic decomposition may only cause local isotopic perturbations in pore-water composition. Filtration of meteoric water through organic-rich soil zones is a continuing source of light carbon for phreatic pore-waters. Highly negative C^{13} values are found in narrow zones near subaerial exposure surfaces. However, the effect is limited, as meteoric waters are recycled and attain rock equilibrium (Allan and Matthews 1977, Meyers and Lohmann 1985).

When considering isotopic changes in pore-waters and precipitates, the degree of openness of the system must be examined. A closed system is a static physico-chemical environment, isolated from surface or near-surface fluids (generally CO_2-rich meteoric water) (Walls et al. 1977). In these settings, the C^{13} composition is inherited from marine sediment and cements, there is no input of new C. Oxygen values may vary due to thermodynamic conditions.

Open systems are active physico-chemical environments that are not isolated from CO_2-rich meteoric water. In these systems del C^{13} and del O^{18} may be variable and inconsistent with marine data. As implied earlier, cycling of water in these systems and progressive modification of the pore fluids, may ultimately result in a closed system equilibrium. Having reached equilibrium, the precipitates of this now-closed system will have their composition controlled by the dissolving carbonate phases (Meyers and Lohmann 1985).

8.5 GENERAL PRINCIPLES OF INTERPRETATION

8.5.1 CARBON ISOTOPES

Marine sediments and precipitates are enriched in C^{13}. Del C^{13} values for these carbonates are in the range of 0 to +4 per mil PDB (Hudson 1977, Dickson and Coleman 1980, Meyers and Lohmann 1985). Carbonates of this origin that retain del C^{13} values in this range are interpreted to approximate the original marine composition. Any subsequent re-equilibration of these early phases occurred in a relatively closed system with the addition of no new C (Walls et al. 1977).

Variable del C^{13} values of carbonate cements imply a change from heavy marine to light organic derived carbon

(Marshall 1981, Meyers and Lohmann 1985). Light C^{13} compositions may be derived from soil/gas CO_2 or organic matter oxidation in meteoric waters. Carbonates of variable del C^{13} ranges that become enriched at depth are used to identify ancient subaerial exposure surfaces in ancient limestones (Allan and Matthews 1977).

Original marine components are most likely to reflect marine compositions, but how does a late burial cement gain a similar del C^{13} value? Late cements with this type of isotopic composition cannot be formed from soil/gas CO_2 contributions and petroleum/gas CO_2 is to variable in CO_2 to be the source of consistent del C^{13} values. The easiest way to explain this is that the del C^{13} signature is inherited from solutions bearing dissolved marine material.

In dissolution-precipitation reactions;

$$H_2O + CO_2 = H_2CO_3$$

$$CaCO_3 + H_2CO_3 = Ca(HCO_3^-)^2 + H^+$$

an input of CO_2 is required. Unless this CO_2 has the same del C^{13} as the carbonate del C^{13}, the precipitated cement will not have the same carbon isotopic signature as the original marine components. For example, dissolution-precipitation during near surface meteoric diagenesis, will result in a precipitate that has a light C^{13} composition due to soil derived CO_2 (Hudson 1975). The same reasoning is applicable to these processes at depth.

Late burial cements with a marine C^{13} composition may be explained by simple solution in the absence of CO_2 (marine water). Aragonite transformation and pressure solution ($CaCO_3 = Ca^{2+} + CO_3^{2-}$) of marine components will preserve a marine C^{13} signature because no new C is added to the system. Between them, these two processes would yield enough $CaCO_3$ to solution to produce carbonate in solution with the same del C^{13} composition as the marine carbonate precursors. The slowness of the process is acceptable within the burial regime, and as Hudson (1975) states "it is simple, it is ubiquitous".

8.5.2 OXYGEN ISOTOPES

The oxygen isotopic composition of water determines that of any carbonate phases precipitated from it. This composition depends primarily on the nature of the water and temperature.

Present-day seawater has a narrow range of oxygen isotopic composition (e.g del O^{18} = 0 per mil PDB at the equator, -6 per mil to -7 per mil in Northern England, Dickson and Coleman 1980). Rain water isotopic composition varies with climatic changes (temperature increase or decrease), the distance from marine source (multiple fractionation due to multiple evaporation/precipitation) and to changes in composition of the marine source (Meyers and Lohmann 1985).

Rain water is depleted in O^{18} in such a manner that it can be correlated to geographical locations. It is more O^{18}-depleted at high latitudes and altitudes, than those which are lower. Near-surface ground waters are directly derived from rain and share its isotopic composition (Hudson 1977).

Variations in carbonate del O^{18} values can be attributed to temperature variations alone, or to temperature variations and changes in pore-water chemistry. Pore-water changes may be due to progressive rock/water interaction or a change in the composition of water (e.g. climatic changes in meteoric water, source changes in subsurface water).

For example, consider early cements whose del O^{18} value is too light to reflect marine conditions. This must indicate precipitation from an early O^{18}-depleted water or re-equilibration of the isotopic composition with water of modified composition or higher temperature during burial (Marshall 1981). Late cements that have light del O^{18} values are commonly attributed to temperature increases depleting the O^{18} content of subsurface waters. If fractionation factors alone cannot explain the magnitude of depletion, the mechanisms of diagenetic evolution and mixing of pore-waters must be examined.

It is natural to relate low del O^{18} values to prolonged contact with meteoric waters which are an abundant source of depleted O^{18} (Hudson 1977). This may occur in the cases of early diagenetic stabilization of unstable carbonate phases (aragonite, high-Mg calcite) and cementation, or it may occur by long-continued isotopic exchange between rock and water. To be able to generate such values, there must be meteoric access to the system. Evidence of meteoric water might be found in del C^{13} values.

8.5.3 RECRYSTALLIZATION

Neomorphism of metastable carbonate phases (e.g. marine cements and sediments) results in the re-equilibration of their isotopic composition. For example, Walls et al. (1977) recognized textural evidence indicating that radiaxial fibrous calcite is a neomorphic product of an earlier marine cement. The del C^{13} value of these cements lies within the range of del C^{13} = +1.6 per mil to +3.5 per mil, suggesting a marine origin and subsurface fluid of similar composition.

The light del O^{18} signature is likely a product of secondary diagenesis; it shows neither a marine or meteoric character. This may result from micro-dolomite inclusions in the cement concentrating O^{18}, from changes in the composition of the pore fluids during burial, and/or from an increase in temperature during burial.

It is unlikely that fractionation of O^{18} by microdolomite can explain the light del O^{18} values in radiaxial fibrous calcite. By volume, these inclusions account for 2% to 20% of the cement usually less than 10%. This is not enough to explain significant O^{18} depletion. Adjacent internal sediments have similar O^{18} values. Depletion by a change in pore-water composition during burial can be discounted, unless the altered waters had the same del C^{13} values of that for marine sediments and cements.

Depletion by an increase in temperature is acceptable, especially since the del C^{13} values suggest a closed system. Similar arguments may be applied to any cement or sediment which displays a recrystallized texture.

8.5.4 DOLOMITE

The chemical reaction of dolomitization is one of dissolution-precipitation in and from an aqueous fluid. The del O^{18} of dolomite is dependent upon the O^{18} content of its precursor as much as it is on water and temperature. It is recognized that the precursor may have much influence upon the del O^{18} of the fluid in a partially open system and in many cases, the dissolving phase being replaced can contribute to the composition of the fluid (Land 1980).

Mattes and Mountjoy (1980) believe that dolomitization of a micrite by slow ion-diffusion and micropore water-flow would establish a micro-equilibrium system which is dominated chemically by the precursor or fluid phase. Any allochthonous HCO_3^- carried in by permeating waters will be buffered by the rock if diffusion gradients are low, or will not be buffered if diffusion gradients are high. In the former case, the dolomite isotopic composition will be differentially uniform relative to the precursor phase due to fractionation differences. In the latter case, the isotopic composition of the dolomite may vary considerably.

For example, the isotopic composition of dolomite would be expected to largely reflect the original isotopic character of micrite if diffusion gradients were low. In this case, allochthonous HCO_3^- would be buffered in a micro-equilibrium dominated by the precursor. Differences due to fractionation between the precursor and replacement phase would exist. Studies suggest that C^{13} should only be slightly enriched and that O^{18} should be 3 per mil heavier in dolomite (Land 1980).

In the above example, the del C^{13} value should reflect the original composition of the micrite. Similarly, more extreme positive or negative values might be expected in dolomitization of limestone which itself was characterized by an extreme isotopic composition (Mattes and Mountjoy, 1980).

Oxygen isotopic compositions of ancient dolomites are depleted relative to Holocene examples. Mattes and Mountjoy (1980), suggest that this may reflect O^{18} depletion with increasing age.

There are three ways to explain progressive O^{18} depletion. Dolomite which is formed either by primary precipitation or by replacement at elevated temperatures, or from fluids depleted in O^{18} relative to sea water (or both), may explain lighter ancient dolomites. Early diagenetic changes to the sediment may leave an isotopic imprint which dominates any later changes caused by re-equilibration at depth (Land 1980, Mattes and Mountjoy 1980).

The notion of "isotopic exchange" was proposed by some workers to account for O^{18} depleted dolomite. At some point in the geologic history of the rock, dolomite crystals would readily "exchange" oxygen with the pore fluids by diffusion but remain otherwise unchanged. This type of re-equilibration is considered to be too slow, and would not account for isotopic inhomogeneities at a single crystal scale. These inhomogeneities would not be preserved if the depleted isotopic composition was due to "massive isotopic exchange" by diffusion in great thicknesses of dolomite (Land 1980).

Preference is given to oxygen depletion through recrystallization accompanying compaction as basinal temperatures exceed 100°C (Land 1980). This mechanism involves on the order of ten pore volumes of water and could account for great thicknesses of depleted dolomite which exhibit localized inhomogeneities. Through the process of dissolution-precipitation, dolomite crystals most affected may inherit a depleted O^{18} composition from the pore fluids.

8.6 RESULTS

The del O^{18} and del C^{13} values of all samples analysed are shown in Table 14 and plotted in Figure 98. Most of the data cluster into two discrete groups, each made up of two subgroups. All results are reported as PDB values.

Group I represents nine analyses of radiaxial fibrous calcite cement from six different samples. All data points lie within a narrow del C^{13} range (+1.6 per mil to +4.1 per mil) but fall into two groupings of del O^{18} values (2 analyses at -6.9 per mil and 7 analyses at -10.2 per mil).

Group II data are the results of micrite analyses, 4 individual samples and 7 extracted from dolomite samples. All eleven data points lie within a narrow del C^{13} range (+0.6 per mil to +3.9 per mil) but the group as a whole shows variable del O^{18} values (-5.9 per mil to -10.2 per mil), trending towards depletion.

Group III consists of 8 dolomite samples. These samples include green dolomicrite, brown dolomite concentrated along stylolites, and grey matrix dolomite. As a group they lie within a narrow range of del C^{13} values (+0.9 per mil to +3.5 per mil) and del O^{18} values (-5.6 per mil to -8.6 per mil).

TABLE 14: ISOTOPE DATA FOR ZETA LAKE MEMBER

Sample	Description	Del ^{13}C per mil PDB	Del ^{18}O per mil PDB
2380.98	Mottled Rad. Fib	3.83	- 6.85
2386.50	White " "	4.12	-10.17
2386.50	Dark " "	3.44	-10.04
2389.49	Lt. Grey " "	2.44	-10.38
2389.49	Brown " "	2.62	-10.46
2392.78	White " "	1.63	- 6.95
2395.64	White " "	2.20	-10.17
2395.64	Brown " "	2.47	-10.12
2416.05	White " "	1.87	-10.06
2371.25	Micrite	3.96	- 5.89
2372.26	"	3.48	- 6.52
2389.77	"	1.94	- 6.39
2392.78	"	.96	- 7.82
2395.64	"	2.35	- 6.62
2412.99	"	.79	- 6.55
2416.05	"	1.05	- 6.65
2419.92-1	"	1.25	- 7.07
2420.84	"	2.02	- 6.14
2440.13	"	.77	-10.21
2440.55	"	.61	- 7.16
2392.78	Matrix Dolo.	2.14	- 7.37
2416.05	" "	.93	- 8.65
2419.92-1	" "	2.60	- 6.59
2420.84	" "	2.77	- 6.58
2372.26	Green Dolomicrite	2.99	- 8.33
2372.48	" "	3.32	- 7.97
2395.64	Brown Dolo.	3.54	- 5.64
2389.77	" "	2.65	- 7.17
2396.07	Dull Calcite	2.29	-10.38
2416.05	" "	.76	- 8.61
2419.92-2	Dull Calcite-Plug	1.74	-10.71
2419.92-3	" " "	.99	-10.86
2419.92-4	" " "	2.00	-10.66
2426.69	" "	1.79	- 8.52
2396.07	Coarse Dedolo. Dolo.	2.84	- 7.53
2396.07	" " Calcite	2.19	- 7.89
2396.07	Fine Dedolo. Dolo.	1.57	- 8.34
2396.07	" " Calcite	X	- 7.20
2419.92-3	Fe-Dolomite	1.13	- 8.75

Figure 98 Stable isotopic composition (per mil PDB) of Nisku Formation main mineral phases.

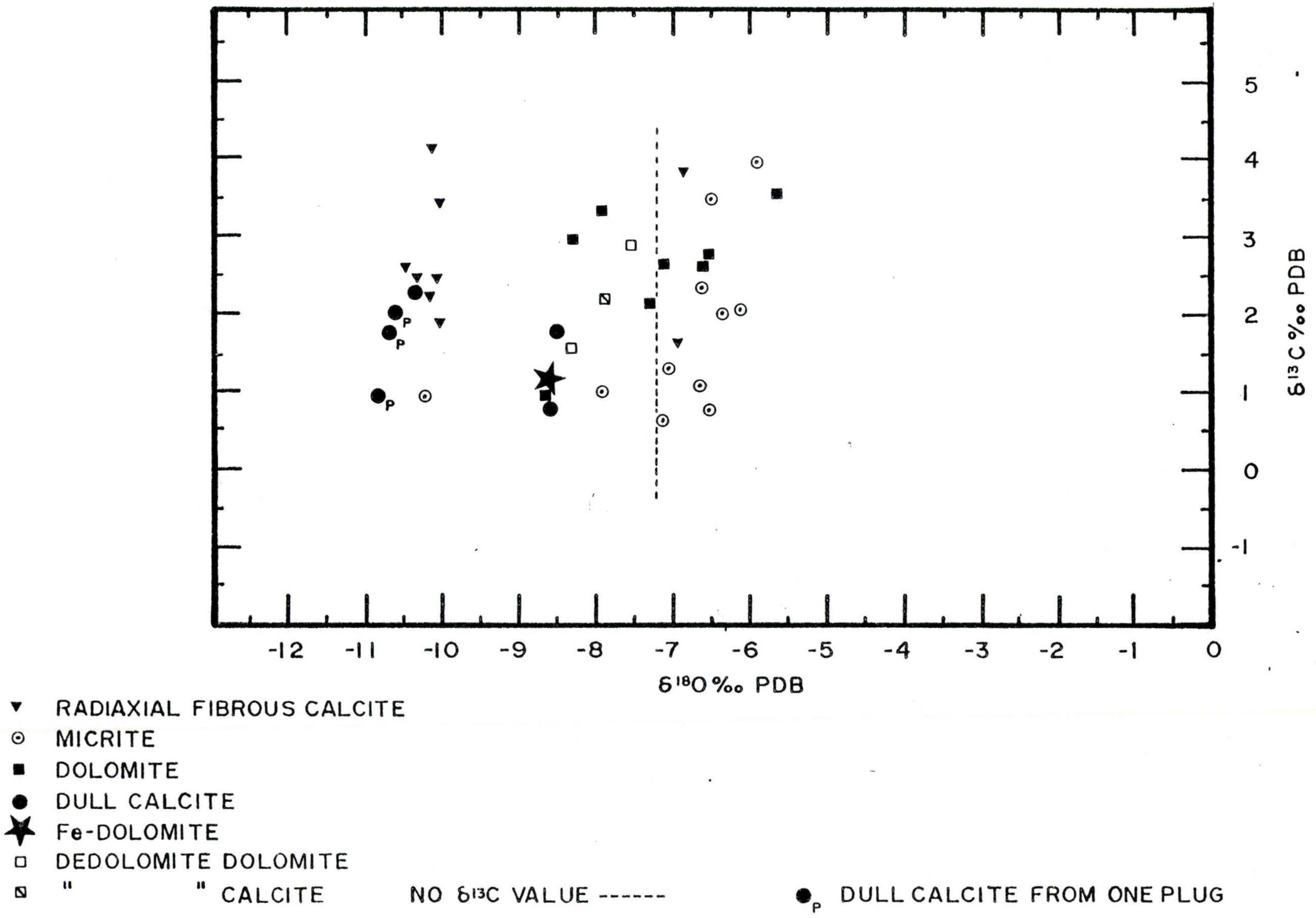
5
4
3
2
1
0
-1
δ¹³C ‰ PDB
-12
-11
-10
-9
-8
-7
-6
-5
-4
-3
-2
-1
0
δ¹⁸O ‰ PDB
P
P
P
▼ RADIAXIAL FIBROUS CALCITE
⊙ MICRITE
■ DOLOMITE
● DULL CALCITE
★ Fe-DOLOMITE
□ DEDOLOMITE DOLOMITE
▨ " " CALCITE
NO δ¹³C VALUE ------
●P DULL CALCITE FROM ONE PLUG

Individually, green dolomicrite and brown dolomite are more enriched in C^{13} than matrix dolomite, and brown dolomite is more enriched in O^{18} than green dolomicrite or matrix dolomite. Matrix dolomite is the isotopically lightest dolomite within this group, brown dolomite the heaviest.

Group IV comprises 6 samples representing dull calcite spar, previously interpreted to be pressure solution derived. This coarse spar lies within a very narrow range of del C^{13} values (+0.8 per mil to 2.2 per mil) and falls into two groupings of del O^{18} values (those at -8.5 per mil and -10.7 per mil). Three samples (labelled P) are from one drill plug and represent fracture-fillings right adjacent, to 15 centimetres away from a major stylolite. The other 3 samples represent 2 dull and 1 subzoned calcite spar.

Other data points not included in these groups are; a) the calcite and dolomite analyses for a coarse and fine crystalline dedolomite, and b) one analysis of late ferroan dolomite cement. These data points are labelled accordingly. Dedolomite analyses (both calcite and dolomite) lie within the groups defined by micrite and dolomite. Late Fe-dolomite has an isotopic composition of del ^{13}C = 1.1 per mil and del O^{18} = -8.8 per mil.

Several features can be seen in the data of Figure 98. These are:

1) All samples have a narrow range of positive del C^{13} values (=0.6 per mil to +4.1 per mil).
2) Dull luminescent and most radiaxial fibrous calcite samples have more negative del O^{18} values than most micrite and dolomite samples.
3) The radiaxial fibrous calcites are not as depleted in C^{13} compared to other groups.
4) Micrite and dolomite samples have more variable del C^{13} values than radiaxial fibrous calcite and dull calcite spar.
5) One micrite sample is comparable to dull calcite in its composition.
6) Dedolomite phases (both calcite and dolomite) lie within the compositional ranges of micrite and dolomite.
7) Late Fe-dolomite (1 sample) is similar in composition to a matrix dolomite and dull calcite sample.

8.7 DISCUSSION

8.7.1 CARBON ISOTOPES

The most important characteristic of the stable isotopic analyses plotted in Figure 98 is that all del C^{13} values lie within the range +0.6 per mil to +4.1 per mil. These values are in accordance with those commonly ascribed to marine carbonates and strongly suggest a closed system after the beginning of burial. For the Group I and II analyses this suggests that radiaxial fibrous calcite and micrite have not been subject to isotopic re-equilibration in pore-waters of non-marine origin. The absence of variable del C^{13} values implies that there were no significant changes in the composition of the pore fluids.

Between micrite and dolomite (Groups II and III, respectively), the latter is generally slightly enriched in C^{13}. Between paired samples (from the same powder), the maximum difference in del C^{13} values is 1.4 per mil, commonly less than 1 per mil. Close examination of the data plotted for Group II and III suggests that the del C^{13} values of dolomite reflect those of the precursor (micrite) and that dolomitization proceeded under a micro-equilibrium system (Mattes and Mountjoy, 1980). For the C^{13} isotopic character of the precursor to be preserved diffusion gradients of the dolomitizing fluid must have been relatively low. The similarity of del C^{13} ranges for micrite and dolomite suggests that these dolomitizing fluids were not grossly different from those of marine origin.

The tightest range of del C^{13} values is associated with samples of dull luminescent calcite (Group IV). These are burial calcite spar samples and the easiest way to explain the tight values is to ascribe them to simple solution (Hudson 1975). Pressure solution is preferred over aragonite transformation as the source of CO_3^{2-} since these cements are post-dolomitization, heal fractures, and most importantly, are seen in veinlets propagating away from stylolites. It is more difficult to explain the C^{13} composition of this spar by changes in pore-water chemistry. The very narrow range of del C^{13} values, between +0.8 per mil and +2.3 per mil might suggest some external CO_2 influence. However, this is likely due to thermodynamic fractionation because del C^{13} is not lighter than that for the lightest micrite.

The carbon isotopic composition for dedolomite phases and Fe-dolomite also lie within the narrow del C^{13} range. For the dolomite component of dedolomite samples this implies that it is of similar composition to other dolomite samples, and likely is the same dolomite. Petrographically and under CL conditions, the two cannot be distinguished. Dedolomitization by dull calcite is the interpretation made in Chapter 6. Dedolomite calcite has a similar C^{13} composition as dull calcite and is believed to be of the same origin (pressure solution derived).

Fe-dolomite also has a del C^{13} value very close to that of dull calcite. A change in the composition of pore fluids is implied because it is dolomite, but like dull calcite, pressure solution is preferred as the source of CO_3^{2-}. Under CL conditions, veinlets of dolomite similar in luminescence to this cement, are seen originating at stylolites, suggesting a pressure solution origin.

From the abundance of data in favor of a marine origin for all samples, any changes to pore-water chemistry could only have occurred if the new carbon being added to the system already had a marine isotopic signature. External CO_2 from the percolation of meteoric water through soil horizons, and that derived from petroleum maturation, was unlikely to have been introduced into this system.

8.7.2 OXYGEN ISOTOPES

All of the mineral phases sampled are depleted with respect to O^{18}. The data plots as being between fresh- and marine-water mean isotopic values, or beyond the mean for fresh-water limestones (Figure 98). For early marine cements and sediments (Group I and II) this implies precipitation from early O^{18}-depleted water or isotopic re-equilibration with water of modified composition, or re-equilibration at an elevated burial temperature.

Similar reasoning applies to dolomite samples. Either dolomitization took place at elevated temperatures or in fluids depleted in O^{18} relative to seawater, or both. Recrystallization of dolomite may account for light del O^{18} values and variability in composition could be the result of an early diagenetic isotopic signature of micrite dominating any later changes due to re-equilibration.

The dull calcite spar and Fe-dolomite are burial cements precipitated from subsurface fluids. It seems unlikely that they were subject to re-equilibration of an earlier isotopic signature. The light del O^{18} values are easily explained by precipitation from a fluid at elevated temperatures, or of modified isotopic composition, or both.

The dolomite component of the dedolomite samples are two of the more O^{18}-depleted dolomite samples. Explanation of these light del O^{18} values is similar to that for other dolomite samples. The calcite component is more problematic. The del O^{18} values are depleted but resemble those for micrite and dolomite. If these were pure precipitates of dull calcite, they should reflect the same isotopic composition. Because dedolomitization is believed to be diffusion controlled (Chapter 6), the heavier isotopic composition may reflect earlier micrite and dolomite compositions which alter the dull calcite del O^{18} signature. Also, the calcite dedolomite components are "bulk rock" analyses. The probability of contamination from micrite is very high, which may be enriching the isotopic composition measured.

8.8 INTERPRETATIONS

Isotopic data (Table 14, Figure 98) support a strongly rock-buffered system. Marine components (Group I and II) retain their original del C^{13} values and non-marine phases (Group III, IV, dedolomite, and Fe-dolomite) have inherited marine del C^{13} values. The lack of any extreme or more variable del C^{13} values suggests that waters with a non-marine signature were not present during the formation and/or re-equilibration of these phases. Bulk chemical composition of the pore-waters did change as evidenced by dolomite phases, but it is believed that these waters were of marine-origin, or had quickly re-equilibrated with the rock composition.

Pressure solution is the source of CO_3^{2-} for dull calcite spar and Fe-dolomite. Pressure-dissolution of the rock released CO_3^{2-} ions of marine carbonate to the pore fluids, resulting in the marine del C^{13} values of these phases. Whether the system was open or closed during pressure solution cannot be precisely determined, though a closed system is preferred. Calcite spar was precipitated from the marine carbonate being dissolved. Late Fe-dolomite could be precipitated via a pressure solution mechanism in a closed system. The change to Fe-dolomite is believed to be a late pressure solution response to very low calcite and high dolomite concentrations along some stylolite surfaces. Dolomite was being dissolved because no calcite was available in the immediate vicinity. Were the system open to external pore fluids, variable del C^{13} values would be expected, unless these fluids had a marine isotopic signature, or quickly re-equilibrated with the rock. Openness is difficult to accept in light of the consistently narrow range of del C^{13} values for all phases samples.

Isotopic re-equilibration and precipitation from pore fluids of marine isotopic composition at elevated temperatures is believed to account for the depleted del O^{18} values measured. There is no evidence to indicate that early O^{18}-depleted or isotopically different fluids were present.

The pattern of del O^{18} values for radiaxial fibrous calcites (Group I) suggests a del O^{18} shift towards lighter values. These cements were originally metastable marine precipitates that now show neomorphic textures. In plane light a former acicular habit of the precursor can be seen, and in CL conditions they show patchy, dominantly dull luminescent characteristics. This is the result of neomorphic conversion of high-Mg to low-Mg calcites during burial (Kendall and Tucker 1973, Lohmann and Meyers 1977). Through the process of partial-dissolution and replacement, isotopic re-equilibration with the pore fluids at elevated temperatures occurred. The lightest del O^{18} values (approximately -10 per mil) suggest that neomorphism was active through much of the burial history, since these values are similar to those for the lightest dull calcite of pressure solution origin. The luminescence of these cements suggests that replacement by dull calcite occurred, hence must have been active during pressure solution. The heavier values may reflect original isotopic compositions, or early/less neomorphosed products.

Micrite del O18 values do not show a shift as described above, but are depleted in O18 nonetheless. These sediments were metastable. They show a patchy but variable dull luminescence. Re-equilibration is believed to have occurred via neomorphism at elevated burial temperatures and due to diffusion of dull calcite through this medium. The more variable del O^{18} values are likely the result of a hetrogeneous primary mineralogy and early Zone 1 and 2 cements in the micrite influencing the final isotopic composition. The lightest del O^{18} value of micrite is similar to that for light radiaxial fibrous cements and dull calcites. This suggests that re-equilibration of micrite was concommittant with that of Group I cements and that diffusion was active. Two different re-equilibration episodes seem unlikely, since both marine sediment and cements attained the same degree of depletion.

Dolomite del O^{18} values are also believed to be the result of isotopic re-equilibration. Recrystallized dolomite concentrations are recognized in thin section and under CL conditions. Through the recrystallization process, the isotopic composition of the pore-waters was inherited by dolomite. The lightest del O^{18} values fall along a narrow range (approximately -8 per mil) which is almost 3 per mil heavier than the lightest dull calcite values. Considering fractionation differences between calcite and dolomite (delta O^{18} = 3 per mil +/- 1 per ,mil, Land 1980), this difference suggests re-equilibration in dolomite attained the same state of depletion as that for Group I and II.

Dedolomite phases were also subject to re-equilibration. The dedolomite dolomite samples are two of the more O^{18}-depleted samples. The above reasoning is applicable to these samples. They were subject to re-crystallization, dedolomitization being a further extension of this process. The calcite dedolomite component del O^{18} values are harder to interpret for reasons stated in the previous section. It can only be said that, based upon the luminescence characteristics and the spatial relationship of dedolomite concentrations to stylolites, this calcite is the same as dull calcite and that the del O^{18} values do not accurately reflect this.

For dull calcite and Fe-dolomite, the depleted O^{18} compositions reflect precipitation at elevated temperatures. The more enriched dull calcite values (at del O^{18} = -8.5 per mil) may be pressure solution derived, or may not be related to pressure solution at all. Watts (1984) and Machel (1984) both suggest two episodes of stylolitization in their diagenetic schemes, of which these heavier cements may be an early precipitate. The lighter dull calcite values are directly associated with stylolites and believed to be the product of pressure solution. Fe-dolomite is approximately 3 per mil heavier in O18 than the lightest dull calcite. Considering fractionation differences it is possible that it formed in fluids of the same isotopic, but different ionic composition, as those that precipitated dull calcite.

8.9 SUMMARY

Isotopic analysis of the main mineral phases suggests that dull calcite and Fe-dolomite are of pressure solution origin. The sources of these cements are the marine components and earlier dolomite phases, for dull calcite and Fe-dolomite, respectively.

Re-equilibration of earlier phases at elevated burial temperatures proceeded to a state of O^{18} depletion similar to that for pressure solution products. This implies that re-equilibration, thus neomorphism, recrystallization, and dedolomitization, stopped when pressure solution ceased.

CHAPTER 9

CONCLUSIONS

9.1 DISCUSSION

9.1.1 STYLOLITIZATION MECHANISMS

Two different types of stylolitization mechanisms have been proposed; the amalgamation mechanism and dolomitization-stylolitization. Each mechanism forms a stylolite by responding to pressure solution differently. The different responses arise from primary features and diagenetic alteration of the original sediment.

"Organic" layers constitute primary features. These originally form as a result of mechanical compaction of the sediment. The primary concentration of organic materials within bedding interiors ultimately determines whether or not a stylolite will form and how large it will be (given ideal conditions). This is the "trigger" for the amalgamation mechanism.

Microstylolites form at organic layers in direct response to pressure solution, concommittant with, or after, a pervasive response through the rock. Where dense concentrations of organic layers occur, a microswarm develops (neonatal stage).

With continued pressure solution, microstylolites of sufficient number (in a swarm) amalgamate to form an incipient stylolite through pressure-dissolution of inter-stylolitic dolomite (early adolescent stage). Dissolution takes place primarily at the numerous microstylolite surfaces, and to a lesser degree at crystal contacts.

Amalgamation continues through middle and late adolescent stages of stylolite growth. The resultant geometry of the stylolite formed is determined by the phase relationships (in-phase or out-of phase) of the amalgamating microstylolites, the principle of superposition of waveforms. Adolescence marks a growth period when the growing stylolite accumulates large quantities of insoluble material. Each microstylolite incorporated contributes to the net thickness of the stylolite.

Stylolites mature into adulthood when the microswarm has near-completely been incorporated into the growing seam. This marks an end to the major accumulation of insoluble materials and the beginning of growth via dissolution at the sockets.

Pressure-dissolution of the sockets on both sides of the stylolite surface arises due to stress inhomogeneities created by the sutures (point-load stresses). insoluble materials accumulated at the surface are derived from included materials released by dissolution of dolomite along the stylolite. This is a significant decrease in the quantity of accumulated material relative to adolescent stage growth. As a result, material is thinned along the limbs of sutures by the increasingly deeper penetrating sutures and striations are formed. Stylolite growth proceeds in this manner until pressure solution ceases or another stylolite is encountered.

Dolomitization of micrite constitutes diagenetic alteration of the original sediments. Due to the different mechanical properties of dolomite and limestone, stress "shadows" develop about dolomite concentrations when subjected to increasing overburden pressures. This results in anisotropic stress distributions that may ultimately lead to conditions conducive to stylolitization of a dolomitic limestone. These stress perturbations are the "trigger" of dolomitization-stylolitization.

The initial response to pressure solution is non-seam solution of calcite at dolomitic concentrations and/or clusters, where stress perturbations are "felt" by the micrite and matrix particles. The response is not pervasive throughout the rock but develops about discrete horizons where conditions (anomalous stress distributions, transport to and away from the site) are suitable for pressure solution.

With continued pressure solution, non-seam solution evolves to form a stylolite. This occurs by continued pressure-dissolution at the site of non-seam solution provided that dolomite abundance is sufficiently high or occurs in a manner that maintains anomalous stress distributions. Young stylolites form primarily at abrupt dolomite/matrix boundaries and in dolomitic matrix. To a lesser degree they form by amalgamation of microstylolites. Microstylolites form as the result of pressure-dissolution about linear/planar arrangements of individual dolomite crystals.

Stylolite growth continues by pressure-dissolution at the surface caused by stress inhomogeneities. Early in its development, growth is strongly influenced by dolomite occurrence. As it gets larger, dolomite dependence is lost and the stylolite may respond to changes in "environmental" parameters that influence its growth and resultant morphology. For example, it may encounter material of differing degrees of cementation and dolomite abundance, or bioclastic particles, that enhance or inhibit pressure solution.

The morphology of a growing stylolite may become more variable and change due to dolomite crystals becoming included as seam material and then shearing socket walls, or penetrating deeper into the socket. Secondary responses to anomalously high stresses within a suture may result in bridging stylolites or non-stylolitic pressure solution features within the suture interior.

The accumulation of dolomite at a stylolite surface results in coalescence through non-seam solution in the immediate vicinity of the stylolite. This results in removal of intervening matrix calcite and recrystallization of the dolomite.

The manner in which stylolites propagate laterally is similar for both the amalgamation mechanism and dolomitization-stylolitization. Removal of material through dissolution in the central body of a stylolite surface results in stresses built-up at its tips. Pressure-dissolution in the region of these built-up stresses allows the stylolite to propagate and relieve the anomalously high stresses, only to be built-up again through removal of more material in the central body. Growth in the direction of shortening cannot occur without propagation, and vice versa.

For the amalgamation mechanism, the bifurcating tips (made up of "horsetails" of microstylolites) represent the propagation mechanism "frozen" in the rock. The microstylolites amalgamate in a "pinching" manner to form an extension of the stylolite by removal of dolomite at the microstylolite surfaces and crystal contacts. For dolomitization-stylolitization, propagation proceeds by non-seam solution of matrix calcite (that is rarely seen as a fan-like array of dolomite crystals) at the stylolite tip.

Amalgamation is not only restricted to microstylolites. "Adult" stylolites, whether of the Lockport or Nisku Formation type, may merge together through pressure-dissolution of interstylolitic carbonate. The resultant seam is a function of the phase relationships (in-phase or out-of-phase) of the amalgamating seams. This type of amalgamation is not to be confused with the amalgamation mechanism which results in the formation of a stylolite. This type of amalgamation results in a stylolite that may be more or less complex sutured.

9.1.2 PERMEABILITY BARRIERS

The statistical analysis of core data for the Nisku Formation, Zeta Lake Member, shows that stylolites do reduce flow across their surfaces. Relative to non-stylolitic data, mean vertical permeability values decrease from micron-scale through millimetre to centimetre-scale stylolites, then increase again at centimetre-scale.

The decreasing trend is attributed to the increasing accumulation of insoluble materials at a stylolite surface as it grows. The most effective permeability barriers are intermediate scale stylolites (millimetre-, and millimetre to centimetre-scale). The increase in mean values at centimetre-scale seams is attributed to the shearing action of sutures penetrating deep into their sockets. This action attenuates insoluble material along the limbs (sides) of a suture; such that the insoluble material becomes so thin that a centimetre-scale stylolite is equivalent to micron to millimetre-scale ones in terms of its ability to be a permeability barrier.

Fractures present in the rock provide an alternative route of vertical flow across a stylolite surface. The result is that mean vertical permeability values of fractured samples do not display an completely ordered pattern relative to stylolite scale.

9.1.3 PRESSURE SOLUTION GENERATED MATERIAL

Evidence of pressure solution generated carbonate was found using cathodoluminescence. Carbonate of pressure solution derivation is related to late-stage diagenetic alterations of the samples examined.

In the Lockport Formation, stylolitization produced a bright-red luminescent dolomite. This is seen filling porosity and pervading crystal interiors. It is found along stylolite surfaces where pressure-dissolution was once active and partially fills fractures. Most importantly, veinlets propagating away from stylolites contain this dolomite phase.

In the Nisku Formation, Zeta Lake Member, stylolitization produced dull luminescent calcite, and to a lesser degree, dull maroon luminescent dolomite. Dull calcite is seen filling porosity and healing broken particle surfaces. It infills fractures and is found as veinlets propagating away from stylolites. This phase is responsible for dedolomite textures adjacent to stylolites and replacement of earlier calcite cement phases. Dull maroon dolomite is seen as veinlets propagating away from stylolites and healing brecciated dolomite crystals. It is luminescently equivalent to pore-occluding Fe-dolomite.

Transport of the pressure solution generated phases away from stylolite sites is primarily by diffusion of thin fluid-films. In the Lockport Formation this accounts for the pervasive nature of bright-red dolomite in crystal interiors. In the Nisku Formation, the dominantly dull luminescent signature of the matrix components, the replacement of crystal interiors, and dedolomitization by dull calcite, support the idea of diffusional transport. Ionic transfer by fluid-flow was also active, once fluid-films emerged from the crystalline medium into pores, and in fractures originating at stylolites.

Geochemical interpretation of the zonal sequences mapped in the Nisku Formation, Zeta Lake Member, support the interpretation of dull calcite as being a burial diagenetic cement that precipitated from reducing pore waters, likely of subsurface origin.

Isotopic analysis of the Nisku Formation main mineral phases support the interpretation of dull calcite and Fe-dolomite being pressure solution derived. It also compliments rather well the neomorphism/recrystallization history of the marine and matrix dolomite components.

9.2 FURTHER RESEARCH REQUIREMENTS

9.2.1 STYLOLITIZATION MECHANISMS

The amalgamation mechanism, as described in Chapter 2 applies to dolomitized sub- to intertidal sediments. The "trigger" to the mechanism is the primary "organic" layering that results from mechanical compaction of unlithified sediment. In transmitted and reflected light microscopy the seam material appears "organic". It does not display any petrographic characteristics of clay minerals. This needs to be confirmed by XRD and chemical analyses.

To further support this mechanism as a general model, study of similar fine-grained carbonate lithologies needs to be done. Analagous features and structures have been described in the literature (Mossop 1972, Wanless 1979), but a comparative study of two or more similar carbonates is required.

The dolomitization-stylolitization mechanism of Chapter 3 applies to a matrix dolomitized reefal carbonate. Similarly, before proposing this mechanism as a general model, a comparative study of other partially dolomitized limestones is needed to confirm or modify this mechanism.

9.2.2 PERMEABILITY BARRIERS

The trend produced by statistical analysis of core data suggests that centimetre-scale stylolites have similar abilities as vertical permeability barriers as do micron to millimetre-scale stylolites. This is believed to result from the shearing action of large sutures past their socket walls.

Further research is required to determine whether or not this type of trend is ubiquitous to all extensively stylolitized carbonates, or just reefal carbonates such as the Zeta Lake Member. The procedure is simple and inexpensive. It requires no technical assistance, just time.

9.2.3 PRESSURE SOLUTION GENERATED MATERIALS

Further research is required to compliment the cathodoluminescent study of the Zeta Lake Member. Trace element analyses are required to substantiate the geochemical interpretations made in Chapter 7. These interpretations were made on a qualitative basis using other investigators data found in the literature, making the conclusion susceptible to warranted criticism.

Trace element analysis is also required of dull calcite spar and dull maroon dolomite: that which is directly related to stylolites (fracture infillings) and that which occludes porosity. The purpose of this would be to establish if there are compositional differences not detected by cathodoluminescence between directly related and inferred phases.

Additional isotopic analyses of Zone 1 and 2 calcite spar cements would be useful (if these zones could be separated) to support the interpretations made in Chapter 7. Calculation of temperatures of formation waters from which the mineral phases were precipitated/re-equilibrated would also be of use to the diagenetic understanding of the Nisku Formation, though not necessary to the recognition of pressure solution generated-cements.

9.3 CONCLUSIONS

Research into the pressure solution phenomenon has lead to the following conclusions:

1) Stylolitization is a response to pressure solution that is initially dependent upon original primary features and diagenetic alteration of the sediment.

2) Once formed, a stylolite may grow in one of two manners; by continued amalgamation or by pressure-dissolution of the sockets. Ultimately, the former evolves into the latter in adult stage growth of the amalgamation mechanism.
3) Both mechanisms of stylolitization propagate laterally in the same manner. The difference is visual. One can commonly see the propagation mechanism "frozen" in the rock if stylolites form by an amalgamation mechanism. For dolomitization-stylolitization, rare occurrences of fan-like arrays of dolomite crystals confirms that the manner in which these stylolites propagate is similar.
4) A stylolite cannot grow vertically without growing laterally. In this sense, stylolites are self-propagating.
5) The shearing action of stylolitic sutures penetrating deep into their sockets attenuates accumulated insoluble material such that large, centimetre-scale stylolites are as much of a permeability barrier as small micron to millimetre-scale stylolites.

6) Direct evidence relating stylolitization to pressure solution generated cements is found as veinlets propagating away from stylolites. The carbonate material that makes up these veinlets is seen elsewhere in the rock in modes of occurrence that are spatially and temporally related to stylolites.

7) Recrystallization and diffusion transport (of pressure solution generated material) accounts for luminescent characteristics of the rock that cannot be related to cementation processes. The result is random luminescent patterns and/or replacement of some pre-stylolitic mineral phases found proximal to stylolites.

This thesis has dealt with three main aspects of the pressure solution phenomenon: stylolitization mechanisms, permeability barriers, and pressure solution generated-cements. It is hoped that the reader now has a better understanding of how stylolites form and develop, and the effects that this process can have on the rock.

APPENDIX A

CATHODOLUMINESCENT MICROSCOPY

Instrumentation Cathodoluminescent observations were made using a Nuclide Corporation ELM-2A Cold Electron Gun Luminoscope. Operating conditions are:

Beam Energy: 12.5 Kv DC

Beam Current: 0.5 milliamp for observation
0.8 milliamp for photography

Spot Diameter: 8 mm spot size at a focus setting of 28%

Gun Type: Cold Cathode

Ambient Gas: Air

Instrumentation: Nuclide ELM-2A Luminoscope
Olympus standard petrographic microscope (magnification 28X)
Olympus OM-2 35 mm SLR camera

Operating instructions for the luminoscope may be found in the accompanying manual supplied by Nuclide Corporation.

Sample Preparation

Standard petrographic thin sections prepared to 30 micron thicknesses were used in this study. These were made by Texaco Canada Resources Ltd.. All thin sections were stained for calcite and dolomite using Alizarin Red-S and Potassium Ferricyanide stains. For cathodoluminescent conditions the cover slips were removed and the thin sections were washed in acetone before use in the Luminoscope.

Photography

Photographs were taken using Kodak Ektachrome EES P800/1600 professional slide film. This film gives the best results. It reproduces CL light intensities and colors accurately and does not vary with the processor.

Camera settings: Film speed 1600 ASA

Plain light exposures at 3 to 6 seconds

Polarized light exposures at 5 to 8 seconds

CL light exposures at 30 to 75 seconds, at 15 second intervals

Due to variable transmitted and CL light intensities inherent in the thin section these exposure times only serve as a general guide. Unfortunately, exposure times must be determined experimentally to find correct exposure times.

For plain light and CL light exposures the image must be focused under plain light conditions. Images must be refocused for polarized light focused.

Suggestions

Do not leave the electron beam on any one spot for any length of time (approximately 2 minutes or longer). This results in burning of the thin section due to long exposure.

APPENDIX B

STATISTICAL ANALYSIS

The vertical permeability and porosity data used for the statistical analysis of Chapter 4 is property of Texaco Canada Resources Ltd., Calgary. Anyone wishing to use this data must request the release of the core analysis for Texaco Bigoray 6-12-52-9W5 from Texaco. For these reasons the data has not been included in this appendix.

Equations

Mean $$\bar{x} = \frac{\Sigma x}{n}$$

Standard Deviation

$$Sx = \sqrt{\frac{\Sigma x^2 - n\bar{x}^2}{n-1}}$$

Population parameter taken to be "n-1". Used to estimate the standard deviation of the population from sample data extracted from the population (e.g. for stylolite classes).

$$\sigma_p = \sqrt{\frac{\Sigma x^2 - n\bar{x}^2}{n}}$$

Population parameter taken to be "n". Used when all populations are taken to be sample data or when finding the standard deviation of the population sample taken to be the population (e.g. for No Seam class).

Confidence Intervals

Used to calculate the standard difference of the mean of samples for larger sample sizes (n>25). Two standard errors of the mean is equivalent to a 5% probability level. Three standard errors of the mean is equivalent to a 1% probability level.

$$\frac{2\ \sigma_p}{n_s} = \text{2 Std. Err. of the Mean}$$

$$\frac{3\ \sigma_p}{n_s} = \text{3 Std. Err. of the Mean}$$

where σ_p = population standard deviation (No Seams)

n_s = number of items in the sample class being compared

T-tests: First Distillation (Large sample method, n>25)

Used to test the hypothesis that a sample (stylolite class) whose mean value is $\bar{x}$ could have come from a population (No Seams class) whose mean value is $\bar{X}$ and whose standard deviation is O_p.

$$t = \frac{\text{Error in Mean}}{\text{Std. Err. of Mean}} = \frac{|\bar{X} - \bar{x}|}{\left(\frac{\sigma_p}{n_s}\right)} = \frac{|\bar{X} - \bar{x}|\sqrt{n_s}}{\sigma_p}$$

Calculated t values are compared to tabulated values of t for a normal distribution at $n_1 + n_2 - 2$ degrees of freedom. Calculated values that exceed normal distribution t values are significant at probability values indicated in tables. Therefore the mean values compared are different.

T-tests: Second Distillation (Small sample method, n<25)

Used to test the hypothesis that one sample (stylolite class) whose mean value is $\bar{x}_1$ and another sample (No Seams class) whose mean value is $\bar{x}_2$ could have come from populations identical both as to mean and variance.

First step is to make a pooled estimate of the population variance.

$$\hat{\sigma}^2 = \frac{n_1 s_1^2 + n_2 s_2}{n_1 + n_2 - 2}$$

n = sample size s^2 = sample variance

Second step is to make a best estimate of the standard error for the difference of the means of the two samples.

$$\hat{\sigma}_w = \sigma\sqrt{\frac{1}{n_1} + \frac{1}{n_2}}$$

Third step is to calculate the t value.

$$t = \frac{\bar{x}_2 - \bar{x}_1}{\hat{\sigma}_w}$$

Calculated t values are compared to tabulated t values for a normal distribution at $n_1 + n_2 - 2$ degrees of freedom. Calculated t values that exceed normal distribution t values are significant at probability levels indicated in tables. Therefore the compared mean values are different.

APPENDIX C

ISOTOPIC ANALYSIS

Preparation and Collection

Sample powders were prepared for isotopic analysis in two different fashions.

Calcite powders (between 2 to 5 milligrams) were placed in glass "boats" made from 6 mm glass tubing sealed at one end. Each glass boat was inserted in a reaction vessel made from 20 centimetres of 9 mm glass tubing sealed at one end. In the reaction vessel the glass boats sat on a 10 cm spacer cut from the narrow end of a pipette. 100% phosphoric acid was added to this level before the insertion of the glass boat. After insertion, the reaction vessels were placed on a vacuum line, evacuated, then sealed with a torch. These vessels were stored upright until it was desired to invoke the reaction. This was done by inverting the vessel, allowing the calcite powder and phosphoric acid to mix. To ensure that only calcite derived CO_2 was measured in the mass spectrometer, the vessels were inverted only 1 hour before being inserted into the mass spectrometer.

Dolomite powders (between 2 to 5 milligrams) were placed in the main body of a carbonate reaction vessel. In the small arm of the vessel 5 millilitres of 100% phosphoric acid was placed. The vessels were then placed on a vacuum line and evacuated. When sufficient vacuum was reached the vessels were closed, removed from the line and inverted, allowing the acid to mix with the sample powder. The vessels were then placed on the vacuum line again.

After 1 hour any calcite CO_2 was collected from each vessel and sealed in 6 mm glass tubes. Due to the nature of the dolomite, this gas would be CO_2 derived from micrite.

After 3 hours the vessels were opened and evacuated, and then closed. This was done to ensure that any calcite derived CO2 was evacuated. The reaction was then allowed to proceed for 72 hours to let the dolomite-phosphoric acid reaction reach completion. After the allotted time, each vessel was opened, evacuated, and the dolomite CO_2 collected and sealed in 6 mm glass tubes.

All reactions were performed at 25^{o} celcius.

Analysis

Measurement of the isotopic ratios was done on a VG Micromass 602D mass spectrometer. Isotopic ratios were measured with precisions better than +/- 0.10 per mil. The measured ratios were then converted to PDB values using phosphoric acid - carbonate fraction factors of O'Neill et al. (1969) for calcite, and of Land (1980) for dolomite.

REFERENCES

Allen, L.R. and Matthews, R.K., 1977. Carbon and oxygen isotopes as diagenetic and stratigraphic tools: data from the surface and subsurface of Barbados, West Indies. Geology, 5, 16-20.

Bathurst, R.G.C., 1971. Carbonate Sediments and Their Diagenesis, Elsevier, Amsterdam, 620 pp.

---------. 1980. Deep-crystal diagenesis in limestones. Revista del Instituto de Investigaciones Geologicas, Universidad de Barcelona, Department de Petrologia i Geoloquimica. 34, 89-100.

---------. 1983. Neomorphic spar versus cement in some Jurassic grainstones: significance for evaluation of porosity evolution and compaction. J. Geol. Soc London. 140, 229-237.

Carpenter, A.B. and Oglesby, T.W., 1976. A model for the formation of luminescently zonal calcite cements and its implications. Geol. Soc of Am. Abstr., 8, 469-470.

Dickson, J.A.P. and Coleman, M.L., 1980. Changes in carbon and oxygen isotopic composition during limestone diagenesis. Sedimentology, 27, 107-118.

Dunham, R.J., 1969. Early vadose silt in Townsend mound (reef), New Mexico, In Depositional environments in carbonate rocks. Friedman, G.M., editor. SEPM Spec. Publ. 14, 139-181.

Dunnington, H.V., 1954. Stylolite development post-dates rock induration. Journ. Sed. Petrol., 24, 27-49.

----------. 1967. Aspects of diagenesis and shape change in stylolitic limestone reservoirs. Proc. Seventh World Petroleum Congress, Mexico, 339-352.

Ebers, M.L. and Kopp, O.C., 1979. Cathodoluminescent Microstratigraphy in Gangue Dolomite, the Mascot-Jefferson City District, Tennessee. Econ. Geology 74, 908-918.

Fairchild, I.J., 1983. Chemical controls of cathodoluminescence of natural dolomites and calcites: new data and review. Sedimentology, 30, 579-583.

Ferguson, C.C. and Harvey, P.K., 1972. Porphyroblasts and "crystallization force": some textural criteria. Discussion. Geol. Soc. Am. Bull. 83, 3839-3840.

Fletcher, R.C. and Pollard, D.D., 1981. Anticrack model for pressure solution surfaces. Geology, 9, 419-424.

Frank, J.R., 1981. Dedolomitization in the Taum Sauk Limestone (Upper Cambrian), Southeast Missouri. Journ. of Sed. Petrology, 51, no. 1, 7-18.

Frank, J.R., Carpenter, A.B., and Oglesby, T.W., 1982. Cathodoluminescence and composition of calcite cement in the Taum Sauk Limestone (Upper Cambrian), Southeast Missouri . Journ. of Sed. Petrology, 52, 631-638.

Garrels, R.M. and Christ, C.L., 1965. Solutions, minerals and equilibria. Harper and Row, New York, 450p.

Grover, G. and Read, J.F., 1983. Paleoaquifer and deep burial related cements defined by regional cathodoluminescent patterns, Middle Ordovician carbonates, Virginia. Amer. Assoc. Petrol. Geol., 67, 1275-1303.

Hudson, J.D., 1975. Carbon isotopes and limestone cement. Geology, 3, 19-22.

------. 1977. Stable isotopes and limestone lithification. Q. Jl. Geol. Soc. Lond., 133, 637-660.

James, N.P. and Choquette, P.W., 1984. Diagenesis 9 - Limestones - The meteoric diagenetic environment. Geoscience Canada, 11, 161-194.

James, N.P. and Klappa, C.F., 1983. Petrogenesis of Early Cambrian reef limestones, Labrador, Canada. Journ. Sed. Petrol., 53, 1051-1096.

Kendall, A.C. and Tucker, M.E., 1973. Radiaxial fibrous calcite: a replacement after acicular carbonate. Sedimentology, 20, 365-389.

Krauskopf, K.B., 1979. Introduction to geochemistry. New York, McGraw-Hill, 617p.

Land, L.S., 1980. The isotopic and trace element geochemistry of dolomite: the state of the art. In Concepts and models of dolomitization Zenger, D.H., Dunham, J.B. and Ethington, R.L., editors. SEPM Spec. Publ. 28, 87-110.

Lohmann, K.C. and Meyers, W.J., 1977. Microdolomite inclusions in cloudy prismatic calcites: proposed criteria for former high-magnesium calcites. Journ. Sed. Petrol., 47, 1078-1088.

Long, J.V.P. and Agrell, S.O., 1965. The cathodo-luminescence of minerals in thin section. Mineralogical Magazine, 34, 318-326.

Machel, H.G., 1984. Facies and diagenesis of some Nisku build ups and associated strata, Upper Devonian, Alberta, Canada. In Carbonate Buildups, SEPM Core Workshop No. 4, Dallas, Texas, 1983.

------. 1985. Cathodoluminescence in calcite and dolomite and its chemical interpretations. Geoscience Canada, 12, no. 4, 139-147.

Marfunin, A.S., 1979. Spectroscopy, luminescence and radiation centres in minerals. Springer-Verlag, Berlin, 352pp.

Marshall , J.D., 1981. Zoned calcites in Jurassic ammonite chambers: trace elements, isotopes and neomorphic origin. Sedimentology, 28, 867-887.

Mattes, B.W., and Mountjoy, E.W., 1980. Burial dolomitization of the Upper Devonian Miette Buildup, Jasper National Park, Alberta, In Concepts and models of dolomitization. Zenger, D.H., Dunham, J.B. and Ethington, R.L., editors. SEPM Spec. Publ. 28, 259-297.

Meyers, W.J., 1974. Carbonate cement stratigraphy of the Lake Valley Formation (Mississippian) Sacramento Mountains, New Mexico. Journ. of Sed. Petrol., 44, 837-861.

------. 1978. Carbonate cements: their regional distribution and interpretation in Mississippian limestones of south New Mexico. Sedimentology, 25, 371-400.

Meyers, W.J. and Lohmann, K.C., 1985. Isotope geochemistry of regionally extensive calcite cement zones and marine components in Mississippian limestones, New Mexico. In Carbonate Cements. Schneidermann, N. and Harris, P.M., SEPM Spec. Publ. 36, 223-239.

Moore, C.H. Jr., Graham, E.A. and Land, L.S., 1976. Sediment transport and dispersal across the deep fore-reef and island slope (-55m to -305m), Discovery Bay; Jamaica. Journ. Sed. Petrol., 46, 174-187.

Moroney, M.J., 1951. Facts From Figures, Penguin Books, Baltimore, Md. 472p.

Mossop, G.D., 1972. Origin of the peripheral rim, Redwater reef, Alberta. Bull. Canadian Petroleum Geology, 20, 238-280.

Nelson, R.A., 1981. Significance of fracture sets associated with stylolite zones. Amer. Assoc. Petrol. Geol., 65, 2417-2425.

Nickel, E., 1978. The present status of cathodoluminescence as a tool in sedimentology. Minerals Sci. Engng., 10, 73-100.

Oldershaw, A.E. and Scoffin, T.P., 1967. The source of ferroan and non-ferroan calcite in the Halkin and Wenlock Limestones. Geol. Journ., 5, 309-320.

O'Neill, J.R., Clayton, R.N. and Mayeda, T.K., 1969. Oxygen isotope fractionation factors in divalent metal carbonates. Journ. Chem. Physics., 51, 5547-5558.

Park, W.C. and Schot, E.H., 1968. Stylolites: their nature and origin. Journ. Sed. Petrol., 38, 175-191.

Pierson, B.J., 1981. The control of cathodoluminescence in dolomite by iron and manganese. Sedimentology, 28, 601-610.

Pingitore, N.E. Jr., 1982. The role of diffusion during carbonate diagenesis. Journ. Sed. Petrol., 52, 27-40.

Pratt, B.R., 1982. Limestone response to stress-pressure solution and dolomitization-discussion and examples of compaction in carbonate sediments. Journ. Sed. Petrol., 52, 3323-328.

Prezbindowski, D.R., 1985. Burial Cementation - Is it important? A case study, Stuart City Trend, South Central Texas. In Carbonate Cements. Schneidermann, N. and Harris, P.M., editors. SEPM Spec. Publ. 36., 241-264.

Prokopovich, N., 1952. The origin of stylolites. Journ. Sed. Petrol., 22, 212-220.

Purser, B.H., 1978. Early diagenesis and the preservation of porosity in Jurassic limestones. Journ. Petrol. Geol., 1, 83-94.

Richter, D.K. and Zinkernagel, U., 1981. Zur Anwendung der Kathodenlumineszenz in der Karbonat petrographie: Geologische Rundschau, 70, 1276-1302.

Rutter, E.H., 1976. The kinetics of rock deformation by pressure solution. Phil. Trans. R. Soc. London A., 283, 203-219

Schofield, K., 1984. Are pressure solution, neomorphism and dolomitization genetically related? Abu Dhabi National Reservoir Research Foundation, (ADREF), Seminar on Stylolites and Associated Phenomena. Relevance to Hydrocarbon Reservoirs. Al Ain, Abu Dhabi, 1983.

Schofield, K. and Adams, A.E., 1986. Burial Dolomitization of the Woo Dale Limestones Formation (Lower Carboniferous), Derbyshire, England. Sedimentology, 33, 207-219.

Scholle, P.A. and Halley, R.B., 1985. Burial diagenesis: out of sight, out of mind! In Harris, P.M. and Schneidermann, N., editors, Carbonate Cements. SEPM Spec. Publ., 36, 223-239.

Selkman, S.O., 1983. Stress and displacement distributions around pyrite grains. Journ. Struct. Geol., 5, 47-52.

Shaub, B.M., 1939. The origin of stylolites. Journ., Sed. Petrol., 9, 47-61

-----. 1949. Do stylolites develop before or after the hardening of the enclosing rock? Journ. Sed. Petrol., 19, 26-36.

Shimamoto, T., 1975. The finite element analysis of the deformation of a viscous spherical body embedded in a viscous medium. Journ. Geol. Soc. Japan, 81, 255-267.

Shinn, E.A., Halley, R.B., Hudson, J.H. and Lidz, B.H., 1977. Limestone compaction-an enigma. Geology, 5, 21-24.

Shinn, E.A. and Robbin, D.M., 1983. Mechanical and chemical compaction in fine-grained shallow-water limestones: Journ. Sed. Petrol., 53, 595-618.

Shukla, V. and Friedman, G.M., 1983. Dolomitization and diagenesis in a shallowing-upward sequence: The Lockport Formation (Middle Silurian), New York State. Journ. Sed. Petrol., 53, 702-717.

Simpson, J., 1985. Stylolite-controlled layering in an homogeneous limestone: pseudo-bedding produced by burial diagenesis. Sedimentology, 32, 495-505.

Sippel, R.F. and Glover, E.D., 1965. Structures in carbonate rocks made visible by luminescence petrography. Science, 150, 1283-1287.

Smith, J.V. and Stenstrom, R.C., 1965. Electron-excited luminescence as a petrologic tool. Geology, 73, 627-635.

Sommer, S.E., 1972a. Cathodoluminescence of carbonates, 1. Characterization of cathodoluminescence from carbonate solid solutions. Chem. Geol., 9, 257-273.

------. 1972b. Cathodoluminescence of carbonates, 2. Geological applications. Chem. Geol., 9, 275-284.

Stockdale, P.B., 1922. Stylolites: their nature and origin. Indiana University Studies, 9, 1-97.

---------. 1926. The stratigraphic significance of solution in rocks. Journ. Geology, 34, 399-414.

---------. 1943. Stylolites: Primary or secondary. Journ. Sed. Petrol., 13, 3-12.

Walken, G.M. and Berry, J.R., 1984a. Natural calcite in cathodoluminescence: crystal growth during diagenesis. Nature 308, 525-527.

Walls, R.A., Mountjoy, E.W. and Fritz, P., 1977. Isotopic composition and diagenetic history of carbonate cements in the Devonian Golden Spike reef, Alberta, Canada. Geol. Soc. Am. Bull., 90, 963-982.

Wanless, H.R., 1979. Limestone response to stress-pressure solution and dolomitization. Journ. Sed. Petrol., 49, 437-462.

Watts, N.L., 1984. The role of carbonate diagenesis in exploration and production from Devonian pinnacle reefs, Alberta, Canada. In-house publication of Texaco Can. Res. Ltd., Calgary, Alberta.

Wong, P.K. and Oldershaw, A.E., 1981. Burial cementation in the Devonian, Kaybob reef complex, Alberta, Canada. Journ. Sed. Petrol., 51, 507-520.

Wuerker, R.G., 1962. Annotated tables of strength and elastic properties of rocks. Soc. Petroleum Engineers, Petroleum Trans. reprint series, 6 (Drilling), 23-45.